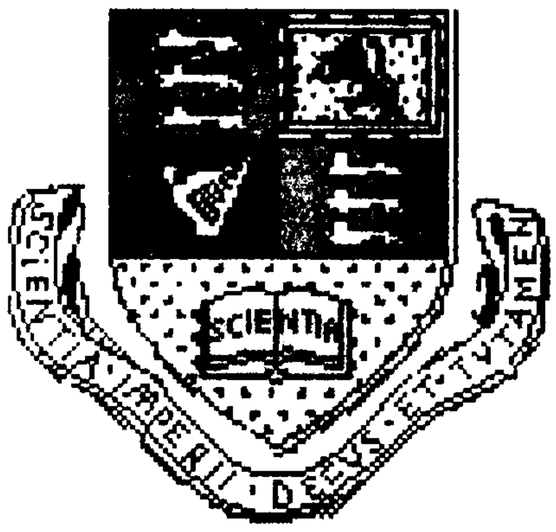
SILICATE GLASS-CERAMICS CONTAINING FLOURIDE FOR APPLICATION IN CERAMIC-MATRIX-COMPOSITES

BY

KULJIRA SUJIROT

Thesis submitted for the
Degree of Doctor of Philosophy of the University of London
and for the
Diploma of Imperial College



Department of Materials,
Imperial College of Science, Technology and Medicine
London SW7 2BP

September 1995

Abstract

The possibility to use a glass in the Na_2O-CaO-Al_2O_3-SiO_2 system with and without partly-substitution of fluorine for oxygen developed by Mukerjee and Rogers [1967] for mechanical application was studied. The fluorine has a significant effect on the kinetics of crystallization in several ways. Firstly, it forms glass with stronger bonds at temperature lower than the glass transition temperature, and facilitates the viscous flow of the glass at higher temperature. Secondly, it decreases the activation energy for crystallization. Thirdly, it acts as a nucleating agent which induced glass-in-glass phase separation. Finally, it affects the crystallization path by forming a metastable phase, which in CSF case is cuspidine.

The cast glass-ceramic was produced sucessfully in the glass with fluorine (CSF) which shows the highest flexural strength of 154 MPa and high fracture toughness, 2.59 MPam1/2. The toughness can be enhanced by inducing microcracks but this inevitably reduced the flexural strength. The highest toughness obtained was 3.71 MPam1/2 and the flexural strength dropped to 100 MPa. Factors controlling the mechanical performance were crystallinity, spherulite morphology and size, and crystal phase.

In the CS base glass which crystallizes one-dimensionally from the surface and sintering was completed before crystallization started, constant heating rate is beneficial for densification. On the other hand, the CSF glass which crystallizes so abruptly that sintering may be halted, high heating rate should be used to shift the crystallization temperature to higher temperature and also to lower the viscosity.

Three types of particulate 'reinforcements' were incorporated to the matrices; i.e. Al_2O_3, ZrO_2, and SiC. Due to less crystallisation at the interface, the CS achieves higher densification than the CSF. From the preliminary study, alumina has the potential to be used in these matrices.

Acknowledgements

I gratefully acknowledge my supervisors, Prof. R.D. Rawlings and Dr. P.S. Rogers who provided critical insight into various aspects of research in glass-ceramics, for their guidance and advice.

I am thankful to the contributions made by a number of colleagues who have shared invaluable time in my English life as well as this research: Bernard Aduda, Ian Davies, Fiona McQuillan, Hasan Alanyali, Charles Shieh, Christopher Von Schweitzer, Titin Kathrina, Belinda Taylor, Charlie Lin, Robert Baxter, Emma Claxton, Christian Colongo, Gloria Velasco, Eliana Fu, Pakamard Saewong, Jesus Imery, Anita Adoba, Emmanuelle Devaux, Lincoln Leatherland and Huseyin Uzun.

I particularly expresses appreciation to all friends in the 'Thai Society' and all Kalayanamitras from Amaravati and Holland park group who uplifted my spirit. My sincere thanks goes to Seeroong Preechanont, Siriporn Pavawongsak, and Hathaichanok Duriyabunleng for their friendship and the interest in my work. In the preparation of this thesis I am especially indebted to Kantadharm Suphamongkhon, Manirat Sensee, and Vinny for their kindness and support.

I wishes to thank all the technical, photographic, and administrative staff, especially R.Sweeney, N.H.V.Salpadoru, M.Hudden, J.Wright, D.Raj, A.Willis, and P.G.Batten, who have contributed their time and provided practical advice and assistance. I also acknowledge the Royal Thai Government for financial support throughout the study.

Finally, my greatest love and gratitude go to my family for their constant encouragement.

September 1995

Annotation

A : constant

a' : uncalibrated CTE of a specimen

a* : CTE of the sample holder

a : notch depth

a_c : critical flaw size

a_0 : interatomic distance

b : heating rate

B: specimen breadth

C : constant

c : volume fraction crystallized

D : diameter

d : average indent diagonal

d : mean crystal diameter

D* : size of clusters > the critical size

E : Elasticity of the material

ε : transducer conversion constant

E_c : activation energy for crystallization

E_η : activation energy for viscous flow

$E_{\eta'}$: activation energy for viscous flow by Moynihan method

E_s : activation energy for sintering

γ : fracture surface energy of new surfaces

g, g´ : geometric factor

γ_i : effective surface energy for fracture initiation

η : viscosity

H_v : Vicker's hardness

I_v : nucleation frequency per unit volume

K : effective overall reaction rate

K_0 : pre-exponential constant

L : length of specimen

λ : mean free path of a glass

M : bending moment

m : integer or half integer

n : Avrami exponent

N_A : number of crystals per unit area

N_v : number of crystals per unit volume

P : applied load

R : gas constant

r : radius of glass particles

ρ' : relative density

ρ_0 : density of a pressed unfired compact of powder

r_0 : initial particle radius

ρ_a: apparent material density

ρ_{air} : density of air

ρ_g : pycnometer density of glass particles

ρ_{H2O} : density of water

ρ_t : true density of the powder

σ : applied flexural stress

s: span length

T : absolute temperature

t : time

T_g : glass transition temperature

$T_{g'}$: temperature marking the extrapolated finish of the transition region in the DTA trace

T_p : crystallization peak temperature

u : crystal growth rate

υ : material Poisson ratio

u : rate of crystal growth.

v : volume fraction of crystalline phase

W : width of the beam

W_1, W_2 : weight of the paper representing the peaks and the amorphous region respectively

W: specimen width

w_{wire} : submerged weight of the wire

Y: compliance factor

Z : flaw shape parameter

ΔG : kinetic barrier to nucleation

ΔT : difference in temperatures

ΔT_{FWHM} : full width of the crystallization peak at half the maximum height

Δx: difference in transducer readings

Contents

Abstract 2
Acknowledgements 3
Annotation 4
Contents 5
List of Tables 10
List of Figures 12

CHAPTER 1 INTRODUCTION 17
1.1 Glass 18
1.2 Monolithic glass-ceramics 20
1.3 Sintered glass-ceramics 22
1.4 Glass-ceramic matrix composites 23
1.5 Aim 24

CHAPTER 2 GLASS 26
2.1 Introduction 26
2.1.1 Glass Formation 26
2.1.1.1 Structural models 27
(i) Goldschmidt's radius ratio criterion 27
(ii) Zachariasen's random network hypothesis 27
(iii) Sun's bond-strength criterion 29
(iv) Kingery's O:Si criterion 30
2.1.1.2 The structure of multicomponent glass-forming systems 30
2.1.1.3 Kinetic approach to glass formation 31
2.1.2 Glass behaviour 31
2.1.2.1 Glass transition 32
2.1.2.2 Viscosity of glass 34
(i) VFT Equation 36
(ii) Urbain's method 36
(iii) Activation energy for viscous flow 36
2.1.2.3 Effect of Fluorine ions 37
2.2 Experimental Procedure 39
2.2.1 Starting materials and glass preparation 39
2.2.2 Chemical analysis 41
2.2.2.1 Wet chemical analysis 41
2.2.2.2 Energy dispersive x-ray spectroscopy (EDS) 41

2.2.3 Density measurements 41
2.2.3.1 True density 41
2.2.3.2 Bulk density 42
2.2.4 Dilatometry 43
2.2.5 Differential thermal analysis (DTA) 44
2.3 Results and Discussion 44
2.3.1 Chemical analysis 44
2.3.2 Glass characterization 46
2.3.2.1 Density 46
2.3.2.2 Coefficient of thermal expansion 47
2.3.3 Kinetic behaviour 47
2.4 Summary 53

CHAPTER 3 CRYSTALLIZATION PROCESS 54
3.1 Introduction 54
3.1.1 Silicate structure 55
3.1.2 Transformation Kinetics 57
3.1.2.1 Nucleation 58
(i) Glass-in-glass phase separation 58
(ii) Time lag effects 59
(iii) Saturation effects 59
(iv) Nucleation catalysts 60
3.1.2.2 Crystallization 60
(i) Surface crystallization 61
(ii) Spherulitic crystallization 63
(iii) Approach to equilibrium 63
3.1.2.3 Certain material properties and crystallizability 64
3.1.2.4 Crystallization in silicate systems 66
3.1.3 Theories of Phase Transformation 66
3.1.3.1 Classical Nucleation theory 68
3.1.3.2 Johnson-Mehl-Avrami Equation 69
3.1.4 Application of thermal analysis to the kinetics of crystallization 71
3.2 Experimental Procedure 75
3.2.1 Microscopic techniques 75
3.2.1.1 Optical Microscopy 76
3.2.1.2 Secondary Electron Microscopy 76
3.2.1.3 Transmission electron microscopy 77
3.2.1.4 Image analysis 77
3.2.2 X-ray diffractometry 78

3.2.2.1 Identification of crystalline phases 78
3.2.2.2 Semi-quantitative analysis of crystalline and amorphous phases 79
3.2.3 Differential thermal analysis 81
3.2.3.1 Determination of activation energy 81
3.2.3.2 Determination of nucleation-rate-curve 81
3.3 Results and discussion 82
3.3.1 Kinetic of crystallization 82
3.3.1.1 Differential thermal analysis (DTA) 82
3.3.1.2 Crystal phase identification 84
3.3.2 Microstructural development 88
3.3.2.1 CS glass 88
(i) Single stage heat treatment 88
(ii) Second stage heat treatment 92
3.3.2.2 CSF glass 92
(i) Single stage treatment 92
(ii) Double stage treatment 96
3.3.3 Controlled crystallization 105
3.4 Summary 114

CHAPTER 4 POWDER ROUTE 115
4.1 Introduction 115
4.1.1 Powder characteristics 116
4.1.2 Fabrication of powder compact 117
4.1.3 Sintering process 118
4.1.3.1 Sintering stages 119
4.1.3.2 Driving force 119
(I) Surface energy 119
(II) Porosity 120
4.1.3.3 Densification mechanisms 120
4.1.4 Theoretical models for glass sintering 121
4.1.5 Sintered glass-ceramics 123
4.1.6 Effect of rigid inclusions 125
4.2 Experimental procedure 126
4.2.1 Powder preparation 126
4.2.2 Dry pressing and Isostatic pressing 126
4.2.3 Characterization techniques 126
4.3 Results and Discussion 127
4.3.1 Powder characterization 127
4.3.2 Differential thermal analysis 127

4.3.3 Densification Study 134
4.3.2.1 Constant heating rate treatment 134
4.3.2.2 Isothermal treatment 136
(i) CS 136
(ii) CSF 145
4.3.2.3 Effect of rigid inclusions 149
4.4 Summary 156

CHAPTER 5 MECHANICAL PROPERTIES 158
5.1 Introduction 158
5.1.1 Strength 158
5.1.1.1 Strength of glass 161
5.1.1.2 Strength of glass-ceramics 162
5.1.2 Fracture toughness 163
5.1.2.1 Critical Flaw Size (ac) 165
5.1.2.2 Fracture surface energy (gf) 165
5.1.3 Hardness and Indentation Toughness 166
5.1.4 Fractography 168
5.1.5 Toughening mechanisms in glass-ceramics 169
5.2 Experimental procedure 172
5.2.1 Flexural strength 172
5.2.2 Plane strain fracture toughness 172
5.2.3 Vicker's microhardness and Indentation toughness 173
5.2.4 Elasticity 173
5.3 Results and discussion 174
5.3.1 Elasticity 174
5.3.2 Flexural strength 176
5.3.2.1 Bulk cast glass and glass-ceramics 176
5.3.2.2 Sintered glass and glass-ceramics 180
5.3.2.3 Glass- and glass-ceramic matrix composites 182
5.3.3. Vicker's microhardness 183
5.3.4 Fracture toughness 188
5.4 Summary 191

CHAPTER 6 SUMMARY 193
6.1 Kinetics considerations 193
6.2 Thermodynamic considerations 194
6.3 Controlled crystallization 195
6.4 Controlled sintering and crystallization 196
6.5 Mechanical properties 197

6.6 Conclusion 198

CHAPTER 7 SUGGESTIONS FOR FURTHER WORK 200
7.1 On matrix characterization 200
7.2 On improvement of the materials 200
7.3 On application 201

REFERENCES 202

Appendix A 213
Appendix B 214
Appendix C 215

List of Tables

Table 1-1 19

Table 2-1 Common constituents of glasses and their influence on properties [Holloway 1973]. 29

Table 2-2 Raw materials used in the glass preparation and conditions under which they were dehydrated. 40

Table 2-3 Nominal batch compositions for the base glass (CS) and base glass with fluoride (CSF). 40

Table 2-4 Wt% of individual cations (compared to total cation content) in CS and CSF glasses analysed by EDS technique. 46

Table 2-5 Fluorine content analysis in wt%. 46

Table 2-6 Density and coefficient of thermal expansion (CTE) in CS and CSF glasses. 47

Table 2-7 Temperatures corresponding to fixed points of CS and CSF bulk glasses from DTA and dilatometric results (within accuracy of ±5˚C) in comparison viscosity by VFT method (Eq. 2-4). 49

Table 2-8 Glass transition temperatures as defined in Figure 1-4 for the calculation of enthalpy of viscous flow by Moynihan's method. 53

Table 2-9 Activation energies for viscous flow at the glass transition temperatures calculated via Arrhenius's (Eh) and Moynihan's (E_η^*) methods. 53

Table 3-1 Comparison of information form JCPDS cards of crystal phases present in the study. 57

Table 3-2 Composition of glass, investigated by Shyu & Wu [1991], which affects the crystallization as shown in Figure 3-5. 67

Table 3-3 Thermal characteristics constants of bulk cast CS and CSF samples. 86

Table 3-4 The apparent activation energy for the initiation of crystallisation and the crystallisation peak range. 86

Table 3-5 Intensity of wollastonite I (d-value 2.98 ˚A) compared with the intensity of cuspidine (Io) (d-value 3.26 ˚A) heat treated at 660˚C for 3 hours and then at different growth temperatures for 30 minutes. 86

Table 3-6 Activation energy for diffusion of various species in silicate glass from literatures 92

Table 3-7 Quantitative EDX analysis of samples undergoing various heat treatments. 94

Table 3-8 Crystallised CS and CSF and their characterisation 109

Table 3-9 Quantitative EDX analysis of samples which have undergone various heat treatments. 112
Table 4-1 Thermal characteristics constants of bulk cast CS and CSF samples. 133
Table 4-2 The apparent activation energy for crystallisation and Avrami exponent in CS and CSF glass powders..... 133
Table 4-3 Significant thermal points reference glass transition temperature from DTA (Tg), sintering temperature from dilatometer (Ts) and temperature starting and finishing crystallization from DTA (Tx and Tf respectively) for CS and CSF (<38 mm) powders at 15˚C/min, within accuracy of ±5˚C..... 136
Table 4-4 Shrinkage rate of CSF powder derived from the former Figure (Isothermal stage: temperature between Tg to the isotherm and CHR stage: temperature between the isotherm to Tsf). 147
Table 4-5 Summary of sinterability of CS powder with rigid inclusions 155
Table 4-6 XRD results of sintered CSF composites (x : 3h660˚C + 1h775˚C and y : 3h660˚C +3h775˚C) 155
Table 5-1 Effect of heat treatment on morphological transformation and flexural strength of 3BaO-5SiO2 glass-ceramics [Freiman et al 1971]. 163
Table 5-2 Elasticity of CS and CSF cast glasses and glass-ceramics 175
Table 5-3 Modulus of rupture (MOR) of CS and CSF cast glasses compared with those of crystallized CSF classified by morphology, size and crystallinity..... 178
Table 5-4 Effect of heat treatment, and crystallinity, on flexural strength of sintered glass-ceramics. 181
Table 5-5 Effect of particulate 'reinforcements' on the flexural strength of sintered CS and CSF (all heat treated for 3 hours at 900˚C)..... 183
Table 5-6 Effect of crystallinity, on hardness of cast CSF cast glass-ceramics. 186
Table 5-7 Effect of heat treatment at different temperatures for 3 hours on Vicker's hardness of sintered CS glass. 186
Table 5-8 Effect of heat treatment, and crystallinity, spherulite radius (Rs), mean free path (l), and critical flaw size on fracture toughness of cast CSF glass..... 189
Table 5-9 Effect of heat treatment at different temperatures for 3 hours on indentation toughness of sintered CS glass. 190
Table 6-1 Characteristic temperatures in ˚C 193

List of Figures

Figure 1-1 Rates of homogeneous nucleation and crystal growth in a viscous liquid [Tammann 1925]. 21
Figure 1-2 Heat treatment schedule for a glass-ceramic. 21
Figure 2-1 Regions of stability of coordination polyhedra with coordination number (CN) according to the radii ratio of the cation and anion (rc/ra) [Goldschmidt 1926]. 28
Figure 2-2 Two dimensional schematic representation of the structure of (a) a crystal, and (b) glass, according to the random network theory [Zachariasen 1932]. 28
Figure 2-3 Temperature dependence of specific volume and coefficient of expansion showing the definition of glass transition and the effect of isobaric cooling and subsequent reheating through the glass transition region. 33
Figure 2-4 (a) A typical DTA plot in the transition region showing extrapolated temperatures for onset and completion of the glass transition, and (b) determination of Tg and dilatometric softening temperatures, Td, by dilatometer. 33
Figure 2-5 The variation of the viscosity of a soda-lime-silica glass as a function of temperature showing the fixed points. 35
Figure 2-6 Weight loss during DTA runs of CS and CSF glass powders in an air atmosphere at heating rate 15˚C/min. 45
Figure 2-7 Dilatometric profiles of CS and CSF cast glass at a heating rate of 10˚C/minute. 48
Figure 2-8 Viscosity curves calculated from VFT's (Eq. 2-4) and Urbain's (Eq. 2-5) methods (P:powder, B: bulk). 50
Figure 2-9 Arrhenius plot of viscosity for CS and CSF. 50
Figure 2-10 DTA profiles in the glass transition region for CS bulk glass at various heating rates (The profiles have been displaced vertically for ease of viewing). 52
Figure 3-1 The ternary phase diagram CaO-CaF2-SiO2 showing the CS and CSF glass compositions. 56
Figure 3-2 Schematic drawing showing anisotropic crystal growth in surface crystallisation. 62
Figure 3-3 Schematic drawing showing different spherulitic morphologies. 62

Figure 3-4 Relationship between temperature, nucleation and crystallisation rates, viscosity, and transient time [Gutzow 1991]. 65
Figure 3-5 The variation of the number density of nuclei with nucleation temperature of glasss with 3.4 wt% fluoride [Mukherjee & Rogers 1968] and with composition shown in Table 3-2 [Shyu & Wu 1991]. 67
Figure 3-6 Schematic graph showing a typical DTA curve of a silicate glass where Tg is glass transition temperature 72
Figure 3-7 Typical crystallisation exotherm. Method for calculating volume fraction crystallised, S(t), in a time, t, and ΔTFWHM is shown. 72
Figure 3-8 Schematic representation of a portion of an x-ray diffraction pattern of a glass-ceramic. 80
Figure 3-9 DTA plots of CS and CSF bulk glass at a heating rate of 15˚C/min 83
Figure 3-10 Variation of characteristic temperatures (Tx,where crystallisation has started and Tp, at the crystallisation peak temperature) with heating rate for CS and CSF bulk glasses. 83
Figure 3-11 Arrhenius plots of CS and CSF bulk glasses calculated from (a) Kissinger's, and (b) Augis-Bennett's equations. 85
Figure 3-12 X-ray diffraction profiles of heat treated (a) CS (wollastonite) and CSF (cuspidine and a mixture of wollastonite and cuspidine) samples, and (b) CSF samples heat treated at 550˚C or 660˚C for 3 hours followed by growth treatment at 750, 800, 850, 900, or 980˚C for 30 minutes. 87
Figure 3-13 Surface crystallisation in, (a) CS glass heat treated at 900˚C, (b) at 950˚C for 60 minutes, and (c) showing microcracks at the plane of weakness and in microstructure. 89
Figure 3-14 CS surface crystallisation (a) thickness of surface crystal layer obtained from several crystallisation temperatures as a function of time, and (b) Arrhenius plot for calculation of activation energy for crystallisation ,Ec 91
Figure 3-15 TEM micrograph showing amorphous phase separation in CSF glass heat treated at 660˚C for 20 hours. 93
Figure 3-16 Backscattered image of opalescent glass heat treated at 750˚C for 60 minutes. 93
Figure 3-17 The development of nuclei into spherulites having undergone a single stage heat treatment at (a) 740˚C 60mins, (b) 820˚C 60 mins, (c) 900˚C 10mins, and (d) 980˚C 20 mins. 95
Figure 3-18 Variation of particle size with time and temperature for CSF glass that has undergone a single stage heat treatment at 740˚C and 820˚C. 97

Figure 3-19 Different types of spherulites were observed in samples heat treated at (a) 550˚C for 30 minutes followed by 750˚C for 30 minutes and (b) 900˚C for 20 minutes. 98
Figure 3-20 The effect of growth time on the number density in specimens heat treated at various nucleation temperatures for 30 minutes and then allowed to grow at 750˚C for different times. 99
Figure 3-21 Effect of nucleation time on the size of spherulites in samples heat treated at 600, 660, and 690˚C for various times and allowed to grow at 750˚C for 10 minutes. 99
Figure 3-22 Nucleation-rate-like curves of CS and CSF glasses obtained from the relation between the DTA peak height and nucleation temperature. 101
Figure 3-23 The effect of growth temperature on the particle radius in specimens nucleated at 550˚C or 660˚C for 30 minutes and then given growth treatments at different temperatures. 103
Figure 3-24 Micrographs representing different morphologies of spherulite developed at (a) and (b) 550˚C for 30 minutes followed by 850˚C for 30 minutes, and (c) and (d) 550˚C for 10 minutes followed by 900˚C for 10 minutes. 104
Figure 3-25 Arrhenius plots of CSF glass showing the effect of fluoride content (3.4 wt% ,modified from Mukherjee & Rogers [1968], and 4.8 wt% [the present study]) and nucleation treatment followed by growth treatment at 750, 800 and 850˚C 106
Figure 3-26 Morphology of crystallised CSF (sample characteristics are shown in Table 5-2). 108
Figure 3-27 Bulk density of (a) CS heat treated at 950˚C for different times and (b) CSF cast glass of different percentage of crystallinity 110
Figure 3-28 Dilatometric curves of (a) CS and (b) CSF samples undergone different heat treatments 111
Figure 3-29 Plot showing effect of the amount of fluorine retained in the CSF crystallised glass on the coefficient of thermal expansion. 113
Figure 4-1 PZD cumulative weight below and weight in band of CS, CSF, SiC, and ZrO2 powders from laser sizer 128
Figure 4-2 Scanning electron micrographs which illustrate typical jagged particles of (a) and (b) glass powders, (c) and (d) coarse and fine SiC, (e) Al2O3, and (f) ZrO2 129
Figure 4-3 DTA profiles of (a) CS and (b) CSF powder glass at different heating rates 130
Figure 4-4 Arrhenius plots via (a) Kissinger's and (b) Augis-Bennett's methods for calculation of Ea. 132

Figure 4-5 Dilatometric plots showing effects of temperature on densification of CS and CSF glass powders. 135
Figure 4-6 Linear shrinkage of CS glass heat treated at 15˚C/min compared with those heat treated isothermally at 732, 759, 777, and 849˚C. The shrinkage at the holding temperature is represented by the vertical drop on the plots. 137
Figure 4-7 Isothermal treatment of CS glass under dilatometry at 750, 780, 800, and 850˚C. 137
Figure 4-8 Shrinkage rate of CS powder derived from Figure 4-7. 139
Figure 4-9 K values derived from Petru's equation (eq.4-6) as a function of sintering temperature (the samples undergone isothermal treatment in a dilatometer). 141
Figure 4-10 Arrhenius plots of the rate constant of sintering (K) vs reciprocal of isothermal temperature for the calculation of activation energy for sintering. 141
Figure 4-11 SEM micrographs showing effect of isothermal treatment under dilatometry at (a) and (b) 750˚C, (c) and (d) 800˚C, and (e) and (f) 850˚C on sinterability of CS glass powder. 142
Figure 4-12 SEM micrographs of Back-scattered images and secondary electron image of edged samples of CS pressureless-sintered samples at (a) and (b) 900˚C, (c) and (d) 1000˚C, and (e) and (f) 1100˚C for 3 hours, respectively. 144
Figure 4-13 Dilatometry plots for CSF glass specimens tested at constant heating rate or with isothermal treatment at 609, 633, 645, and 665˚C. The shrinkage at the holding temperature is represented by the vertical drop on the plots. 146
Figure 4-14 Isothermal treatment of CSF glass vs time under dilatometry at 605, 633, 645, and 655˚C. 146
Figure 4-15 SEM micrographs and Back-scattered images of CSF samples pressureless-sintered at (a) 750˚C and (b) 900˚C for 3 hours, respectively. 148
Figure 4-16 Effect of addition of reinforcements on densification of CS glass. 150
Figure 4-17 Effect of reinforcement type and volume fractions on densification of CSF glass 150
Figure 4-18 Scanning electron micrographs showing the effect of (a) and (b) Al2O3, (c) and (d) ZrO2 on sinterability in CS and CSF glasses and , (e) SiC(fine), and (f) SiC (coarse) particles on sinterability in CS, all heat treated at 900˚C for 3 hours. 152

Figure 4-19 Scanning electron micrographs showing the interface between the particles, (a) ZrO2, (b)Al2O3, (c) coarse SiC, and (d) fine SiC, and the CS glass. 153
Figure 5-1 Common strength tests (a) tensile, (b) compression, and (c) three-point bending tests. 159
Figure 5-2 Three point bend test configuration, (assuming friction if zero): (a) schematic diagram of a beam subject to 3-point loading, (b) Bending moment diagram (M = f(X)), and (c) Shear force diagram (s = f(X) = dM/dX. 159
Figure 5-3 Cracking sequences obtained by Vickers indentation test during loading (+) and unloading (-) [Hamidouche et al 1994]. 167
Figure 5-4 Schematic drawings illustrates typical sharp crack in glass and glass-ceramic materials and toughening mechanisms in monolithic and composite structures. 170
Figure 5-5 The relationship between crystallinity and Young's modulus of cast CSF glasses. 175
Figure 5-6 A plot showing the effect of morphological parameters, (a) crystallinity and (b) spherulite radius, on flexural strength of CSF glass. 177
Figure 5-7 displays micrographs of the fracture surfaces 179
Figure 5-8 Plot showing the effect of sintering temperature on flexural strength. 181
Figure 5-9 Typical indents in cast and sintered samples 184
Figure 5-10 Plot shows the effect of (a) crystallinity and (b) spherulite radius on Hv in CSF cast glass 185
Figure 5-11 The effect of sintering temperature on Hv in CS and CSF glasses. 187
Figure 5-12 The effect of spherulite radius on critical flaw size. 189
Figure 5-13 Plot shows the effect of sintering temperature on normalised fracture toughness (Kc). 190
Figure C-1 Free energy of nucleus as a function of size. Some critical size must be exceeded before the nucleus becomes stable. 215

CHAPTER 1

INTRODUCTION

The development of glass-ceramics is a recent advance in the science of materials. Glass-ceramics are polycrystalline solids prepared by the controlled crystallisation of glass. The concept of controlled crystallisation of glass involves the separation of a crystalline phase, in the form of tiny crystals, from glassy parent phase. The number of crystals, their growth rate, and thus also their final size are controlled through suitable heat treatment [Strnad 1986]. The controlled heat treatment results in one or more crystalline phases together with a residual glass phase. An extensive range of properties can be realised through manipulating the volume fraction, nature, size, and shape of the crystalline phase [McMillan 1979]. Owing to their versatile nature, the applications are also varied, ranging from domestic usage [Shen *et al* 1989], biomedical application [Vogel 1985], through to heavy electrical engineering and microelectronics [Tammala 1991].

Many glass compositions have been studied for the production of glass-ceramics since their discovery at Corning Glass works [Anon 1957 and Stookey 1960]. Most commercial compositions are based on silicate crystalline phases. Glass-ceramics are useful well above the softening point of the parent glass composition though they are subject to creep deformation via diffusion through the residual glassy phase at higher temperatures, (generally >600˚C). Another major problem with glass ceramics, as with all ceramic materials, is that of brittle fracture and low fracture toughness. When an inherent or introduced flaw, particularly at the surface, is subject to tensile stresses, rapid propagation of the flaw can occur leading to catastrophic failure of the component.

The development of new useful monolithic glass-ceramics from oxide systems is becoming increasingly difficult [Tashiro 1985]. A barriers to the development of useful

monolithic glass-ceramics is the limitation of the glass composition, as adequate viscosity at the liquidus must be achieved to allow shaping of the required glass article. There are three main directions in compositional development of new and useful glass-ceramics. One is to extend the search from simple oxide systems to the wider field of mixed anion systems [Lewis *et al* 1979]. The second trend is the extension of the search from monolithic glass-ceramics to sintered glass-ceramics [Rabinovich 1982 &1985]. The final trend is the development of composite materials that contain reinforcements, i.e. particulate matter [Von Schweitzer 1994 and Taylor 1994], short fibres, or continuous fibres [Prewo *et al* 1986 and Kim 1989], embedded in a glass-ceramic matrix. Physical and mechanical properties of some glasses, glass-ceramics fabricated by conventional casting and powder routes, and glass-ceramic matrix composites are given in Table 1-1.

1.1 Glass

The word *glass* has various meanings. In everyday language this term designates a fragile and transparent material well known since antiquity. In scientific language its range of meanings is much broader and is difficult to define with precision as it is subject to evolutionary change. One of the most frequently quoted definitions is that proposed in 1945 by the American Society for Testing Materials: "Glass is an inorganic product of fusion which has cooled to a rigid condition without crystallising". This definition is satisfactory for those glasses with which we are most familiar but is unnecessarily restrictive- glasses are characterised not only by the absence of crystallinity but also by their ability to pass progressively and reversibly to an increasingly fluid state as the temperature is increased. In the course of this change there is a modification of properties known as *glass transition*, the significance of which will be discussed further in section 2.1.2.1. Thus, the following definition of a glass can be adopted: "A glass is a non-crystalline solid exhibiting the phenomenon of glass transition" [Zarzycki 1990].

Table 1-1 Density, coefficient of thermal expansion, modulus of rupture, elastic constants, hardness, and fracture toughness of glass, glass-ceramic, and glass-ceramic matrix composites.

Materials	Density (kg/m^3)	CTE / MK^{-1}	E / GPa	H / MPa	σ / MPa	K_{1c} / MPa $m^{\frac{1}{2}}$	References
Glass							
Soda-lime silica	2.40-2.55		74	6.0	65	0.75-0.82	Wiederhorn 1969
Ca-Si-Al-O-N	2.78-2.92		105-130	6.0-8.3			Lewis 1989
Canasite ($Ca_5Na_4K_2Si_{12}O_{30}F_4$)	2.623	11.4	72.3		48±10% (tensile)	0.78±11%	Ogumi et al 1987
Cast glass-ceramics							
Silceram	2.9	7.5	121	7.2	174		Ponton 1986
Mica+apatite		(20-300°C)	70-88	5.0	140-180	1.2-2.1	Holand et al 1991
		8-12					
Curved phlogopite + cordierite	2.5	(20-400°C)	70	8.0	90-140	2.0	Vogel et al 1989
		75-125					
Canasite ($Ca_5Na_4K_2Si_{12}O_{30}F_4$)	2.624	12.8	85		125±4% (tensile)	4-5	Ogumi et al 1987
Sintered glass-ceramics							
CP1	3		115	5.07	98±13	1.09±0.13	Taylor 1994
Glass-ceramic matrix composites							
CP1/Ti20 vol%	2.95		86.3		93±2	1.52±0.87	Taylor 1994
CP1/Ag 10 vol%	3.46		85.2		133±12	1.61±0.14	Taylor 1994

1.2 Monolithic glass-ceramics

For any given bulk glass, the tendency and ability to crystallize can be expressed in terms of nucleation and crystal growth curves as shown in Figure 1-1, which illustrate rates of homogeneous nucleation and crystallization in a glass [Tamman 1925]. Below the equilibrium melting temperature there exists a temperature interval, referred to as the metastable zone, in which nuclei do not form at a detectable rate, owing to the fact that the very small crystal nuclei have melting temperatures significantly below that of the bulk material. Crystals can grow in this region, however, if nuclei of a sufficient size are provided by 'seeding' (heterogeneous nucleation). At temperatures below this region the crystallization process is governed by the rate of formation of nuclei and the crystal growth rate. As the temperature decreases further, nucleation and crystallization rates increase, as shown, passing through maxima. The increasing viscosity of the glass hinders the atomic rearrangement and diffusion processes necessary for nucleation and crystal growth. Eventually, at still lower temperatures, the viscosity becomes so high that nucleation and crystallization processes cease. Normally, the glass in bulk form is subject to a controlled heat treatment, as illustrated in Figure 1-2, which converts the glass to a glass ceramic.

Successful preparation of glass-ceramic materials depends crucially on ensuring the formation of a sufficiently large number of uniformly distributed crystal nuclei throughout the bulk of the glass which continue to grow at increased temperature until the crystalline phase occupies a volume that generally lies between 50 % and 100 % of the original glass volume [Strnad 1986]. Internal nucleation must be sufficient to produce a fine-grained body and to avoid the adverse effects of directional crystallization from the glass surface. Efficient bulk crystal nucleation is made possible through the use of "nucleating agents". Various materials added in small amounts are successfully used as nucleating agents, for example, precious metals (e.g. Ag, Pt, Au) usually added as chlorides, oxides (e.g. TiO_2, ZrO_2, P_2O_5, Fe_2O_3, Cr_2O_3, V_2O_5), fluorides (e.g. LiF, MgF_2, CaF_2), and sulphides (FeS, MnS). Crystal growth upon the nuclei must also be controlled to avoid large crystals whose grain boundaries frequently

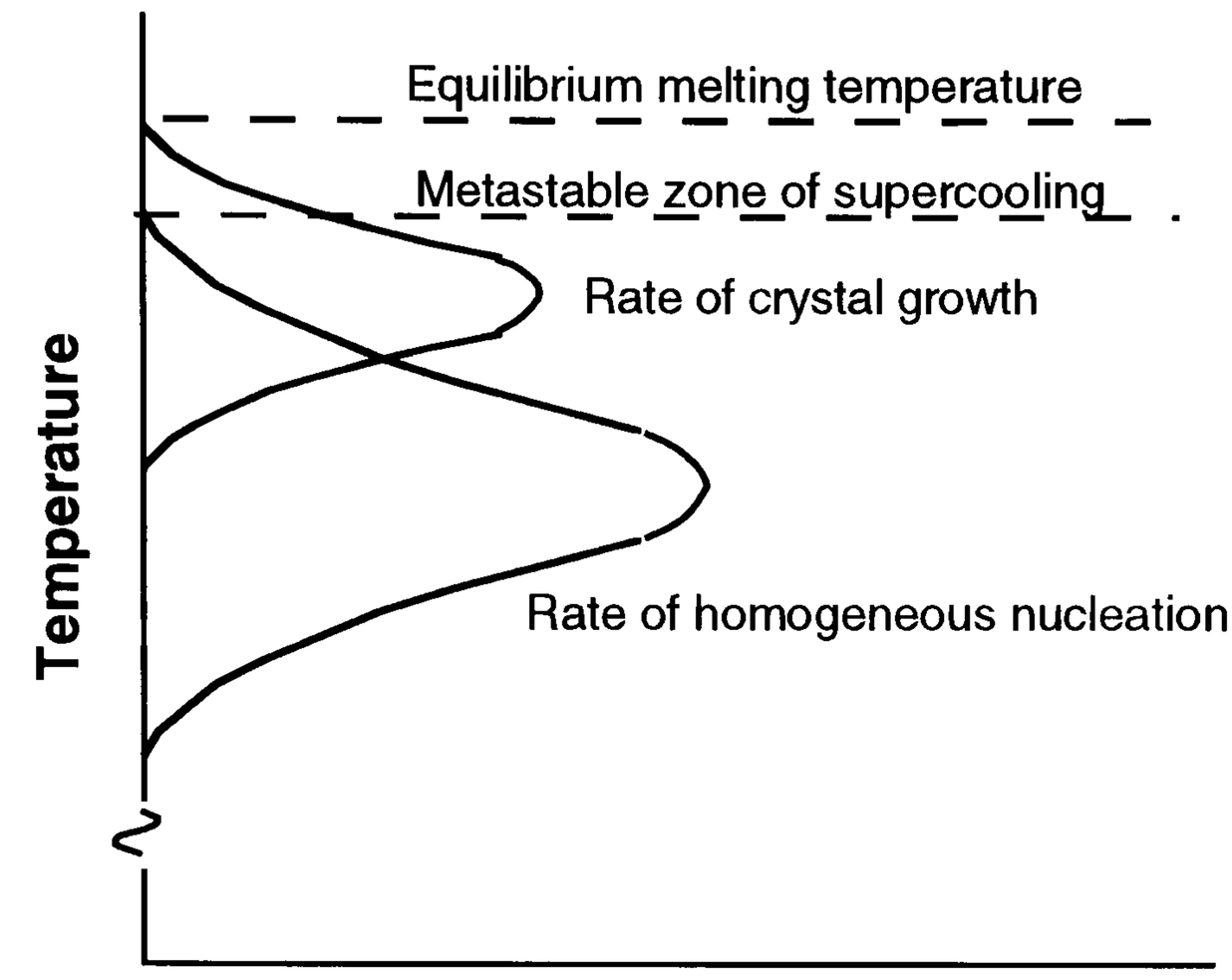


Figure 1-1 Rates of homogeneous nucleation and crystal growth in a viscous liquid [Tammann 1925].

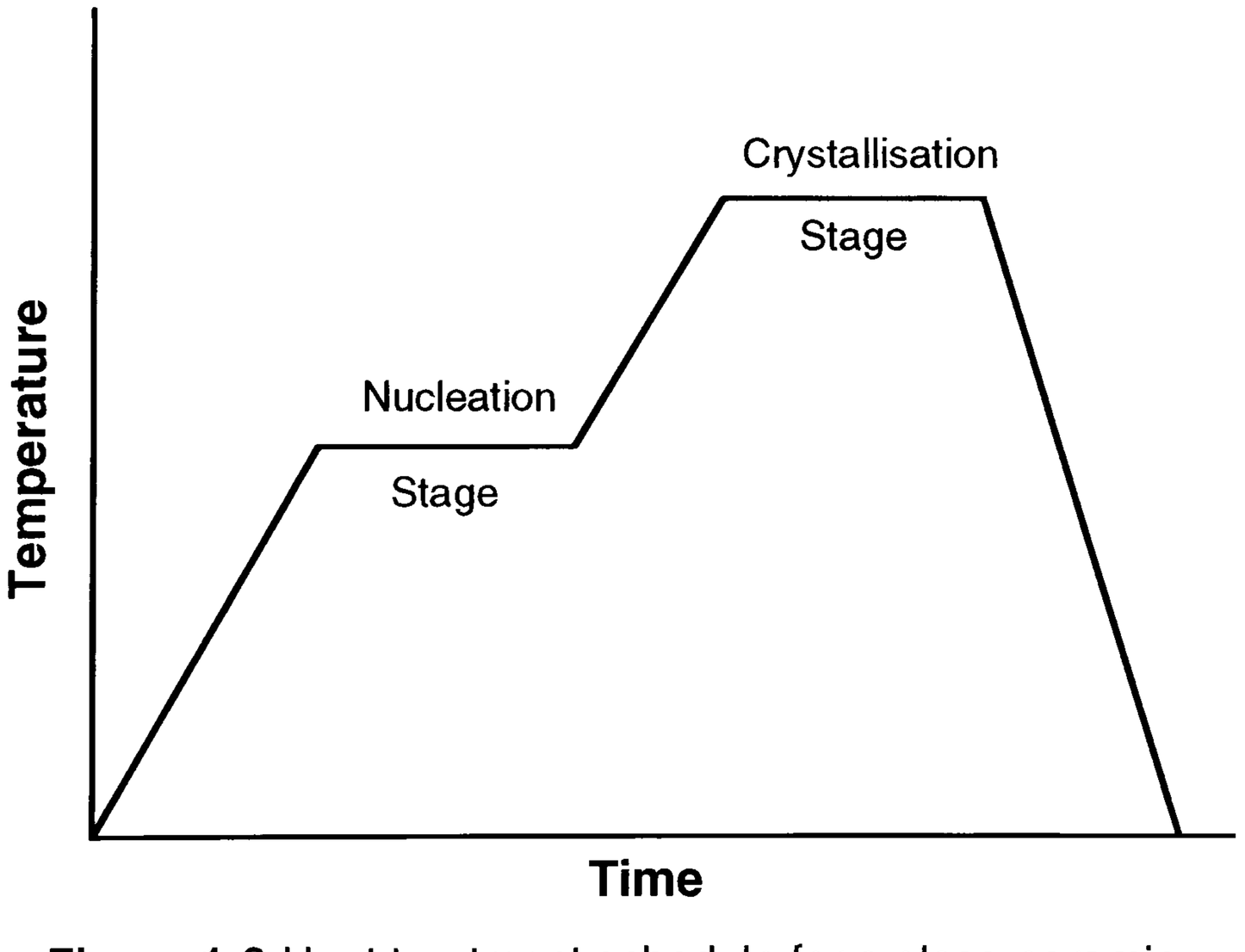


Figure 1-2 Heat treatment schedule for a glass-ceramic.

act as "weak link" routes during crack propagation. Additionally, deformation through gravitational sag or warpage due to volume changes during crystallization in a thermal gradient must be controlled in order to maintain the shape of the original glass article.

1.3 Sintered glass-ceramics

As an alternative to bulk route preparation, the glass may be reduced to powder and then suitably compacted into desired shapes by techniques such as die or isostatic pressing, slip-casting, and tape-casting, followed by sintering in a similar manner to that employed for a 'conventional' ceramic to provide either a fully dense component or a preform suitable for use in subsequent processing [Partridge 1994]. The powder particles derived by this route are generally in the range 1 to 30 μm, although this can vary depending on the degree of comminution achieved. The surfaces of the particles are in a highly damaged state and consequently the glass particles are highly susceptible to surface crystallization. Accordingly, it is possible to produce glass-ceramics from a much wider range of composition than for monolithic glass-ceramics [Tashiro 1985].

Preparation of glass by sintering rather than melting allows the reduction of processing temperatures and the formation of complex shapes. The practical melting temperature of a glass is significantly higher than the thermodynamic melting point (the liquidus temperature) of a crystal mixture of the same composition, because high viscosity at the liquidus temperature slows the dissolution of particles and arrests refining of the glass [Rabinovich 1985]. Below the liquidus only amorphous starting particles may be sintered to a bulk glass, while above the liquidus crystalline starting particles will melt before, or simultaneously, with the consolidation. Below the liquidus crystallization may occur in the course of sintering, thus arresting it, whereas above the liquidus there is no danger of crystallization and the consolidation may be improved by an increase in temperature or time. However, at higher temperature the viscosity of the glass decreases more rapidly and precautions need be taken so as to prevent deformation of the article.

1.4 Glass-ceramic matrix composites

Hot-pressed glass- and glass-ceramic matrix composites are the highest strength ceramic-matrix composites available and they also exhibit high values of toughness [Phillips 1992]. The key to the successful development of glass matrix composites lies in the fact that the glass matrix can be readily deformed and made to flow in its low viscosity state at elevated temperatures. Glass-ceramics provide the unique capability to densify a composite in the glassy state and then subsequently crystallise the matrix to achieve high temperature stability [Prewo *et al* 1986]. There are several reasons why glass-ceramics have provided useful matrices for composites. Firstly, the glasses provide a choice of a wide range of coefficients of thermal expansion (CTE) ; secondly, they permit relatively low processing temperatures compared with true ceramics, and finally, they have lower elastic moduli than engineering ceramics.

Ideally the CTE of the reinforcement (α_r) should be equal to or slightly higher than that of the matrix (α_m) [Phillips 1989]. Having α_r higher than α_m can be beneficial in two respects [Prewo & Brennan 1989]. Firstly, the matrix will be placed in residual compression which will result in enhancement of its load-induced cracking strain. For composites in which the matrix failure strain is lower than that of the reinforcement and which therefore begin failing by multiple matrix microcracking, the increased matrix failure strain will give improvements in performance. The second effect when $\alpha_r \geq \alpha_m$ is that some radial shrinkage of the reinforcement from the matrix can occur, which can result in a decrease in the interfacial bond strength and a resulting improvement in toughness and strength.

As softening point of glasses is around 800°C, good quality composites with low porosity matrices might be expected to be produced by hot pressing at temperatures below 1000°C. However problems can arise due to the nucleation and growth of crystalline phases and this has to be taken into account in optimising the fabrication conditions [Davies *et al* 1990]. In general, processing temperatures for glass-based systems tend to lie in the range 900-1200°C, as opposed to >1600°C for hot-pressed engineering ceramics [Rice & Lewis 1989].

The relatively low elastic moduli of glass-based matrices is valuable because the reinforcement efficiency in a matrix depends on the ratio of the moduli of reinforcements and matrix, E_r/E_m. Young's moduli of glasses and glass-ceramics lie typically in the range 60-90 GPa, while those of engineering ceramics are typically 250-400 GPa. Thus better load transfer occurs in a glass or glass-ceramic matrix which for a given matrix stress level implies greater strengthening [Warren 1992].

Particles that can be incorporated into glass-ceramics may be classified as either inert or active. Inert reinforcements include metals, alumina, silicon nitride, and silicon carbide which serve the function of diverting or delaying the progress of the crack front with no change taking place in the reinforcing particles. In general, care has to be taken that excessive reaction does not take place between the matrix material and the toughening material since this may negate the effectiveness of the particles through solution into the matrix, reducing the 'sharpness' of the interface. The various inert particles employed are generally in the size range 1 to 100 μm, with the optimum being in the range 5 to 20 μm. The reinforcements are normally incorporated into the matrix body via the powder route with a mixture of powder matrix material (in precursor glass form) and articles being prepared and shaped using ceramic manufacturing technology.

1.5 Aim

The present study investigates the feasibility of utilising wollastonite-based compositions in the oxide quaternary system similar to that developed by Mukherjee & Rogers [1967], with and without partial substitution of fluorine for oxygen, as matrices in glass-ceramic matrix composites. The main objectives were two fold. The first objective was to gain insight into how glass characteristics, i.e. viscoelasticity and thermodynamics, affect the crystallisation and sintering processes. The second objective was to study the effects of different fabrication routes, i.e. conventional casting and powder sintering, on the mechanical properties of the glasses/glass-ceramic products and to investigate the feasibility of improving the mechanical properties through incorporation of particulate reinforcements into the glass/glass-ceramic matrix.

Chapter 1 introduces general approaches for the development of glass-ceramics. Each of the following chapters in the thesis provide a summary of current knowledge and theoretical understanding in addition to a discussion of the experimental results and analysis of the processing and properties of the materials under investigation. Chapter 2 covers the basic principles of glass formation and structure prior to discussing the kinetics of glass formation and the influence of fluorine on glass properties. Chapters 3 and 4 present the fundamental principles of crystallisation and sintering. Crystallisation in bulk cast glass is then characterised to develop insight into the factors which determine the microstructure, and thus mechanical properties, of glass-ceramics. These issues are of considerable importance in fabricating glass-ceramics and glass-ceramic matrix composites via a powder route where the competition between viscous sintering and crystallisation determines the conditions under which densification can be achieved. The effect of particulate reinforcements on the densification of glass-ceramic matrix composites is also discussed. Chapter 5 deals with the mechanical properties of glass-ceramics produced via both monolithic and powder routes, and of glass-ceramic matrix composites. Chapter 6 summarises the factors determining the ability of the glass under investigation to be employed as a parent glass for glass-ceramic matrix composites. The mechanical properties of the glass-ceramics and the composites are correlated with the main processing variables.

CHAPTER 2

GLASS

2.1 Introduction

Glasses are among the most ancient materials in human history and constitute a fascinating group of materials both from the fundamental and applied standpoints. Glasses present the challenge of studying disordered solids with difficult thermodynamic and kinetic problems which have not yet been completely resolved. However, in the past three decades the understanding of glass has been significantly advanced. New types of glass have been discovered and these play an increasing role in modern optics (lasers), electronics, energy conversion, and medicine (bio-materials).

This chapter focuses on the general properties of glasses in the quaternary system, Na_2O-CaO-Al_2O_3-SiO_2, based on Mukherjee and Rogers' study [1968] in relation to the glass structure and behaviour. The thermodynamics and kinetics of glass formation are elaborated and the effect of fluorine on glass is investigated.

2.1.1 Glass Formation

Glass formation is a kinetic phenomenon; any liquid, in principle, can be transformed into glass if cooled sufficiently quickly and brought below the transformation range [Paul 1990]. For a substance which can be cooled to a glass state, there is no discontinuous volume change and no exothermic effect corresponding with the change from liquid to *solid* state. Instead, the viscosity of the melt increases progressively as the temperature falls and eventually the viscosity attains values which are so high that for all practical purposes the substance behaves as a *rigid body*. On this basis, it is clear that glass may be regarded as a *supercooled liquid* since the melt is cooled through the temperature zone in which crystallisation might occur but the liquid-like structure is

retained. Either an atomistic or a kinetic approach may be used to understand the nature of glass formation.

2.1.1.1 Structural models

Many researchers have postulated different atomistic hypotheses correlating the nature of the chemical bond, and the geometrical shape of the groups involved, with the ease of glass formation. It should be pointed out that, although these empirical hypotheses explain glass formation in some liquid systems, a unified hypothesis capable of explaining the phenomenon of glass formation in all known systems has yet to be developed.

(i) Goldschmidt's radius ratio criterion

According to Goldschmidt [1926], for a simple oxide of the general formula A_mO_n, there is a correlation between the ability to form glass and the relative sizes of the oxygen and A atoms (Figure 2-1). Glass-forming oxides are those for which the ratio of ionic radii R_A/R_O lies in the range 0.2 to 0.4. Following classical considerations of crystal chemistry for ionic structures, the ratio is directly related to the coordination number of the central cation. The ratio proposed above thus implies tetrahedral coordination.

(ii) Zachariasen's random network hypothesis

Zachariasen [1932] considered the relative glass-forming ability of oxides and concluded that the ultimate condition for glass formation is that a substance can form extended three-dimensional networks lacking periodicity with an energy content comparable with that of the corresponding crystal network. From this condition he derived four rules, the so-called *random network theory*, for oxide structures, that allow one to choose those oxides which tend to form glasses. The rules are the following:

1. An oxygen atom is linked to not more than two glass-forming atoms.
2. The coordination number of the glass-forming atoms is small.
3. The oxygen polyhedra share corners with each other, not edges or faces.
4. The polyhedra are linked in a three-dimensional network.

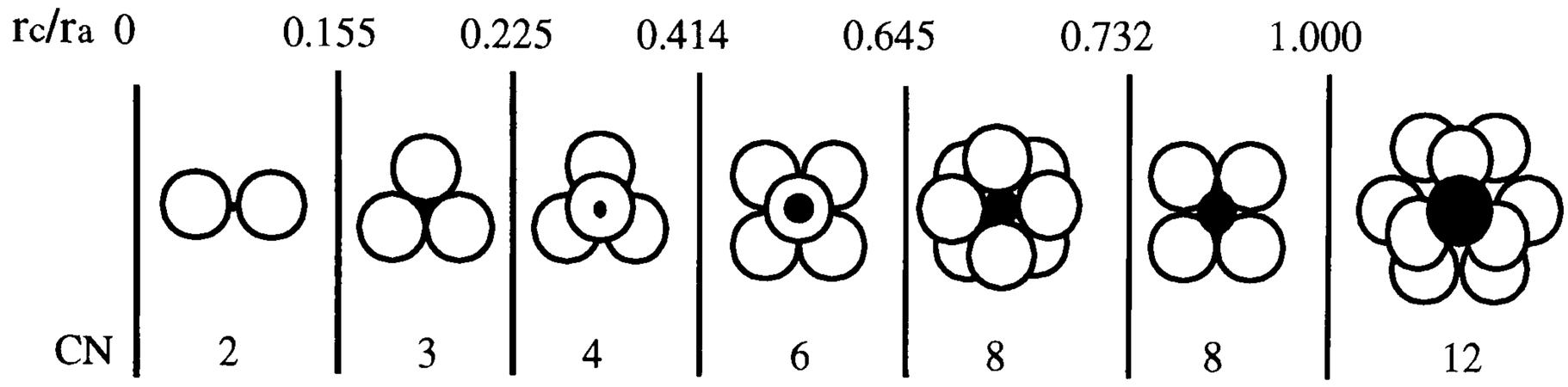


Figure 2-1 Regions of stability of coordination polyhedra with coordination number (CN) according to the radii ratio of the cation and anion (r_c/r_a) [Goldschmidt 1926].

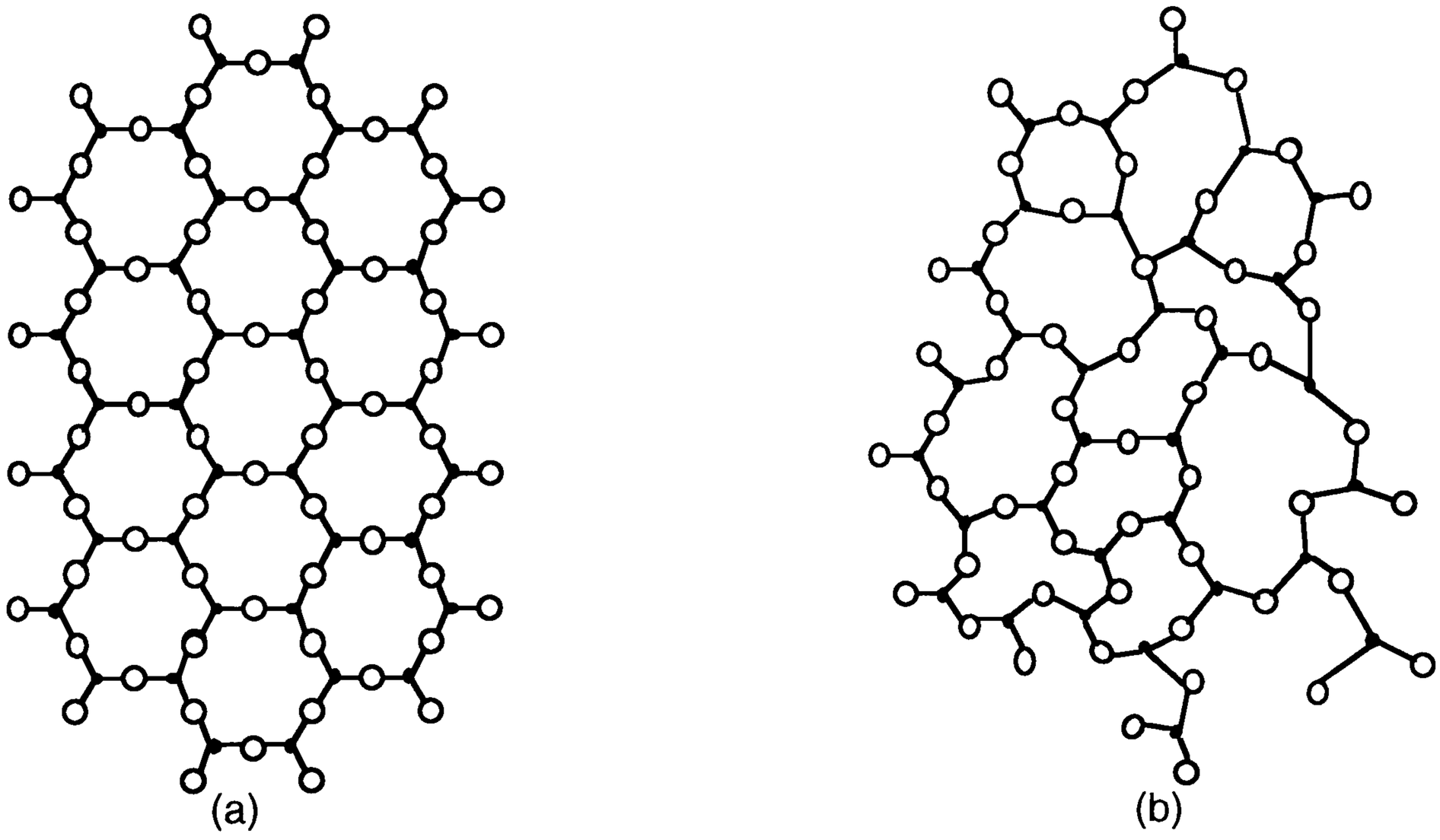


Figure 2-2 Two dimensional schematic representation of the structure of (a) a crystal, and (b) glass, according to the random network theory [Zachariasen 1932].

Table 2-1 Common constituents of glasses and their influence on properties [Holloway 1973].

SiO_2	Basic glass-former (network former). Crystalline silica has very high melting point- liquid silica has very high viscosity. High concentration of silica in a glass confers high softening temperature, low thermal expansion, and good chemical durability.
Na_2O	Network modifier. Markedly lowers softening point. Raises thermal expansion and ionic conductivity. Reduces durability.
CaO	Network modifier. Inhibits mobility of alkali ions, hence increases resistivity and durability of alkali glasses. Shortens the working range.
Al_2O_3	Intermediate. Can join network in AlO_4 tetrahedra which are different size from SiO_4. Strongly suppresses devitrification; increases viscosity and therefore makes melting and refining more difficult.

Figure 2-2 illustrates the structure of a crystal and of a glass according to the random network theory. It has been used to characterise the roles which glass composition plays in the structure. According to Zachariasen the one essential ingredient in an oxide glass is a *network former*. The other classes of oxides used in glass-making are designated *network modifiers* if, like Na_2O, they disrupt the continuity of the network. The alkali metal oxides and alkaline earth oxides are network modifiers (See Table 2-1). An oxide is defined as *intermediate* if it can either join the network or can occupy interstices in the network.

(iii) Sun's bond-strength criterion

Since the process of atomic rearrangement which takes place during crystallisation of a material may involve the breaking and reforming of interatomic bonds, it may be reasonable to expect a correlation between the strength of these bonds and the ability of the material to form a glass. Sun [1947] suggested that the stronger the bonds, the more retarded will be the rearrangement process and hence the more readily will a glass be formed. From Sun's calculations, glass-forming oxides have single bond strengths greater than 380 kJ/mol while modifiers have bond strengths less than 250 kJ/mol.

(iv) Kingery's O:Si criterion

As the addition of alkali or alkaline earth oxides to SiO_2 increases the ratio of O to Si and breaks up the three-dimensional network, Kingery [1960] proposed that the ease in forming glasses from the melt and the stability of the resulting glasses change continuously with the O:Si ratio. Most glasses which are simultaneously readily fusible and stable have an O: Si ratio in the range of 2.25 to 2.75. In general, when this ratio becomes equal to or greater than 3, special precautions must be taken to obtain a glass and the resultant glass is not very stable.

2.1.1.2 The structure of multicomponent glass-forming systems

The tendency towards glass formation will be much increased if a system consisting of several components can have a wide variety of structural configurations. This can often result in good glass-forming properties despite the fact that none of the components can be regarded as a true glass former. This is particularly noticeable in fluoride glasses. The pattern of the glass structure in such cases goes beyond the rules formulated by Zachariesen, as it consists of octahedral $[AlF_{6-a}O_a]$ units linked in one, two, and partly even three dimensions by F and O atoms.

The glass forming tendency usually increases with the incorporation of network modifiers because of the increase in structural configuration possibilities. However, as more alkali or alkaline earth oxide is added, increasing to ratio with the glass former to greater than 1:2, the network becomes more and more disrupted as some tetrahedra are bonded to only two other tetrahedra. Glass formation becomes progressively more difficult because the rates of nucleation and crystallisation in the glass become much more rapid as alkali or alkaline earth oxide is added. In the composition range between disilicate ($A_2O{\cdot}2SiO_2$ or $AO{\cdot}2SiO_2$, A being the metallic ion) and metasilicate ($A_2O{\cdot}SiO_2$ or $AO{\cdot}SiO_2$), chainlike structures should exist, although direct evidence for this is lacking. At alkali concentrations above the metasilicate, isolated islands and rings, as well as chains, of silicon-oxygen tetrahedra should be the major structural features [Doremus 1973].

The distribution of non-bridging atoms and, accordingly, that of the cations, is often not continuous throughout the network, because it can be advantageous in the balance of energetic and entropic factors that the structural skeleton of the network former is largely destroyed in certain regions whilst maintained almost without change in others.

2.1.1.3 Kinetic approach to glass formation

Whether or not a given liquid will crystallise during cooling before the glass transition temperature, *Tg, is* reached is strictly a kinetic problem involving the rate of nucleation and crystal growth on the one hand and, on the other, the rate at which thermal energy can be extracted from the cooling liquid. Cooling rate, density of nuclei and various material properties such as crystal-liquid surface tension, and entropy of fusion etc. have been suggested as significant factors which affect the tendency of different liquids to form glasses [Turnbull 1961].

Uhlmann [1972], developing Turnbull's idea, has provided some useful guidelines for glass formation by using theoretical time-temperature- % transformation (T-T-T) curves to specify critical cooling rates in terms of material constants. In the case of single-component materials or congruently melting compounds, if the nucleation frequency and rate of crystal growth are constant with time, then the volume fraction crystallised, χ, in a time, t, may be expressed as:

(for small values of χ) $$\chi = \frac{1}{3}\pi I_v u^3 t^4 \qquad [2\text{-}1]$$

where I_v is the nucleation frequency per unit volume, and

u is the rate of crystal growth.

Both nucleation frequency, I_v, and rate of advance, u, are inversely proportional to the viscosity of the liquid. The kinetics of crystallisation will be discussed further in Chapter 3.

2.1.2 Glass behaviour

As non-equilibrium solids, glasses possess a variable excess stored energy and hence the thermal history conditions are important in determining certain properties. Due to

the relative immobility of ions at room temperature in a glass structure which precludes the formation of the lower energy crystalline structure configuration, glass retains its amorphous configuration. The temperature between two states at which glass deformation changes from elastic behaviour to time-dependent viscoelastic deformation is called the *glass transition temperature (T_g)*. Since the transition from one behaviour to the other is continuous then T_g is not a unique transformation but depends on testing method (see below); also, in contrast to crystalline solids, no true *melting point* is observed but instead there is a progressive softening.

2.1.2.1 Glass transition

Shown schematically in Figure 2-3 is the temperature dependence of a typical macroscopic property such as hardness, H, or Poisson's ratio, ν, during isobaric cooling and subsequent reheating of a glass-forming liquid through the glass transition region [Scherer 1990]. This hysteresis between the cooling and reheating curves is a consequence of the fact that, irrespective of whether the system is being cooled or heated, it attempts to move with time towards the same equilibrium state at any given temperature. In practice it is observed that, at constant pressure, the position of the transition point, T_g, is not fixed but varies slightly with the *rate* at which the liquid is cooled. Rapid cooling has the effect of shifting the break defining T_g towards higher temperatures whilst slow cooling displaces T_g towards lower temperatures. For this reason it is preferable to substitute for T_g the concept of *a transition interval*, where the upper and lower limits are defined respectively by the highest and lowest heating rate used, or else *an isothermal* T_g, which is extrapolated from T_g values at various heating rates to zero heating rate.

A typical DTA plot in the transition region is shown in Figure 2-4a. The maximum or overshoot in the curve is influenced by the sigmoidal shape of the curve in Figure 2-3. Moynihan [1993] found that a correlation exists between the width of the glass transition region measured using DTA during heating and the activation energy for viscous flow, E_η^*. This was demonstrated by the constancy of a dimensionless parameter

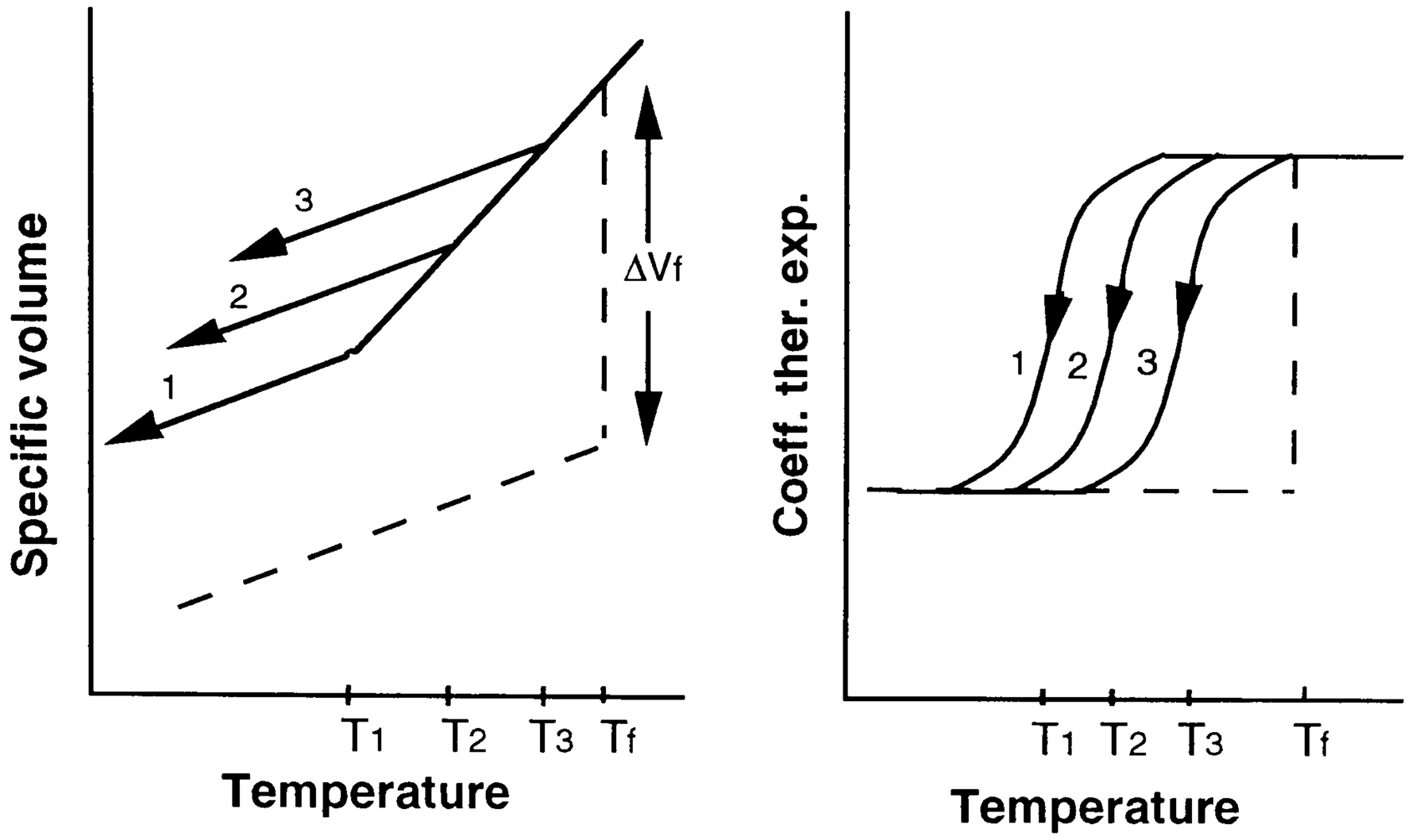
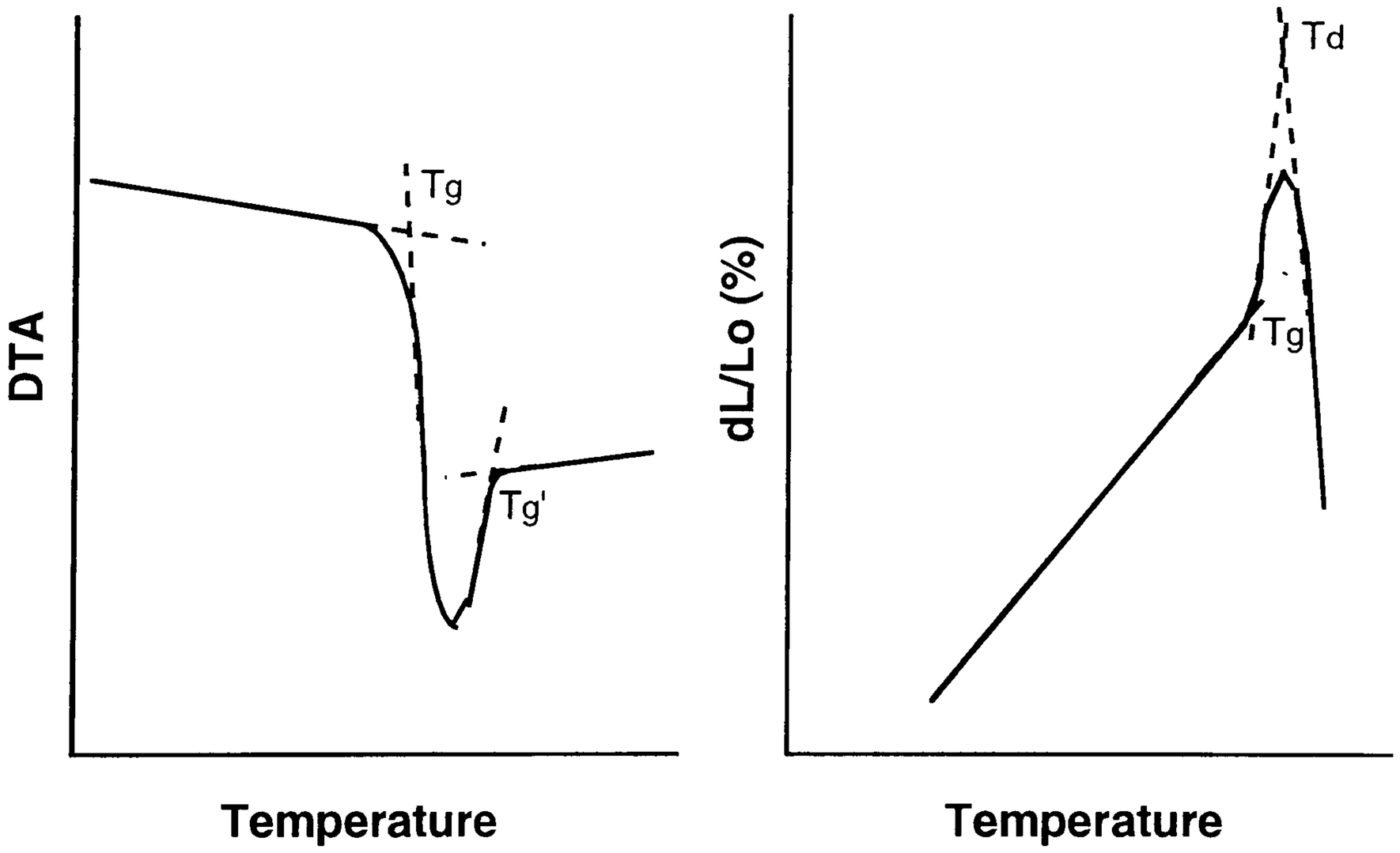


Figure 2-3 Temperature dependence of specific volume and coefficient of expansion showing the definition of glass transition and the effect of isobaric cooling and subsequent reheating through the glass transition region.



(a) (b)

Figure 2-4 (a) A typical DTA plot in the transition region showing extrapolated temperatures for onset and completion of the glass transition, and (b) determination of T_g and dilatometric softening temperatures, T_d, by dilatometer.

$$C = \frac{E_{\eta}^{*}}{R}\left(\frac{1}{T_g} - \frac{1}{T_{g'}}\right) \qquad [2.2]$$

where T_g and $T_g{}'$ are temperatures marking the extrapolated onset and finish of the transition region in the DTA trace and R is the gas constant.

Dilatometry is another technique normally used to determine the T_g of a glass. The procedure consists of measuring the expansion of a glass specimen as a function of temperature, though it is necessary to use a well-annealed glass to avoid the effects of quenching shown in Figure 2-3. The intersection of the straight lines corresponding to the expansion of the glass before and after the transition determines T_g (Figure 2-4b). Dilatometer also permits the determination of the dilatometric softening temperature which corresponds to the final fall in the expansion curve (Figure 2.4b). This point is reached when the specimen begins to flow (collapse) under the mechanical action of the dilatometer spring and is the temperature corresponding to a viscosity of ~ $10^{11.3}$ Pa·s, though this will vary with the type of apparatus (elastic constant of the spring) and thus has only a comparative value.

2.1.2.2 Viscosity of glass

For a given composition, the variation of viscosity, η, with temperature is large (Figure 2-5). Since, in practice, certain intervals of viscosity have particular importance, a series of standard viscosity values has been adopted. A given glass is then characterised from the point of view of its viscous behaviour by the temperatures which correspond to these standard values and which are called *fixed points*.

It should be noted that the *transformation temperature,* T_g, constitutes a particularly important fixed point, corresponding to a viscosity of approximately 10^{13} Pa·s. Koide *et al* [1990] found that the viscosity at the glass transition temperature increases as the heating rate decreases, approaching 10^{12} Pa·s at zero heating rate for all glasses. The *annealing point* and *strain point temperatures* correspond to viscosities of 10^{13} and $10^{14.5}$ Pa·s respectively and are related to the relaxation time of internal stresses. At the

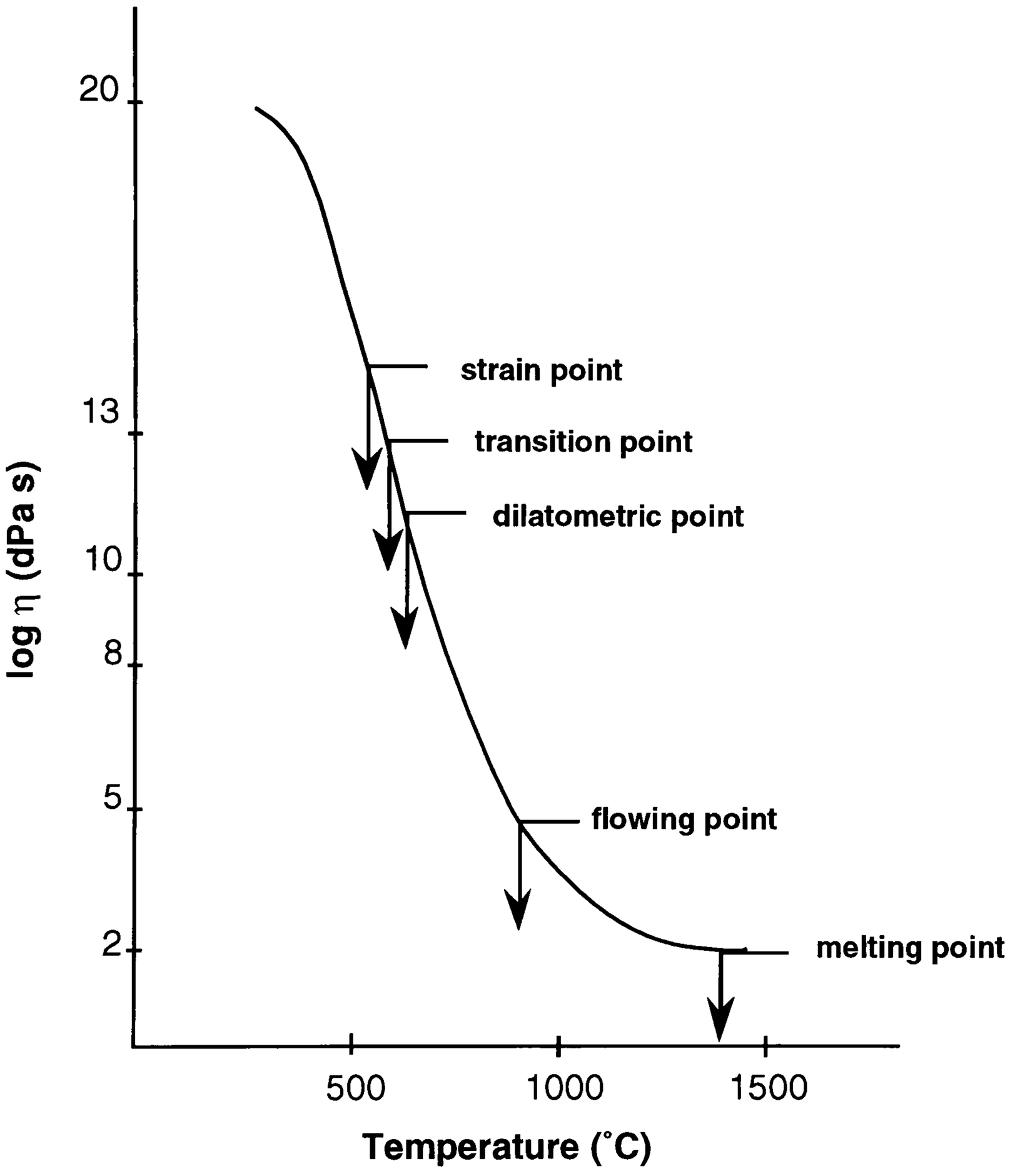


Figure 2-5 The variation of the viscosity of a soda-lime-silica glass as a function of temperature showing the *fixed points*.

annealing point the internal stresses are relaxed in about 15 minutes whilst at the strain point this stress relief requires about 2-3 hours. Variation of viscosity with temperature can be analysed by VFT equation, Urbain's method, or activation energy for viscous flow method.

(i) VFT Equation

In the early 1920's it was found independently by Vogel, Fulcher, and Tammann and Hesse, that for many glass melts the following equation gives a good representation of the variation of viscosity over a wide range of temperature:

$$\log \eta = A + \left(\frac{B}{T - T_0} \right) \qquad [2\text{-}3]$$

where A, B and T_o are constants for a particular melt. Values of η at three temperatures are sufficient to determine the three constants A, B and T_o.

(ii) Urbain's method

Urbain [1981] predicted viscosity from the absolute temperature and composition of the *silicate melts*. Firstly, the constituent oxides are split into three categories: glass formers, modifiers, and intermediates (see definition in Table 2-1). These categories are then used to predict the viscosity of the melt. Using the absolute temperature (known), T (K), and the empirical constants A and B (see Appendix A), the viscosity can be calculated from:

$$\eta = AT \exp\left(\frac{10^3 B}{T} \right) \qquad [2\text{-}4]$$

It should be noted that this method does not take into account the effect of mineralisers such as OH^- or F^- which have an important role in lowering the viscosity.

(iii) Activation energy for viscous flow

Viscous flow in a liquid involves the movement of atoms or groups of atoms relative to one another. As the temperature rises there is an increase in the probability of a

particular unit possessing sufficient thermal energy to surmount the energy barrier. Considerations such as this lead to an equation of the form:

$$\eta = A\exp\left(\frac{E_\eta}{RT}\right) \qquad [2\text{-}5]$$

where A is a constant for the glass,

T is the temperature (K), and

R is the gas constant.

E_η is a measure of the magnitude of the energy barrier and is usually called the "activation energy for viscous flow". However it should be noted that at temperatures above that where $\eta \sim 10^8$ Pa·s, the viscosities of most glass-forming melts begin to exhibit a marked non-Arrhenius temperature dependence.

2.1.2.3 Effect of Fluorine ions

Fluorine incorporation in glass melts, glasses, ceramics, and glass-ceramics has been used for a variety of purposes, e.g. as an opacifying agent in the production of opal glasses [McMillan 1979], as a dopant in fused silica waveguides to lower the refractive index [Dumas *et al* 1982], and as a fining agent in glass melts [Hirayama & Camp 1969]. Fluorine was found to greatly facilitate batch melting due to the fact that it markedly lowers the liquidus temperature of the glass by approximately 50-100°C [Salama 1990]. It also significantly lowers the temperature at which crystallisation starts and increases crystallisability. This indicates that a lower activation energy is needed to induce crystallisation with the addition of fluorine, assuming that the pre-exponential term in (Eq.2-6) does not change significantly.

As early as 1941 Dietzel [Dietzel 1941] suggested that mutual substitution of oxygen and fluorine ions in silicate melts occurs without great disturbance to the arrangement of the other ions because of the equality of their radii. However, the smaller charge associated with F^-, compared to O^{2-} necessitates a compensatory mechanism within the glass structure. This may occur through the breakdown of the strong Si-O-Si linkage in the structure and the bonding of the terminals of the chains to two fluorine ions, i.e. 2 ~Si-F, and as a result the glass network structure will be weakened [McMillan 1979].

The direct effect of breaking down the network is to lower viscosity [Kingery 1960] and to increase direct current conductivity and thermal expansion [Singer & Tomozawa 1989].

Rabinovich and coworkers [Rabinovich *et al* 1989] demonstrated that Si-F bonds are strong enough to survive temperatures greater than 2000°C; however, it is normally difficult to retain significant amounts of fluoride in silicate glasses at elevated temperatures as in cases of simple silicate glass melting from a batch, most of the F^- ions volatile during decomposition of the batch components before substitution of Si-F for SiO_2 bonds can occur at higher temperatures. It has been proposed [Rabinovich *et al* 1989] that moisture decomposes or reacts with F^- and the silica network, forming HF and Si-OH. This hot HF attacks the network according to

$$\text{Si-OH + F-Si -----> Si-O-Si + HF}\downarrow \qquad [2\text{-a}]$$

At higher temperature, some of the F^- ions can be released as a result of formation of siloxane bonds, i.e.

$$SiO_2 + 4HF \text{ ------> } SiF_4\downarrow + 2H_2O \qquad [2\text{-b}]$$

However, Rabinovich [1983] found that the volatilisation of F^- as SiF_4 is significantly reduced with increased basicity of the melt. He proposed that at high temperatures, asymmetry resulting from thermal vibration may create a situation where 3 oxygens provide relatively good screening to one of the silicons and that the 4th oxygen may move closer to the 2nd silicon atom. The fluorine ion may completely replace the 4th oxygen and thus a tetrahedron [SiO_3F] is formed. However, the more basic a glass composition, i.e. the greater the number of nonbridging oxygens, the smaller the number of F^- ions which can be incorporated into the network; they remain mostly in the coordination spheres of other cations. The F^- ions which have moved into the spheres of M^+ and M^{2+} ions result in the formation of crystalline fluorides in the glass. The fluoride mostly precipitates from the glass in a crystalline form, i.e. below the liquidus, and prior liquid-liquid phase separation may occur only at high fluorine content.

2.2 Experimental Procedure

2.2.1 Starting materials and glass preparation

The raw materials used in the glass preparation and the conditions under which they were dehydrated are shown in Table 2-2. The SiO_2 and Al_2O_3 were dried in large platinum dishes in an electric muffle furnace while the remaining powders were placed in pyrex dishes in an electric fan-assisted oven. The amount of moisture was kept to a minimum by storing the dried powders in a desiccator containing self-indicating silica gel. Two kinds of calcium silicate glass batches were produced; one was a calcium silicate glass with the addition of Na_2O and Al_2O_3 (CS) and the other was a 3.8 mol% fluoride substituted glass (CSF), i.e. CaF_2 was partially substituted for CaO. Their nominal and batch compositions are given in Table 2-3.

The glasses investigated in this report were prepared by mixing appropriate amounts of dried powder in a 3D-rotating blender for 1 hour followed by melting in a platinum crucible at 1420°C for 2 hours. The glass was then quenched into iced water, keeping the glass in the crucible intact from the water. The resultant glass fragments were crushed in a cobalt tungsten carbide-lined Tema mill to a particle size of <150 μm. Each batch was melted three times, with intermediate quenching and crushing, in order to obtain a homogeneous glass. CaF_2 was introduced into the CSF batch prior to the 3rd melt by mixing thoroughly and then melting in a crucible covered by a Pt-lid so that the loss of fluoride will be minimised.

After the final melt the molten glass was quickly removed from the furnace and poured onto a clean hot stainless steel plate (500-550°C) and transferred to an annealing furnace at approximately the glass transition temperature (T_g) in order to relieve internal stresses.

Table 2-2 Raw materials used in the glass preparation and conditions under which they were dehydrated.

Raw materials	Temperature (˚C)	Time (hours)
SiO_2 (Brazilian α-quartz crystal and precipitated silica BDH AnalR)	900	3
Al_2O_3 (BDH AnalR calcined)	1350	3
$CaCO_3$ (BDH AnalR)	150	3
CaF_2 (BDH GPR extra pure)	150	3
$Na_2CO_3.10H_2O$ (BDH AnalaR)	150	3

[Note: BDH - general chemical suppliers, GPR - general purpose reagents, AnalR - international standard for analytical reagents, representing maximum permitted levels of impurities]

Table 2-3 Nominal batch compositions for the base glass (CS) and base glass with fluoride (CSF).

	CS (wt%)	CSF (wt%)
Batch composition		
SiO_2	43.45	44.56
Al_2O_3	5.49	5.56
$CaCO_3$	44.40	35.02
Na_2CO_3	6.66	6.85
CaF_2	-	8.01
Chemical composition		
SiO_2	56	54.5
Al_2O_3	7	6.8
CaO	32	24.0
Na_2O	5	4.9
CaF_2	-	9.8
in which F	-	4.8

2.2.2 Chemical analysis

2.2.2.1 Wet chemical analysis

Wet chemical analysis was utilised to measure the amount of fluoride. 0.1 gram of CSF glass sample was fused with 1 gram of Na_2CO_3 at 1000°C for 12.5 minutes. When cooled, the solution was leached with water and filtered. Water was added to the resultant sample followed by 1.5 ml of 1+1 acitic acid to make pH 6.7. The solution was then diluted to 100 cc. The fluoride was measured by ion selective electrode. The result was compared with that from standard solution made from CS glass.

2.2.2.2 Energy dispersive x-ray spectroscopy (EDS)

Selected area quantitative chemical point analysis was obtained using a JSM-35 SEM equipped with energy dispersive x-ray spectroscopy and ZAF software. Due to the limitations of the equipment, light elements (lighter than Na) could not be detected and hence fluorine analysis was conducted via a wet chemical technique using a fluorine selective electrode.

The samples for EDS were polished down to 1 μm surface finish and carbon coated to prevent surface charging as the carbon does not interfere with the spectrum of the specimen. The EDS procedure consisted of selecting a small region on the sample surface and analysing the energy of the X-rays emitted from this area. This enabled the determination of the elements present and their relative amounts in this area. Peaks corresponding to the four major elements present in the material; i.e. Na, Ca, Al, Si, were found. No other significant peaks were noticeable.

2.2.3 Density measurements

2.2.3.1 True density

Liquid pycnometry was used to determine the true density of powder in the cases when all pores in the particles are penetrated by the fluid and so the volume of fluid displaced is equal to the volume of solid phases. The dry weight, w_1, of the calibrated pycnometer

bottle was measured and then approximately a quarter of the bottle was filled with finely powdered glass, with the weight of the bottle, powder and the stopper, w_2, being noted. Distilled water together with a tiny drop of soap solution, which reduces the surface tension of water, aids in wetting and minimises the floating of micron-size particles, was added to cover the powder. The accuracy of this technique depends on wetting the particles completely and eliminating air bubbles and thus the bottle and its content were placed under vacuum to remove all trapped air. Having completed evacuation the water was allowed to reach room temperature and then the bottle was topped up with distilled water and weighed again, w_3. The temperature of the water was noted for accurate determination of the density, as the density of water varies with temperature (see Appendix B). Finally, the bottle was emptied, cleaned and refilled with only distilled water and reweighed, w_4. The true density of the powder was calculated using:

$$\rho_t = \left[\frac{w_2 - w_1}{(w_4 - w_1) - (w_3 - w_2)}\right](\rho_{H_2O} - \rho_{air}) + \rho_{air} \qquad [2\text{-}6]$$

where ρ_t is the true density of the powder (Mg/m^3)

ρ_{H2O} is the density of water (Mg/m^3), and

ρ_{air} is the density of air (Mg/m^3).

2.2.3.2 Bulk density

Using an immersion method based on Archimedes' principle, the apparent density of the bulk glass was calculated. The samples were initially cleaned with acetone and trichloroethane in an ultrasonic bath for 15 minutes and then allowed to dry naturally, with the dry weight in air, w_5, being measured. Samples were then placed in a dish containing distilled water together with a small drop of soap solution. The dish was first placed in a vacuum chamber to evacuate the air trapped in pores and then, with the aid of a wire support, the submerged weight of the samples, w_6, was measured. Finally, the samples were removed from the water, with excess surface water being removed from the sample and then the wet mass in air, w_7, was obtained. The bulk material density was calculated using:

$$\rho_a = \left[\frac{w_5}{(w_7 - w_6) + w_{wire}}\right]\rho_{H_2O} \qquad [2\text{-}7]$$

where ρ_a is the apparent material density (Mg/m^3), and

w_{wire} is the submerged weight of the wire.

2.2.4 Dilatometry

The apparatus for dilatometry consisted of a silica specimen support tube in which the specimen was placed with a spring-mounted silica thrust rod which was in contact with one face of the sample. The thrust rod was connected to a linear variable differential transducer which monitored the movement of the rod and hence the expansion, or contraction, of the specimen. Calibration of the equipment showed the transducer output to be 0.836 mV/μm. The temperature of the specimen was measured by a Pt-13Rh thermocouple placed next to the specimen inside the tube and the output of the transducer and thermocouple were monitored on a two channel chart recorder. The uncalibrated coefficient of thermal expansion, α', was evaluated by measuring the slope of the temperature vs transducer output curves.

$$\alpha' = \frac{\Delta x}{\varepsilon L \Delta T} \qquad [2\text{-}8]$$

where α' is the uncalibrated CTE of the specimen ($10^{-6}K^{-1}$)

Δx: is the difference in transducer readings (mV)

ΔT is the difference in temperatures (°C)

L is the length of specimen (m), and

ε is the transducer conversion constant (mV/μm)

Corrections accounting for the absolute expansion of the equipment during the experiment were made using alumina and palladium calibration materials. The correction factor (α*) was applied to the experimental CTE to give a more accurate value for the coefficient of thermal expansion, α .

$$\alpha = \alpha' + \alpha^* \qquad [2.9]$$

where α' is the CTE of the specimen ($10^{-6}K^{-1}$), and

α^* is the CTE of the sample holder ($10^{-6}K^{-1}$)

2.2.5 Differential thermal analysis (DTA)

A Stanton Redcroft STA 780 thermal analyser connected to a STA-780 furnace and Commodore CBM 4032 running DAPS 2 software was used to establish any thermodynamic change within the materials. All experiments were performed with platinum crucibles (5mm diameter x 5mm high), calcined alumina reference material, and an air atmosphere with flow rate 65 ml/minute.

Although a relatively low mass (20 mg) of glass powder samples were used to estimate the loss of fluorine during the melting process, for the assessment of thermal events, a relatively high mass (50 mg) was required due to the limited energy change associated with thermodynamic events in the glass.

2.3 Results and Discussion

2.3.1 Chemical analysis

Chemical analysis of CS and CSF parent glass was conducted using the energy dispersive x-ray spectroscopy (EDS) for cations (Table 2-4) and wet chemical and DTA weight loss techniques for fluorine (Table 2-5 and Figure 2-6). It can be seen that:

1) There is good agreement between the batch and experimental amounts of cations present in the specimens.

2) CS glass exhibits a higher wt% of cations (Table 2-4) than for CSF glass though this was attributed to oxygen and fluorine not being detected by EDS.

3) In order to investigate the glass formability, all anions present were assumed to be oxygen which gave O:Si ratios of 1.67 and 2.94 for CS and CSF respectively. Thus, according to the Kingery criterion (see section 2.1.1.1(iv)) CS and CSF compositions should form glass, although CSF less readily than CS.

4) Analysis by various techniques (Table 2-5) confirmed that a negligible amount of fluorine was lost from the CSF glass during the preparation process even though fluorine is expected to be lost at temperature greater than 700˚C (Figure 2-6).

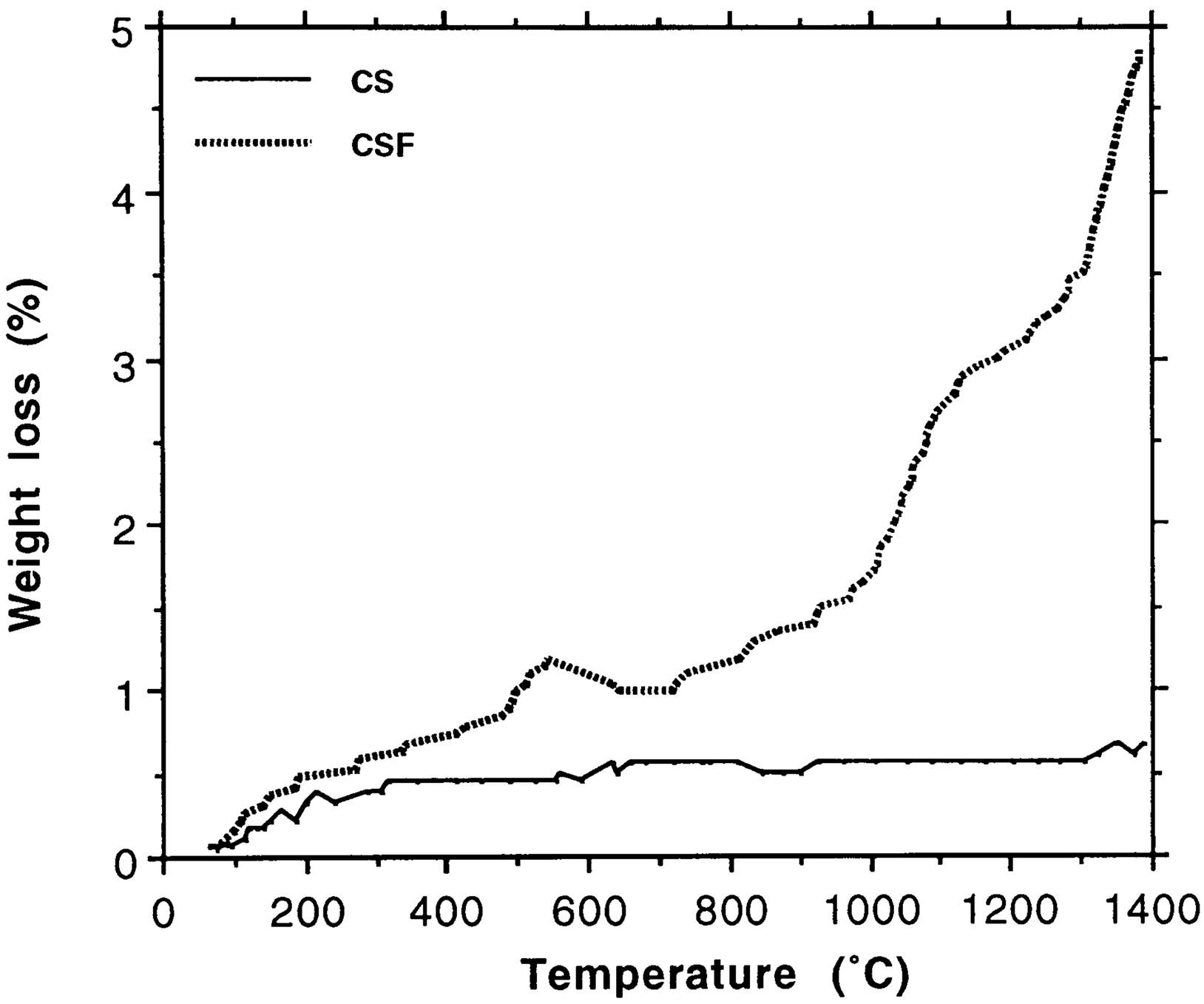


Figure 2-6 Weight loss during DTA runs of CS and CSF glass powders in an air atmosphere at heating rate 15˚C/min.

Table 2-4 Wt% of individual cations (compared to total cation content) in CS and CSF glasses analysed by EDS technique.

Element	CS		CSF	
	sample	batch	sample	batch
Na	6.6	6.6	6.6	6.4
Ca	40.5	40.5	40.3	39.3
Al	6.6	6.6	6.6	6.4
Si	46.3	46.4	46.3	45.1
% cations	56.5	56.5	42.4	54.9
O:Si	1.7	1.7	2.9	1.6

Table 2-5 Fluorine content analysis in wt%.

Analytical technique	CS	CSF
Titration	0.04 ± 0.03	4.75 ± 0.06
Ion selective electrode	used as blank	4.27
DTA weight loss	0.66	4.85

2.3.2 Glass characterization

2.3.2.1 Density

Table 2-6 shows the effect of fluoride addition in to the CS glass. The density change is a direct consequence of the formation of less directed bonds and hence the structural skeleton collapses into closer packing [Rabinovich 1983], i.e. a reduction of the molar volume. Fundamentally, fluoride ion packing fractions are much higher than those of oxide ions in silicates. For instance, fluoride ions occupy 57% of the available space in a ZBLAN (Zr-B-La-Al-N) glass [Bansal *et al* 1983] whereas in vitreous silica, oxygen ions fill only 44% of the volume. These can be compared to a random closed-packed array, which would be expected to have a packing fraction of 0.636. The above results are in agreement with the present study in that both true and bulk densities of CSF glass are higher than those of CS glass.

Table 2-6 Density and coefficient of thermal expansion (CTE) in CS and CSF glasses.

Properties	CS	CSF
True density (Mg/m^3)	2.700	2.724
Bulk density (Mg/m^3)	2.695	2.720
$CTE/_{MK^{-1}}$	6.65	10.64

2.3.2.2 Coefficient of thermal expansion

The CTE is very sensitive to changes in chemical composition. Dilatometric profiles of the variations of length in glass specimens with temperature are illustrated in Figure 2-7. As shown in Table 2-6, 4.8 wt% of fluorine substituted for oxygen increased the CTE of the glass by about 60%.

The reason for the difference in the CTE may be twofold: the annealed state of the sample and the structure of the glass. As with crystals, the thermal expansion of glass is due to unsymmetrical atomic vibration with increased temperature. It is possible that the annealing of the specimen could have altered the atomic arrangement of the glass, and thus have affected the thermal expansion of the glass. In the case of the CS glass, the structure might have arranged itself in such a way as to be similar to single-chain wollastonite, for which the CTE is ~ $4.5x10^{-6}$ K^{-1}. The negatively charged non-bridging fluorine atoms could have increased the polarisability, and thus the anharmonicity of the lattice vibrations, leading to an increase in the coefficient of thermal expansion.

2.3.3 Kinetic behaviour

In the T_g region, the anharmonicity of lattice vibrations increases to an extent beyond which the elastic lattice forces are no longer dominant. As the anharmonicity of the lattice vibrations plays a role in determining both CTE and T_g, it is perhaps not unexpected that there is a relationship between these parameters; generally, the greater the thermal expansion coefficient the lower the T_g value, as has been observed in the present study (Table 2-6 and Table 2-7). As well as the glass transition temperature, the dilatometric softening point and the viscosity of both CS and CSF glass are shown in

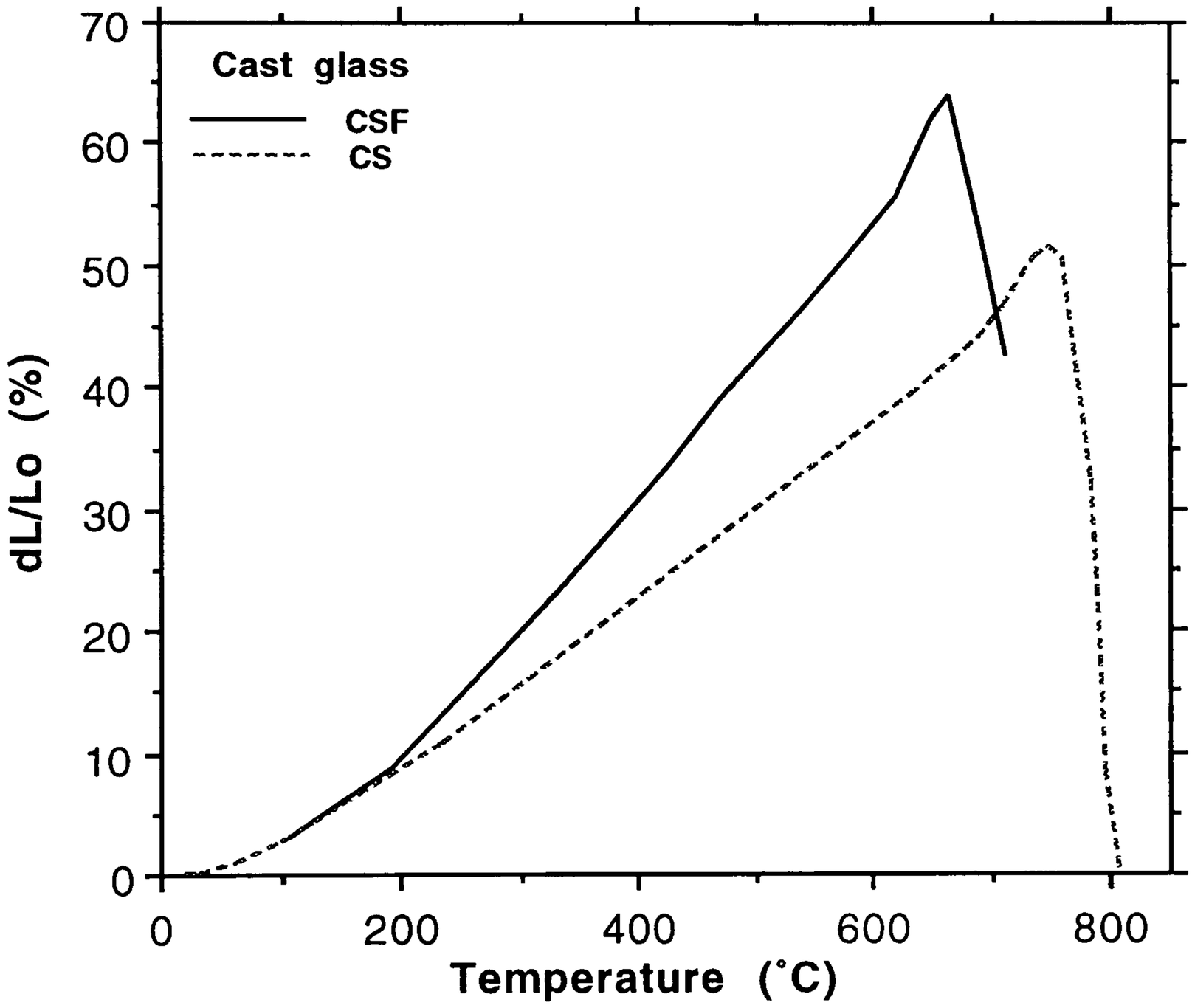


Figure 2-7 Dilatometric profiles of CS and CSF cast glass at a heating rate of 10˚C/minute.

Table 2-7 Temperatures corresponding to fixed points of CS and CSF bulk glasses in comparison viscosity by VFT method (Eq. 2-4).

Fixed points	log (η)	Temperature (°C)			
		VFT (calculated)		Experimental data	
		CS	CSF	CS	CSF
glass transition	13.3	985	908	686	613
dilatometric softening	11.3	1051	985	770	664
melting point	2	>1500	1365	1308	1083

Table 2-7. According to the VFT equation (Eq. 2-4), viscosity values at three temperatures are sufficient to calculate the viscosity profile of a glass. Thus, another fix point obtained from the DTA curves, namely the melting point which corresponds to $\log(\eta) = 2$ Pa·s, was employed.

Figure 2-8 illustrates the resultant viscosity profiles according to the VFT method in comparison with the viscosity of CS and CSF melts calculated by Urbain et. al.'s method [Urbain *et al* 1981]. The Urbain curves appear insensitive to fluorine addition, while the VFT curves indicate that glass with fluorine (CSF) exhibits lower viscosity values than does CS glass at higher temperatures. It should be noted, however, that the viscosity values obtained from Urbain's method agreed with that of CSF calculated by the VFT equation at high temperatures (>1300°C). In bulk samples (designated by --B after the glass composition designation), the viscosity of CSB glass is initially lower than that of CSFB glass until the temperature reaches 850°C. At higher temperatures, the tendency reverses, i.e. the viscosity of CSB is higher than that of CSFB. Similar behaviour occurs in powder glasses, but the transition temperature where the viscosity of CSF powder (CSFP) starts to be lower than that of CS powder (CSP) is shifted to a lower temperature of approximately 700°C.

The effect of surface area on the viscosity decreases at higher temperature for both glasses. It can be seen that the curves of the same composition converge as the temperature increases until they merge at ~950°C for CSF and at ~1050°C for CS. At higher temperatures, the viscosity is insensitive to the surface area of the glasses.

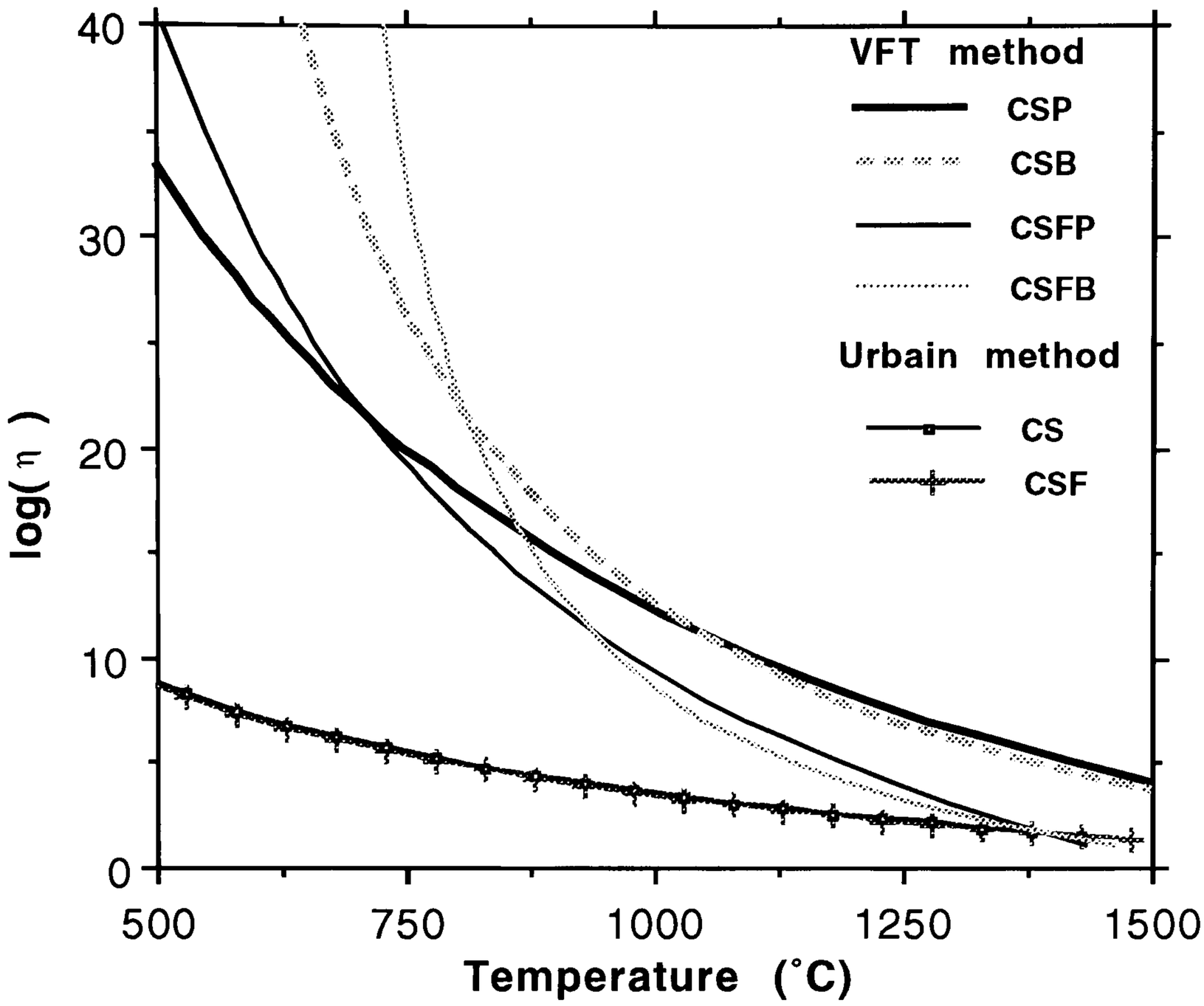


Figure 2-8 Viscosity curves calculated from VFT's (Eq. 2-4) and Urbain's (Eq. 2-5) methods (P:powder, B: bulk).

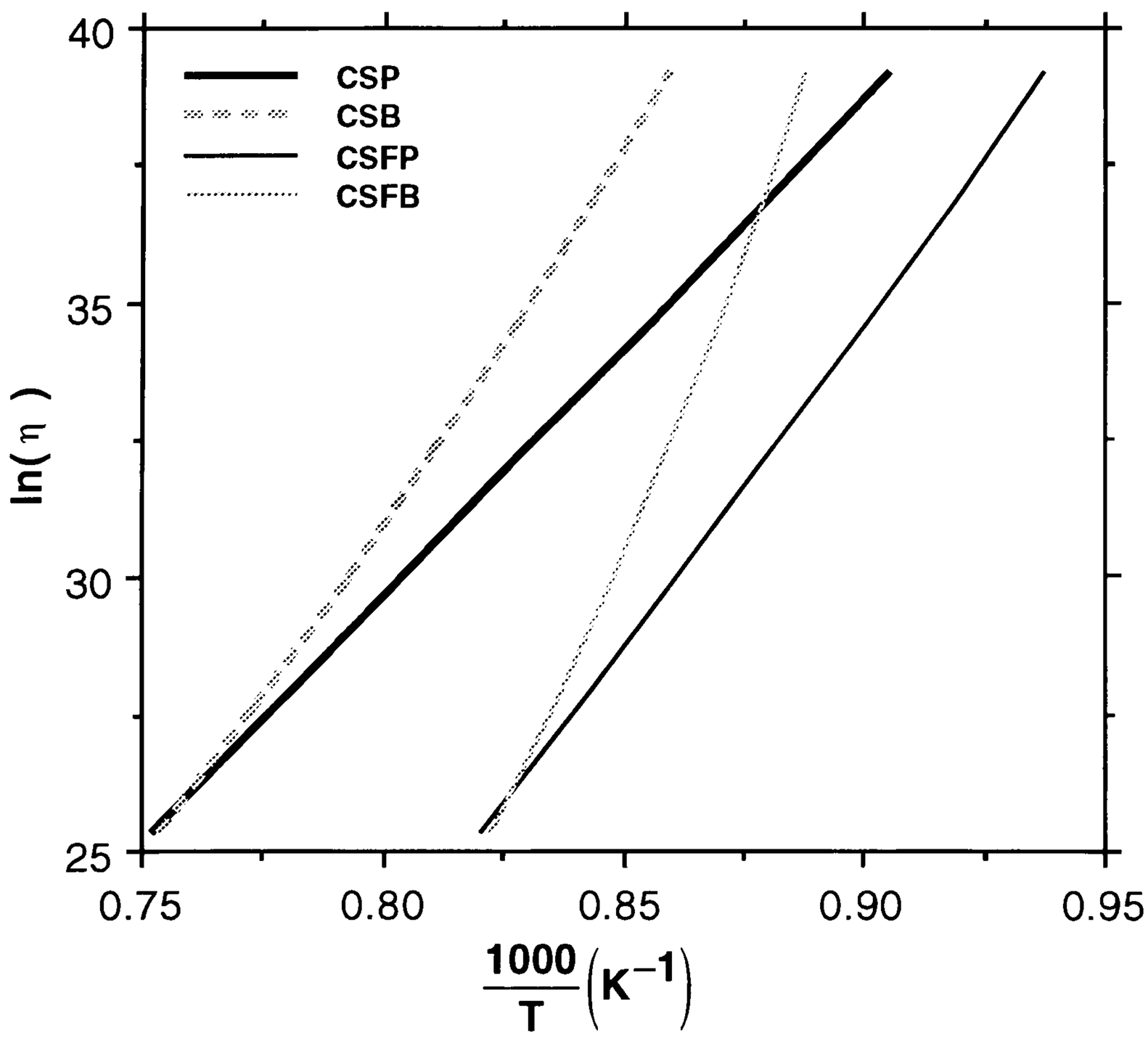


Figure 2-9 Arrhenius plot of viscosity for CS and CSF.

Despite these differences for both CS and CSF glasses, the shear viscosity exhibits Arrhenius behaviour i.e. a straight line can be fitted through the data points of the log viscosity versus $\frac{1}{T}$ plots of Figure 2-9 to give the activation energies E_η presented in Table 2-9.

T_g regions form DTA plots of CS powder glass are shown in Figure 2-10. Table 2-8 lists the values of T_g *and* T_g' as defined in Figure 2-4, for CS and CSF glasses in both bulk and powder forms. These values were utilised in calculating the activation energy for viscous flow, E_η^*, via Moynihan's method (Eq.2-21), and the resultant E_η^* are compared with the values obtained via Arrhenius method (Eq. 2-6), from the slopes of the curves of Fig. 2-9, in Table 2-9. It can be seen that the activation energy obtained from Arrhenius' method agrees with that from Moynihan's method in that they both exhibit lower activation energies for the fluorine-containing cases, implying that fluorine facilitates the viscous flow of the glass. It should be pointed out that $E_\eta > E_\eta^*$ (with the exception of CS powder) which was attributed to E_η being interpolated from the viscosity profile in the higher temperature range whilst E_η^* was calculated at a temperature ~T_g.

In CS glass, the activation energy for viscous flow in bulk form is higher than that of powder form which implies that the powder form has higher crystallisation tendency than in bulk form. On the other hand, the activation energy for viscous flow in CSF glass in bulk form is lower than that of powder form which implies that the powder form has lower crystallisation tendency than in bulk form. One possible explanation is that crystallisation occurs instantaneously on the powder surface which retards bulk crystallisation.

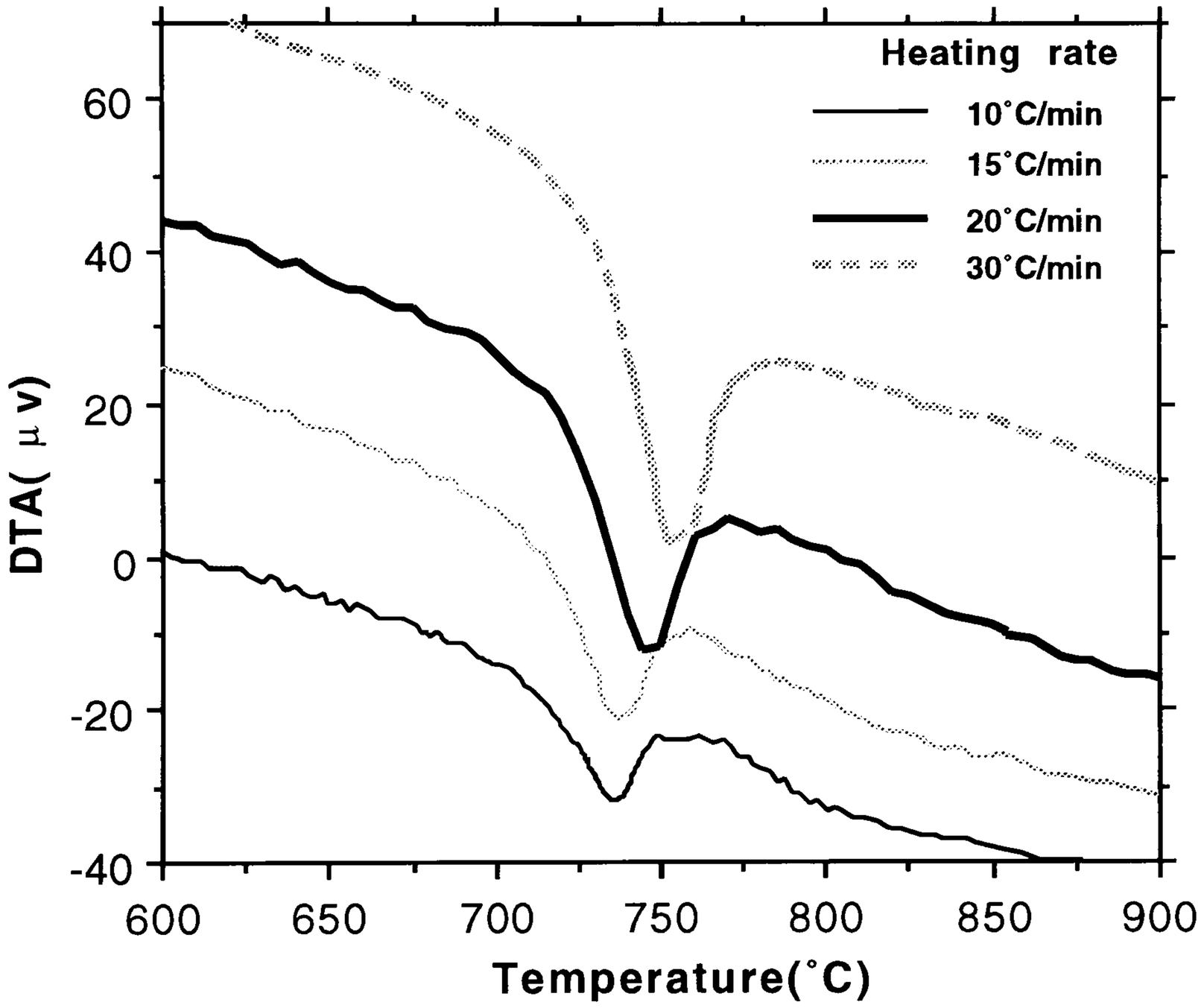


Figure 2-10 DTA profiles in the glass transition region for CS bulk glass at various heating rates (The profiles have been displaced vertically for ease of viewing).

Table 2-8 Glass transition temperatures as defined in Figure 1-4 for the calculation of enthalpy of viscous flow by Moynihan's method.

Heating rate	CS bulk		CS powder		CSF bulk		CSF powder	
(°C/min)	Tg	Tg'	Tg	Tg'	Tg	Tg'	Tg	Tg'
10	706.9	747.9	686.4	717.9	613.2	643.7	613.6	639.9
15	712.4	750.0	688.3	747.5	-	-	614.2	665.7
20	719.1	763.3	699.3	743.3	611.2	659.8	619.1	668.5
25	-	-	699.4	748.2	617.8	665.9	620.1	674.1
30	728.8	772.0	-	-	-	-	625.7	677.5
35	-	-	-	-	627.2	683.3	-	-

Table 2-9 Activation energies for viscous flow at the glass transition temperatures calculated via Arrhenius's (E_η) and Moynihan's (E_η^*) methods.

Sample	Activation Energy (kJ/mol)	
	E_η	E_η^*
CSbulk	1061	985±60
CS powder	717	875±88
CSF bulk	1542	616±80
CSF powder	866	652±22

2.4 Summary

The quaternary system under investigation, Na_2O-CaO-Al_2O_3-SiO_2, forms glass readily. Materials with partial substitution of fluorine for oxygen in the system also readily form glass but with an increased tendency to crystallise (c.f. Kingery's criterion). It was found that negligible amounts of fluorine were lost during the preparation process. Fluorine affected the glass properties in such a way that the density, the coefficient of thermal expansion, and the glass transition temperature are all increased. In addition, fluorine has a significant effect on the viscosity. It forms glass with stronger bonds at temperature lower than the glass transition temperature, as reflected from higher viscosity in this range. In contrast, at higher temperature it facilitates the viscous flow of the glass. Surface area also has great effect on the viscosity in the range higher than $\log(\eta) = 12$.

CHAPTER 3

CRYSTALLISATION PROCESS

3.1 Introduction

As a non-equilibrium solid, glass is a substance in a metastable state in that it would have a lower free energy if crystallised into one or more stable 'solid' phases. The development of controlled crystallisation of glasses brought about an important class of materials, i.e. glass-ceramics [Stookey 1960 and James 1982]. There are several important requirements to consider in choosing a glass-ceramic system. The composition must form a glass with adequate viscosity at the liquidus to allow shaping of the required glass article. Internal nucleation must be efficient, in order to produce a fine-grained body, and to avoid the adverse effects of directional crystallisation from the glass surface. Crystal growth upon the nuclei must also be controlled to avoid large crystals whose grain boundaries frequently act as planes for easy fracture propagation. In order to maintain the shape of the original glass articles, deformation through gravitational sag, or warpage due to volume changes during crystallisation in a thermal gradient, must be controlled. Thus knowledge of the overall kinetics is of practical importance in controlling the ultimate microstructure and properties of glass-ceramic materials.

Two of the most important distinguishing features of crystallisation mechanisms in silicate melts are related to their high viscosity and the crystallographic characteristics of silicate phases [Lewis *et al* 1979]. High viscosity will enhance localised segregation of solute or impurities at the crystal/liquid interface whilst the small differences in free energy between silicate phases of similar composition (shown by the frequency of polymorphism) results in a high probability of kinetically preferred metastable phases being formed.

The present chapter discusses the correlation between the properties of glass and the crystallisation process. In the first section, a review of the current knowledge concerning silicate structure, general kinetics, including formulated kinetic theories for crystallisation, will be discussed. This will lead to considerations of methods for the control of the crystallisation of the glass. Practical experimental methods for determining the nucleation and crystal growth rate, in addition to global evaluation of the crystallisation process, will be followed by experimental results and discussion. Some physical and thermal properties of the crystallised glass will also be correlated with the microstructure of the glass/glass-ceramics.

3.1.1 Silicate structure

The structure of silicate glasses, as proposed by Varshal [1989], is based on the crystallochemical similarity of the structure of the crystals and their respective glasses. If the present CS base glass were to be simplified to a lime-silica composition of approximately 35CaO:65SiO_2 wt% which when cooled down from molten glass, should give rise to a mixture of quartz (SiO_2) and wollastonite ($CaO{\cdot}SiO_2$). as shown in the ternary diagram of Figure 3-1 [Mukerji 1965].

Natural wollastonite crystals are often mixtures of monoclinic and triclinic forms, both forms having a nearly identical diffraction pattern (Table 3-1). The distinction of monoclinic para-wollastonite and triclinic wollastonite is their interrelation in a projection along the [001] direction. The difference exists only in the packing of the chains, which account for the often observed intimate intergrowth of both crystal phases [Ohsato & Sugimura 1986]. Wollastonite is used in applications ranging from bowling balls to automobile fenders, from ceramic tile to automobile brakes, and from industrial insulation board to protective industrial coatings [Bauer *et al* 1994].

The effect of partial substitution of CaF_2 for CaO (the CSF glass) may induce 2-liquid formation and would be expected to crystallise into wollastonite ($CaO{\cdot}SiO_2$) and rankinite ($3CaO{\cdot}2SiO_2$).

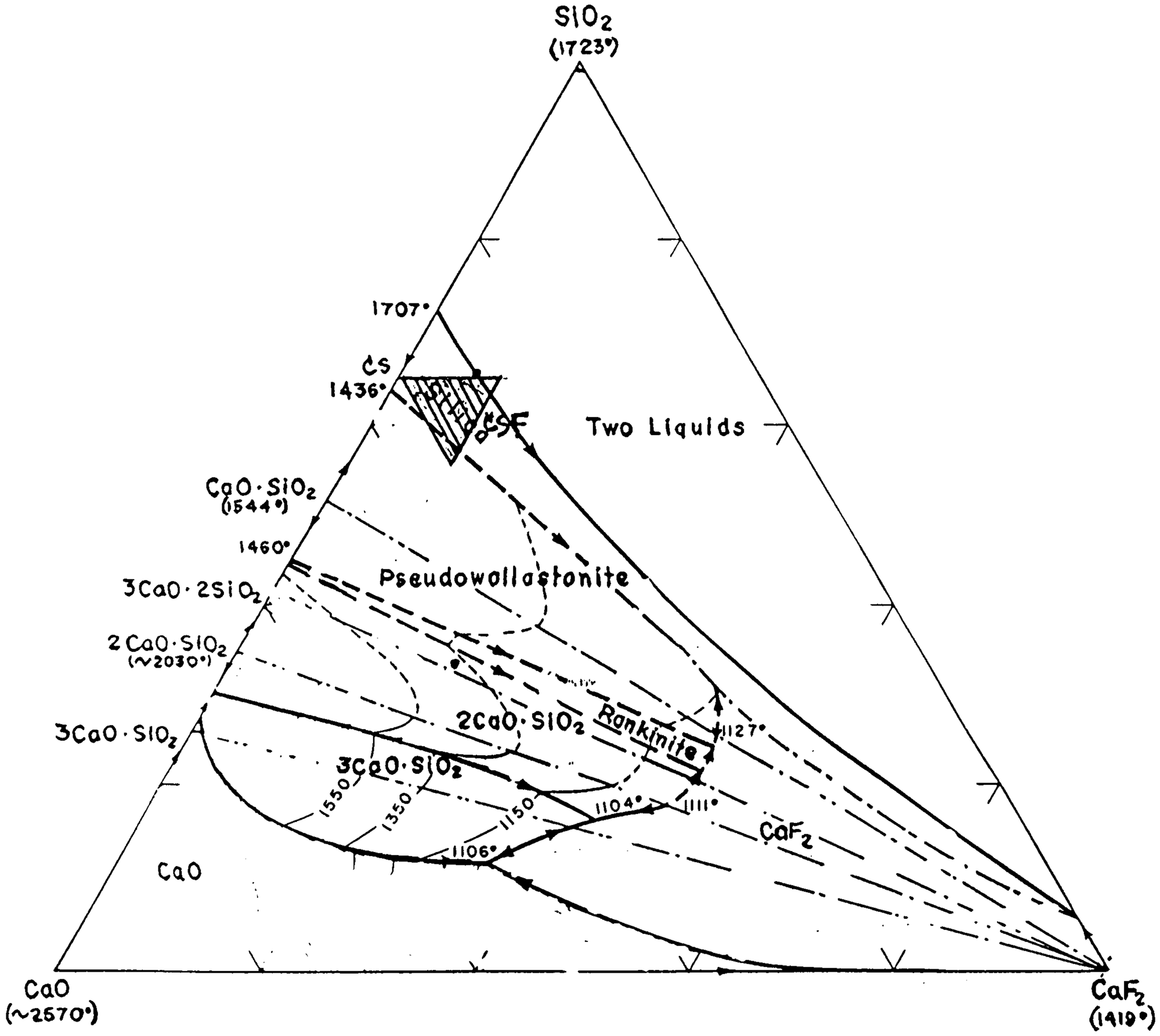


Figure 3-1 The ternary phase diagram CaO-CaF_2-SiO_2 showing the CS and CSF glass compositions.

Table 3-1 Comparison of information form JCPDS cards of crystal phases present in the study.

	β–wollastonite		Para-wollastonite		α–wollastonite		Rankinite		Cuspidine	
JCPDS-No.	27-1064		43-1460		31-300		23-124		41-1474	
Formula	$CaSiO_3$		$CaSiO_3$		$CaSiO_3$		$Ca_3Si_2O_7$		$Ca_4F_2Si_2O_7$	
System	triclinic		monoclinic		triclinic		monoclinic		monoclinic	
D_X	2.90		2.91				3.00		2.98	
d-value	d(˚A)	I/I_0	d(˚A)	I/I_0	d(˚A)	I/I_0	d(˚A)	I/I_0	d(˚A)	I/I_0
	3.830	85	3.840	40	5.67	60	4.49	30	3.258	25
	3.510	75	**3.519**	50	3.419	70	3.84	50	**3.061**	100
	3.314	100	**3.319**	60	**3.235**	100	3.79	50	2.946	16
	3.086	60	3.091	45	**3.219**	100	3.38	20	2.933	18
	2.977	30	**2.978**	100	2.816	70	3.20	60	**2.898**	30
	2.721	30	2.560	14	2.798	60	**3.18**	70	**2.873**	50
	2.556	45	2.481	25	2.784	60	**3.02**	100	2.552	8
	2.477	25	2.354	14	2.449	70	2.91	60	2.310	8
	2.340	30	2.350	16	1.998	70	**2.72**	80	2.019	12
	2.302	50	2.306	35	1.984	60	2.59	30	1.959	10
	1.918	25	2.186	25	**1.970**	100	2.58	30	1.883	10
	1.759	35	1.831	14	1.832	60	2.52	30	1.821	12

The effect of fluoride can be deduced theoretically from the stoichiometric formulae of the CS and CSF glasses as follows

CS: $CaO+2SiO_2 \rightarrow CaO\cdot SiO_2 + SiO_2$ [3-a]

CSF: $CaF_2+4CaO+9SiO_2 \rightarrow CaF_2 + 3CaO\cdot 2SiO_2 + CaO\cdot SiO_2+ 6SiO_2$ [3-b]

3.1.2 Transformation Kinetics

The crystallisation of a homogeneous phase, liquid or glass, is not a transformation which is produced throughout the whole volume at once: it begins and extends progressively from *discrete centres* distributed throughout the mass [McMillan 1979 and Zarzycki 1991]. Accordingly, the heat treatment of glasses to produce a glass-ceramic typically involves two or more steps: a lower temperature step to induce

nucleation, and one or more higher temperature treatments to promote growth of the crystalline assemblage and to develop the desired microstructure.

3.1.2.1 Nucleation

In this stage the agglomerations which can serve as the starting points for the development of ordered regions are formed [McMillan 1979 and Zarzycki 1991]. These agglomerations or *embryos*, which form and disappear according to structural fluctuations produced by thermal agitation, have different and constantly fluctuating sizes. Such an embryo must attain a certain critical size to be able to serve as a starting point for the development of the new (crystalline) phase; i.e. to constitute a *nucleus.*

Nucleation which occurs in a totally random manner throughout the entire system is said to be *homogeneous*. The necessary condition for this to happen is that all volume elements of the initial phase must be structurally, chemically and energetically identical. In practice, this is difficult to achieve: the surface itself already constitutes an inevitable imperfection. In this case, the energy necessary for the formation of a nucleus is lowered for these sites, and the nucleation will preferentially occur at the interface. This process is an example of *heterogeneous nucleation.* Practically, many factors influence the nucleation process in glass, in particular glass-in-glass phase separation, time lag effects, saturation effects, and nucleation catalysts.

(i) Glass-in-glass phase separation

There is a range of silicate compositions and temperatures below the liquidus where the equilibrium solid cannot form directly from an undercooled single-phase liquid. Thermodynamics requires either a prior liquid-liquid phase separation or a simultaneous formation of the second liquid to form [Cahn 1969 and Charles 1969]. The driving force behind every segregation process is the decrease in the free energy of the whole system which results from an increase in the ordered state.

In baria-silica [Seward *et al* 1968 and James 1982] and lithia-silica [Greer & Kelton 1991] glasses, evidence was found for an additional enhancement in nucleation due to

the presence of phase separation. However, there was no evidence for a significant enhancement of crystal nucleation at the interface between amorphous phases in these two systems. Thus prior phase separation would be imagined to be effective in the control of the crystal size by limiting growth within a phase, even though growth rates might not be significantly affected [Lewis *et al* 1979]. The dimensions of the crystallites are, in the first instance, found to be dependent on the phase boundaries of the droplets in which they grow.

(ii) Time lag effects

Most of the kinetic treatments concerning nucleation of glass assumed a time-independent concentration of sub-critical nuclei. However, if the melt is highly viscous, e.g. in the case of SiO_2, or on high undercooling, a transient time during which the equilibrium concentration is established must be taken into account [Zdaniewski 1978 and Gutzow *et al* 1990]. The time during which the nuclei production rate is increasing to its steady state value is usually called the time lag (τ) [Kelton *et al* 1983]. Specific material parameters such as the surface energy of the nuclei, activation energy of diffusion, and the VFT temperature (see 2.3.3) sensitively influence the kinetic nucleation process and determine whether transient effects are important for glass formation [Richter 1989]. Time-lag can also be a result of non-ideality of the solution and elastic strain in segregation processes in highly viscous liquids [Bartels *et al* 1990].

(iii) Saturation effects

Zanotto and Weinberg [1988] demonstrated that for homogeneous nucleation, saturation effects are possible due to the reduction in volume available for nucleation as a result of crystal growth, while for the case of heterogeneous nucleation, an additional mechanism causing saturation is the encapsulation (ingestion) of heterogeneous nucleation sites during crystal growth. At a later stage, when the period of nucleation is finished, the average cluster size of the distribution evolving in a regular solution becomes larger than that found in an ideal solution. This is due to the higher number of clusters formed initially in the ideal solution and the resulting depletion as, for further

growth of the larger clusters, the smaller clusters must be dissolved. The time needed for the process of dissolution contributes significantly to the hindrance of the growth of the larger clusters.

(iv) Nucleation catalysts

In practice, crystal nucleation is usually controlled through adding a nucleating agent into the parent glass. Nucleating agents are materials which are added to, and are completely soluble in, the parent-glass at the melting and working temperatures, but which initiate efficient bulk nucleated crystallisation during the carefully controlled heat treatment of the parent glass [Salama 1990]. Nucleating agents may initiate crystallisation in one or more of the following ways:

1. Weaken the silica network by breaking its continuity, act as a flux and affect viscosity [Saraswati 1990].
2. Induce phase separation either on cooling or heating of the parent glass [Tomozawa 1977].
3. Act as a surface active agent and reduce the critical size of an embryo required to form a stable nucleus [Salama 1990].
4. Alter molecular mobility, thus changing crystallisation behaviour [Drummond III 1990].

3.1.2.2 Crystallisation

After formation of stable nuclei in the parent phase, crystallisation proceeds through growth of the new phase. While nucleation is highly critical in the production of microcrystalline glass-ceramics, the crystallisation process is also of considerable importance in the controlled crystallisation of glasses as it determines the morphology of the phase produced. Two crystallisation stages can be distinguished: the crystal growth stage and the crystallisation approach to equilibrium. In the growth stage, the crystalline particle grows at a certain rate at the expense of the surrounding phase [Stephenson & White 1967]. The rate of growth of the new phase is generally controlled by:

(i) the rate at which the irregular glass structure can be re-arranged into the periodic lattice of the growing crystal;

(ii) the rate at which energy released in the phase transformation process can be eliminated, that is: the rate of heat flow away from the crystal-glass interface.

As far as the final stage of crystallisation is concerned the driving force is a consequence of the reduction in total interfacial energy or the reduction in curvature of the boundary [Anderson *et al* 1984]. This leads to the diminishing of the fibrous appearance of the spherulite

Three modes of crystallisation occurred in the present study which could be classified as surface crystallisation, spherulitic crystallisation, and approach to equilibrium which is common when the crystallised volume fraction reaches 0.95 and the crystals rearrange to achieve the equilibrium state.

(i) Surface crystallisation

The development of crystallisation from the surface is critically dependent on the state of the surface [Klingsberg 1964 and Bergeron & De Luca 1967]. Differences in composition between the surface and interior regions, as a result of superficial condensed-phase impurities (atmospheric dust) or the presence of flaws and other heterogeneities, are possible causes for the initiation of surface crystallisation [Morey 1930; Scott & Pask 1961; and Mattox 1967]. Glasses which crystallise in this way show a characteristic crystal structure in which the crystals grow inwards from the surface, often oriented perpendicular to it (Figure 3-2). The crystal growth rate is constant until the crystallisation fronts from opposite faces meet at which point a plane of weakness is created, which is detrimental to mechanical performance.

(ii) Spherulitic crystallisation

Spherulites commonly occur in silicate minerals found in igneous rock [Johannsen 1931] and some synthetic silicate glasses [Freiman *et al* 1972; Carpenter *et al* 1986; and Shyu & Wu 1991b]. In inorganic glasses spherulitic crystallisation is often preceded by

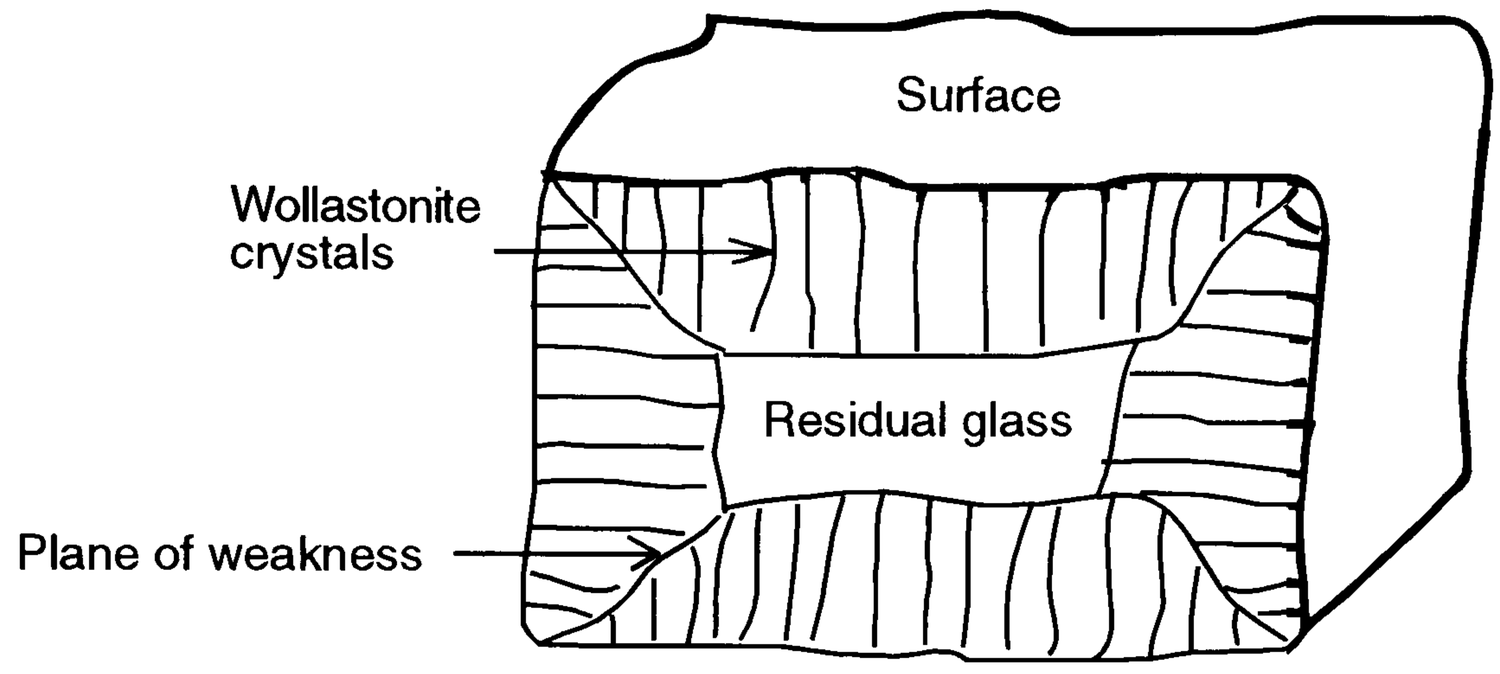


Figure 3-2 Schematic drawing showing anisotropic crystal growth in surface crystallisation.

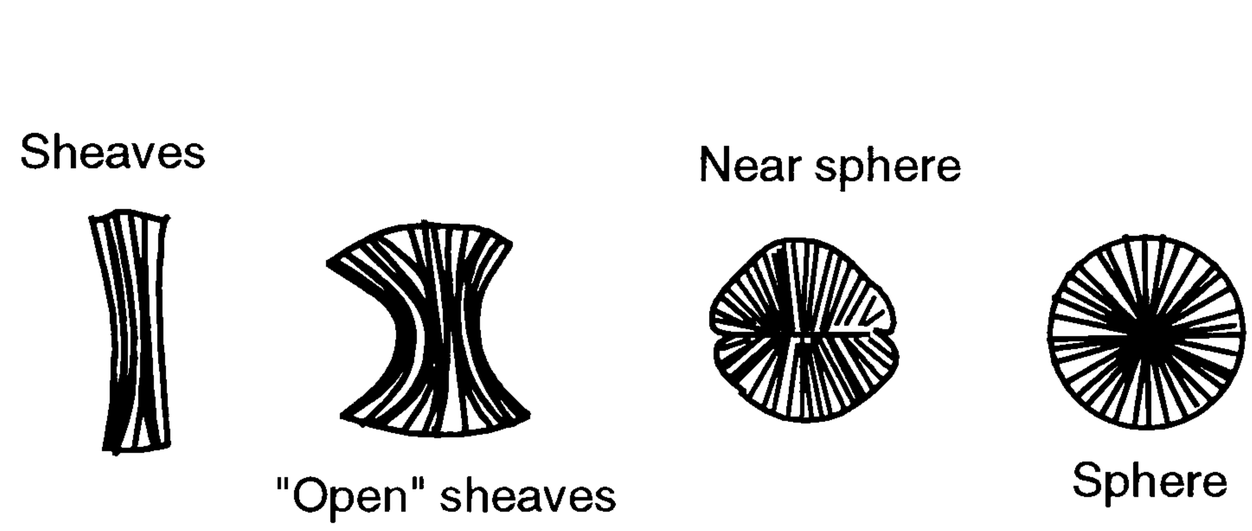


Figure 3-3 Schematic drawing showing different spherulitic morphologies.

(ii) Spherulitic crystallization

Spherulites commonly occur in silicate minerals found in igneous rock [Johannsen 1931] and some synthetic silicate glasses [Freiman *et al* 1972; Carpenter *et al* 1986; and Shyu & Wu 1991b]. In inorganic glasses spherulitic crystallization is often preceded by phase separation [Ohlberg *et al* 1962]. Spherulites are transient morphological forms produced during the rapid growth of crystals when the rate of growth exceeds that of diffusion [Zdaniewski 1978].

The fibres constituting the spherulites are most commonly encountered when the composition of the earliest crystals differs significantly from the overall composition, for in these conditions at the crystal-glass interface the crystal becomes depleted of the components required for growth and is then dependent for continued growth on diffusion from elsewhere [Keith & Padden 1963]. The accessible volume from which the crystal surface can draw the necessary components for growth is greatest at protuberances on the crystal growth front, and in particular at the tip, which accounts for the fibrous character. If the fibrous growth is in a fast-growing direction, perturbations on its faces will result in branching. The directions of growth of the branches are controlled by the interference of the diffusion fields of other branches, resulting in the spherulitic morphology eventually becoming radial.

There are different types of spherulitic morphology based on these orientated fibres (Figure 3-3), namely: (a) "straight" sheafs and "open" sheafs - bundles of fibres which are divergent at both ends, (b) near spheres - two hemispheres united through a common cord, and (c) spheres and ellipsoids [Freiman *et al* 1971]. The spherulites are not entirely crystalline as some residual glass phase remains inside [Zanotto & James 1988] and the chemical composition in the residual glass varies with heat treatment due to crystal formation.

(iii) Approach to equilibrium

Two types of crystal rearrangement to approach the equilibrium state can be observed in all microstructures which contain fibrillar morphologies when annealed for long times

or at high temperatures [Lewis *et al* 1979]. The first type is interpreted as a *selective coarsening* of the fibrillar crystals; the main driving force stems from a reduction in the large surface area of the fibrils. The second type of rearrangement is secondary crystallization involving the residual glass which consists mainly of 'impurities' driven out of the crystal phase(es). The secondary crystal size is much smaller than the spherulitic growth unit and independent of the initial nucleation density. These mechanisms may be utilised to achieve the ideal microstructure of a structural ceramic, i.e. that of a completely crystalline material with submicrometer grain size. However, this microstructure is rarely achieved because of the tendency to trap residual glass between the slowly growing facet planes of the anisotropic crystals or at grain boundaries or triple-junction nodes [Raj 1981].

3.1.2.3 Certain material properties and crystallizability

Analyses of the kinetics of volume nucleation in silicate systems in which the crystallising phase has the same composition as the parent glass show striking similarities [James 1985]. The relationship between material properties and crystallizability is summarised in Figure 3-4 [Gutzow *et al* 1990]. The values of T_{max}/T_m, where T_{max} is the temperature of maximum nucleation and T_m the effective melting point, are in the range 0.54 to 0.59 whilst T_{max} is always a temperature somewhat above T_g. Values of T_d/T_m,where T_d is the "just detectable" nucleation temperature (nucleation rate (I) =10^6 $m^{-3}s^{-1}$), are in the range 0.62 to 0.66. At T_g, no nucleation is expected to be observed since the steep rise in viscosity at about T_g will provide an effective "cut off".

For materials which have similar viscosity curves, a low melting point (or liquidus) favours vitrification; this corresponds to a high T_g/T_m. In general, however, such a simple relationship between ease of vitrification and temperature should not be expected as the melting point depends on the properties of the liquid and the crystal, while T_g depends on the properties of the supercooled liquid. However, for a large number of glass-forming liquids, it has been recognised [Sakka & McKenzie 1971] that T_g/T_m »2/3 is usually required for vitrification.

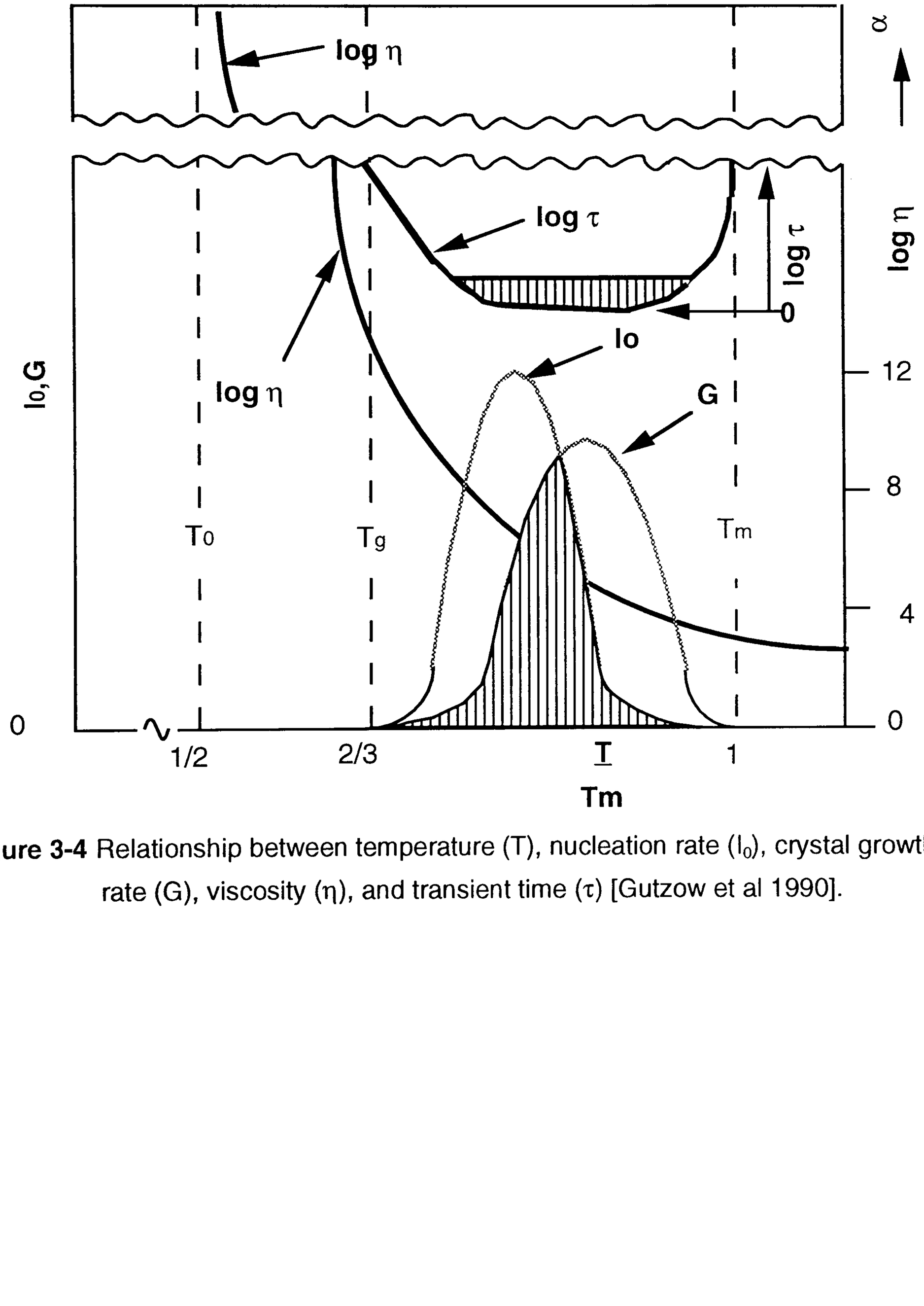


Figure 3-4 Relationship between temperature (T), nucleation rate (I_0), crystal growth rate (G), viscosity (η), and transient time (τ) [Gutzow et al 1990].

PAGE

MISSING

IN

ORIGINAL

Table 3-2 Composition of glass, investigated by Shyu & Wu [1991], which affects the crystallization as shown in Figure 3-5.

Composition	MgO	CaO	SiO_2	P_2O_5
Base glass (CSP)	11.2	37.2	33.3	18.3
CS1	11.2	35.55	34.95	18.3
CS2	11.2	33.9	36.65	18.3
CP1	11.2	38.85	33.3	16.65
CP2	11.2	40.5	33.3	15

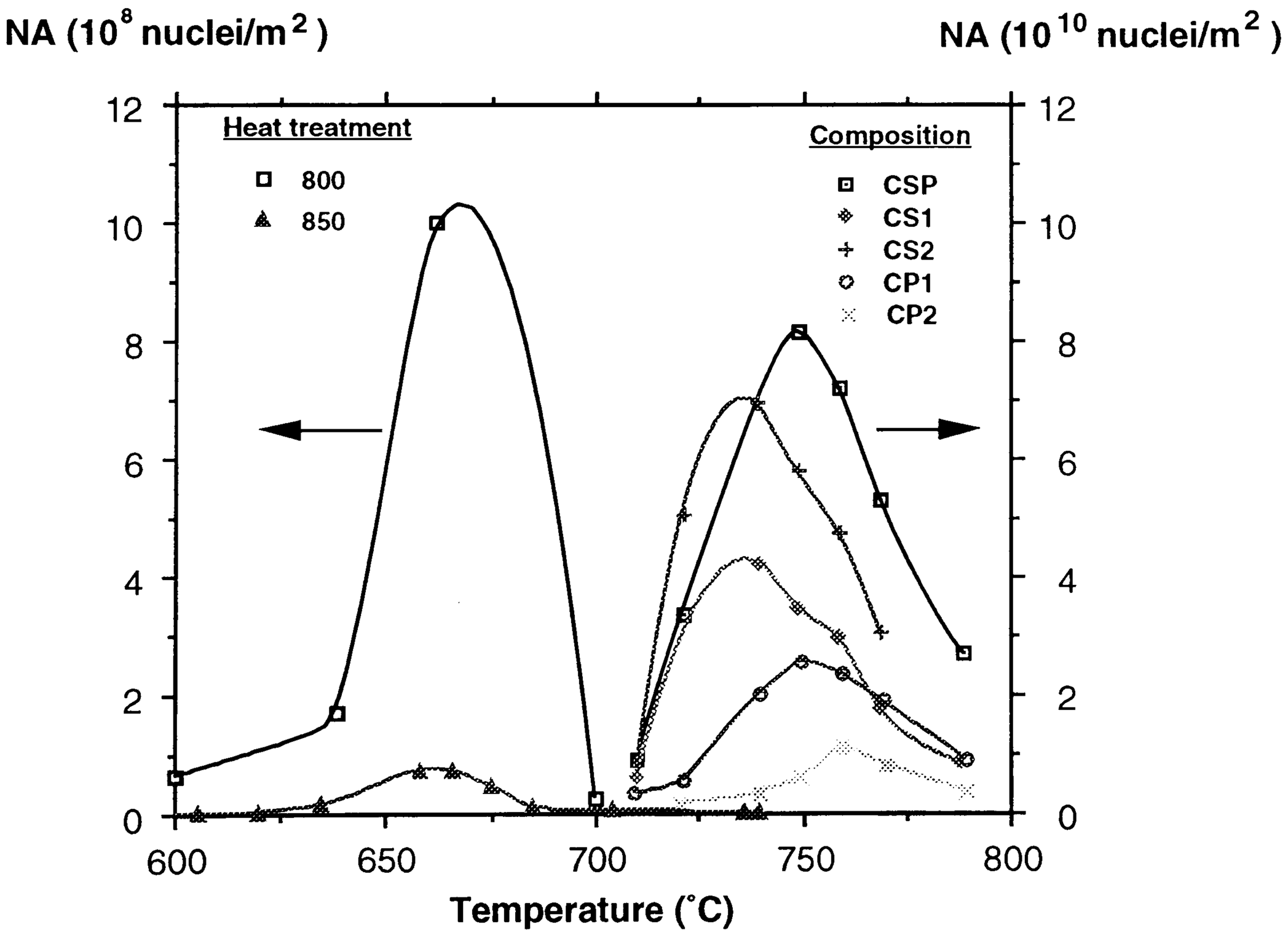


Figure 3-5 The variation of the number density of nuclei with nucleation temperature of glasss with 3.4 wt% fluoride [Mukherjee & Rogers 1967] and with composition shown in Table 3-2 [Shyu & Wu 1991].

overall kinetics is of practical importance in controlling the ultimate microstructure and properties of glass-ceramic materials. Almost all the kinetic methods used in thermal analysis are based on the equation

$$\frac{dX}{dt} = f(X,T) \qquad [3\text{-}1]$$

where dX/dt is the rate of reaction,

$f(X,T)$ is a function of the amount reacted at time t, and

T is the absolute temperature

Mathematical expressions are extensively employed by materials scientists to infer the mechanisms of phase transformation with these expressions usually being based on either classical nucleation theory (CNT) or Johnson-Mehl-Avrami (JMA) theory.

3.1.3.1 Classical Nucleation theory

In the simplest classical model, proposed by Volmer & Weber [1925], Becker & Doring [1935], and Turnbull & Vonnegut [1952], a "droplet" of the new, product phase, is considered to form in the supersaturated (supercooled) parent phase. It is assumed that the droplets have a uniform structure, composition and properties identical to those of the product phase and differ only in form and size. The minimum free energy, ΔG^*, required to form a stable nucleus is called the *thermodynamic barrier* to nucleation. To evaluate the rate of homogeneous nucleation it is assumed that the critical nuclei are formed by random molecular fluctuations. Assuming that the size distribution and formation of the nuclei are governed by statistical fluctuations, the probability that a fluctuation would be critical to form a nucleus is proportional to $exp(-\Delta G^*/kT)$. If the jump across the nucleus-matrix interface is controlled by a free energy of activation, ΔG_a, the rate of nucleus formation, I (the number of nuclei formed per second per unit volume), is given (see appendix C) by an expression of the form:

$$I = A(T)\exp\left(-\frac{\left(\Delta G_a - \Delta G^*\right)}{kT}\right) \qquad [3\text{-}2]$$

where ΔG_a represents the *kinetic barrier* to nucleation and

$A(T)$ is a weakly temperature-dependent prefactor.

Figure 3-4 shows how the nucleation rate, I, depends on temperature. For small super--coolings, the barrier ΔG^* is high and I is very small. On decreasing the temperature, I then increases rapidly to the temperature at which $\Delta G^* \sim \Delta G$, which corresponds to a maximum nucleation rate. For lower temperatures, where $\Delta G_a \gg \Delta G^*$, the diffusion phenomenon dominates and I is progressively reduced.

Provided that the particles of the new phase grow from a multi-component homogeneous solution, then the classical theory states that their composition will equal the equilibrium composition. During isothermal growth, the growth rate can be determined by the rate of diffusion of material in the solution or through reactions on the surface of the phase boundary. In diffusion-controlled growth, the dimensions of the particles of the new phase increase proportional to the square root of time; in surface reactions, they increase linearly with time.

The theory has only recently been tested by quantitative modelling in lithium disilicate glass [Greer and Kelton 1991]. It was demonstrated that reasonable temperature-dependent material parameters are obtained by fitting steady-state nucleation frequencies and effective time-lags for nucleation as a function of temperature. However, a comparison made between the experimentally determined and predicted (CNT) temperature-dependence of the nucleation rate in glass showed that precise thermodynamic data, i.e the free energy of activation for transport across liquid-crystal interface (ΔG_D) are not necessarily required [Weinberg & Zanotto 1989]. It was concluded that the temperature-dependence of the classical homogeneous nucleation rate is still a matter of controversy.

3.1.3.2 Johnson-Mehl-Avrami Equation

Another theory which is extensively used by materials scientists to describe the kinetics of phase transformation was derived by Johnson-Melh-Avrami. Johnson & Mehl [1939] and Avrami [1939] proposed that the nuclei are regarded as being discrete and randomly distributed, and are assumed to be activated simultaneously at the beginning of the transformation. The transformation is then completed by the impingement of

growing spheres centred on these nuclei sites. In its basic form the theory describes the evolution with time, t, of the volume fraction crystallized, χ, in terms of the nucleation frequency per unit volume, I_v, and the crystal growth rate, u

$$\chi = 1 - \exp\left[-g\int_0^t I_v\left(\int_{t'}^t u\,d\tau\right)^m dt'\right] \qquad [3\text{-}3]$$

Here, g is a geometric factor which depends on the shape of the growing crystal,

t' and τ are time at which the growth rate is approximately constant, and

m is an integer or half integer which depends on the mechanism of growth and the dimensionality of the crystal.

For interface-controlled growth when u is independent of time, m assumes the values 1, 2, and 3 for one-, two-, and three-dimensional growth respectively. For diffusion-controlled growth where u decreases as $t^{-1/2}$, m assumes the values 1/2, 1 and 3/2 for the respective dimensionalities of growth. For the important case of isothermal crystallization with nucleation rate and growth rate independent of time, equation 3-3 can be integrated to yield

$$\chi = 1 - \exp\left(-g' I_v u^m t^n\right) \qquad [3\text{-}4]$$

where $n=m+1$ for $I_v \neq 0$, and

g' is a new shape factor.

Therefore, by measuring the crystal nucleation and growth rates at a certain temperature it is possible to calculate the volume fraction transformed with time and to compare it with experimentally determined values. Equation 3-4 can be taken as a detailed specific case of Johnson-Mehl-Avrami (JMA) relation:

$$\chi = 1\text{-}\exp[-(Kt)^n] \qquad [3\text{-}5]$$

where n is a dimensionless exponent called the *Avrami exponent*,

K has the effective overall reaction rate and is usually assigned an Arrhenius temperature dependence

$$K = K_0 \exp\left(-\frac{E}{RT}\right) \qquad [3\text{-}6]$$

where K_o is a frequency factor;

E is the activation energy describing the overall crystallization process,

R is the gas constant, and

T is the absolute temperature.

Eq.(3-5) is usually written as

$$ln\,ln(1-\chi)^{-1} = ln\,K + n\,ln\,t \qquad [3\text{-}7]$$

This expression is normally employed to infer the mechanisms of phase transformation from the values of n, that is, the slope of the $ln\ ln(1-\chi)^{-1}$ versus $ln\ t$ plot (see Table 3.2). The linearity of such plots is taken as an indication of the validity of the JMA equation.

3.1.4 Application of thermal analysis to the kinetics of crystallization

Thermal analysis is a very useful tool for studying the kinetics of reactions, including crystallization of glass, as it is both a rapid and convenient means [Borchardt 1956 and Geiger 1993]. Differential thermal analysis (DTA) and differential scanning calorimetry (DSC) have been used extensively for the study of the kinetics of phase transformations and chemical reactions [Brown 1988]. Several studies [Bansal *et al* 1983; Augis & Bennett 1978; and De Bruijn *et al* 1981] have compared variable-heating-rate calorimetry methods with isothermal calorimetry and concluded that equivalent kinetic parameters are obtained. In DTA the peak is simply the point at which the a particular reaction is finished. Normally, in DTA the maximum rate of reaction occurs at a point prior to the peak temperature [Wendlandt 1974]. However, it appears that as long as a consistent point is chosen (e.g. peak temperature, onset temperature, etc.) to represent a given crystallization event in series of DTA traces with different scan rates, activation energies in agreement with DSC results will be obtained.

The work of Clinton *et al* [1970] and Buri *et al* [1971] has shown that DTA can provide kinetic data in agreement with high temperature microscopy and high temperature x-ray measurements. A schematic representation for a DTA trace for crystallization of a glass to a glass-ceramic is illustrated in Figure 3-6. The discontinuity in the baseline of the curve is associated with the glass transformation whereas the adjacent exothermal maximum corresponds to separation of the crystalline phase(s). Melting of the

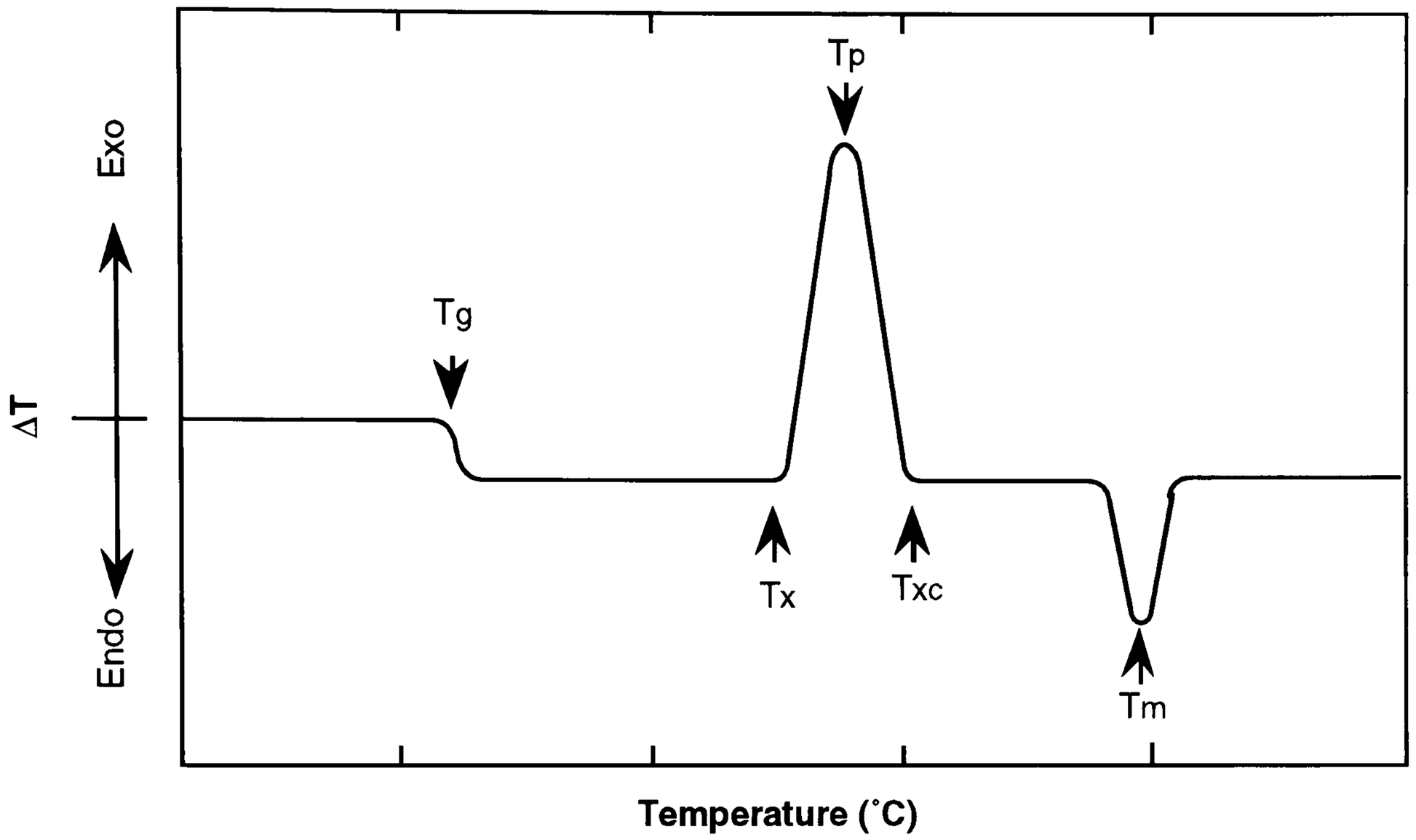


Figure 3-6 Schematic graph showing a typical DTA curve of a silicate glass where T_g is glass transition temperature; T_x the beginning of crystallisation; T_p peak temperature; T_{xc} crystallisation finish; and T_m melting temperature of a crystal phase.

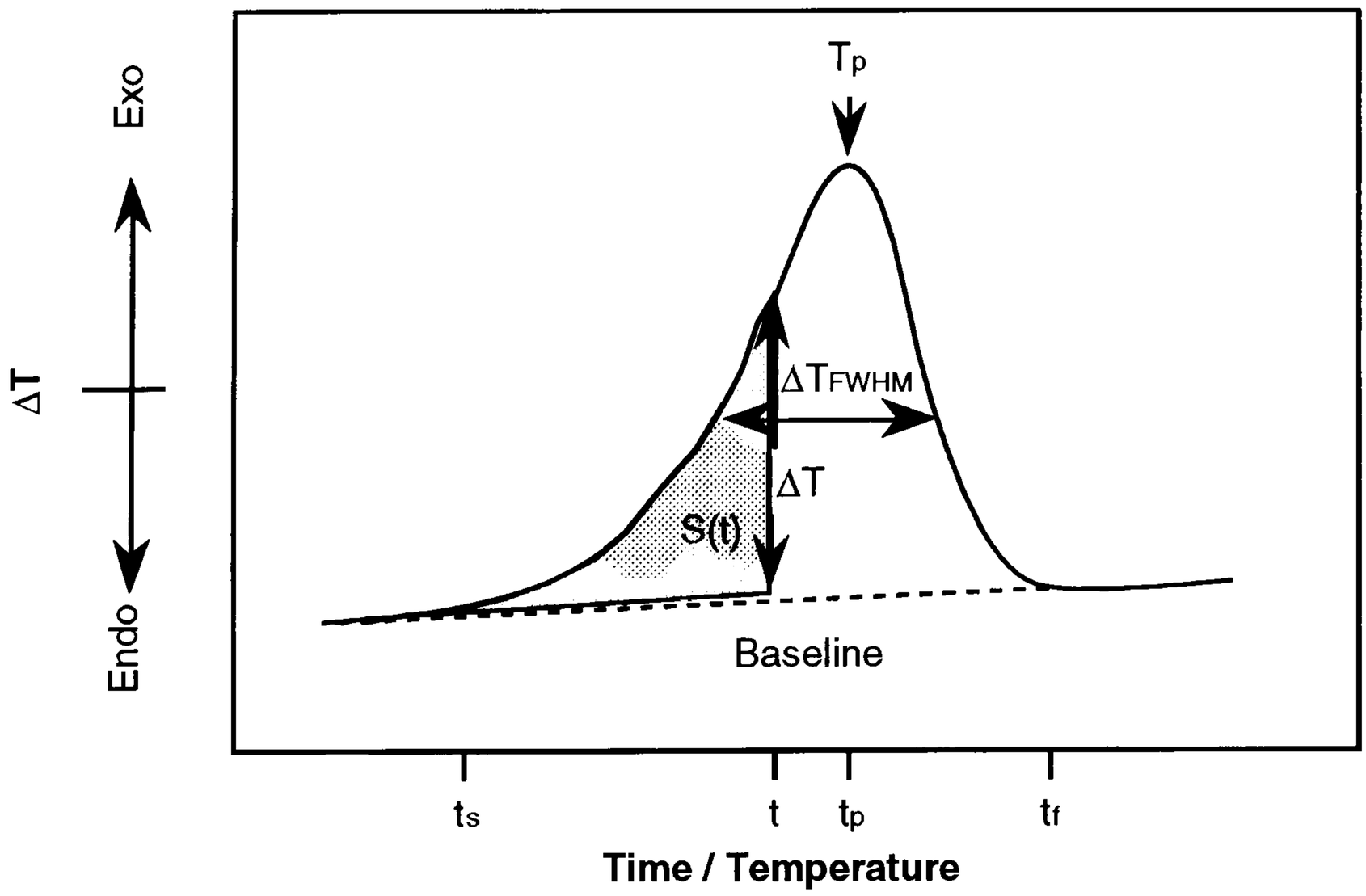


Figure 3-7 Typical crystallisation exotherm. Method for calculating volume fraction crystallised, S(t), in a time, t, and ΔT_{FWHM} is shown.

crystalline phase at a higher temperature appears as a minimum on the DTA curve. During crystallization of the glass an exothermic peak is observed because the enthalpy of the crystal is lower than that of the glass. The enthalpy corresponding to the area under the peak is equal to the heat of reaction. The fraction of glass crystallized at any time and/or temperature is proportional to the amount of heat evolved. Figure 3-7 illustrates the fraction of material crystallized at a time t, χ, which can be determined from the ratios of the area (S_t) between t_s (the time at which crystallization starts) and t, to total area (S_{total}) under the curve between t_s and t_f (the time at which crystallization is completed).

There are several factors which influence the shape and position of the differential thermal analysis peak but the dominant one is the nature of the reaction itself [Kissinger 1956 & 1957]. The shapes of the DTA crystallization peaks are closely related to mechanism of crystallization and therefore depend on factors such as the presence of nucleating agents: sharp peaks are indicative of bulk crystallization while broader peaks are indicative of surface crystallization. Other experimental variables are sample mass, size, and heating rate. The variation of peak temperature with heating rate is used to analyse the crystallization kinetics of glass. For a glass not containing any nucleating agent, and therefore undergoing surface nucleation, the temperature of the exothermic crystallization peak is a function of particle size. Since there is a larger total surface area with fine particles than with coarse particles, crystallization of the fine particles will occur at a lower temperature. However, if a nucleating agent is added, crystallization will take place simultaneously throughout the glass, i.e. bulk nucleation, and the difference between the crystallization peak temperatures of coarse and fine particles should ideally be zero.

Several researchers [Kissinger 1956; Matusita *et al* 1975; Sakka *et al* 1977; Augis & Bennett 1978; Marotta & Buri 1978; Matusita & Sakka 1979a and 1979b; Hayward *et al* 1987] proposed methods for determining the activation energy for crystal growth in glass from DTA curves through analysing the peak height and shape on the basis of the nucleation and growth equations. Assuming that the rate of increase of the volume

fraction of crystals, χ, reaches a maximum at a temperature T_p, all these methods are based on the Avrami treatment of transformation kinetics and define an effective crystallization rate coefficient having an Arrhenian temperature dependence. In general, however, the temperature dependence of the nucleation frequency is far from Arrhenian; and the temperature dependence of the crystal growth rate is also not Arrhenian when a broad range of temperature is considered [Uhlmann 1969]. Upon taking account of the temperature dependence of the crystallization rate coefficient, all the methods are shown to lead to similar conclusions [Yinnon and Uhlmann 1983].

All the mathematical methods for the analysis of data obtained from non-isothermal thermoanalytical studies of crystallization of glass-forming liquids are also based on the JMA treatment of transformation kinetics and define an effective crystallization rate coefficient having an Arrhenian temperature dependence. A modified form of the JMA equation (equation 3-8, cf 3-5) which takes into account the dependence of k on t is used for nonisothermal crystallization [Tang & Chaudhuri 1983].

$$-\ln(1-\chi) = \left(\int_0^t k(t)dt\right)^n \qquad [3\text{-}8]$$

Several of the most commonly employed methods of mathematical analysis have been critically reviewed by Yinnon and Uhlmann [1983]. They are mostly based on an equation developed by Kissinger [1957]:

$$\ln\left(\frac{T_p^2}{\beta}\right) = \frac{E}{RT_p} + C \qquad [3\text{-}9]$$

where T_p is the crystallization peak temperature (K),

β is the heating rate,

E is the activation energy for crystallization,

R is the gas constant, and

C is a constant.

A modification to the Kissinger method was made by Augis & Bennett [1978] through taking into account the temperature of the cold junction (T_0). They showed that

$$\ln\left(\frac{T_p - T_0}{\beta}\right) = \frac{E}{RT_p} + C \qquad [3\text{-}10]$$

The activation energy for crystallization is estimated from the slope (E/R) of a linear plot of either $ln(T_p^2/\beta)$ versus $1/T_p$ (Kissinger's method) or $ln(T_p-T_0)/\beta))$ versus $1/T_p$ (Augis-Bennett's method).

Augis & Bennett [1978] also noted that reactions with the same E but different n show a crystallization peak at the same temperature. The value of n determines the shape of the peak; the higher the value of n, the narrower the peak. They gave the following expression for estimating the value of n:

$$n = \frac{2.5}{\Delta T_{FWHM}}\left(\frac{RT_p^2}{E}\right) \qquad [3\text{-}11]$$

where ΔT_{FWHM} is the full width of the crystallization peak at half the maximum height (see Figure 3-7).

Weinberg [1991] and Matusita & Sakka [1979a] pointed out that precise interpretation of non-isothermal crystallization experiments must account for the nature of the crystal growth law. However, if one employs sufficiently slow heating rates and/or produces a sufficiently large number of nuclei in an experiment in which site saturation is evident, then one may interpret the data with Kissinger-like plots even though $k(T) \neq \exp(-E/RT)$.

3.2 Experimental Procedure

3.2.1 Microscopic techniques

Microscopy techniques, i.e. optical microscopy (OM), scanning electron microscopy (SEM), and transmission electron microscopy (TEM), were utilised to study the microstructural development of samples. Electron microscopy permits detailed study of the process of conversion of glass into a glass-ceramic material. In addition to qualitative evaluation of morphological changes, it also permits quantitative measurements, especially of the number of particles, their size and distribution, determination of the overall volume of the separated phase, etc. An image analyser was used to assist quantification of the microstructural parameters. Quantitative chemical

analysis was obtained via energy dispersive X-ray spectroscopy (EDS) and wet chemical analysis.

Samples for microstructural analysis were initially ground flat on a steel plate using alumina Lapmaster No 1400 grit in an ethane-diol slurry. Once flat, the specimens were polished on a diamond lapping wheel with 12-, 6-, 3-, and 1 μm diamond paste, respectively, until a scratch-free surface was obtained. After each polishing, samples were removed from the polishing disc and cleaned in an ultrasonic bath. Polished unetched samples were used to assess the porosity of materials. To enhance contrast for microstructural observation, the polished faces of some samples were etched using a 2 vol% HF solution for 15 seconds. The purpose of etching is to develop a visible image contrast by means of difference in corrosion resistance of different phases to the etching solution. Glass-ceramics in which a crystalline phase is precipitated form a glass phase, contain crystalline and residual glass phase. Owing to the difference in corrosion resistance to the etching solution, a visible image contrast between glass phase and crystalline phase is produced. In this study, the glass phase is less corrosive-resistant than the crystalline phase, if HF is used as an etching solution.

3.2.1.1 Optical Microscopy

Measurements of the thickness of surface crystallization layer were determined using a Reichert Nr 311237 optical microscope with a graticule in an eyepiece, and calibrated with a standard stage graticule. Polarised light was used to obtain additional contrast.

3.2.1.2 Secondary Electron Microscopy

Samples for secondary electron microscopy were mounted onto aluminium stubs using glue. The electrical conductivity of the samples is poor and thus it was necessary to paint the sides of the samples with silver dag to make electrical contact with the aluminium stub and then coat the surface with a conducting layer of gold, approximately 200 A° thick, by vacuum deposition to prevent charge build up during observation. The gold layer also assists in reflecting the light in optical microscopy. The samples were examined using a JEOL T-200 and JEOL T-220 scanning electron

microscope utilising both the secondary and backscattered modes at accelerating voltages of 15 or 20 kV.

Selected area quantitative chemical point analysis was obtained using a JSM-35 SEM equipped with energy dispersive x-ray spectroscopy and ZAF software. Samples were prepared as described in section 2.2.2.2.

3.2.1.3 Transmission electron microscopy

Transmission electron microscopy examination was employed to observe glass-in-glass phase separation using a JEOL-120CS microscope. Samples were cut from glass specimens and mounted on a metal substrate with a high temperature "Lakeside" temporary cement. This was followed by first mechanically polishing one surface of the sample and then grinding and polishing the opposite surface of the sample to a thickness ~100 μm. Acetone was used to wash the specimens and the samples were again mounted on the metal substrate with "nail varnish solution" and further polishing until a thickness of ~ 50 μm was achieved. The samples were again washed with acetone and glued onto a 3.05 mm diameter Cu-grid. The samples were transferred to an ion beam thinning machine (Gatan Dual Ion Mill) and using a liquid nitrogen cooled stage an Ar-ion beam was directed at the substrate until a hole was seen. At this point material at the edge of the hole was thin enough for TEM study and the specimens were coated with a carbon conducting layer by vacuum deposition to prevent charge build-up during observation.

3.2.1.4 Image analysis

An image analysis system consisting of an Olympus 386 computer running CUE-2 Morphometry software and linked to an Olympus BH-2 optical microscope via a Sony XC-77E CCD video camera module was used to evaluate the microstructure of specimens. SEM micrographs were used for the analyses and an average was taken from at least 5 measurements on different micrographs corresponding to different areas of the sample. More than 300 features were typically counted.

The specimens of glass to be examined were submitted, after quenching, to either single or double heat treatment. Single stage treatments were performed at temperatures between 740 to 980°C whereas double stage treatments were divided into a heat treatment at a nucleation temperature, T_n, in the range 550-690°C, followed by a growth treatment, T_{gr}, in the range 750-900°C. It should be noted that at the growth temperature, those pre-existing clusters with a size greater than the critical size at the growth temperature, D^*, will tend to grow while all others will shrink. To a very good approximation [Hammel 1966], the final number of observable crystals is simply the number of clusters for which diameter, D, is larger than D^*. Number of crystals per unit area, N_A, and D were determined and the average number of crystals per unit volume (N_v), was calculated using Hilliard's equation [Hilliard & Cahn 1961]:

$$N_V = \frac{N_A}{D} \qquad [3\text{-}12]$$

3.2.2 X-ray diffractometry

3.2.2.1 Identification of crystalline phases

Identification of phases, crystalline or glassy, was undertaken using X-ray diffraction (XRD) analysis of powder and bulk samples. A Philips PW 1710 X-ray diffractometer, with CuK_α wavelength 0.154178 nm and an internal program that automatically scanned through the desired 2θ range, was used to measure the intensity of the coherently scattered radiation from the specimens. All samples were placed on a silicon (111) single crystal disc which was spun during the measurements to reduce anisotropy effects. Solid samples were ground flat and polished to a 6 μm finish and mounted on the disc using plasticine whereas powder samples were ground to a fine consistency using an agate pestle and mortar. A thin layer of powder was deposited on the silicon disc by allowing an acetone slurry to evaporate. The analysis was performed on a diffractometer operating at 40 kV and 40 mA and continuous scanning was used at a scan speed of 1°/min. Diffraction patterns were indexed using JCPD (Joint Committee on Powder Diffraction) data cards.

3.2.2.2 Semi-quantitative analysis of crystalline and amorphous phases

A British Standard method (BS6699:1986) was employed for the determination of the crystallinity content of glass-ceramics. A typical x-ray diffraction pattern of a glass-ceramic consists of diffraction peaks produced by the crystalline components, the broad diffraction effect (hump) produced by the glassy (amorphous) material, and a background component which is essentially linear. This is shown schemetically in Figure 3-8. The ratio of the integrated intensity arising from the crystalline material (i.e. the area above the linear background) to the integrated intensity of the amorphous halo is a measure of the crystalline content of the glass-ceramics.

The calculation is made by firstly drawing a straight line across the diffraction pattern such that it passes through those places in the pattern (see Figure 3-8) having d-spacings of 0.404 nm and 0.237 nm (i.e. at 22.0° and 38.0° (2θ) respectively). This line represents the linear background associated with the diffraction pattern. The areas which are contained within the regions defined by these d-spacings and which are above the linear background only are taken into consideration in the calculation. This is followed by the definition of the amorphous region between 0.404 nm and 0.237 nm by drawing a line through the mid-point of the variation of the diffracted intensity representing the hump and interpolating its path below those diffractions which are due to crystalline material. Then, those parts of the paper delineated as representing the peaks and the amorphous region are cut out and each of these areas are weighed to the nearest 0.001 gram. Finally, the percentage of the crystallinity is determined from the following equation:

$$\text{Crystallinity } (\%) = \frac{W_1}{W_1 + W_2} \times 100 \qquad [3\text{-}13]$$

where W_1 and W_2 are the weight of the paper representing the peaks and the amorphous region respectively.

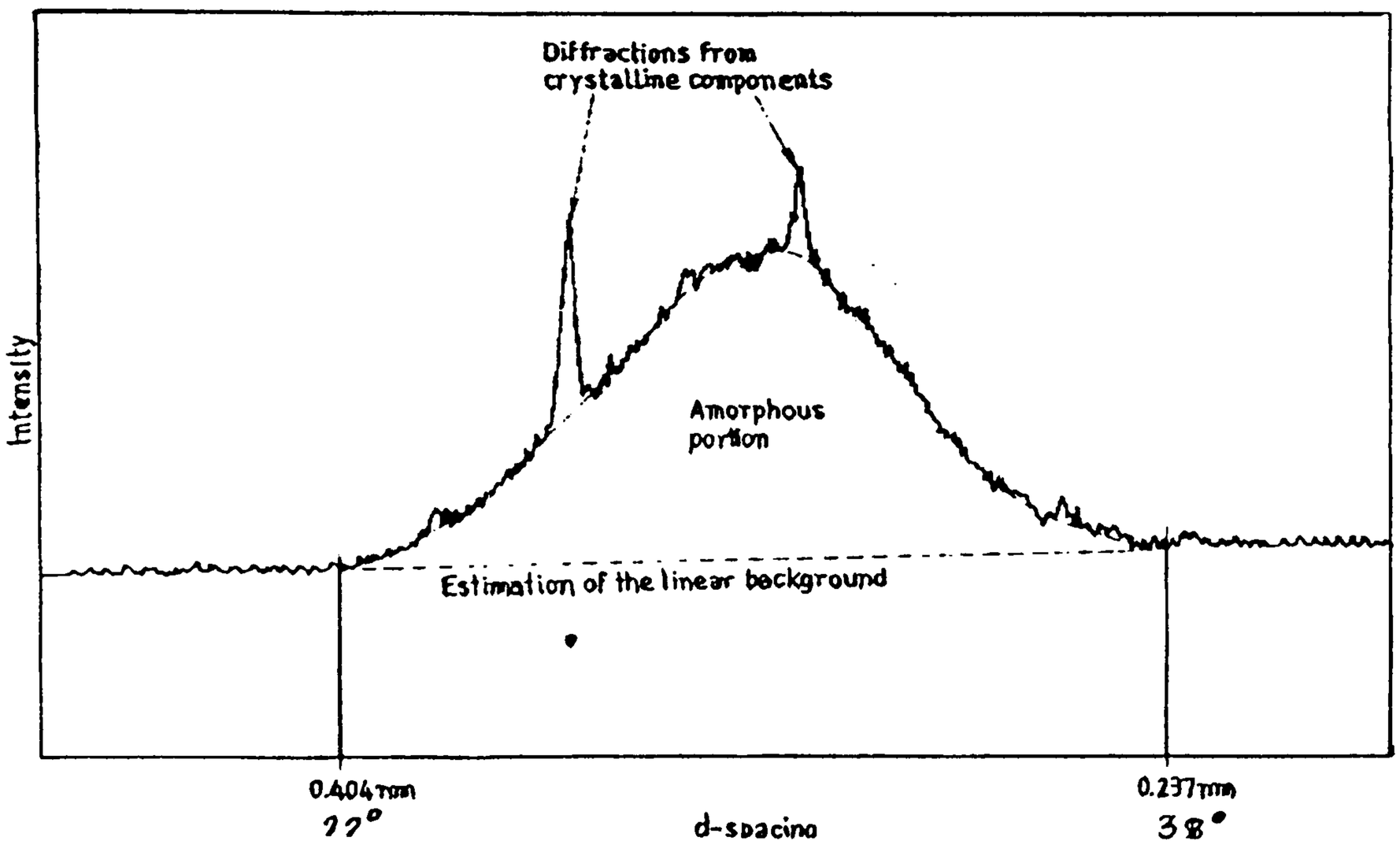


Figure 3-8 Schematic representation of a portion of an x-ray diffraction pattern of a glass-ceramic.

3.2.3 Differential thermal analysis

3.2.3.1 Determination of activation energy

The DTA equipment and experimental settings have been previously described in section 2.2.5. The experiments were conducted from room temperature up to 1200°C at heating rates of 5, 10, 15, 20, 25, 30°C/min. Samples of different forms, i.e. powder, bulk cast, and molten glass, were employed. Powder samples were crushed, ball-milled and sieved to produce a particle size <38 μm. To reduce the effect of surface crystallization, small bulk samples of approximate weight 50 mg were cut from a large glass casting. A flat surface was ground on one face of the bulk sample to obtain good thermal contact with the platinum crucible.

The isothermal glass transition and crystallization temperatures were obtained from extrapolation of the values at different heating rates. For analysis of the data acquired, Arrhenius-type equations which had been adapted by Kissinger [1957] (Eq. 3-9) and Augis & Bennett [1978] (Eq. 3-10) were used to calculate the activation energies.

3.2.3.2 Determination of nucleation-rate-curve

A number of DTA methods [Marotta *et al* 1982, Ray & Day 1990, and Weinberg 1991] have been proposed for the determination of the temperature dependence of crystal nucleation rates in glasses via DTA measurements. It was proposed that the total number of nucleations per unit volume, N, is given by the sum of (a) the surface nucleation, N_s, (b) the bulk nucleation formed during the DTA run, N_b, and (c) the bulk nucleation formed during the previous heat treatment of nucleation, N_n. Owing to the low specific surface of the bulk sample and to the high heating-rate (15°C/min), the difference between the crystallization peak temperature, $T_{p'}$, or peak height, H_p, of the as-quenched sample and of the previously-nucleated sample can be expressed as a function of the nucleation number, N_n, forming during heat treatments. When these parameters are plotted as a function of the nucleation temperature, the graph closely resembles the classical nucleation rate curve.

The CS and CSF glass powders were heat-treated in the selected nucleation range for 3 hours and then the heating continued up to 1200°C. The height of the crystallization peak and the peak temperatures were then measured. The nucleation-rate-like curves were obtained from plotting these parameters against the nucleation temperatures.

3.3 Results and discussion

3.3.1 Kinetic of crystallization

3.3.1.1 Differential thermal analysis (DTA)

In Figure 3-9, DTA profiles obtained at a heating rate of 15°C/min show the typical effects of fluoride addition to bulk samples. Several thermal events can be observed. The CS glass exhibits one small peak temperature at 1125°C while CSF powder shows two exothermic peaks, one at 763±5°C representing the crystallization of cuspidine, and the other at 882±5°C corresponding to the crystallization of wollastonite (see section 3.3.1.2 for phase identification). It can be seen that the fluoride had some significant effects on the crystallization kinetics, i.e. lowering the crystallization temperature to about two-thirds of the fluoride-free crystallization temperature and, from the area under the curves which indicates the degree of crystallization (exothermic reaction), increased the degree of crystallization up to approximately 10 times.

Table 3-3 shows the thermal characteristic constants of these samples derived from the DTA runs at different heating rates. In order to calculate the isothermal temperatures of the reactions, i.e. the temperatures where crystallization started (T_x) and the crystallization peak temperature (T_p), extrapolation curves of heating rates vs T_x and T_p were plotted in Figure 3-10. The isothermal temperature so obtained are presented in Table 3-3 together with R^2, correlation coefficient. The extrapolated values at zero heating rate (isotherm) for the temperatures when crystallization started, T_x, and crystallization peak, T_p, derived from DTA profiles, with accuracy of ±5°C, are 958 and 1108°C for CS glass, and 802 and 822°C for CSF glass, respectively.

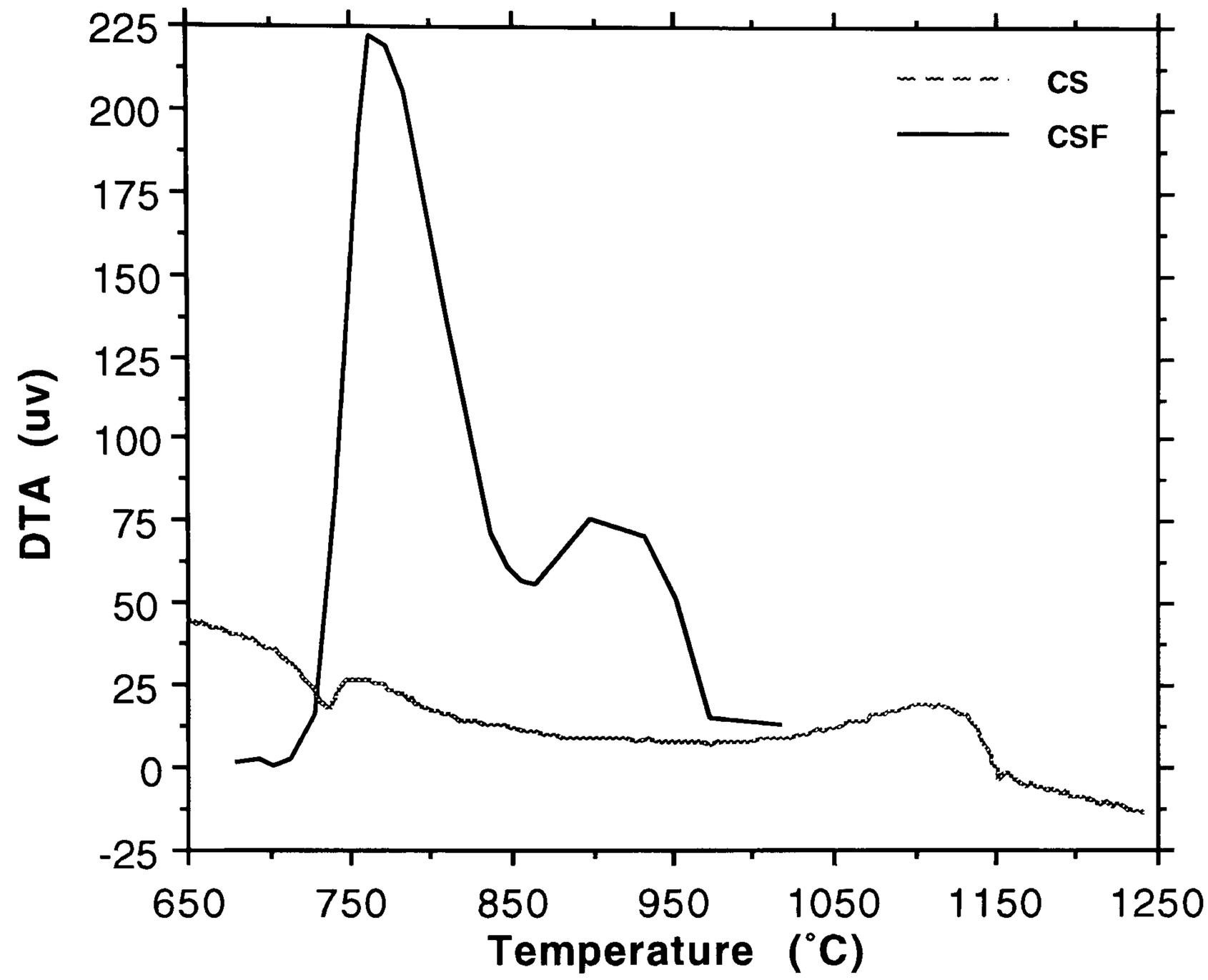


Figure 3-9 DTA plots of CS and CSF bulk glass at a heating rate of 15˚C/min.

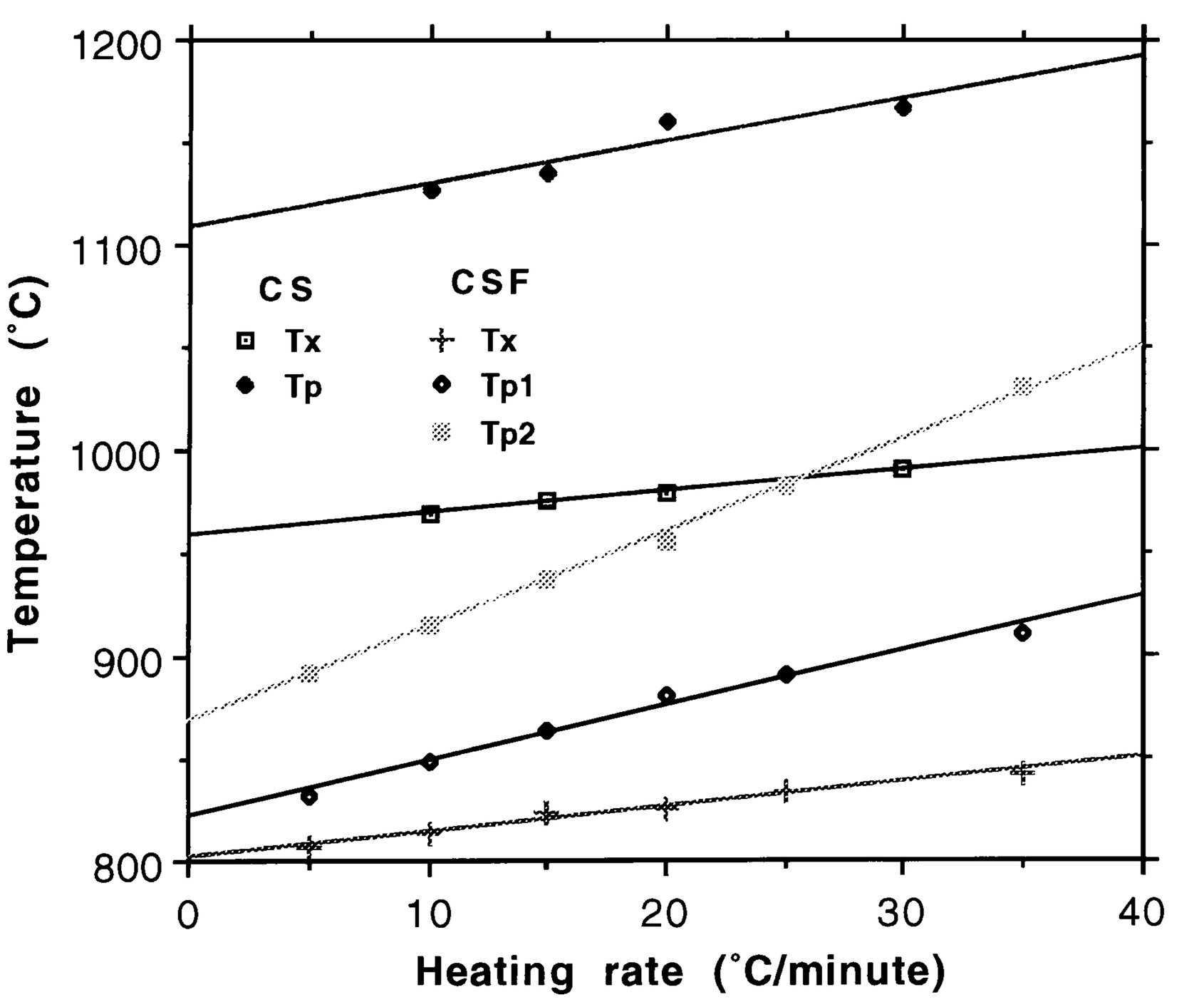


Figure 3-10 Variation of characteristic temperatures (T_x,where crystallisation has started and T_p, at the crystallisation peak temperature) with heating rate for CS and CSF bulk glasses.

The data were analysed via Kissinger's (Eq.3-9) and Augis & Bennett's (Eq.3-10 and 3-11) methods to determine the activation energy for crystallization and the Avrami exponent. The plots for the two glasses are compared in Figure 3-11 and the kinetic parameters for crystallization are shown in Table 3-4. Activation energy for the initiation of crystallization (E_a at T_x) in CS glass closely resembled the Ea at T_g (985 kJ/mol-- see Table 2-9) whereas in CSF glass the E_a at T_x was slightly lower than the E_a at T_g (616 kJ/mol) indicating that the atomic arrangement of the CS glass before crystallization was very similar to that at the glass transition temperature.

The activation energy at T_p for CS was close to that of calcium ion diffusion in glass (466* kJ/mol) [Bansal & Doremus 1986] while the Ea at T_p of the first peak for CSF was similar to that of sodium ion diffusion in glass (96† kJ/mol) [Frischat 1970], which is in agreement with the work done by Mukherjee & Rogers [1968]. E_a at T_p for the second peak in CSF was slightly higher than that from the first peak. Nevertheless, it is still of the same order as that for sodium ion diffusion. The greater mobility of Na^+ ions in the glass, as compared with Ca^{2+} ions, will lead to greater reactivity of the glass phase and hence higher crystallizability. The Avrami exponents indicate that surface crystallization (0.78) predominates in CS glass whereas bulk crystallization (3.01) predominates the first peak in CSF glass.

3.3.1.2 Crystal phase identification

The crystallising phases in these glasses were examined by XRD analysis in terms of d-spacing and relative peak intensities compared with the JCPDS patterns. Typical XRD patterns of crystallized CS glass were identified as wollastonite, whereas crystallized CSF glass contained cuspidine or a mixture of cuspidine and wollastonite depending on heat treatment; these are illustrated in Figure 3-12a.

In order to identify the sequence of crystallization in CSF glass, a series of heat treatments were performed and the crystalline phases evolved were identified. The

---

* Ca diffusion in $Na_2O{\cdot}2CaO{\cdot}3SiO_2$ glass in temperature range 460-600°C

† Na diffusion in SiO_2 glass in temperture range 600-800°C

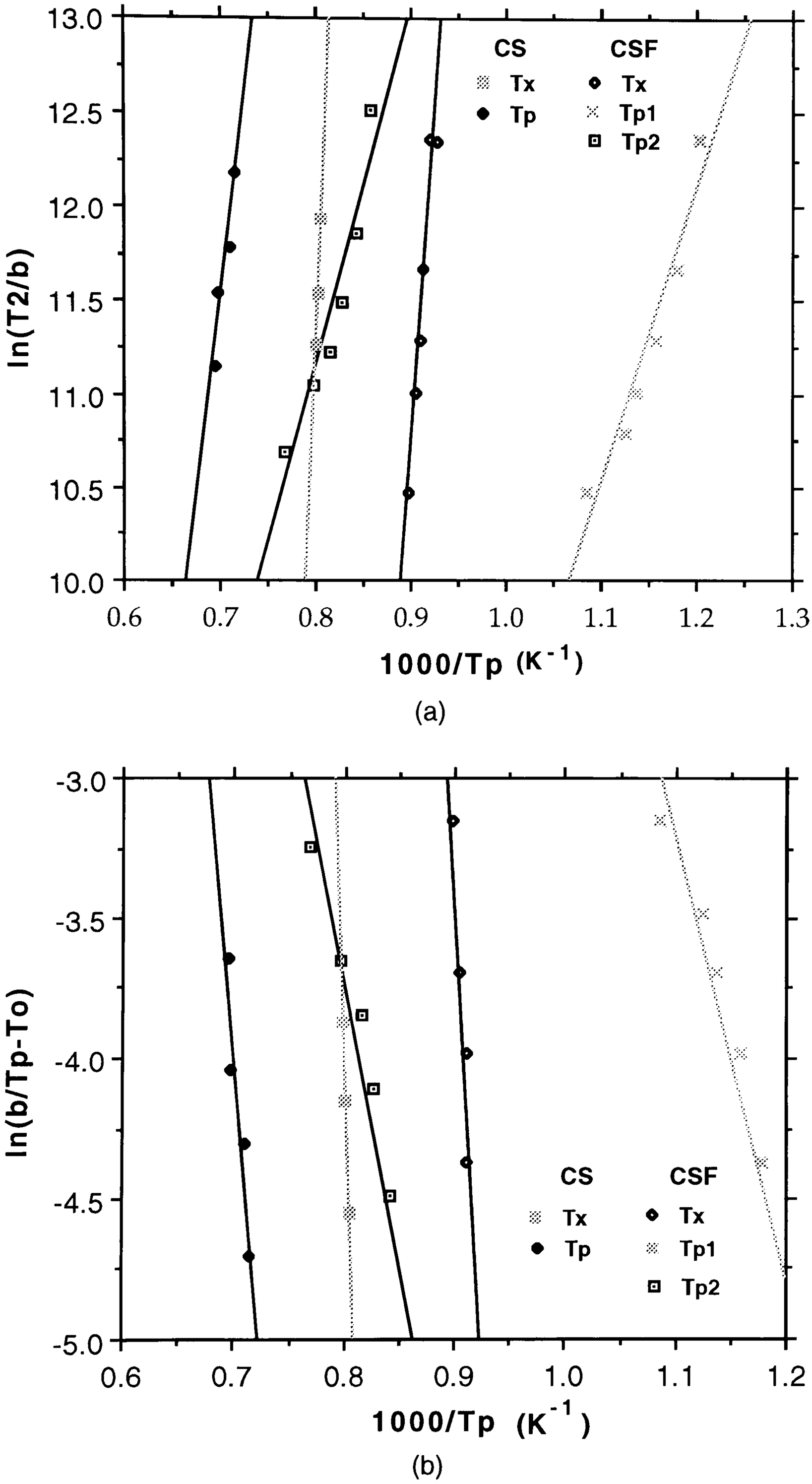


Figure 3-11 Arrhenius plots of CS and CSF bulk glasses calculated from (a) Kissinger's, and (b) Augis-Bennett's equations.

Table 3-3 Thermal characteristics constants of bulk cast CS and CSF samples.

Heating rate	CS		CSF		
	T_x	T_p	T_x	T_{p1}	T_{p2}
10	969	1127	813	848	916
15	974	1135	824	864	937
20	978	1160	825	879	954
25	-	-	833	890	981
30	990	1167	-	-	-
35	-	-	842	911	1030
Isotherm*	958	1108	802	822	868
R^2	0.989	0.879	0.971	0.987	0.997

*isotherm is the isothermal temperature obtained by extrapolation to zero heating rate

Table 3-4 The apparent activation energy for the initiation of crystallisation and the crystallisation peak range.

Sample	Temperature	Kissinger		Augis-Bennett	
		Ec (kJ/mol)	R^2	Ec (kJ/mol)	R^2
CS					
	T_x	986	0.996	994	0.966
	T_p	366	0.904	374	0.908
CSF					
	T_x	566	0.953	572	0.953
	T_p(1st peak)	130	0.941	132	0.842
	T_p(2nd peak)	159	0.923	167	0.932

Table 3-5 Intensity of wollastonite I (d-value 2.98 ˚A) compared with the intensity of cuspidine (Io) (d-value 3.26 ˚A) heat treated at 660˚C for 3 hours and then at different growth temperatures for 30 minutes.

Sample designation	Growth temperature (˚C)	I/I_0
660-800	800	-
660-900	900	62.2
660-980	980	85.8

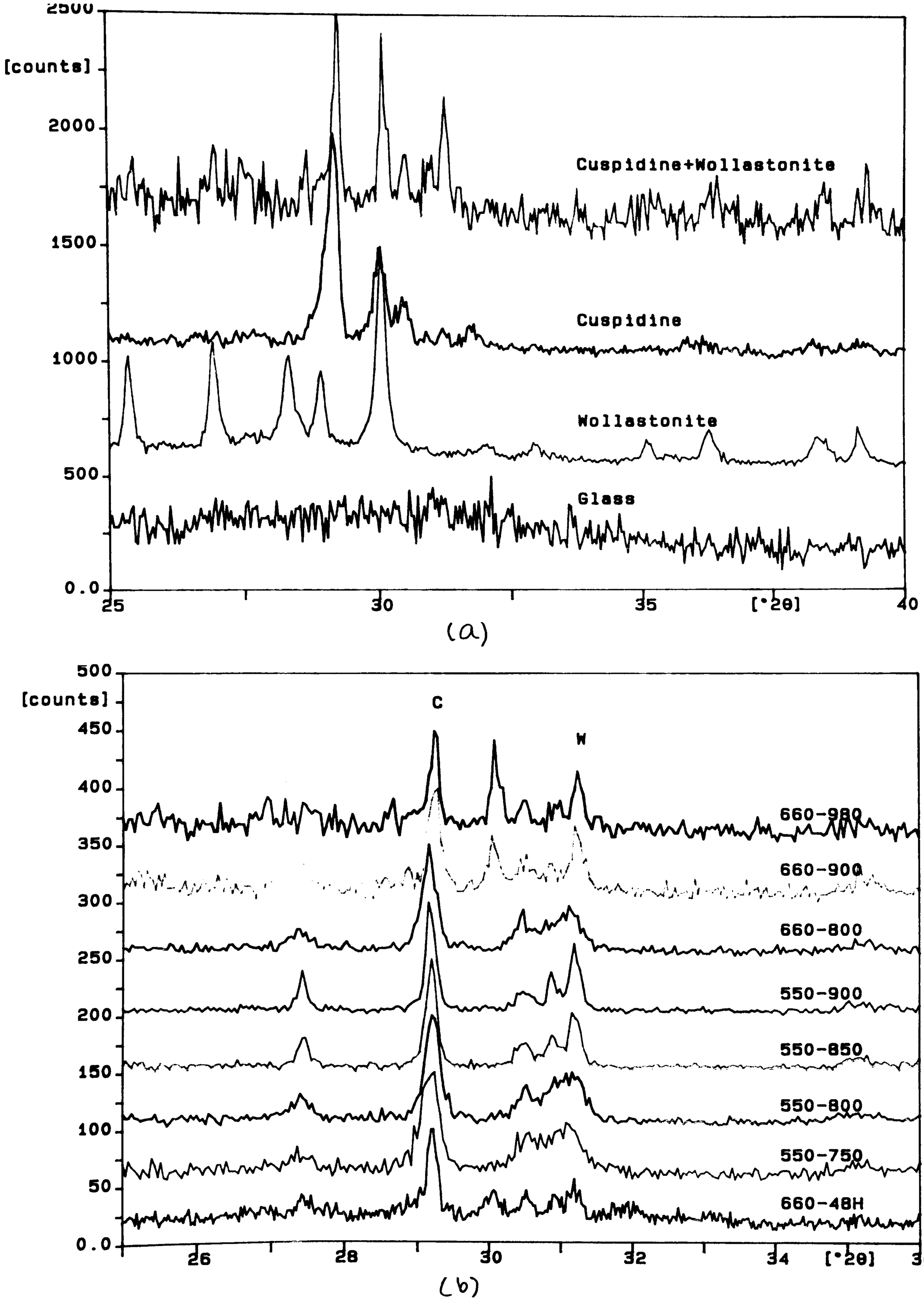


Figure 3-12 X-ray diffraction profiles of heat treated (a) CS (wollastonite) and CSF (cuspidine and a mixture of wollastonite and cuspidine) samples, and (b) CSF samples heat treated at 550°C or 660°C for 3 hours followed by growth treatment at 750, 800, 850, 900, or 980°C for 30 minutes.

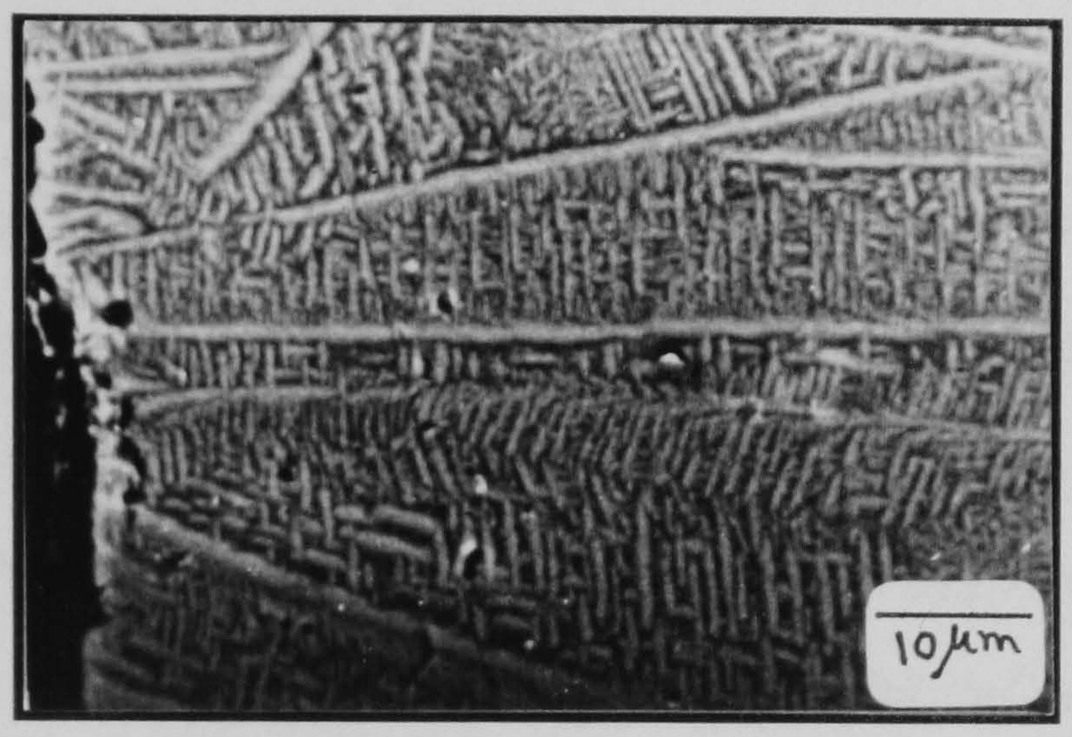
results are summarised in Figure 3-12b. It can be seen that both nucleation and growth temperatures profoundly affect the crystallising phases. The x-ray pattern from samples that have undergone only nucleation treatment at 660°C for 48 hours revealed that cuspidine was present. Nucleation at 550°C only gave rise to one crystal phase, cuspidine, at growth temperatures, while nucleation at 660°C leads to crystallization of cuspidine at growth temperature ≤ 800°C, but crystallization of both cuspidine and wollastonite occurs at growth temperature ≥ 900°C. This implies that, in CSF glass, cuspidine is the major crystalline phase below 800°C and wollastonite occurs as the second phase at temperature higher than 900°C. The intensity of the wollastonite peak, with a d-value of 2.98, (compared to the intensity (I_0) of the peak with a d-value of 3.26, representing the highest peak for cuspidine), increased with increasing temperature above 900°C, suggesting that the proportion of wollastonite was greater the higher the temperature (see Table 3-5).

3.3.2 Microstructural development

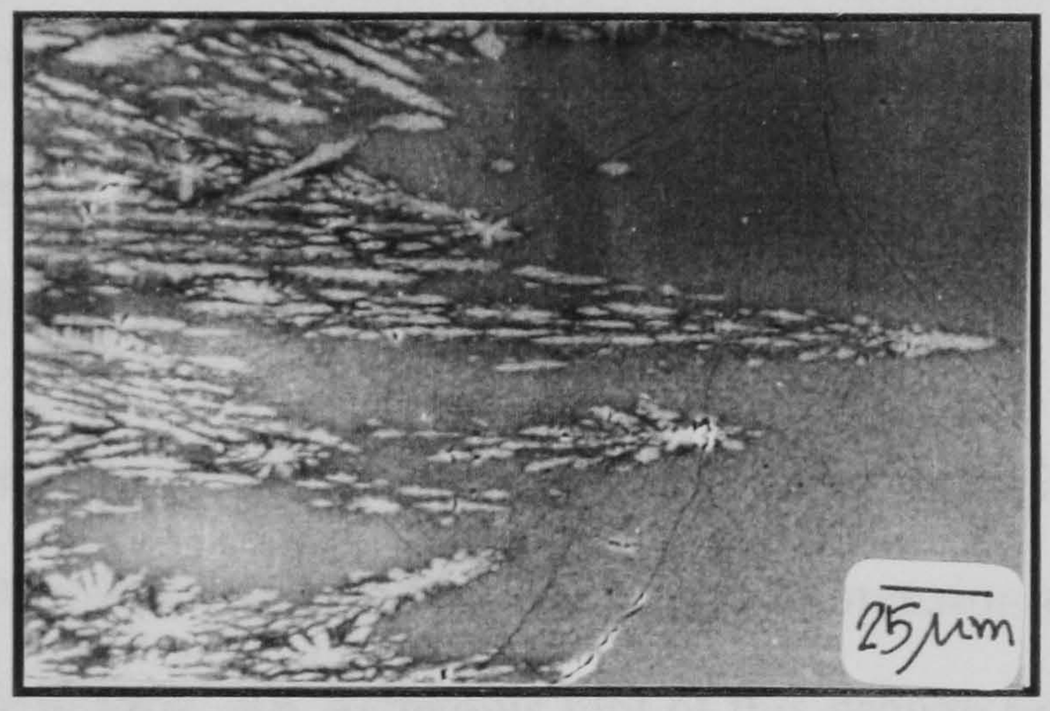
3.3.2.1 CS glass

(i) Single stage heat treatment

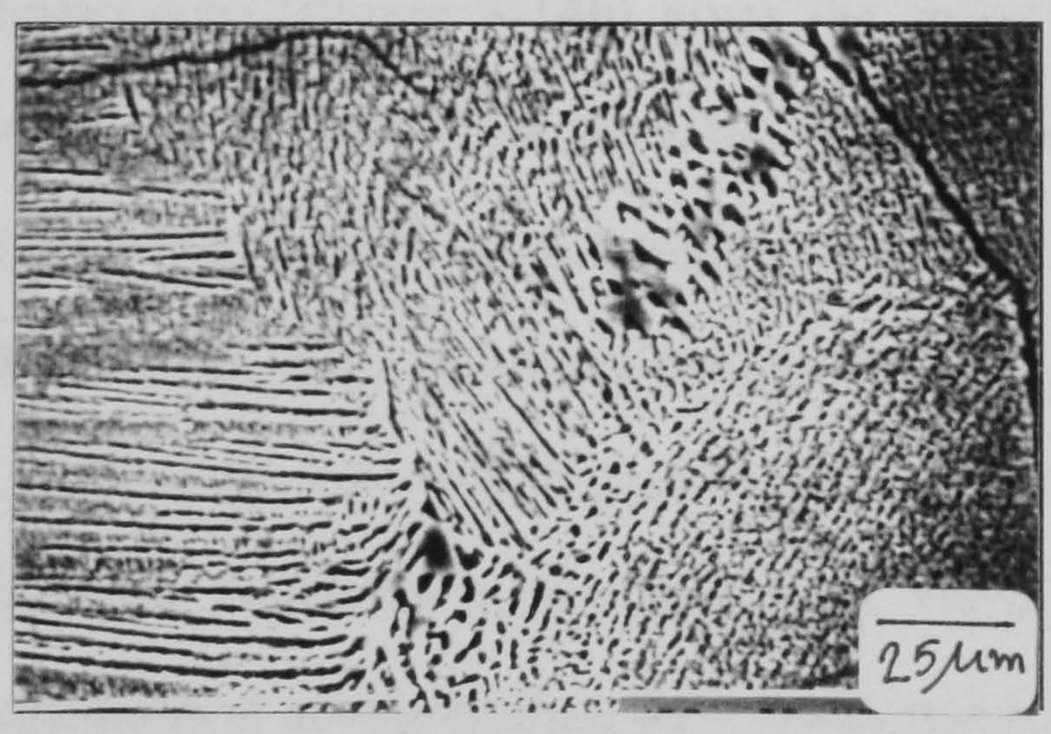
This section is concerned with the microstructural development in samples heat treated in the growth temperature range without any prior nucleation heat treatment. No heat treatment, in the range 800-950°C, was found to cause homogeneous nucleation and volume crystallization in CS glass. However, a surface-nucleated crystalline layer was observed and found to be composed mainly of crystals growing in a fibrous manner with a strong preferential orientation approximately normal to the specimen surface (Figure 3-13a). The primary crystallization was followed by secondary crystallization of residual glass trapped between the primary crystals. These secondary crystals grew perpendicular to the primary crystals and parallel to the surface. Both types are in acicular form but the former were much longer than the latter. At higher heat treatment temperature (950°C) the crystals were developed in coarser morphology (Figure 3-13b).



(a)



(b)



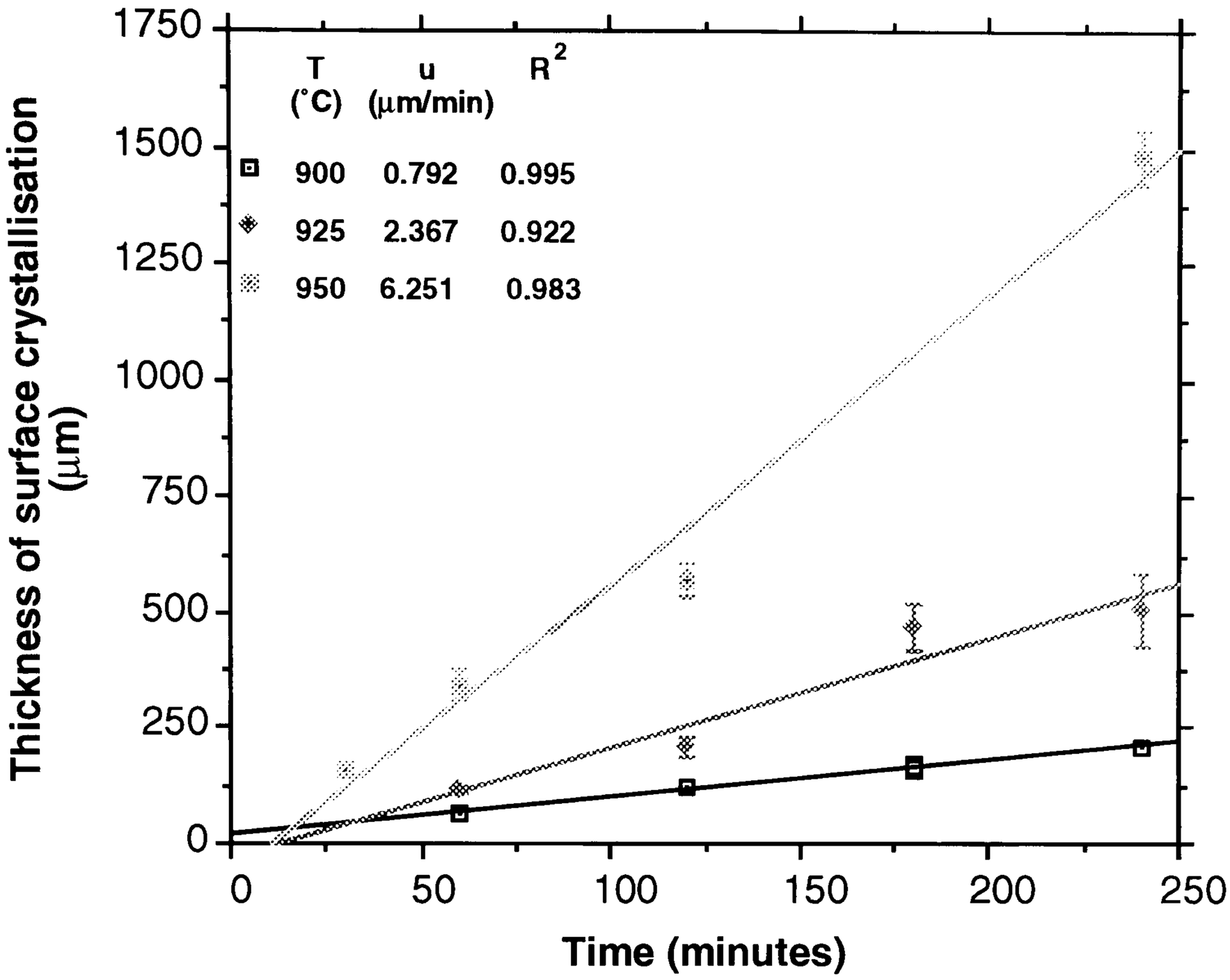
(c)

Figure 3-13 Surface crystallisation in, (a) CS glass heat treated at 900˚C, (b) at 950˚C for 60 minutes, and (c) showing microcracks at the plane of weakness and in microstructure.

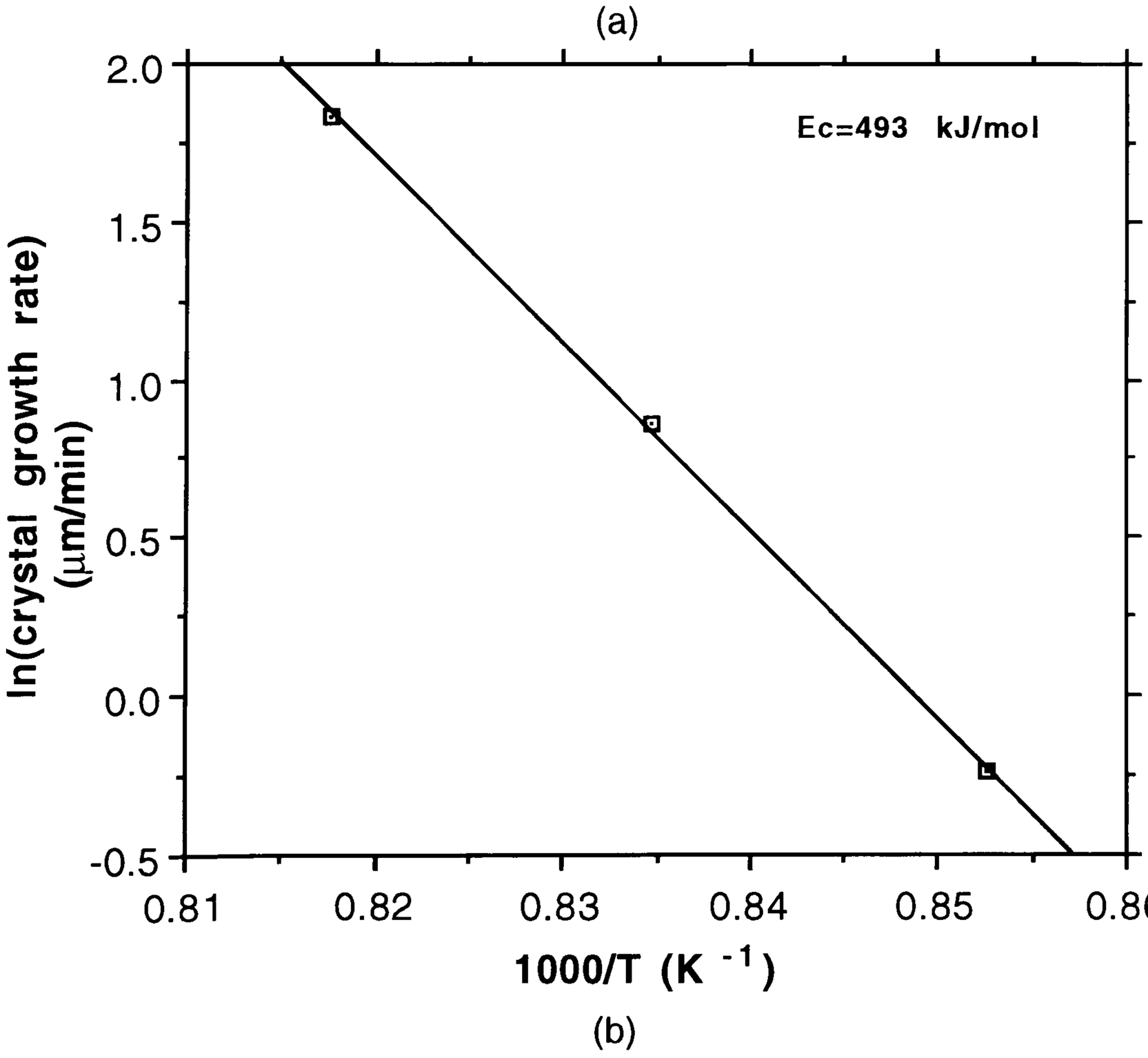
As the crystals grow further, a plane of weakness is formed where the crystal fronts meet (Figure 3-13c). Some cracks appear to be associated with a plane of weakness whereas others seem to ignore this microstructural features.

The CS glass crystallized from the surface with wollastonite crystals. The composition of the CS glass (approximately $CaO{\cdot}2SiO_2$) was different from that of wollastonite crystals ($CaO{\cdot}SiO_2$); i.e. there was a higher concentration of SiO_2 in the glass matrix. The high viscosity of this composition retarded the wollastonite to grow laterally. The protuberance was the only way that crystal can grow and thus giving rise to fibril structure, thus the crystals grew in fibrous manner toward the centre of the glass bulk. Therefore the kinetics of crystal growth appear to be governed by rearrangements in the glass in front of the growing crystal and growth is interface-controlled while the morphology seemed to be determined by the decreased rate of diffusion in the 'impurity' enriched region around the crystals.

The results of the measurements of crystal growth under optical and scanning electron microscopes are given in Figure 3-14a. The largest dimension of the primary crystals increased linearly with time. An Arrhenius plot of this growth rate against reciprocal of absolute growth temperature (Figure 3-14b) gives the activation energy of crystal growth as 493 kJ/mol which is higher than the value obtained from DTA profiles at T_p, 366 kJ/mol. Considering that the former technique was performed isothermally in the temperature range 800-950°C while the latter was performed at different heating rate giving $T_p > 1100$°C and that the viscosity of glass is very sensitive to the heating rate, it could be deduced that these values are in the same range. The large activation energies suggest that simple diffusion is not controlling the growth kinetics [Freiman *et al* 1971]. They are in the same range as the bond strength of glass-forming oxides, compared to the Sun's bond-strength criterion (section 2.1.1.1(iii)), or as the activation energy for diffusion of glass-forming or intermediate species (see Table 3-6).



(a)



(b)

Figure 3-14 CS surface crystallisation (a) thickness of surface crystal layer obtained from several crystallisation temperatures as a function of time, and (b) Arrhenius plot for calculation of activation energy for crystallisation ,Ec

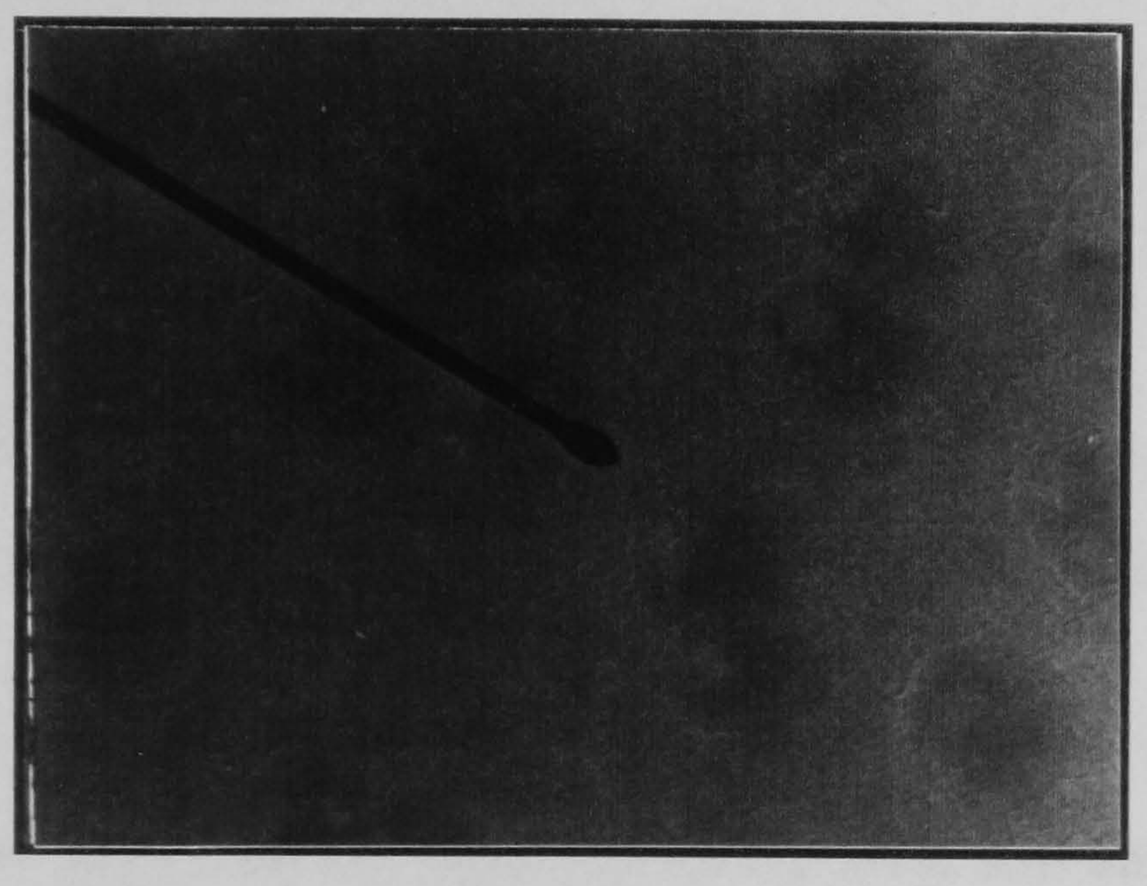


Figure 3-15 TEM micrograph showing amorphous phase separation in CSF glass heat treated at 660˚C for 20 hours.

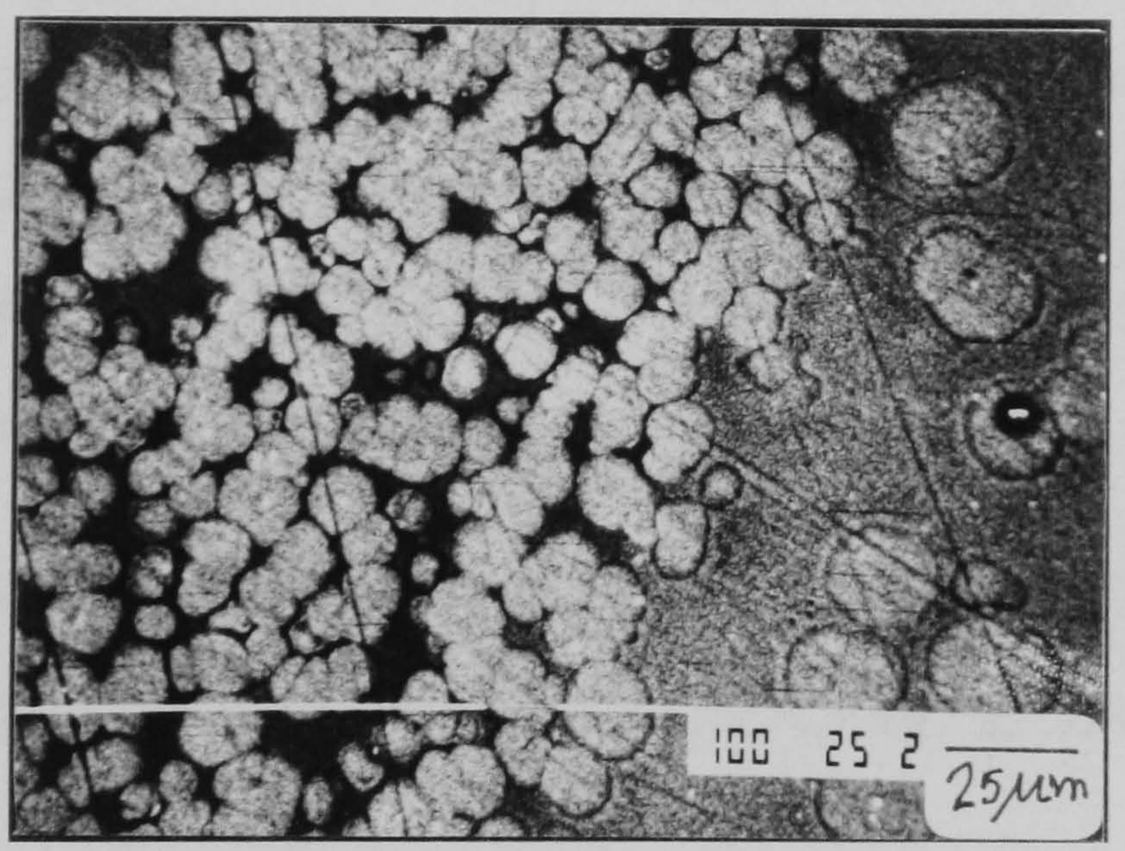


Figure 3-16 Backscattered image of opalescent glass heat treated at 750˚C for 60 minutes.

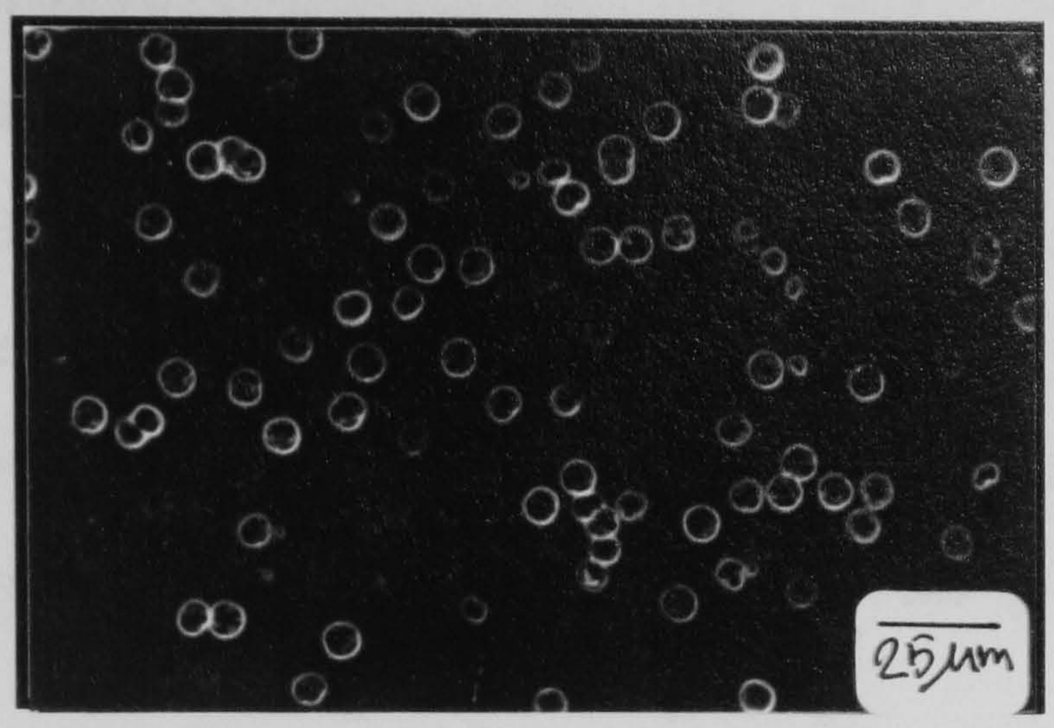
A backscattered image of the opalescent glass revealed that spherical nuclei occurred preferentially in the area rich in the element of lower atomic weight (Figure 3-16). Moreover, the rim of the nuclei appeared darker than the nucleus itself with a lighter halo on the periphery. SEM/EDS microscopic examination (Table 3-7) indicates that the nuclei are Ca-rich whereas the residual glass matrix is Na-rich. The nominal Ca:Si ratio in the base glass is 0.43. When heat treated, the Ca:Si ratio tends to remain constant at 0.50 in the crystal nuclei, while it tends to decrease in the glass matrix; i.e. the residual glass is Si-rich and thus giving rise to higher viscosity. On the other hand, the Na:Al ratio in the crystals is reduced from 1.14 to ~0.4 when heat-treated at a temperature lower than 800°C and to ~0.25 at a temperature higher than 800°C.

The development of the amorphous droplets may be induced by the fluoride ions to form cuspidine-like glass droplets whose structure, while still amorphous, has atom arrangements similar to those in cuspidine. This is supported by the EDS analysis which shows that the nuclei are Ca-rich. In addition, there is a striking difference between Na:Al ratio in nuclei and in matrix. In most cases, this ratio in the nuclei is much lower than in the matrix, which implies the diffusion of Na^+ ions away from the nuclei or the Na^+ ions are dispelled from the crystal phase as '*impurities*'. Presumably, the enrichment of the glassy phase with Na^+ ions at the boundary between the spherulite and the glass during the first stages of spherulitic crystallization lowers its viscosity and more readily allows subsequent crystallization to proceed.

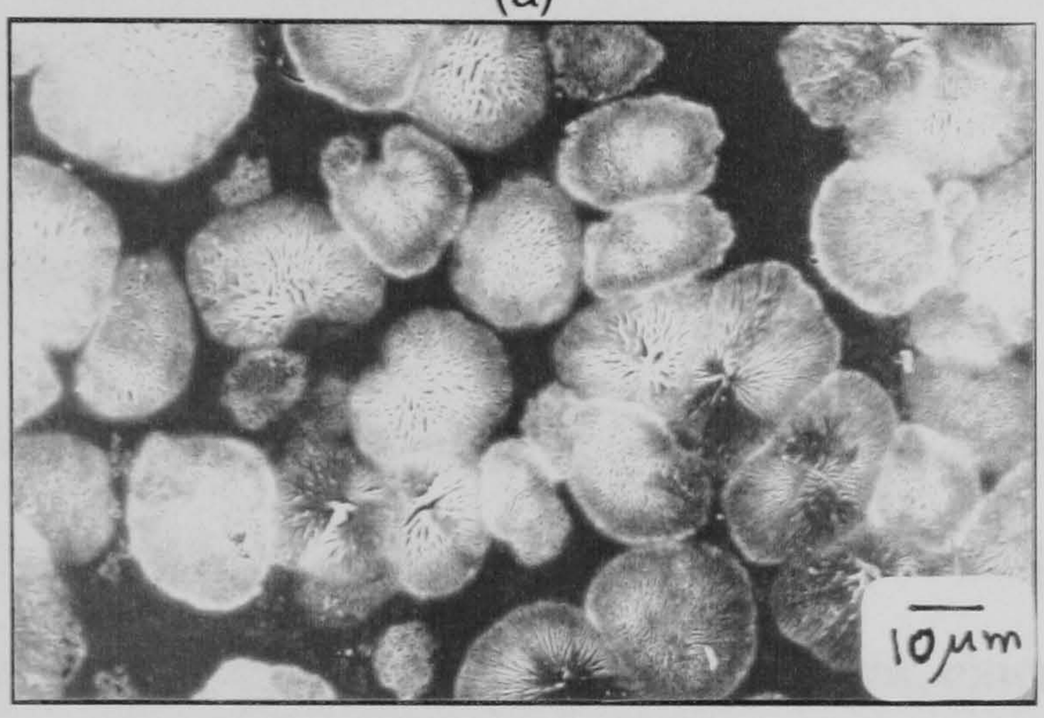
Figure 3-17 shows the development of nuclei into spherulites which are formed at a temperature higher than the nucleation range, e.g. 740, 820, 900, and 980°C. At 740°C,

Table 3-7 Quantitative EDX analysis of samples undergoing various heat treatments.

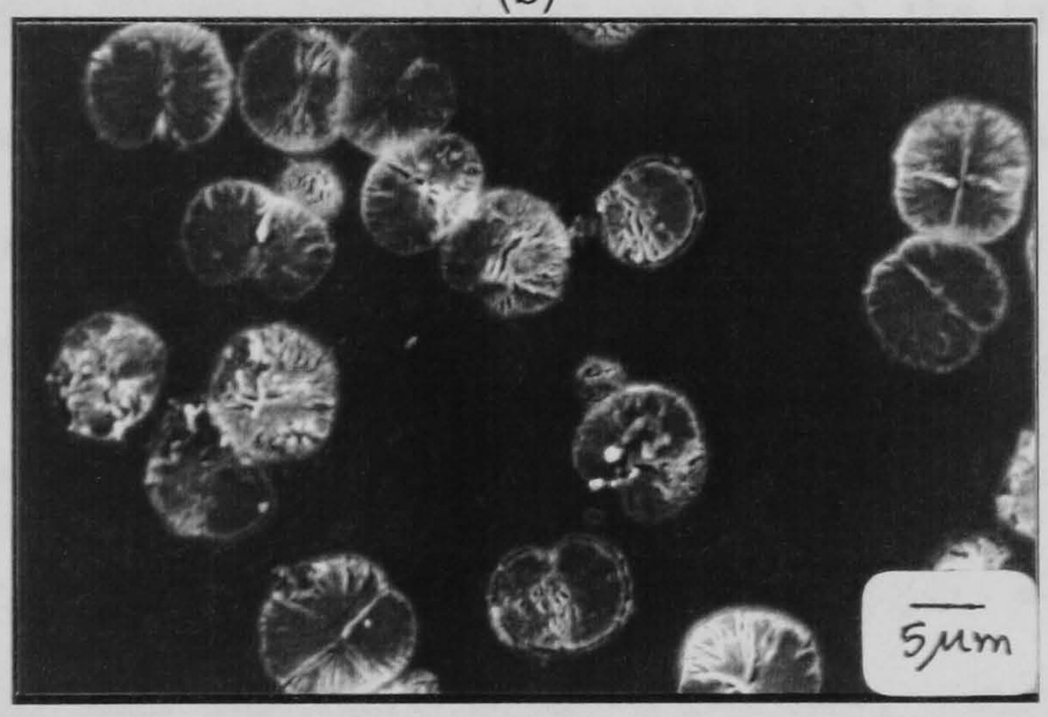
Heat treatment		**Element mol ratio**			
time	temperature	Ca:Si		Na:Al	
(mins)	(°C)	nuclei	matrix	nuclei	matrix
10	900	0.43	0.43	1.14	1.14
60	820	0.50	0.40	0.43	1.33
60	850	0.50	0.25	0.25	0.83



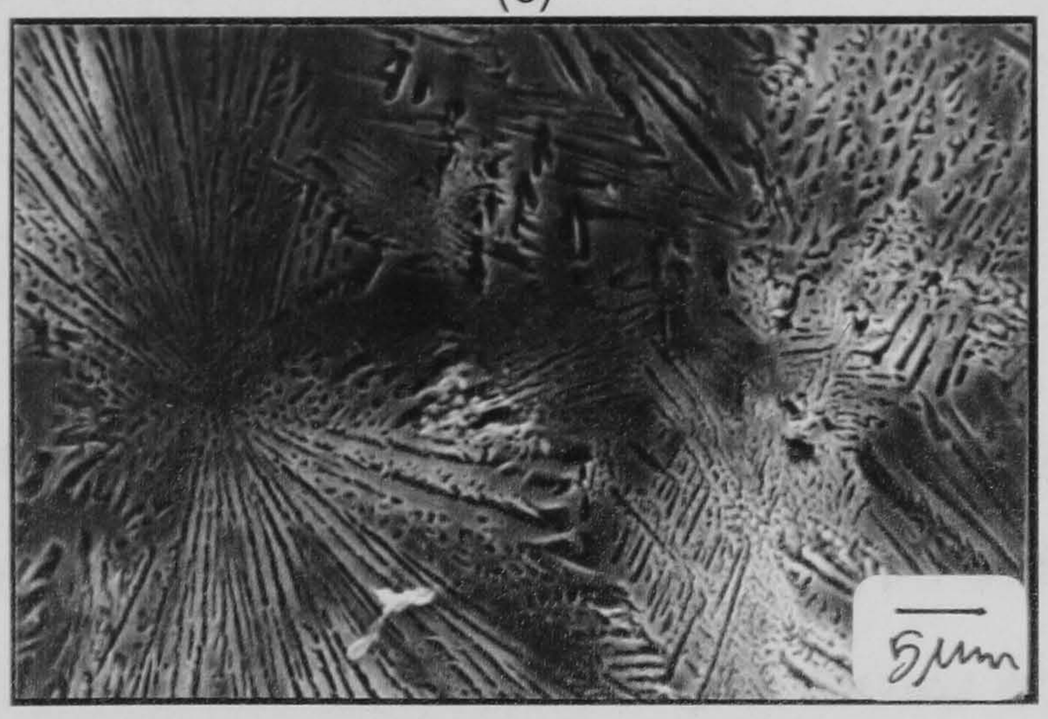
(a)



(b)



(c)



(d)

Figure 3-17 The development of nuclei into spherulites having undergone a single stage heat treatment at (a) 740˚C 60mins, (b) 820˚C 60 mins, (c) 900˚C 10mins, and (d) 980˚C 20 mins.

glass droplets were formed (x-ray diffraction results of this sample shows no crystalline phase), and seem to remain the same size no matter how long the heat-treatment was continued (Figure 3-18). On the other hand, the crystallites started to form from the centre of the droplets at 820°C and grew with time. Needle crystals radiate from the centre at 900°C giving a spherulitic structure and as spherulites impinge upon each other, a more mishaped and irregular spherulite microstructure is formed (see 980°C micrograph).

(ii) Double stage treatment

Effect of nucleation treatment

Different types of spherulites were observed in samples given different nucleation treatments (Figure 3-19). When undergoing high nucleation temperature, the individual crystals, radiated from a common centre to form spherulites, extended in length and also grew laterally to form thicker rods. On the other hand, the sample which had been nucleated at a low temperature exhibited fine crystals. It was suggested by Keith and Padden [1963] that the presence of small quantities of mobile impurities in a glass can have a significant effect on the crystallization process and that spherulites with different rugosities have been predicted for systems where the diffusivity of impurities can be altered. In this system, the diffusivity of Na^+ ions also altered in the residual glass since the composition of the glass changed with time/temperature. It was found that prior heat treatment affects morphology of spherulites in such a way that the fibrous structure was more refined when the sample was treated at temperature just higher than the glass transition temperature than at higher temperatures.

Figure 3-20 shows the effect of growth time on the number of nuclei on specimens heat-treated at various nucleation temperatures for 30 minutes and then given a growth treatment at 750°C. The nuclei number density decreases dramatically within 20 minutes for all nucleation temperatures and was rather insensitive to growth temperature at longer growth times. Similarly, the size of nuclei in the initial period of 20 minutes was very sensitive to the nucleation time, but after 30 minutes any further

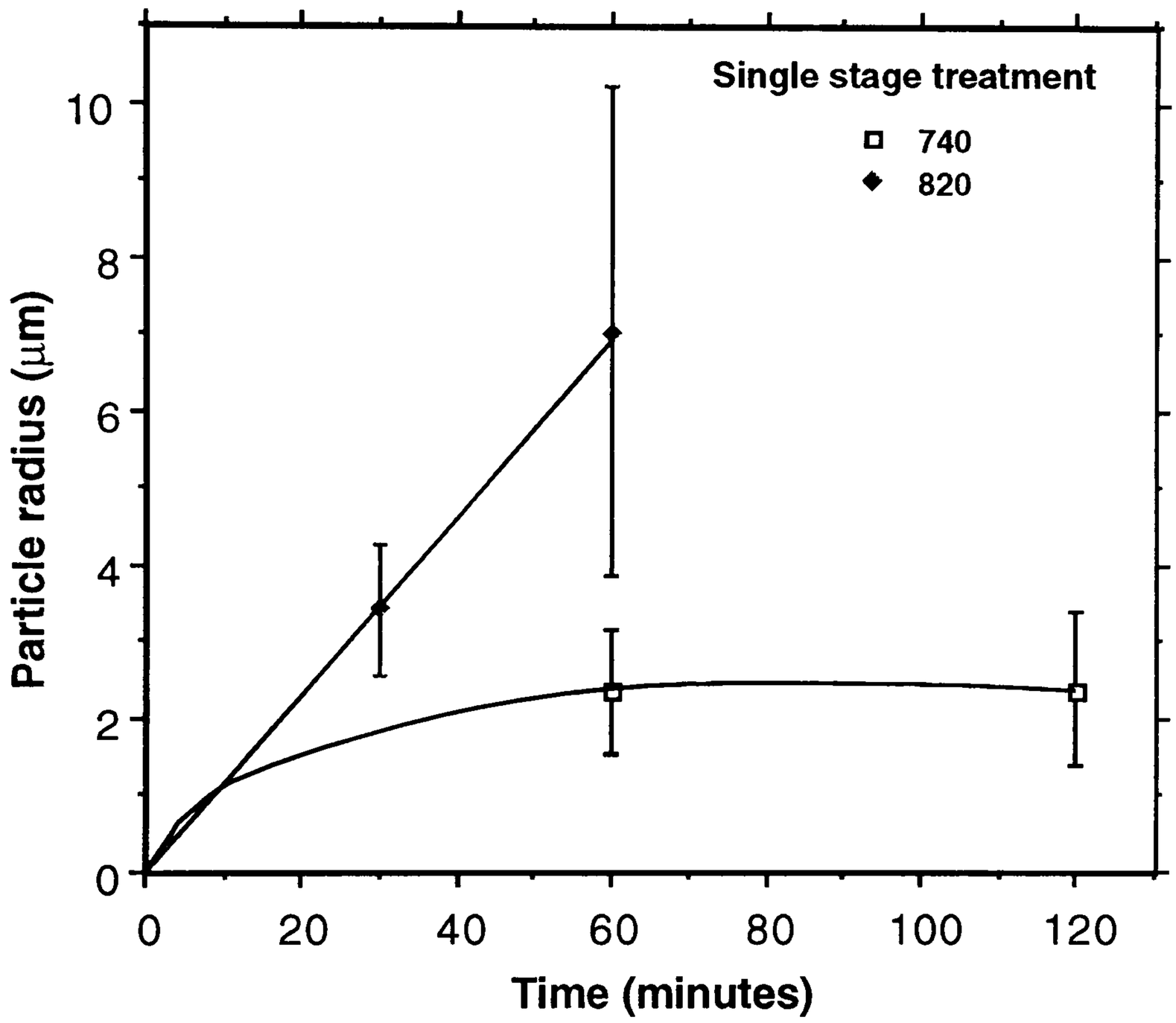
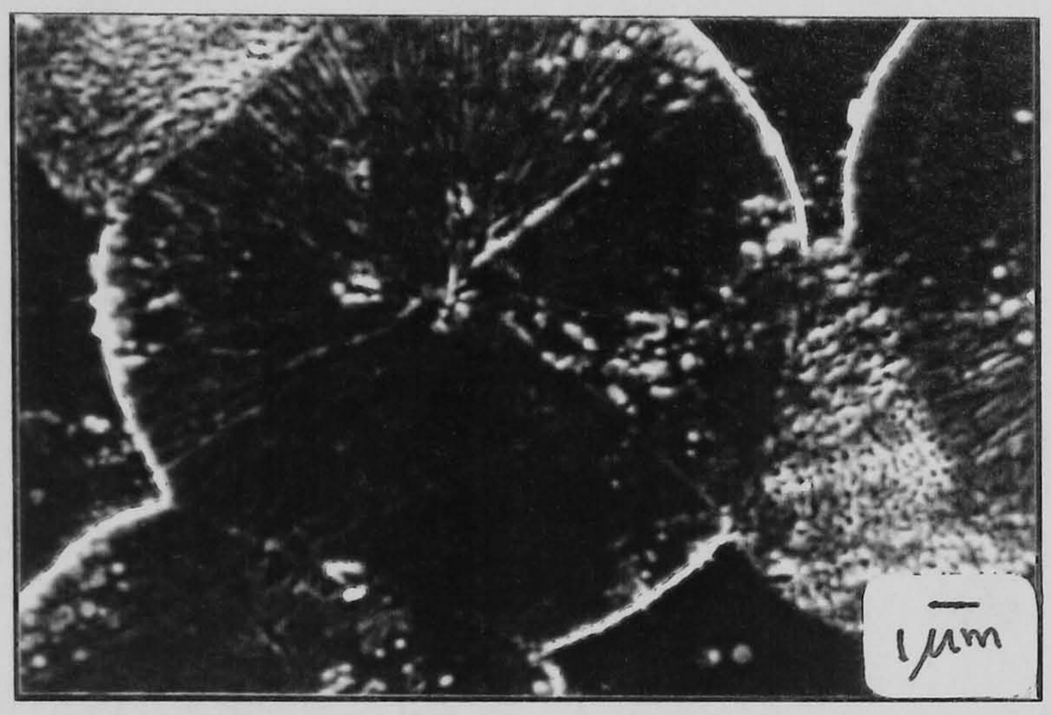
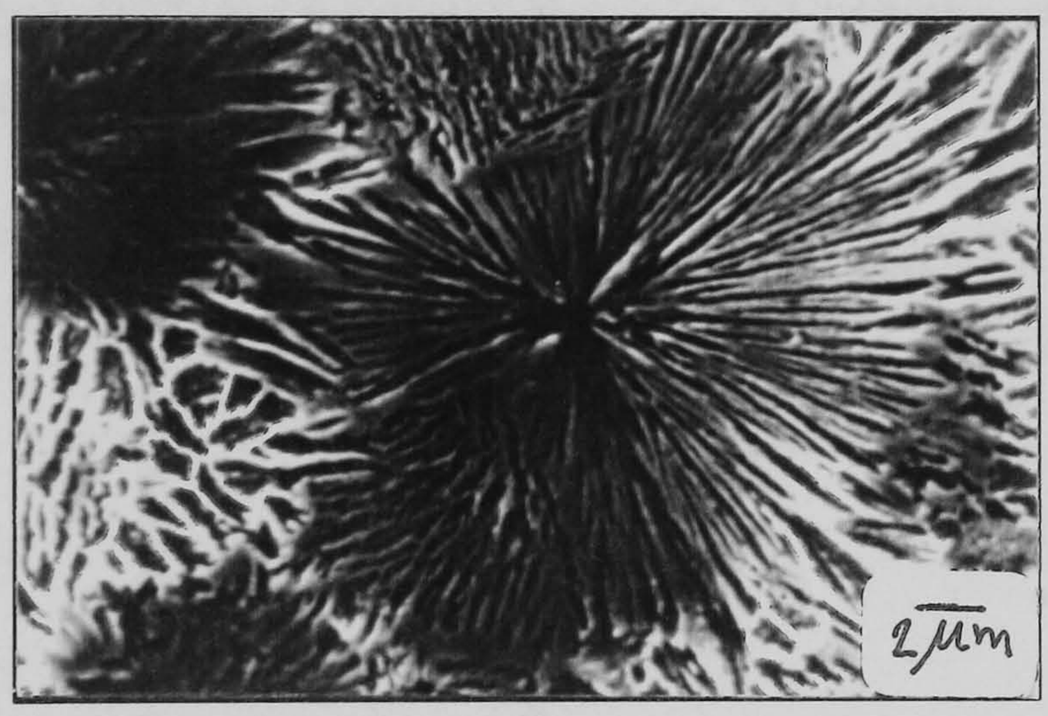


Figure 3-18 Variation of particle size with time and temperature for CSF glass that has undergone a single stage heat treatment at 740˚C and 820˚C.



(a)



(b)

Fig. 3-19 Different types of spherulites were observed in samples heat treated at (a) 550˚C for 30 minutes followed by 750˚C for 30 minutes and (b) 900˚C for 20 minutes.

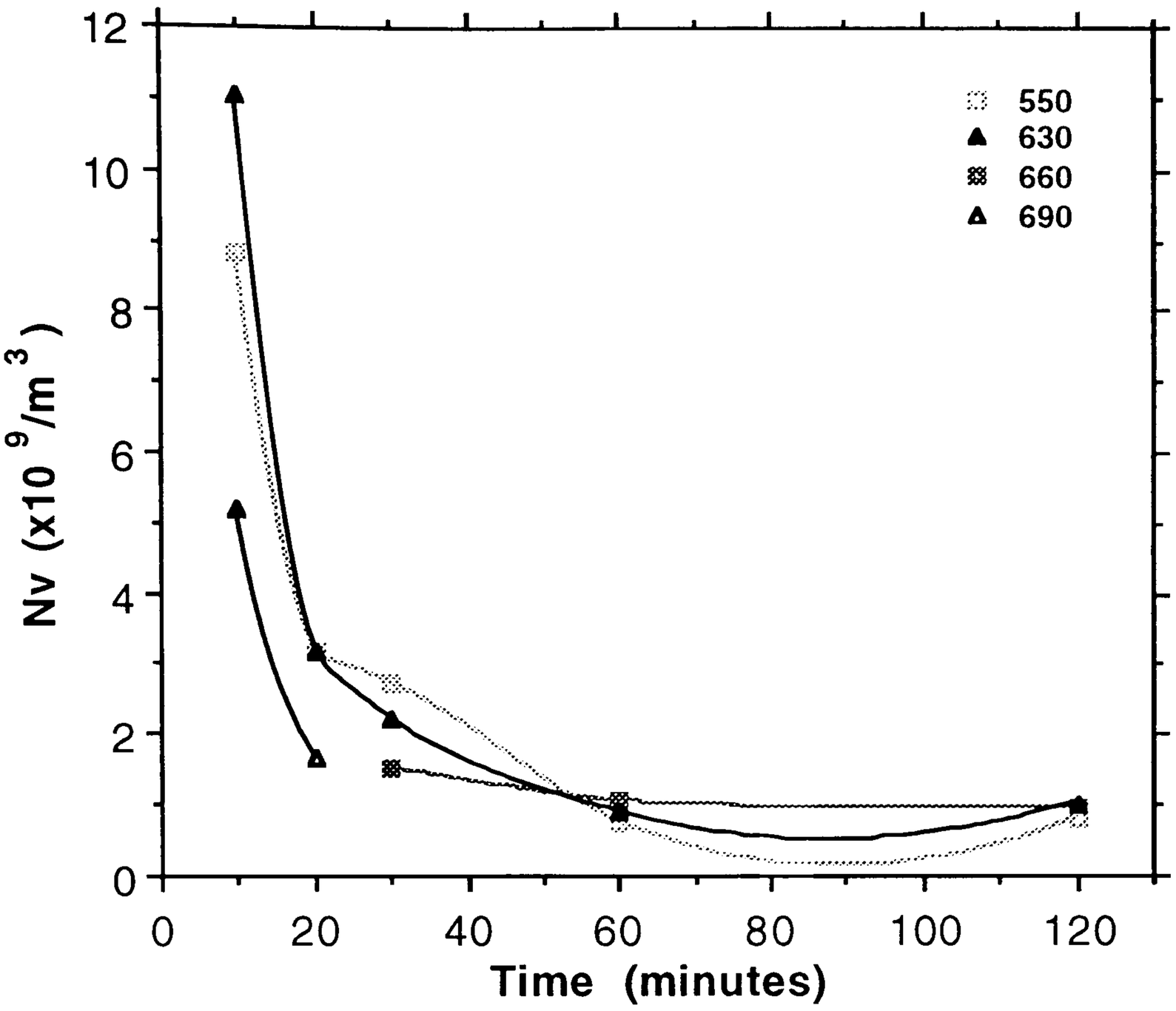


Figure 3-20 The effect of growth time on the number density in specimens heat treated at various nucleation temperatures for 30 minutes and then allowed to grow at 750°C for different times.

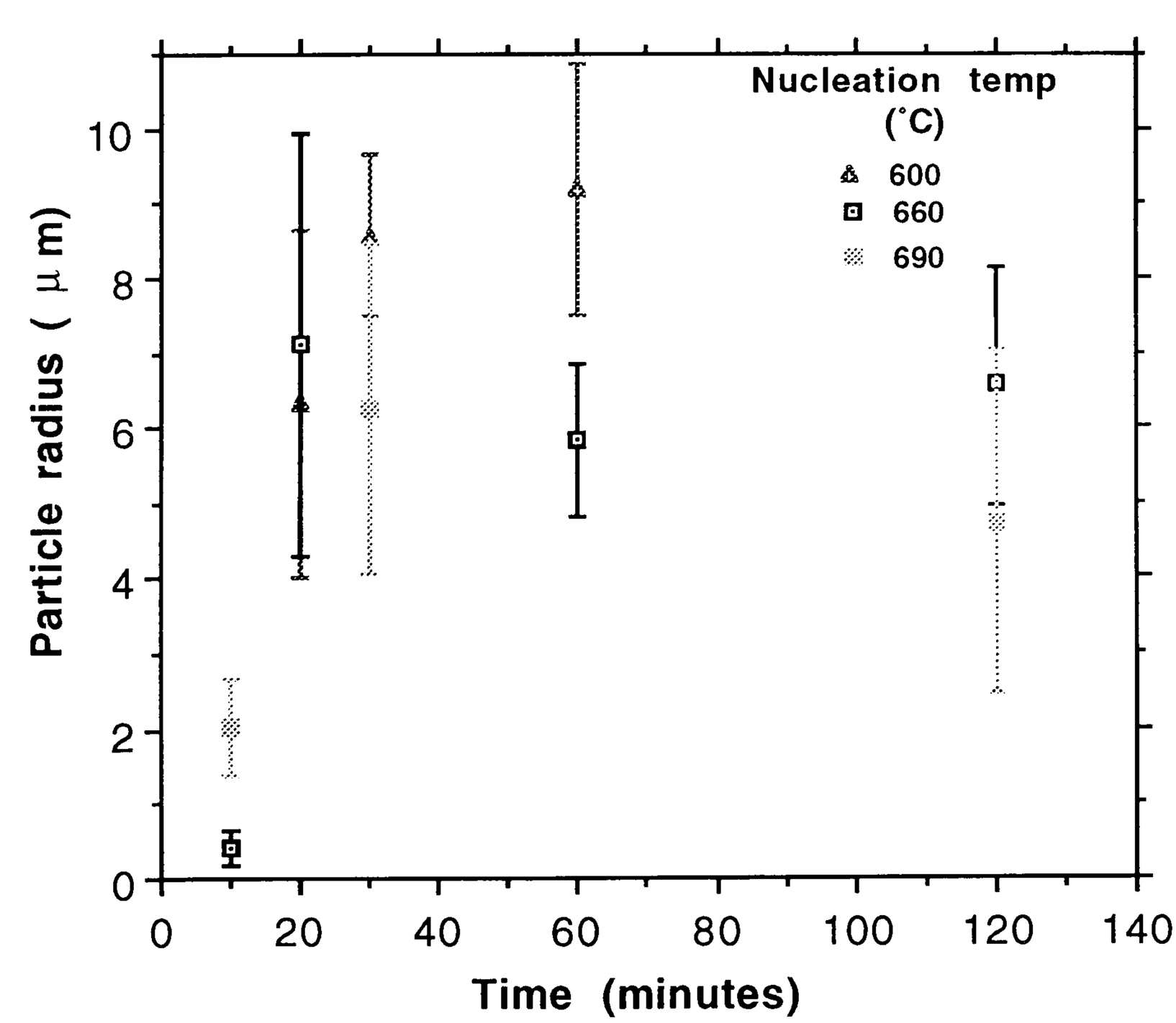


Figure 3-21 Effect of nucleation time on the size of spherulites in samples heat treated at 600, 660, and 690°C for various times and allowed to grow at 750°C for 10 minutes.

nucleation treatment has practically no effect on the number of nuclei or the size of spherulites produced (Fig.3-21). Possible explanations for the generally decreased number of growth centres and the increase of the average size of spherulites with nucleation time is that the glass was saturated with nuclei of different sizes but nuclei of smaller size are subject to dissolutions at the higher growth temperatures (see Appendix C).

It can be concluded tentatively at this stage that the variations of nucleation time and/or temperature treatment affect number of nuclei and spherulite morphology and thus the microstructure of the glass-ceramics. A possible explanation is that the nucleation heat treatment causes gradual changes in the glass structure, which in turn causes differences in subsequent growth behaviour at higher temperatures.

In order to construct the nucleation-rate-like curve from DTA profiles obtained from isothermal runs, various researchers [Marotta *et al* 1982 and Ray & Day 1990] assumed that the temperature or the height of the DTA crystallization peak represents the concentration of nuclei in the glass. Figure 3-22 shows how the DTA peak height (H_p) varies for CS and CSF glasses when nucleated at the temperatures shown for 3 hours. No appreciable change in H_p occurs in CS glass until it is heat treated at 850°C. A similar effect was observed in CSF glass, but the maximum H_p occured at 600°C. It was shown earlier that the CS glass is surface-nucleated and the CSF glass is nuclei saturated from the cooling down of the melt, nonetheless, the '*nucleation-rate-like curve*' could be deduced.

However, the exothermic peak combines the energies for both nucleation and crystal growth and unless these processes are separable, has no definite physical significance. The entropy difference between the initial and transition states is lower when the material has received a nucleation heat treatment although such a treatment did not essentially affect the maximum crystallization rate [Bansal & Doremus 1984]. Thus, it is not inclusive to conclude that the change in the exothermic peak was dependent only upon the number of nuclei present in the glass but rather the whole viscoelastic and thermodynamics condition of the glass take part in the modification of the peak.

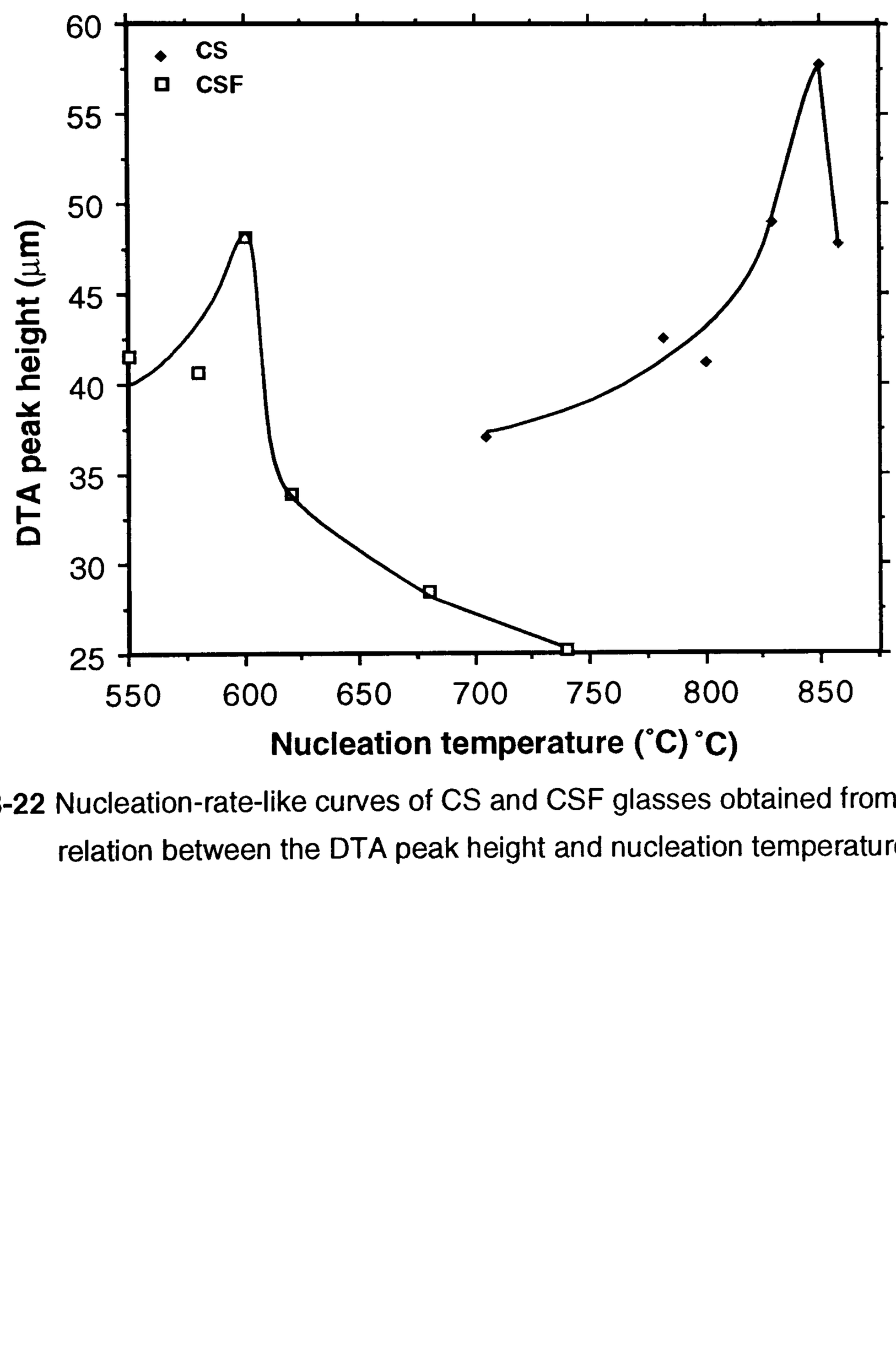


Figure 3-22 Nucleation-rate-like curves of CS and CSF glasses obtained from the relation between the DTA peak height and nucleation temperature.

However, the nucleation-rate-like curve does assist in determining the temperature where crystallization started and its maximum which will be very useful when considering the competition between crystallization and sintering in glass produced via powder route (see Chapter 4).

Effect of growth treatment

There is a dramatic change in size and morphology of the spherulites when undergoing the growth stage at different temperatures. It can be seen in Figure 3-23 that the growth rate for spherulite size decreased when undergoing higher growth temperatures (compare specimens nucleated at 550˚C and heat treated at 750˚C or 800˚C). Also specimens nucleated at 550˚C or 660˚C for 30 minutes give rise to different degrees of nuclei saturation and the lower nucleation temperature exhibits a higher growth rate. This may be partly because the distribution of the nuclei was sporadic and the distance between each nucleus was large enough to allow the nuclei to grow for a longer time before impingement occurred. It is worth noting at this stage that as the spherulites impinge upon each other the determination of the spherulite size is subject to inaccuracy due to the morphology of the spherulites being distorted to form non-spherical shapes.

The major roles of heat treatment in the growth region are to affect the size and morphology of the "spherulites", until the transformation from cuspidine to wollastonite occurs. According to the intersecting growth theory [Haller & Macedo 1968], spherulitic growth begins from spherical particles and proceeds until the entire volume of the material is filled with spherulites. At this point some glass remains at the grain boundaries and between the arms of the spherulites. "Impurities" concentrated in this glass affect the subsequent crystallization process significantly [Freiman *et al* 1972].

As shown in Figure 3-24a, the crystallization of glass in a secondary process causes the diminishing of the fibrous appearance of the spherulites. This transformation is believedto be a recrystallization of the fine spherulites arms (fibrils), promoted by the instability of the large interfacial area of the fibrous, spherulite structure. SEM studies also show that wollastonite started growing from the cuspidine fibres, disrupting the

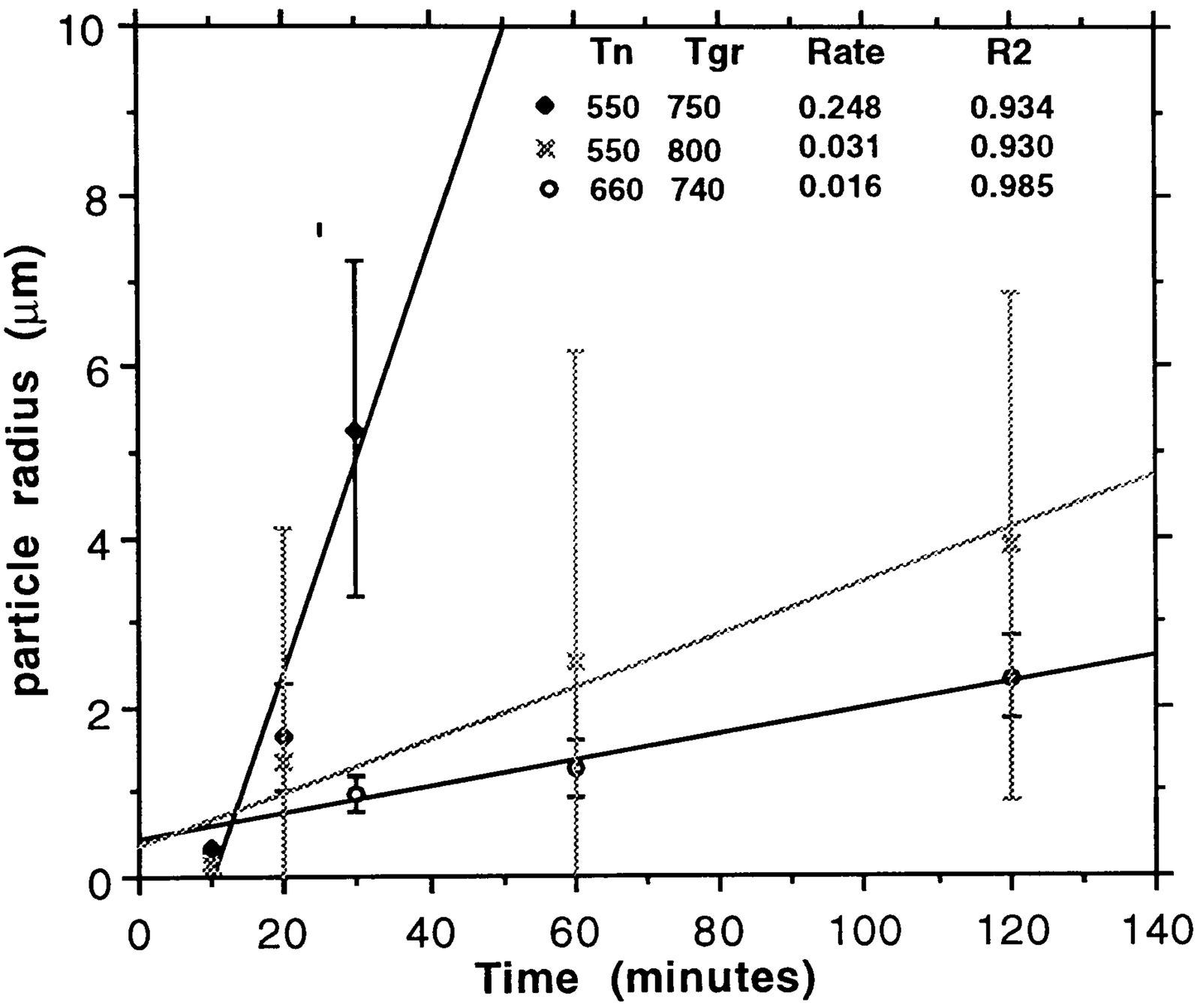
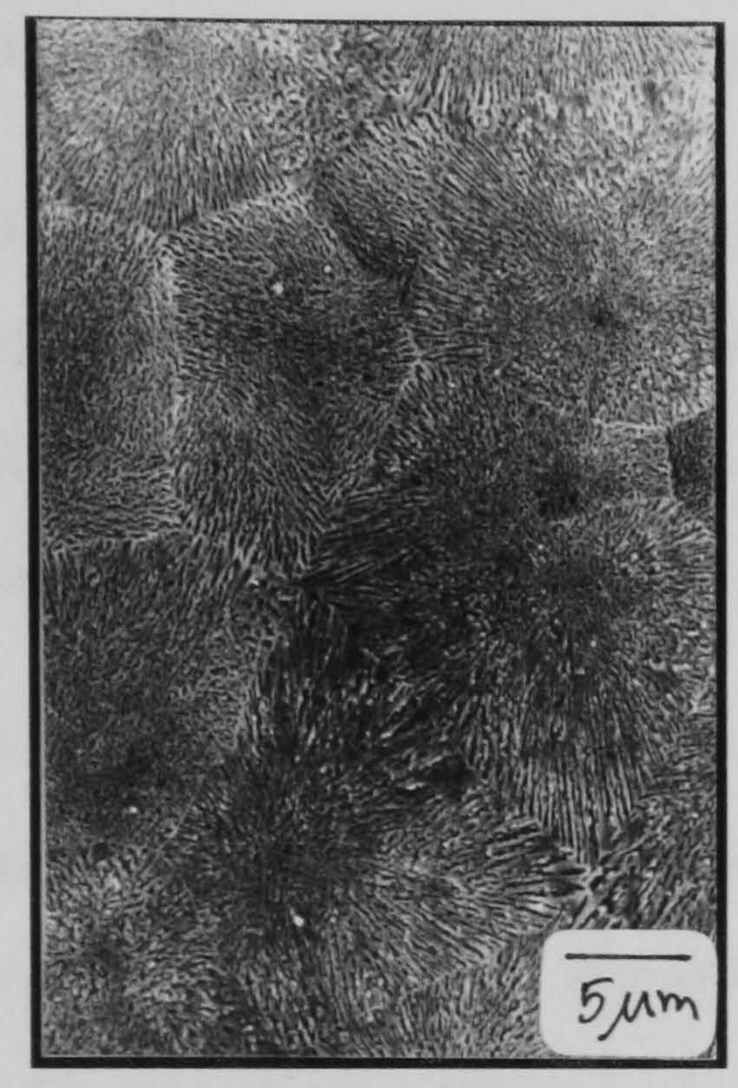
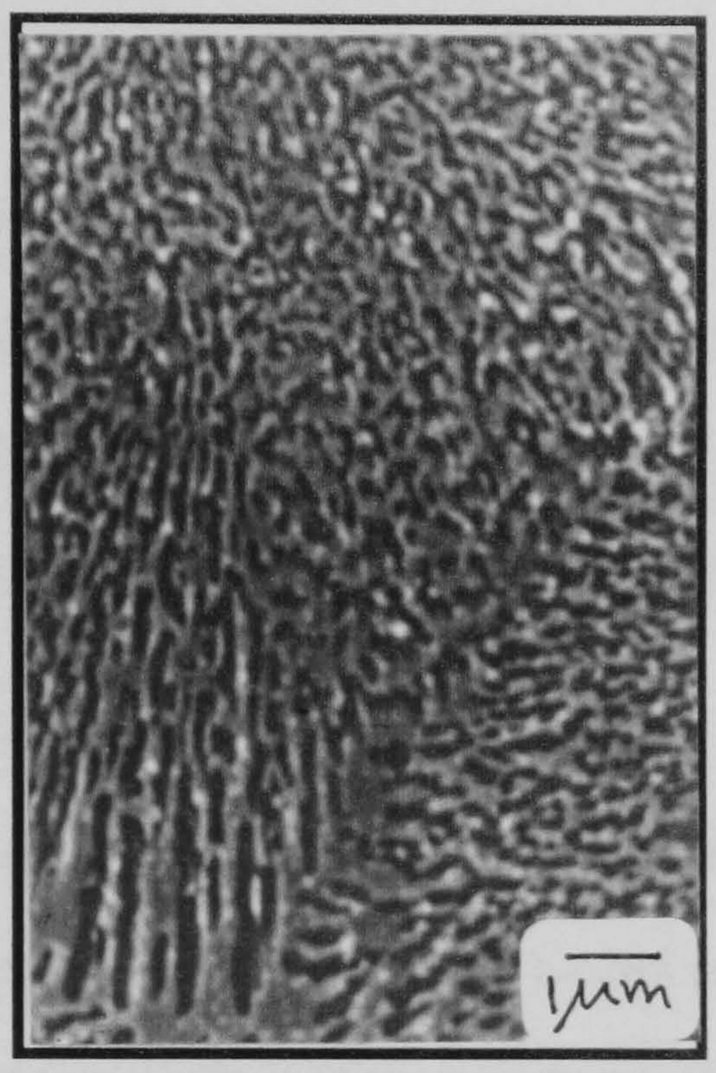


Figure 3-23 The effect of growth temperature on the particle radius in specimens nucleated at 550˚C or 660˚C for 30 minutes and then given growth treatments at different temperatures.



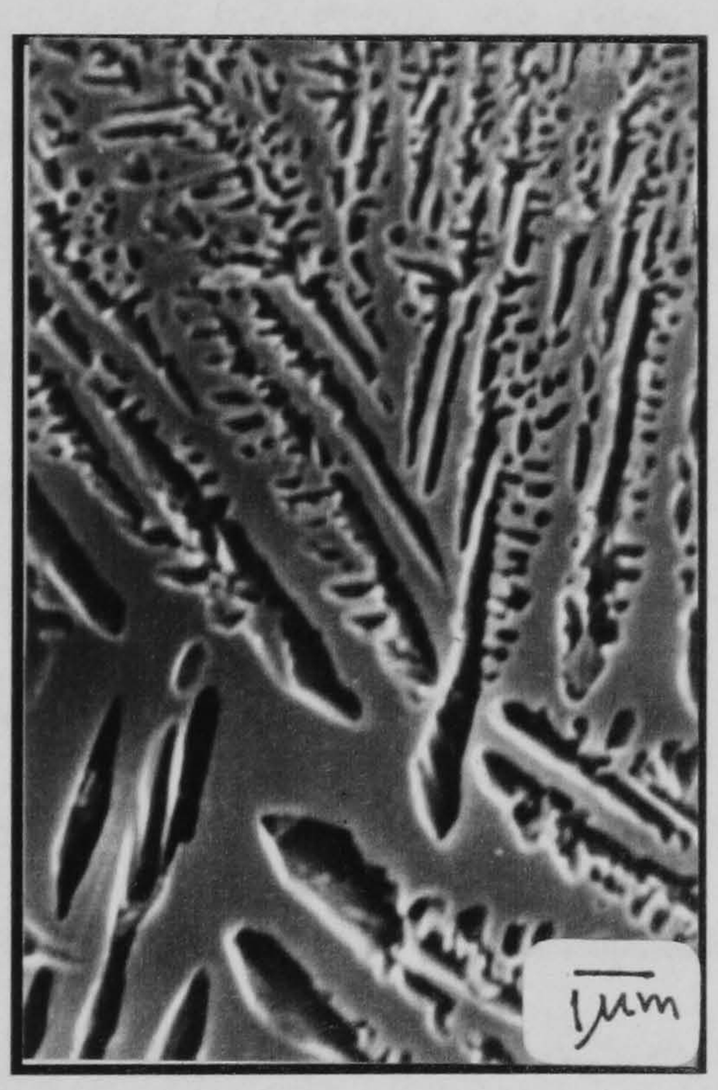
(a)



(b)



(c)



(d)

Figure 3-24 Micrographs representing different morphologies of spherulite developed at (a) and (b) 550˚C for 30 minutes followed by 850˚C for 30 minutes, and (c) and (d) 550˚C for 10 minutes followed by 900˚C for 10 minutes.

fibrous structure. Near 800°C, the cuspidine became thermodynamically unstable and most of it transformed into wollastonite. It is proposed that the CaO forms more wollastonite by reacting with SiO_2 in the glass matrix and the fluoride in the CaF_2 may react with Na^+ ions in the glass and form NaF, thus becoming volatile.

The secondary crystallization occurred between primary crystals. This rearrangement is slow compared with the initial nucleation and growth because the residual glass present possessed more silicon atoms which increase its viscosity. The overall crystallization rate in this stage was substantially lower than the rate of spherulitic crystallization.

Figure 3-25 shows Arrhenius plots of number of nuclei at various nucleation temperatures of CSF glass compared with similar glass with 3.4 wt% fluorine studied by Mukherjee & Rogers [1968]. It can be seen that the number of nuclei in CSF glass (4.8 wt% fluorine) is insensitive to the nucleation temperature which confirms that the glass is saturated with nuclei before heat treatment. However, the glass with smaller amount of fluorine is very sensitive to the nucleation treatment and a large difference between the activation energy for nucleation obtained from samples which have undergone nucleation treatments and allowed to grow crystals at 800°C (86 kJ/mol) and at 850°C (272 kJ/mol) was observed. The activation energy at 800°C is close to that for sodium ion diffusion in glass [Frischat 1970] and this would be the case if the process were controlled by the movement of 'impurities' (Na^+ ions) away from the forming nuclei. At higher growth temperature (850°C) the activation energy is comparable to the activation energy obtained via DTA methods of the first peak temperature in CSF profiles, which is 235 kJ/mol. This value is predicted by Sun [1947] to be the bond strength between the glass modifiers. The difference in the measured value for activation energy for crystallization seems to be related to differences in the viscosities of the liquids in which the crystallization reaction occurs.

3.3.3 Controlled crystallization

From the knowledge obtained from section 3.3.1 and 3.3.2, CSF glass samples of various degree of crystallinity were prepared for mechanical testings. The

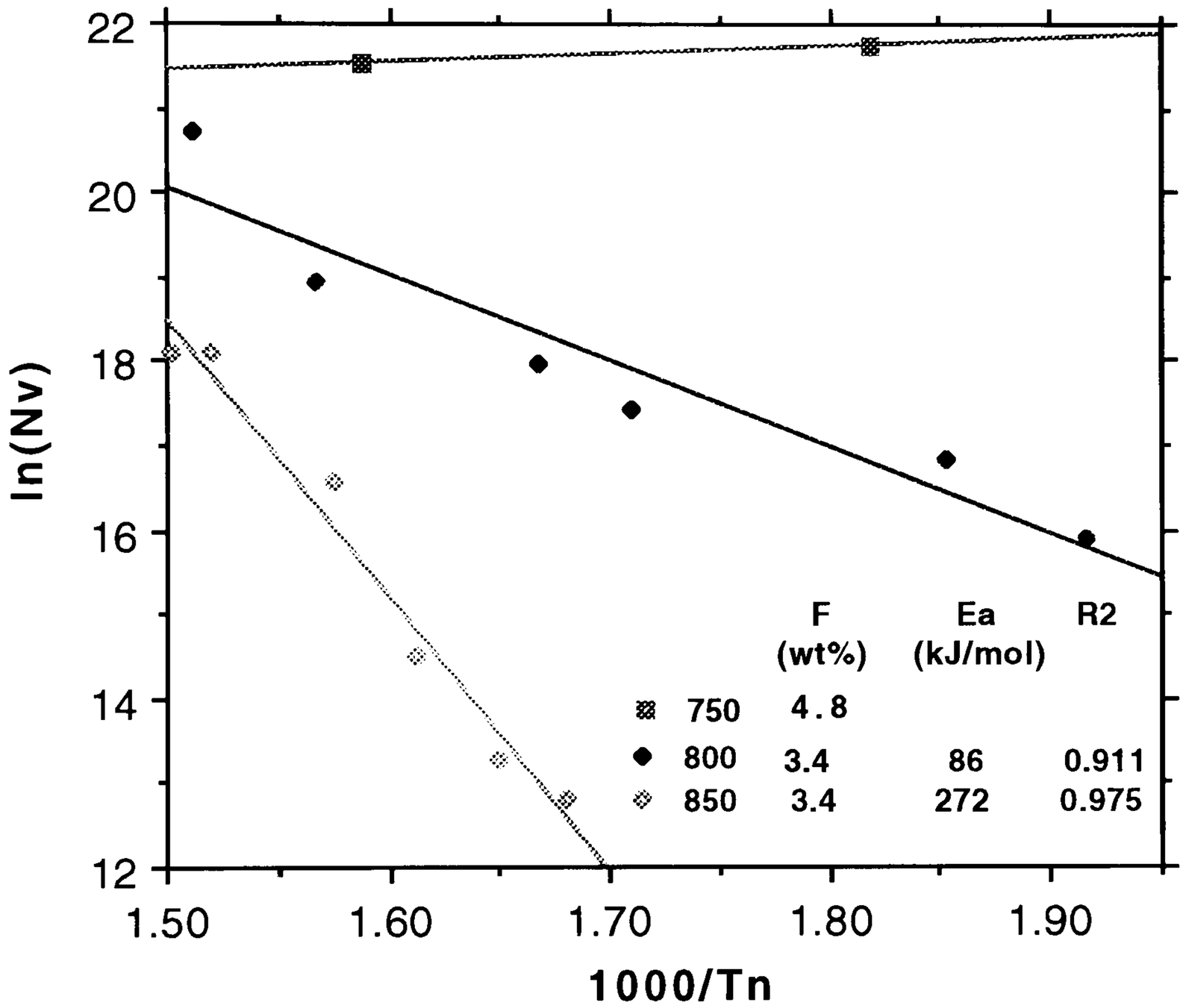


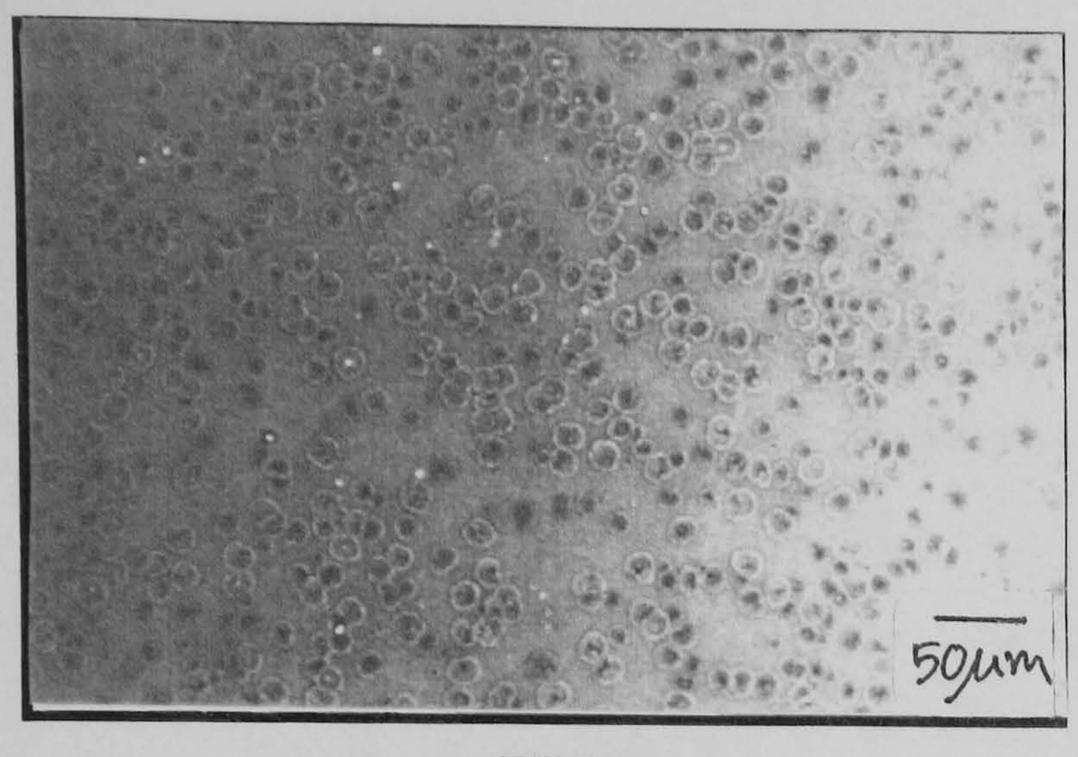
Figure 3-25 Arrhenius plots of CSF glass showing the effect of fluoride content (3.4 wt% ,modified from Mukherjee & Rogers [1968], and 4.8 wt% [the present study]) and nucleation treatment followed by growth treatment at 750, 800 and 850˚C

crystallization in the glass was controlled so that different spherulite morphologies of a various degree of crystallinity be obtained. Two types of spherulites were produced: round and sheaf. The microstructures obtained are displayed in Figure 3-26. Sample designations, heat treatment, amount of retained fluoride, crystallinity and crystal phase present are shown in Table 3-8.

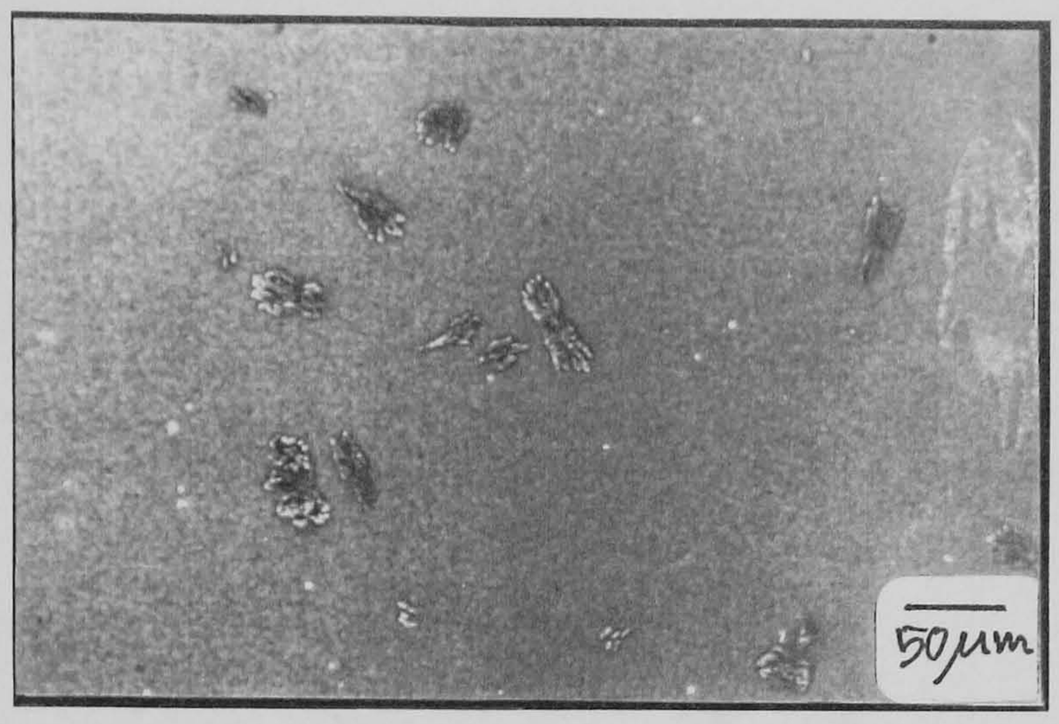
The crystallinity was determined by x-ray diffraction (XRD). It should be noted that the XRD technique was more accurate at high crystallinity because of less interference from the glass halo.

The density of CS cast glass increases slightly as the crystallinity increases, while the density of CSF glass was inversely proportional to the crystallinity (Figure 3-27). The density of CS glass is to be expected as the structure of the crystal is more ordered, and thus denser than the loose structure of glass. However, the density of CSF glass exhibits an opposite trend. Since the theoretical density of cuspidine and wollastonite are 2.90 and 2.84 Mg/m^3 [JCPDS], respectively, it is not surprising that the density decreases with crystallinity because at low crystallinity, the crystal phase is cuspidine but at higher crystallinity the cuspidine disintegrated into the lower density phase, wollastonite. Generally, porosity does not develop during the conversion from the glass to ceramic state since the overall volume changes are very small. The volume increase is due to the production of crystals and/or residual glass of lower density than the original glass. This may explane why the glass-ceramic density is lower than that of the parent glass.

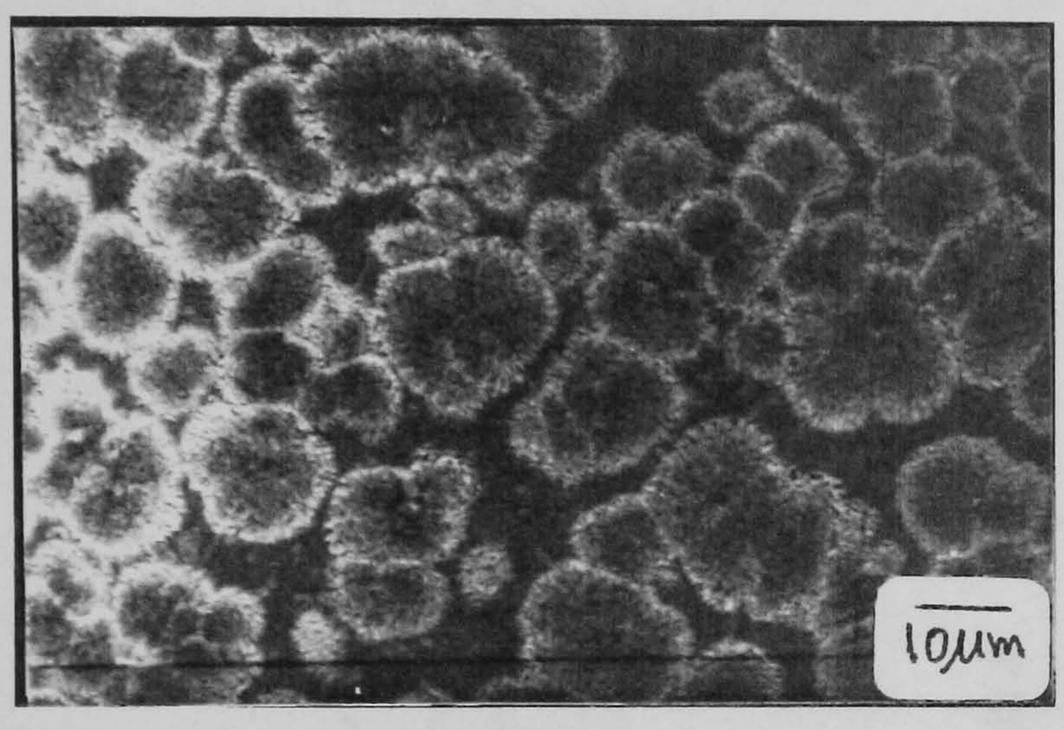
The effect of heat treatment on coefficient of thermal expansion is markedly influenced by the crystallinity. Figure 3-28 shows the dilatometric profiles of CS cast glass with different crystallinity. The specimen heat-treated at a temperature lower than 900°C exhibited a curve resembling that found for the specimens treated at 950°C but the latter showed very low expansion when heated from room temperature up to about 350°C. At higher temperature it expanded at the same rate as the others and then collapsed at 50°C higher. It was found that, in CS glass, the coefficient of thermal expansion was



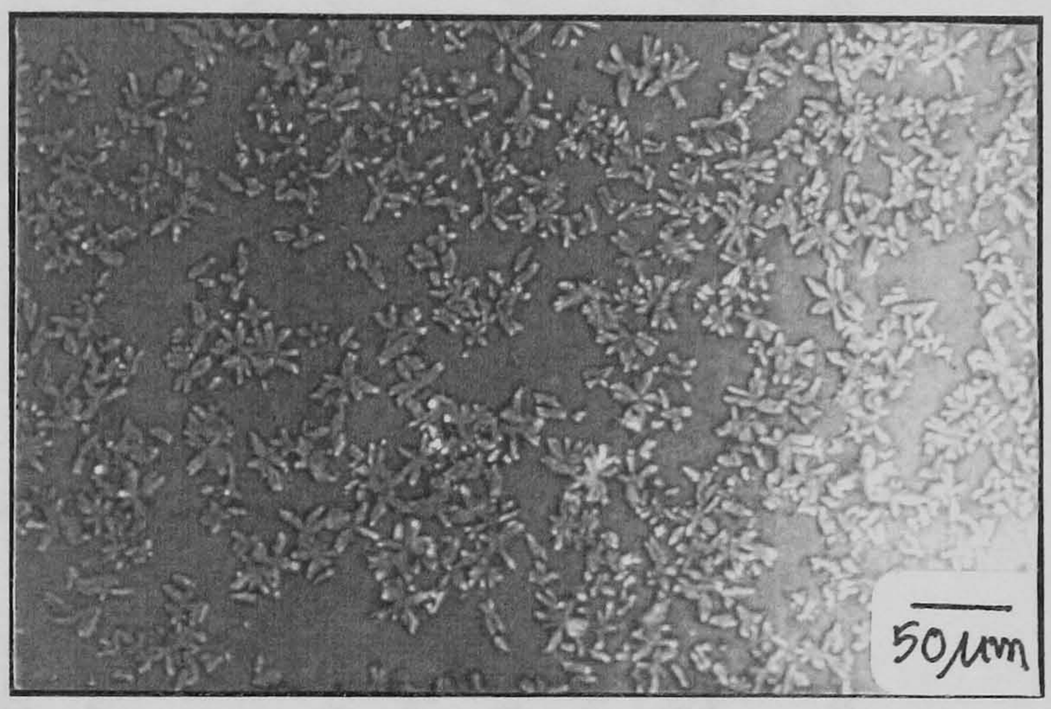
FR2



FS1



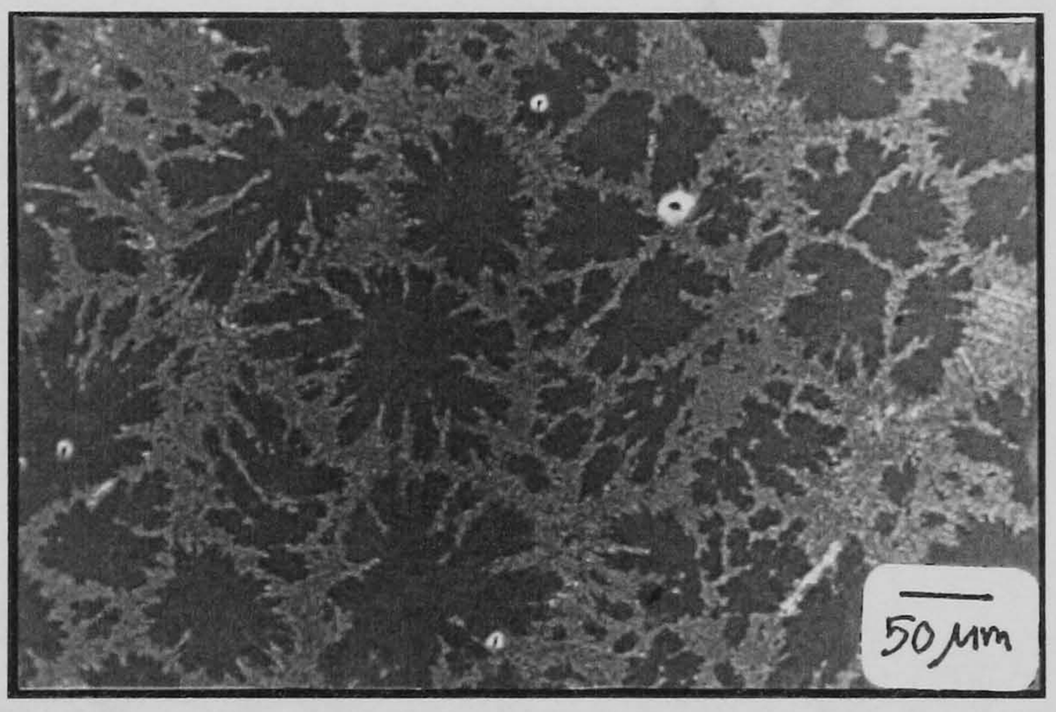
FR3



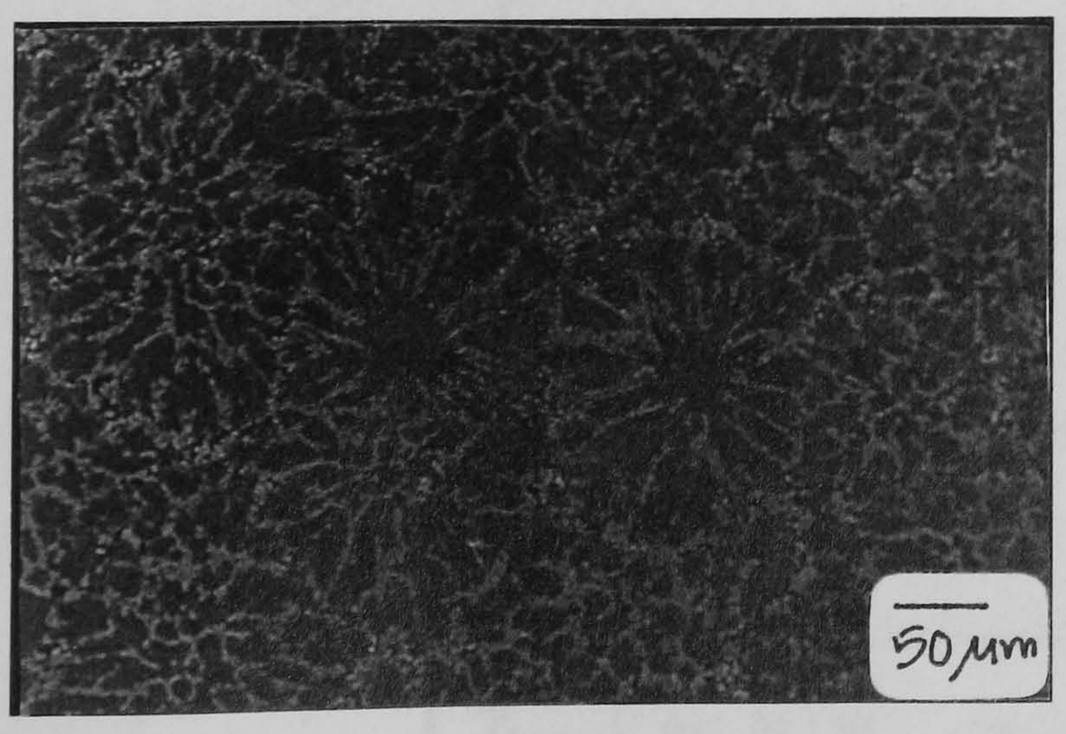
FS2



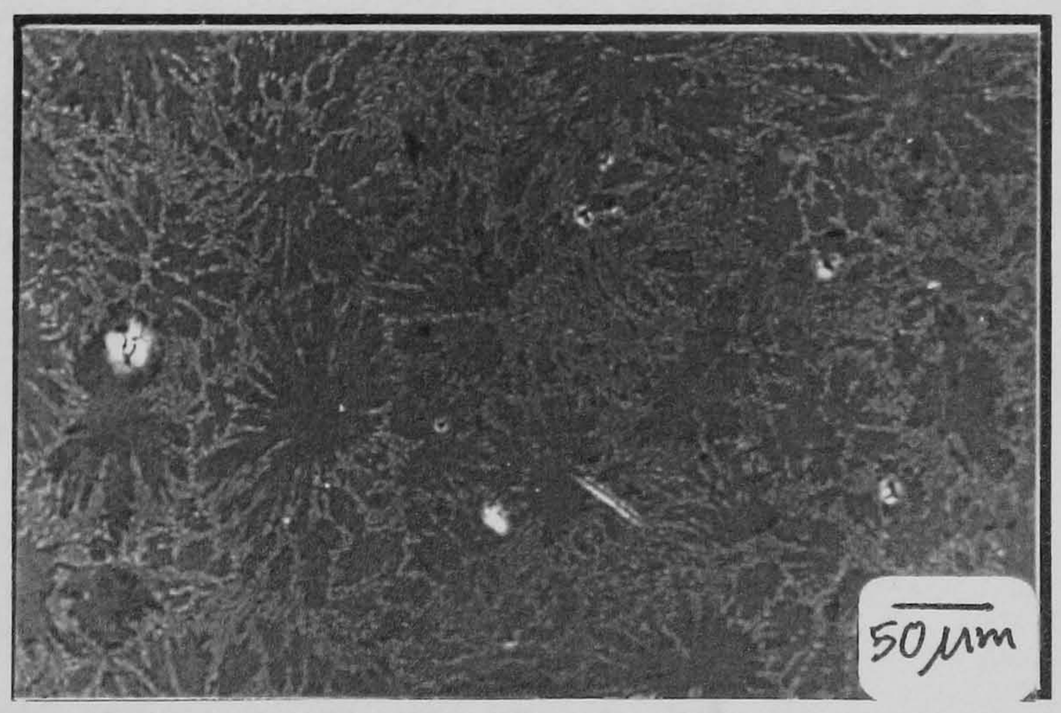
FR4



FS3



FS4



FS5

Fig. 3-26 Scanning electron micrographs showing spherulite morphology undergoing heat treatment shown in Table 3-8.

Table 3-8 Controlled crystallisation in CS and CSF glass-ceramics and their physical and thermal characterisations.

Sample	Nucleation		Growth		Morphology	F^-	crystallinity	Density	CTE	Crystal phase	
	T (˚C)	t*	T (˚C)	t*		(wt%)	(%)	(Mg/m^3)	(x 10^{-6} K^{-1})	C§	W†
CS1	-	-	850	30 m		-	§	2.73	6.66	-	√
CS2	-	-	900	60 m		-	§	2.78	6.84	-	√
CS3	-	-	950	6 h		-	§	2.74	5.54	-	√
FR1	-	-	800	10 m	round	**	32.8	2.72	9.16	√	-
FR2	-	-	820	60 m	"	**	50.6	2.71	6.21	√	-
FR3	600	72 h	750	48h	"	**	73.8	2.68	6.81	√	-
FS1	-	-	900	10 m	sheave	2.8	23.9	2.73	10.42	√	-
FS2	660	15 h	900	5 m	"	2.6	42.2	2.72	9.94	√	-
FS3	660	30 m	820	60 m	"	**	73.4	**	9.14	√	-
FS4	-	-	800	24 h	"	3.3	91.0	2.68	6.05	√	-
FS5	660	48 h	800	24 h	"	3.1	89.4	2.70	7.35	√	√
FS6	-	-	850	60 m	"	3.6	99.0	2.63	6.00	√	√

* time in m: minute or h: hour; ** unmeasured value; C§ :cuspidine; W† : wollastonite, §: not measured.

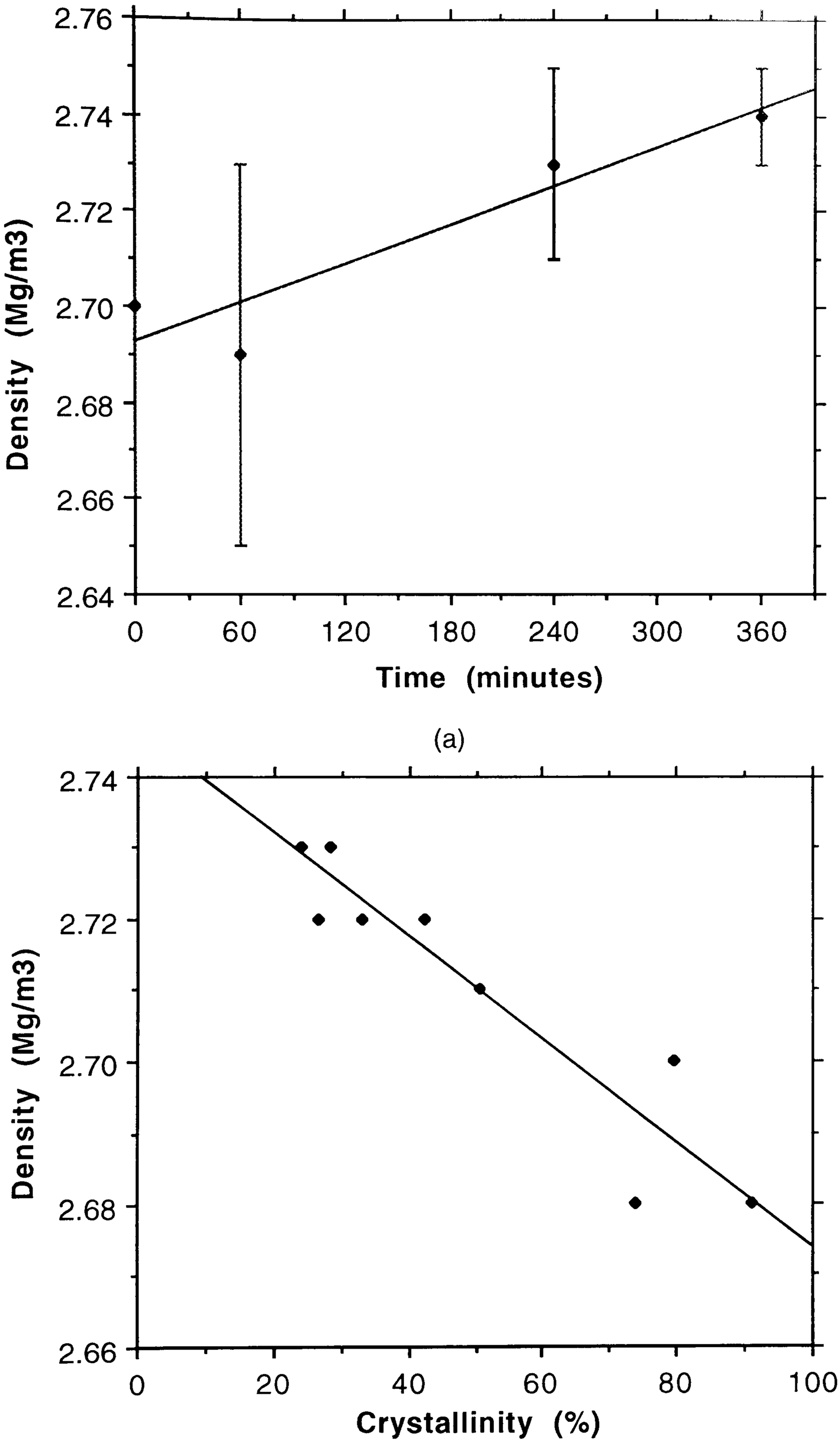


Figure 3-27 Bulk density of (a) CS heat treated at 950˚C for different times and (b) CSF cast glass of different percentage of crystallinity

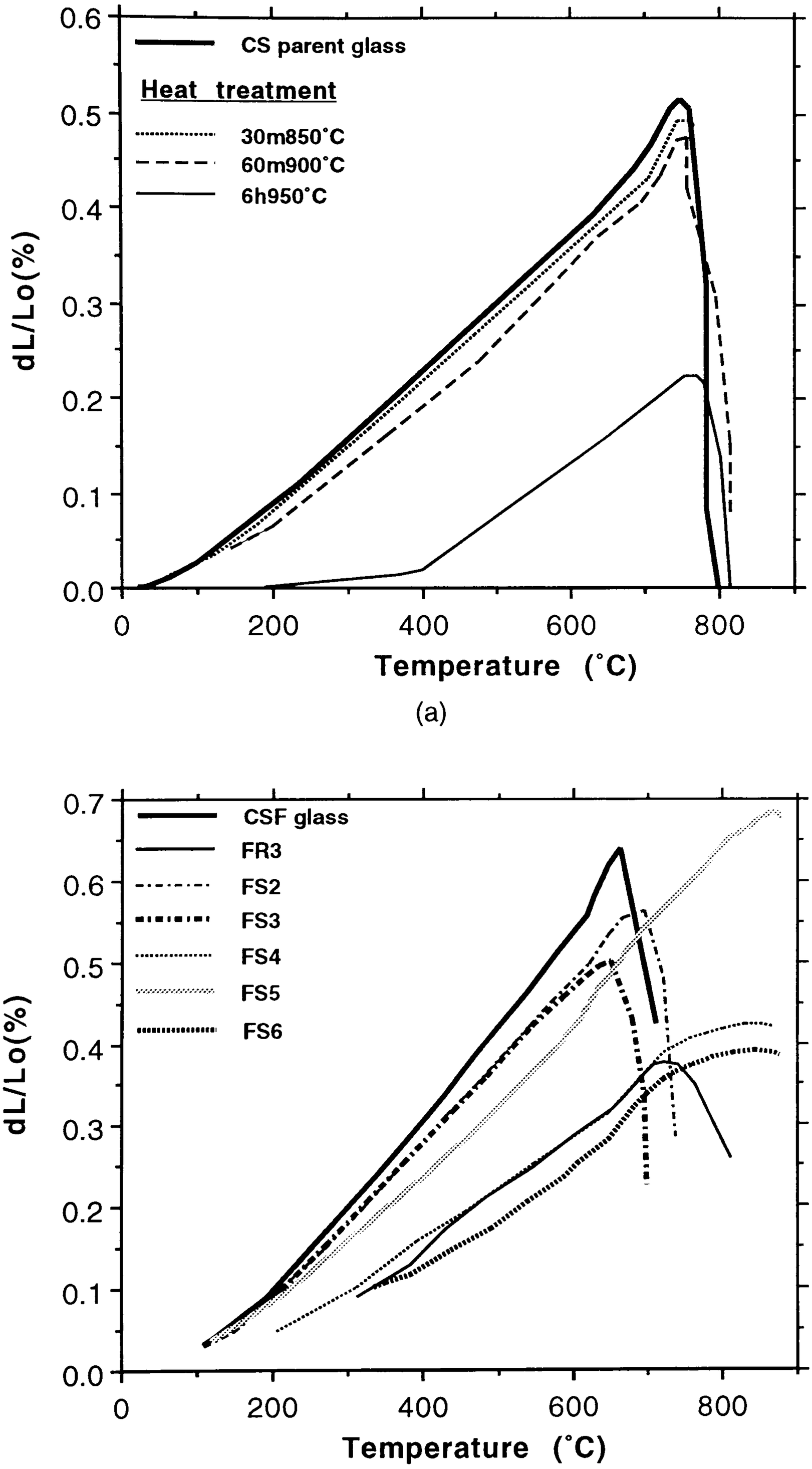


Figure 3-28 Dilatometric curves of (a) CS and (b) CSF samples undergone different heat treatments

Table 3-9 Quantitative EDX analysis of samples which have undergone various heat treatments.

Sample	Element mol ratio			
	Ca:Si		Na:Al	
	nuclei	matrix	nuclei	matrix
FS2	0.50	0.43	0.25	1.00
FS5	0.50	0.40	0.25	1.29
FR3	0.50	0.38	0.44	1.33

dominated by either the glass or the crystal phase. The CTE of CS glass, ~7 x 10^{-6} K^{-1}, was larger than that of the wollastonite crystals, ~4.5 x 10^{-6} K^{-1}. The glass crystallized at 900°C for 60 minutes exhibits glass-like dilatometric curve, while glass crystallized at 950°C for 240 minutes shows a remarkably different profile, i.e. more like that of the crystalline phase, wollastonite.

On the other hand, the CTE of crystallized CSF glass is directly proportional to the amount of retained fluorine in the glass which corresponds to the cuspidine to wollastonite ratio developed at any particular heat treatment.

The CTEs of heat treated CSF glasses are higher than that of CS glass and collapsed at lower temperature (Figure 3-28). The crystallized CSF with crystallinity lower than 50% showed similar expansion behaviour to the CSF glass, but at higher crystallinity the CTE reduced to 6x10^{-6} K^{-1}, which is approximately the same as that of fully-crystallized CS glass. Moreover, the samples did not collapse even at temperature higher than 850°C. Figure 3-29 shows that the CTE of crystallized CSF glass is directly to the amount of retained fluorine in the glass. Generally, the higher the heat-treatment temperature, the lower amount of the retained fluorine in the glass and the higher amount of wollastonite developed, thus giving rise to lower CTE. The type of cracking induced by thermal mismatch will depend on whether the spherulites contract more or less than the matrix during cooling. In CSF case, the spherulites contract more, cracking is circumferential around the spherulites.

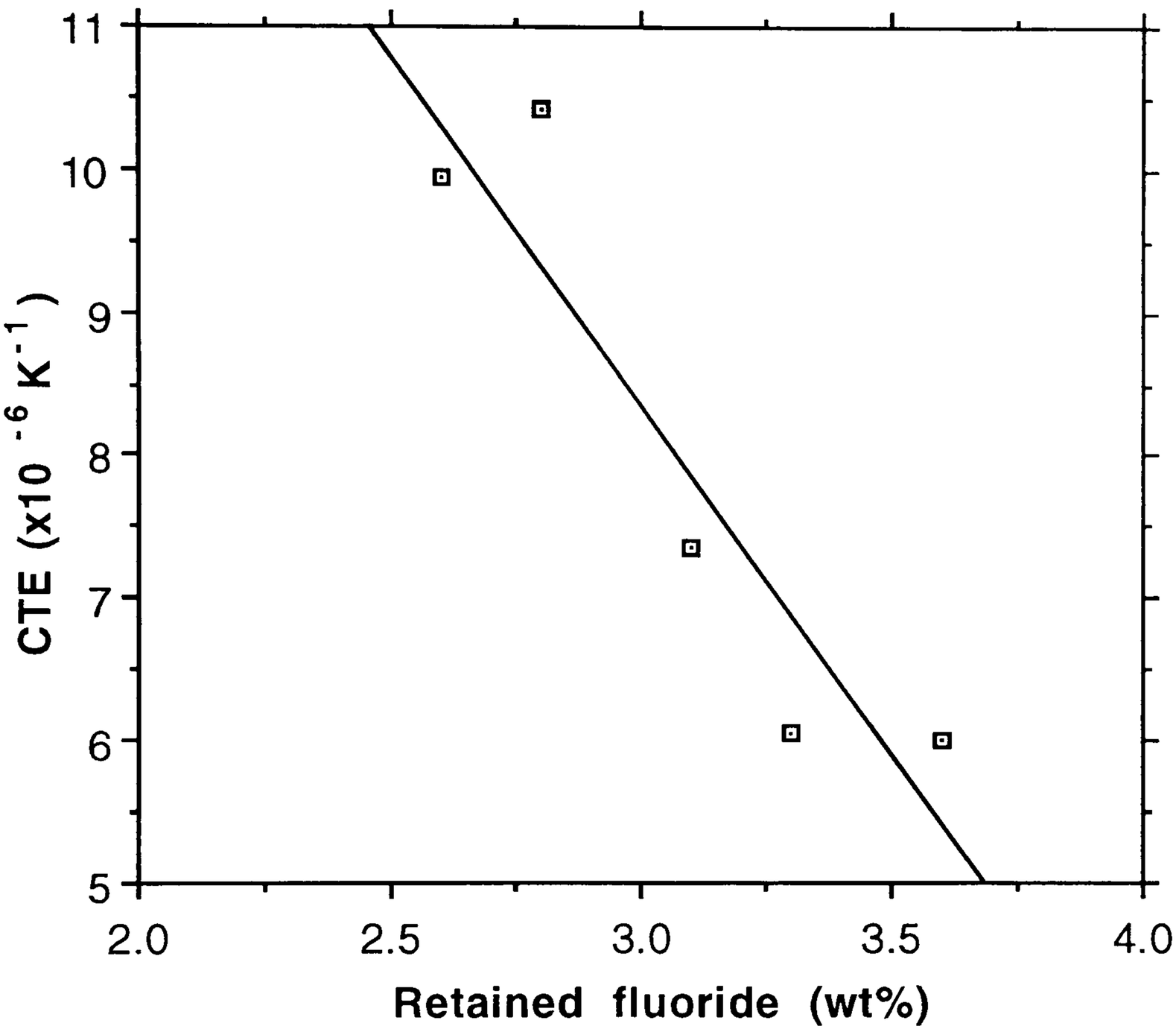


Figure 3-29 Plot showing effect of the amount of fluorine retained in the CSF crystallised glass on the coefficient of thermal expansion.

3.4 Summary

The crystallization of CS glass is surface-nucleated in the form of wollastonite crystals growing one-dimensionally into the bulk glass. The activation energy for crystal growth, 493 kJ/mol, is close to values for glass-forming oxides bond strengths [Sun 1947] and it would be expected for calcium diffusion in glass [Bansal & Doremus 1986]. The addition of fluoride (CSF) affects the kinetics of crystallization in several ways. Firstly, it decreases viscosity at $T > T_g$, and thus decreases the activation energy for crystallization. Secondly, it acts as a nucleating agent which induces glass-in-glass phase separation; i.e. crystallization emanates in three-dimensional growth mode which leads to an increase in crystallinity. Finally, it affects the crystallization path by forming cuspidine which is a metastable phase that will decompose to form the more stable phase, wollastonite, at higher temperature.

The transformation of CSF glass into a micro-crystalline material involved the following metastable stages between the initial and final crystalline states, some of them occurring concurrently: (i) liquid phase separation, (ii) nucleation and spherulitic growth of cuspidine, covering crystallinity range of 5 to 90%, and (iii) transformation of cuspidine leading to stable wollastonite which occurs much more slowly than the nucleation and crystallization stage at crystallinity >90% .

The CSF glass is nuclei-saturated when allowed to cool to room temperature before reheating. The kinetics of spherulite growth appear to be governed by diffusion of sodium ions, in the glass in front of the growing crystals, as indicated by the small activation energy, 130 kJ/mol. The transformation of cuspidine to wollastonite involves the loss of fluorine (evidence DTA analysis) and sodium ions into the glass.

The CTE of the crystallized CS was comparatively close to those of the CS glass up to certain percentage of crystallinity, but the CTE in CSF glass depends on the crystallinity. The bulk density of CS glass increases with crystallinity while the opposite was observed for CSF glass.

CHAPTER 4

POWDER ROUTE

4.1 Introduction

Glass-ceramics can be produced either by bulk crystallisation of formed glass objects [McMillan 1979 and Strnad 1986] or by sintering and crystallisation of pressed glass powders [Rabinovich 1979, Kumar & Tamala 1978, Panda & Raj 1989, Von Schweitzer 1993 and Taylor 1994] in one heat treatment. The recent interest in the sintering of glass arises from the fact that glasses are less prone than ceramics to processing flaws arising from packing defects. For example, large agglomerates can produce flaws in the sintering of ceramics [Evans 1982], but glasses usually sinter to full density even when the green microstructure is non-uniform. In theoretical work, Bordia & Raj [1986] suggested that the ability of the glass to relax shear stress by viscous flow is the reason why problems of differential sintering are alleviated. The glass route to net-shape sintering is, therefore, an attractive process for making a variety of materials including composites.

There are some problems which have to be overcome if a glass powder is to be sintered and heat treated to produce a glass-ceramic. Pre-existing surfaces can act as nucleation sites, and the crystallites may grow from the surface of every glass particles toward the centre. Crystallisation of the surface of the vitreous particles inhibits sintering and consequently pores remain in the product [Clark & Reed 1986]. Most researchers agree that the success of producing near full density, high strength materials depends on how far the sintering proceeds before it is halted by crystallisation [Rabinovich 1982; Sridharan & Tomozawa 1992]. Therefore, in glass-ceramics fabricated by sintering, crystallisation must be delayed until sintering is well-advanced, if a pore-free, fine and uniform structure is to be obtained. Consequently, the kinetics of sintering and

crystallisation plays an important role in determining the sinterability of glass powder to produce glass-ceramics.

This chapter studies the effect of crystallisation on sintering of CS and CSF glass powders. The feasibility of utilising these powders as the matrix for a composite is investigated by their densification characteristics. The effect of rigid particles; i.e. alumina, zirconia, and silicon carbide, of various volume fraction on the sinterability of the systems will be examined. The following section is a review of current knowledge of the sintering parameters, models, and effect of rigid inclusions.

4.1.1 Powder characteristics

The changes the microstructure undergoes during sintering are influenced by a number of factors which are determined by the chemical and physical properties of the material as well as the particle packing configuration of the green body. In order for the process to function rapidly at temperatures below the melting point, a powder of large surface area is utilised to obtain a large driving force toward equilibrium. The green microstructure is a starting point for the processing and its design is a ready means to influence the course of sintering. The green microstructure is in turn largely determined by the powder characteristics. The principal factors consequently become particle size distribution, particle packing, shape, and size.

The packing efficiency in a green compact can be easily increased by choosing the particle or granule size distribution such that each successive smaller size is one-seventh of the previous size [Barringer *et al* 1984]. However, this is not considered desirable since it would result in different rates of sintering in different locations of the same compact. Instead, a narrow but fine particle size distribution is preferred in the manufacturing of high performance ceramics. The sintering ability of a compact decreases with a broader particle size distribution [Rhodes 1981].

Even though a smaller particle size yielded a faster rate of densification in the early stage, it did not assure a high final density [Liniger & Raj 1988]. Complete densification required a high co-ordination number, which is the ratio of the contact

points in the structure to the total number of particles in the structure, a high green density, and a uniform packing density. Precompaction and granulation of the powder will enhance the packing efficiency in final compaction. However, excessive precompaction pressure results in hard granules which survive the final compaction process and retain their identity in the green compacts. Each granule thus has its own centre of shrinkage during sintering, resulting in residual voids between the granules and incomplete densification of compact as a whole.

Practically, nonuniform packing is detrimental to sintering from the very beginning of the sintering process. On the particle scale, it can be seen that forces acting on one particle will be different from particle to particle will certainly give rise to rearrangement. On the polyhedra scale, polyhedra with co-ordination numbers greater than the average will try to shrink more and at a greater rate than the average. Constraint by the average shrinkage behaviour will give rise to disruptive, tensile stress. On the agglomerate scale, it has been experimentally shown [Lange & Metcalf 1983] that agglomerates with a lower bulk density than the average will produce circumferential, cracklike voids. Thus, disruptive processes due to differential shrinkage behaviour are expected to occur at all scales.

Cutler & Henrichsen [1968] have shown that compacts of nonspherical particles have departed significantly from the behaviour predicted for spheres. Crushed glass (non-spherical particles) sintered five times faster than the spherical particles of the same size. They assumed that this was due to the sharper radii at the points of contact between the glass powders. Cahn & Heady [1970] suggested that sphere contacts had only normal forces, whereas jagged particles produced shears and torques which were probably important in particle rearrangement leading to densification.

4.1.2 Fabrication of powder compact

The initial pressing of the powder is aimed at giving a shape to the specimen as well as enabling it to be handleable. Its major goal, however, is to lead to uniform density in the

consolidated (green) part. Two types of cold-pressing can be defined: uniaxial and isostatic.

Uniaxial pressing is the process by which ceramic powders are consolidated inside a cavity, into a predetermined shape, through the use of pressure applied in a uniaxial direction. The compaction force is generally applied only vertically, by counteracting mechanical or hydraulic ram. As pressure is applied, particles move to fill interstices and maximise packing. Air is driven out between the punch and the die walls. Initially, the material increases in density by particle sliding and rearrangement, according to the forces exerted on them. As the punches continue their movement, considerable resistance is generated by the compact. At this point, considerable deformation, compaction, extensive crushing and fragmentation of the powder occurs.

As the punches retract from the compact, the residual stress within the part is translated into a relaxation of dimensions. As a result, upon ejection from the die cavity dimensional growth occurs. The extent of this growth is dependent upon the material itself and the compaction pressure employed. This 'spring back' effect creates some common problems associated with dry pressing, such as end-capping, fracture and delamination of the powder compact.

Isostatic cold-pressing is a process which consists in forming components from a dry powder by uniform pressing in all direction [Kennard 1991]. The principle is to enclose the powder in a bag and to submerge it in a fluid medium through which hydrostatic pressure is applied. The uniform application of pressure leads to a very homogeneous compaction of the powder and to very consistent densities.

4.1.3 Sintering process

Sintering is the result of atomic motion, stimulated by an increase in temperature, which provides the interparticle bonding needed to hold together and consolidate a powder mass [German 1991]. Particles sinter together to eliminate the high surface energy associated with solid-gas interfaces (driving force of densification). Sintering can occur as a result of bulk transport, which results in densification, or surface material transport,

which contributes to interparticle bonding without densification. In glass system, most of the densification occur by viscous flow, surface transport is generally insignificant until crystallisation started.

4.1.3.1 Sintering stages

Investigation of sintering behaviour has commonly been simplified by considering the densification to take place in stages. The sintering process is usually modelled in three stages. In the *initial stage*, the individual particles of the green compact, which remain readily identifiable, are bonded together by the growth of necks between the particles and a grain boundary forms at the junction of the two particles. Usually, but not always, the particle centres approach each other. The relative amounts of neck growth and shrinkage that takes place depend upon the mass-transport mechanisms that are operative. As the necks impinge upon each other, an interconnected pore and particle structure known as the *intermediate stage* of sintering develops. Eventually the pores become isolated from each other at the beginning of the *final stage*. Shrinkage is usually observed during all stages of the process, although under some conditions pore growth and compact swelling (overfiring) can occur during the final stage.

4.1.3.2 Driving force

The driving force for sintering is the reduction of the total surface and interfacial energy of the system, thus decreasing the free energy of the system. As the temperature is increased, the atoms acquire some degree of mobility and a compact of particles undergoes changes of morphology that reduce the overall surface free energy.

(I) Surface energy

When the solid glass particles come into intimate contact, attractive forces act to hold the solid bodies together thus preventing them from falling apart. This can lead to the formation of necks between the spherical bodies and to a reduction in surface area. An increase in the surface area of the powder may be expected to result in an increase in the sinterability of the powder compact. Discontinuities in powder compact lead to many centres for shrinkage. In such multimodel sintering, discontinuities widen as shrinkages

occur in opposite directions, there by lowering the overall density. Zones composed of agglomerates, clusters of tiny crystallites, are also detrimental to the sintering of the glass compact. They densify in early and intermediate stages of sintering in such a way that smaller pores are eliminated, which induces the nearby larger pores to grow in size [Ross *et al* 1982].

(II) Porosity

Porosity is almost always present in ceramics that are prepared by powder compaction and heat treatment. Upon firing, pores initially present in a ceramic can change in shape and form either channels or isolated spheres, without necessarily changing in size [Shields 1991]. More commonly, however, both the size and shape of the pores are altered during the firing process. The pores become smaller and more spherical in shape as sintering is continued.

Kingery *et al* [1976] noted that a pore-grain boundary will always migrate towards its centre of curvature. A pore with flat sides is stable and represents the transition between pore shrinkage and pore growth conditions. The stable, flat-sided pore can in turn be modelled as polygon with vertex angles equal to the ceramic's dihedral angle. Emanating from each vertex would be the grain boundaries for the surrounding grains. By extrapolating this model into 3-D, Kingery arrived at a critical pore size/ grain size ratio for a given dihedral angle. Pore shrinkage, and thus densification, would occur only for pores smaller than the critical ratio.

4.1.3.3 Densification mechanisms

In essence, densification can be considered as the process of shrinking and, ultimately, eliminating pores. Before firing, almost the entire porosity of a ceramic material is represented by open pores. Porosity remains entirely open until about 85% relative density is reached, at which stage closed porosity begins to be detectable [Budworth 1968]. The closed porosity increases slowly at first and then more rapidly until, at about 95% relative density, all the porosity is closed. In the event that the pores became

closed during the firing process, a comparison of the true (theoretical) density before and after sintering would give an indication of the quantity of closed pores.

The possible mechanisms that might provide mass transport have been more or less understood for sometime [Kuczynski 1949; Kingery & Berg 1955; and Coble 1958], although an unambiguous determination of the relative importance of various of these mechanisms has often been difficult if not impossible.

It is quite probable that more than one of the sintering mechanisms will be active during the initial sintering of most materials, and the over-all behaviour of the compact will be the result of the interplay among these mechanisms. High relative surface diffusion or vapour transport could result in entry into the intermediate or even the final stage of sintering after relatively little shrinkage. On the other hand, a low surface diffusivity and vapour pressure would result in maximum shrinkage before the onset of the intermediate and final stages. The former case would tend to give some strengthening without shrinkage, and, therefore, good dimensional stability, while the latter would tend to result in high density. However, macroscopic flow (viscous or plastic) caused by stresses in the proximity of curved surfaces is the important mechanism that control sinterability in glass.

4.1.4 Theoretical models

Exner [1980] presented a systematic survey of concepts for deriving equations for isothermal shrinkage (linear or volume shrinkage, increase of density, or decrease of porosity). Models developed to explain the sintering of glasses are based on two spheres of equal size to ease the understanding of the process. The first model explaining sintering by viscous flow was proposed by Frenkel [1945]. According to this model, the energy dissipated in viscous flow is equal to the energy lost by the decrease in surface area during densification so the densification takes place through flow driven by surface tension, γ. The equation that was derived by Frenkel is:

$$\frac{\Delta L}{L_0} = \frac{3\gamma t}{4r\eta} \qquad [4\text{-}1]$$

where $\frac{\Delta L}{L_0}$ is fractional reduction in length of the powder compact,

γ is the surface tension,

t is time.

η is the viscosity, and

r is the radius of the glass particles

The validity of Frenkel's viscous flow model was confirmed by Kuczynski & Zaplatynskyj [1956], Cutler [1969], Kingery *et al* [1976] and Giess *et al* [1984]. They suggested that the surface tension did not change much with temperature but the viscosity was exponentially related to the temperature, although the latter may only be true for a narrow range of temperatures.

Using Frenkel's energy balance concept, Mackenzie & Shuttleworth [1949] calculated the rate of densification of a viscous body containing closed spherical pores. The interior of each pore has a negative pressure equal to $\frac{2\gamma}{r}$ which is balanced by the positive pressure on the exterior of the compact tending to consolidate it. Here "r" stands for pore size. Their proposed equation is

$$\frac{d\rho'}{dt} = \frac{3\gamma}{2r_0\eta}(1-\rho') \qquad [4\text{-}2]$$

where ρ' is the relative density which is the ratio of bulk density to true density,

r_0 is the initial particle radius

Among various parameters in Equations 4-1 and 4-2, ones which change with glass composition would be surface energy, γ, and viscosity, η. Thus the overall densification of a glass compact with identical geometry but different composition should be given by

$$\frac{dF(\rho)}{dt} = \frac{C\gamma}{\eta} \qquad [4\text{-}3]$$

where C is a constant and

$F(\rho)$ is a function of relative density which increases with increasing density.

Thus, the rate of densification can be increased by increasing the temperature and changing the composition to lower the viscosity of the glassy material.

In constant heating rate sintering, using the heating rate $\beta = dT/dt$

$$dF(\rho) = \left(\frac{C\gamma}{\beta}\right)\left(\frac{dT}{\eta}\right) \qquad [4\text{-}4]$$

where $(C\gamma/\beta)$ can be regarded as a constant.

An empirical model for initial through final shrinkage was developed by simply applying a function related to first-order chemical reactions that expresses the progressive change in density of sintered compacts. The equation for the sintering kinetics of polydisperse powder is

$$K = \frac{1}{t} ln \frac{\rho_g - \rho_0}{\rho_g - \rho_t} \qquad [4\text{-}5]$$

where K is the rate constant of sintering,

ρ_o the density of a pressed unfired compact of powder,

ρ_g the pycnometer density of the glass particles, and

ρ_t the density of the sintered compact after time *t*..

An activation energy for the sintering process was obtained when the temperature dependence of K was described by an Arrhenius relation

$$K = K_0 \, exp\left(-\frac{E_s}{RT}\right) \qquad [4\text{-}6]$$

where K_0 is a pre-exponential constant.

In a system which sintered successfully to zero porosity [Clark & Reed 1986], the activation energy for sintering was comparable to the activation energy of viscous flow. When the apparent activation energy for the sintering process was lower than that of viscous flow, sintering was found to proceed at a slower rate because the precipitated crystalline phase retarded viscous flow and the shrinkage of the pores.

4.1.5 Sintered glass-ceramics

The most desired characteristic of glass-ceramics formed by the sintering of powder is a non-porous body. Obtaining this property has been met with difficulties and limited success because in the case of ceramic materials made from glass powders, pre-existing

surfaces act as nucleation sites, and the crystallites may grow from the surface of every glass particle toward centre.

Rabinovich [1987] found that glass-ceramics which exhibit efficient bulk nucleation are unsuitable for processing via a powder route because, on heat treatment, they rapidly develop crystalline phases which inhibit further sintering. It has been further proposed that glasses in which the nucleation of crystal phases is predominantly heterogeneous (i.e. surface rather than bulk nucleated) are more suitable for powder processing because the overall rate of crystallisation is much lower than in materials exhibiting efficient homogeneous nucleation. Thus, by delaying the crystallisation process, the chances of sintering to high density are enhanced. Glasses which are usually capable of surface crystallisation at relatively low viscosity may be successfully sintered either before crystallisation or simultaneously with crystallisation. Viscous sintering of a glass can be done either isothermally [McCoy & Heuer 1988] or at constant heating rate (CHR) [Panda & Raj 1989].

On the two temperature characteristics of crystallisation namely, crystallisation start temperature (Tx) and crystallisation peak temperature (Tp), Tx is more relevant in determining sinterability, i.e. the viscosity at the Tx has better correlation with the viscous sinterability of crystallisable glass system [Panda *et al* 1989].

The viscous sintering rate is inversely related to viscosity of the glass, and because CHR can shift crystallisation peak temperature (T_p) to higher values compared to isothermal sintering, lower viscosity regions can be accessed before crystallisation [Panda & Raj 1989]. In other word, densification can be controlled by changing the heating rate [Panda et at 1989]. It reflects the fact that crystallisation depends upon 2 kinetic steps, nucleation and growth, whereas densification depends only upon viscous flow. Because nucleation depends not only upon viscosity but also upon undercooling (see section 3.1.2.1), a slower heating rate favours the crystalllisation process, relative to the sintering process which depends only upon viscosity.

4.1.6 Effect of rigid inclusions

The sintering of compacts of particles with rigid inclusions has received considerable attention recently [Rahaman & De Jonghe 1987, Bordia & Scherer 1988, Sudre & Lange 1992] as the physical and mechanical properties of the composites can be considerably improved if sintering is controlled. It is now widely recognised that inclusions and heterogeneities can have important effects on sintering. Inclusions of different elastic moduli and thermal expansivity induce differential sintering rates, which in turn produce transient stresses during sintering [Selsing 1961 and Evans 1982]. The nature of the interface between the second phase and matrix will also influence their fracture mechanical properties [Hasselman & Fulrath 1966, Lange & Radford 1971].

Bordia & Raj [1986] proposed as the matrix shrinks, the constraint imposed by rigid particles generates a shear stress in the matrix and a tensile hoop stress at the particle-matrix interface. Unless the shear stress can be relaxed by shear flow in the matrix, the hoop stress will become locked-in, causing the sintering rate to fall, thus retarding the densification rate of the composite and generating flaws. However it was later shown that the magnitude of the stresses that might develop within the compact is too small to produce any significant retardation of the matrix densification [Scherer 1987]. Further variations on this approach proposed that cracks that pre-exist in the matrix powder open under the hydrostatic tensile stresses and allow the adjacent matrix regions to densify.

Mechanical adherence is obtained in high CTE matrices, which leads to strengthening, The matrix contracts around the particles on cooling and so provides bonding. In poorly-bonded systems micromechanical stress concentrations will develop on loading. Strengthening will therefore only be seen for matching or high CTE matrices and even this improvement will be limited.

4.2 Experimental procedure

4.2.1 Powder preparation

The glass prepared by fast cooling from the melt was reduced to powder by using a tungsten carbide Tema mill. To produce particle size less than 38 μm, the powder was crushed for 5 minutes. By sieving, particles larger than 38 μm were removed. After grinding, the powder was placed in a bottle in a desiccator to avoid contact with environmental humidity. The particle size distribution was determined by laser diffraction method with a Malvern 3600 particle size analyser.

4.2.2 Dry pressing and Isostatic pressing

To prepare cold pressed samples, powder was placed into a steel die. A unidirectional force was applied through upper and lower punches with a manual press. In order to minimise the 'springback' effect, the applied pressure employed in the present work were just high enough to hold the powder compact in shape, 10 MPa. After the sample was pressed it was placed in a desiccator.

To prepare samples by isostatic pressing, samples were previously pressed by uniaxial pressing to the desired shape. Each sample was placed in individual plastic bags and sealed with the application of heat. The equipment used was a Atansted Fluid Power Press and a pressure of 3000 MPa was applied. Two different kinds of samples were prepared: 6.6mm diameter x 10mm long cylinders for dilatometry and 4x34x8 mm^3 bars for mechanical testings.

4.2.3 Characterisation techniques

The characterisation techniques employed for sintered CS and CSF glass were essentially the same as described for the bulk cast glass. Details of the sample preparation and experimental procedure were described in the previous chapters: density in 2.3.3 (i), differential thermal analysis in 2.3.3 (iv), dilatometry in 2.3.3 (iii), and scanning electron microscope in 3.5.1 (ii).

4.3 Results and Discussion

4.3.1 Powder characterisation

Powders utilised in the sintering study were CS and CSF crushed glass powders, and three rigid reinforcement particles were used, namely, alumina, zirconia, and silicon carbide. All powders were dried and sieved (-38 μm) before being characterised by laser particle size analysis and scanning electron microscopy. Particle size distributions displayed in Figure 4-1 reveal that the CS and CSF glass powders were in similar size range, between 1 to 40 μm with the average size smaller than 10 μm, but the filler particles were bigger with an average size larger than 15 μm. However, it should be borne in mind that the laser particle sizer gives the distribution in weight percent, therefore a few particles with large volumes will greatly increase the weight percent of the higher size ranges. The particle size ranges and densities are shown in Table 4-2. Figure 4-2 shows scanning electron micrographs which illustrate typical jagged particles of glass powders and of SiC and Al_2O_3 particles, and agglomerated ZrO_2 particles.

4.3.2 Differential thermal analysis

Differential thermal analysis (DTA) profiles obtained from CS and CSF glass powder samples are shown in Figure 4-3. Basically, the DTA profiles are very similar to the ones obtained from the bulk glasses; i.e. one and two exotherms for CS and CSF glass, respectively, and the thermal characteristics points; i.e. glass transition temperature, T_g, crystallisation starting point, T_x, and peak temperatures, T_p, increased with increasing heating rate. However, several thermal events have been altered by the presence of high surface area of the powdered glasses.

Firstly, the shape of the exotherms was more distinct for the CS glass; i.e., the peaks are narrower and larger than those of the CSF glass, which is opposite to the results obtained from bulk glasses. Secondly, the exotherms occur at lower temperatures than for the bulk glasses; i.e. in CS by approximately 125˚C and 230˚C for the start and peak

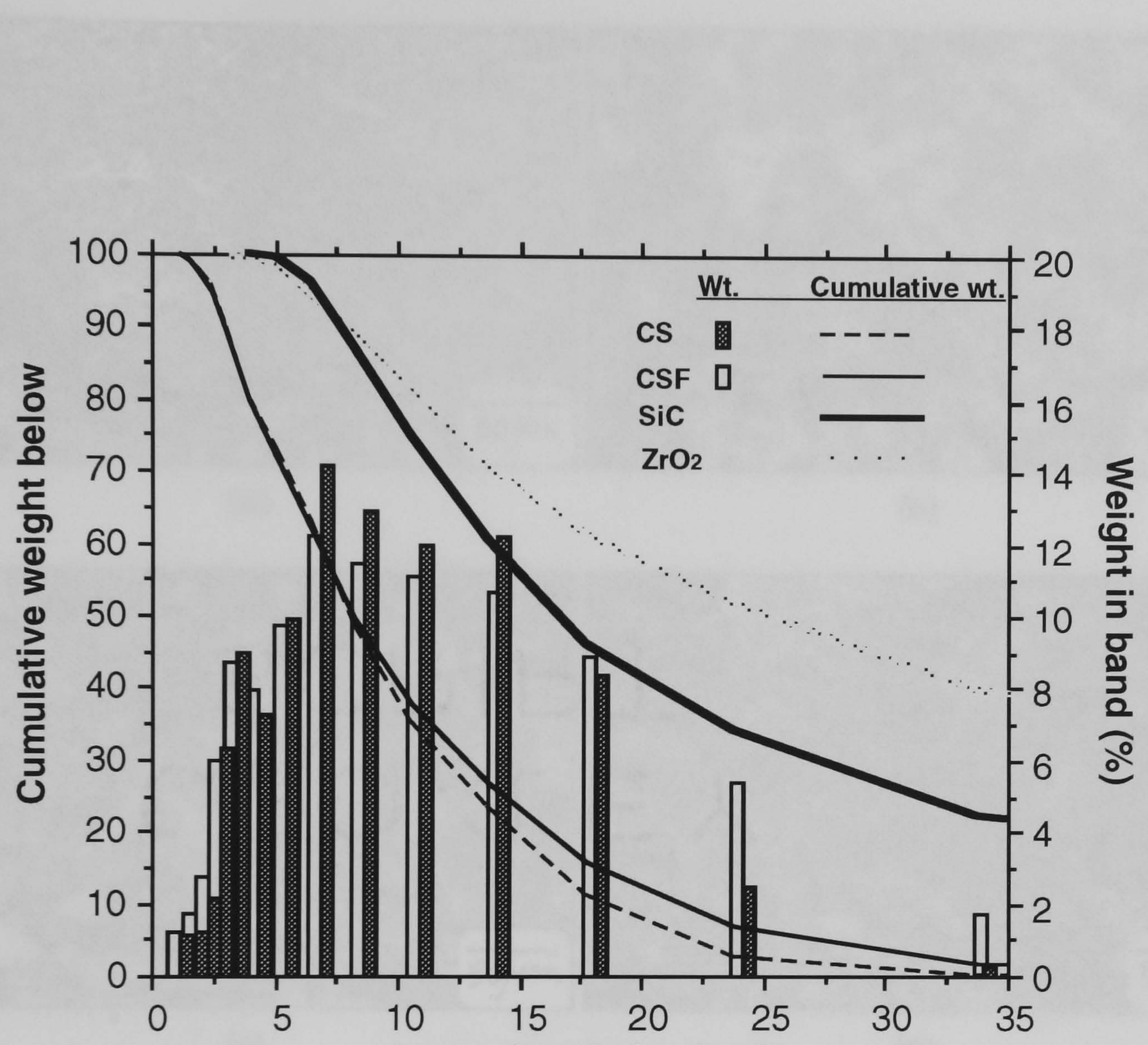
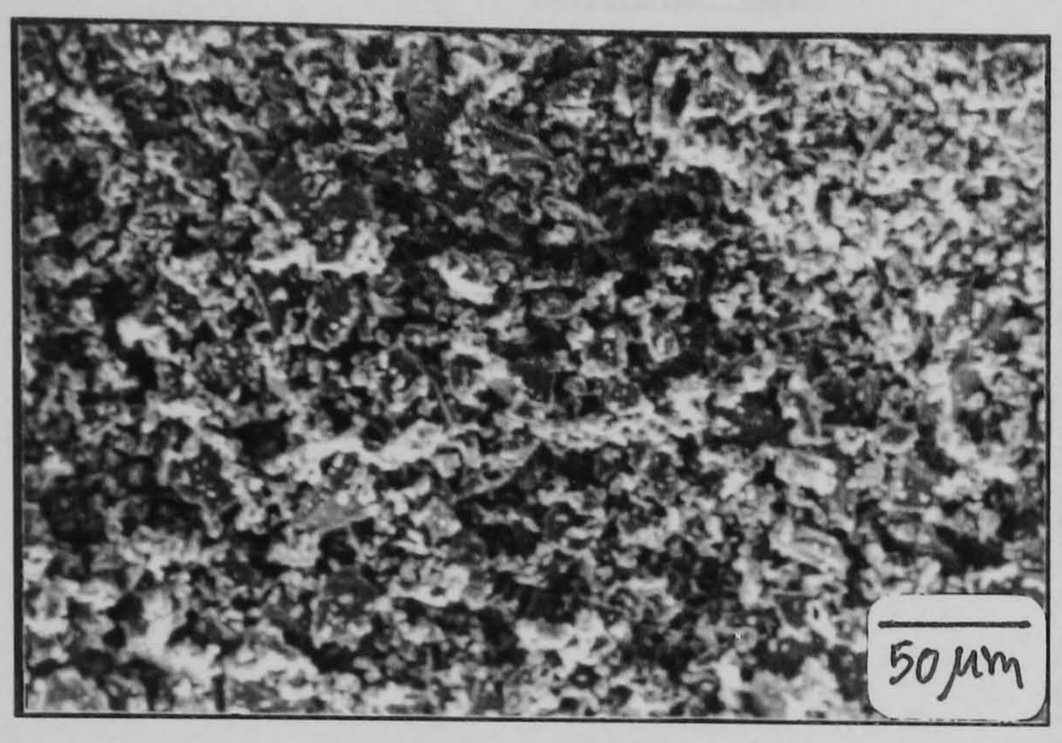


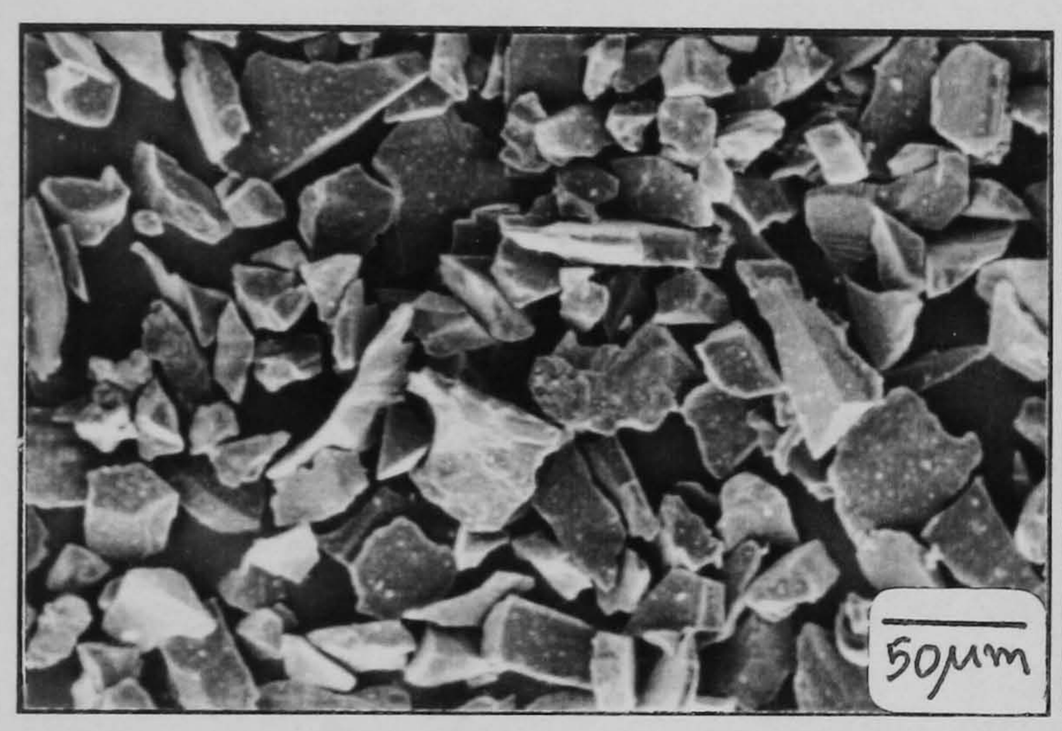
Figure 4-1 PZD cumulative weight below and weight in band of CS, CSF, SiC, and ZrO_2 powders from laser sizer



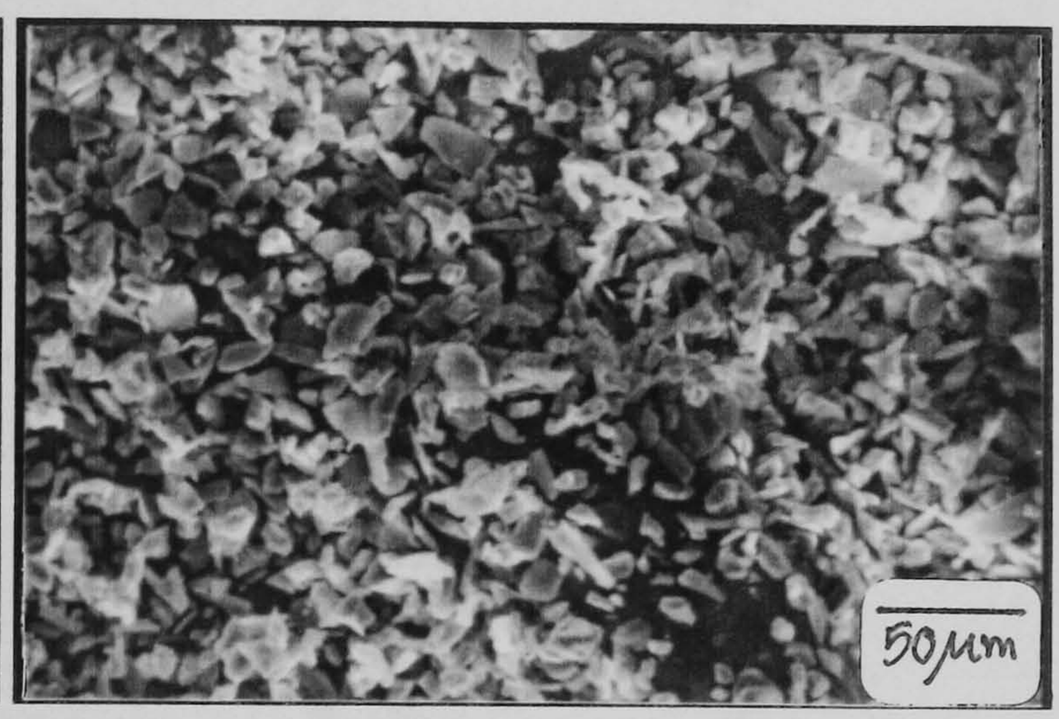
(a)



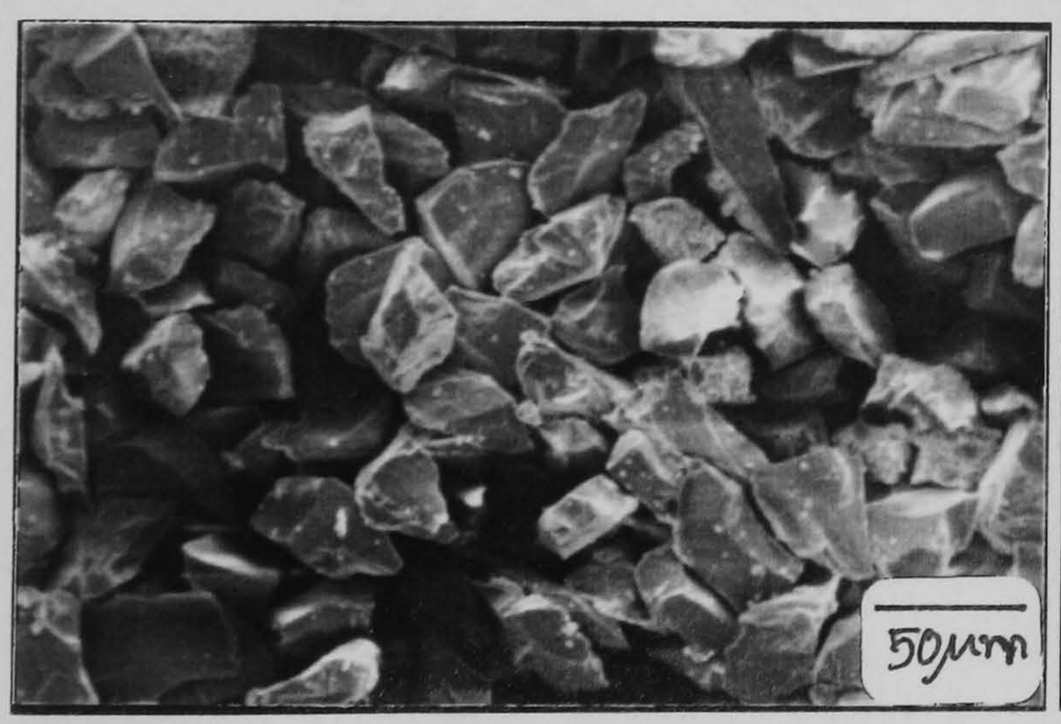
(b)



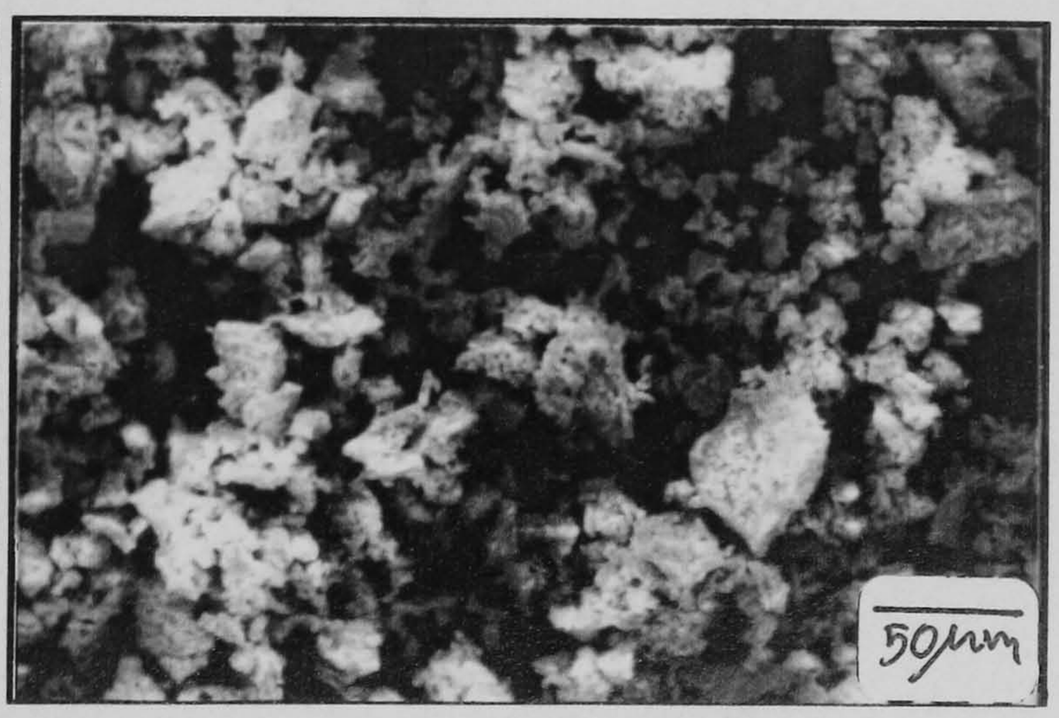
(c)



(d)



(e)



(f)

Figure 4-2 Scanning electron micrographs which illustrate typical jagged particles of (a) and (b) glass powders, (c) and (d) coarse and fine SiC, (e) Al_2O_3, and (f) ZrO_2

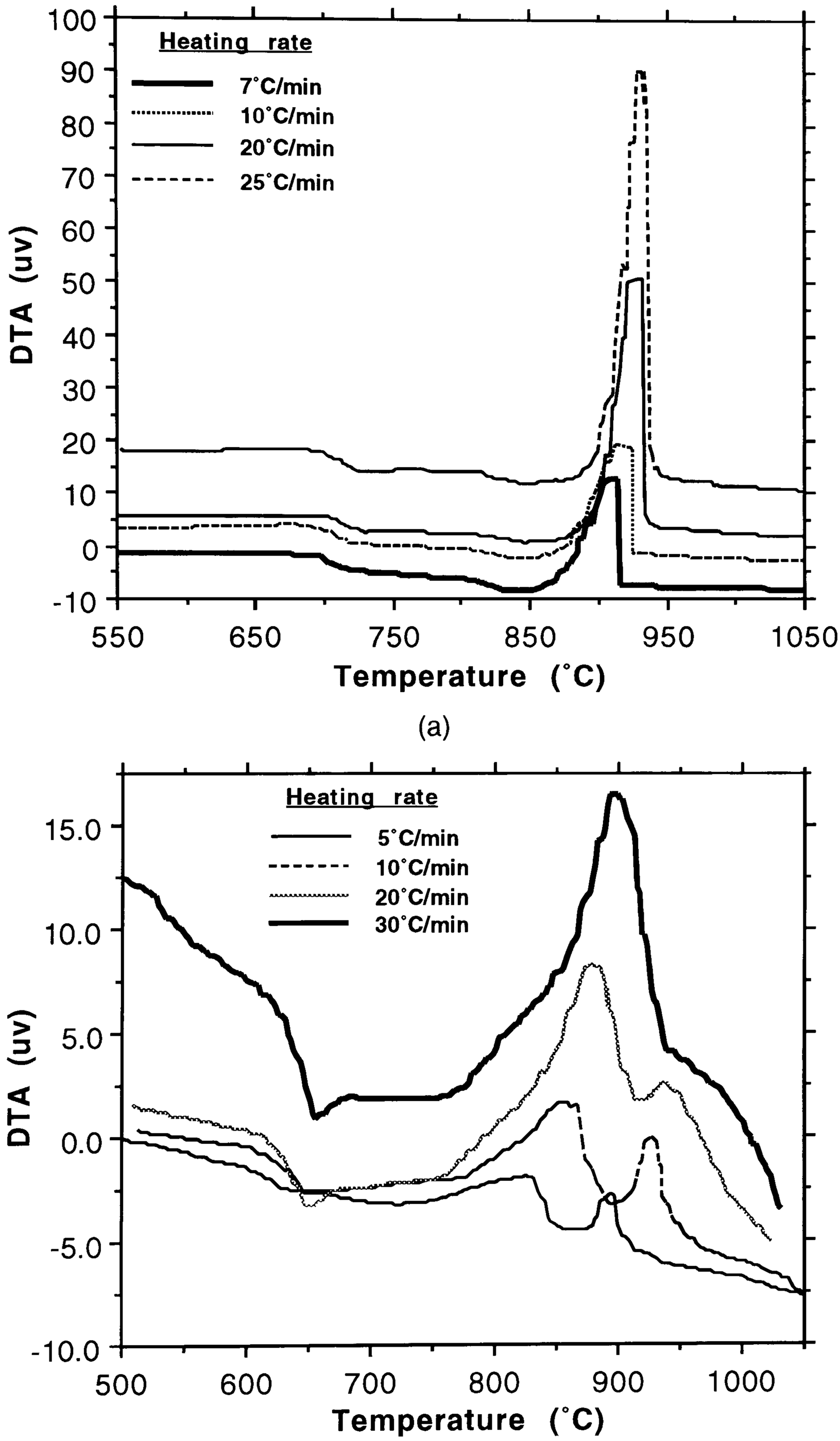
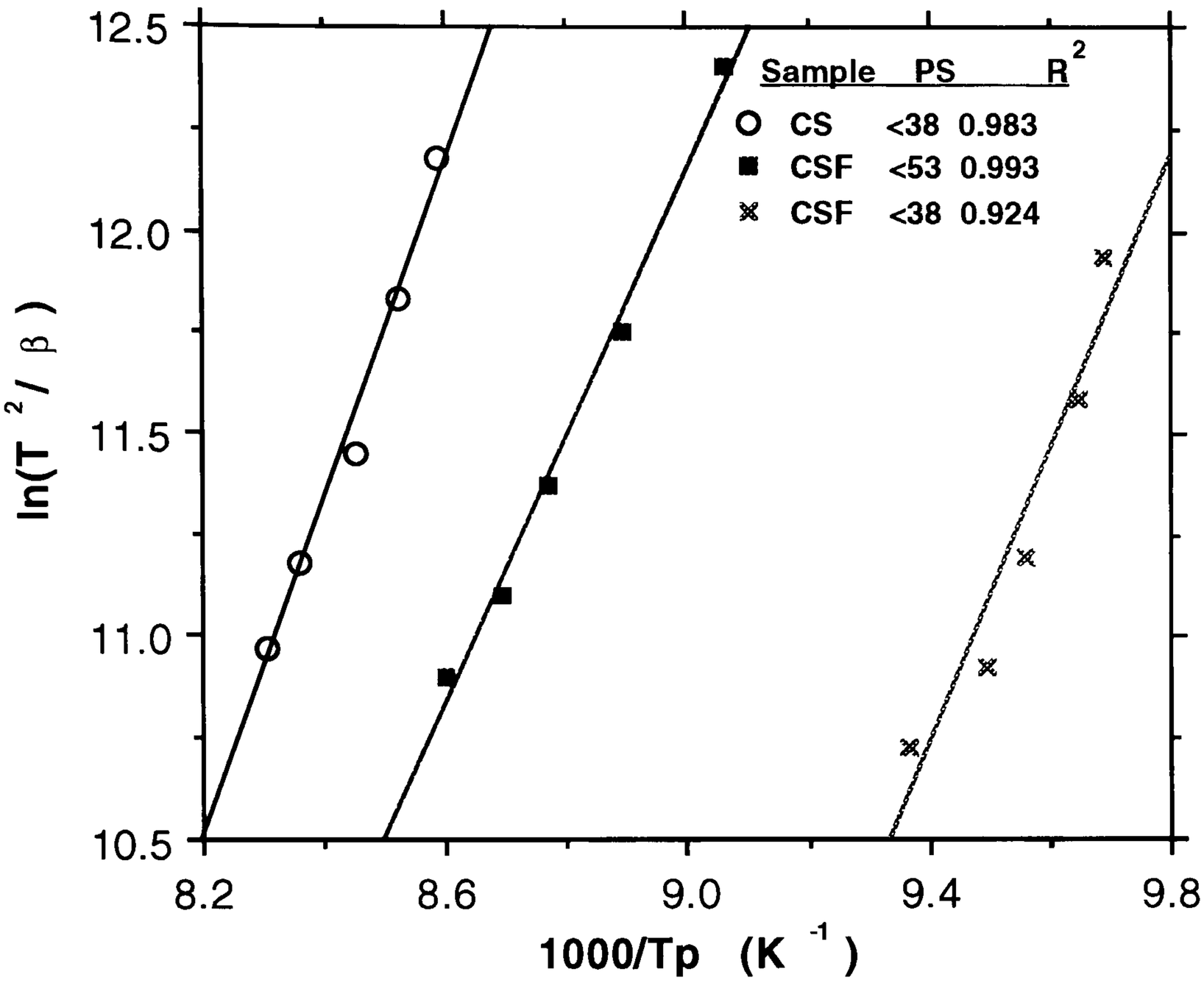


Figure 4-3 DTA profiles of (a) CS and (b) CSF powder glass at different heating rates

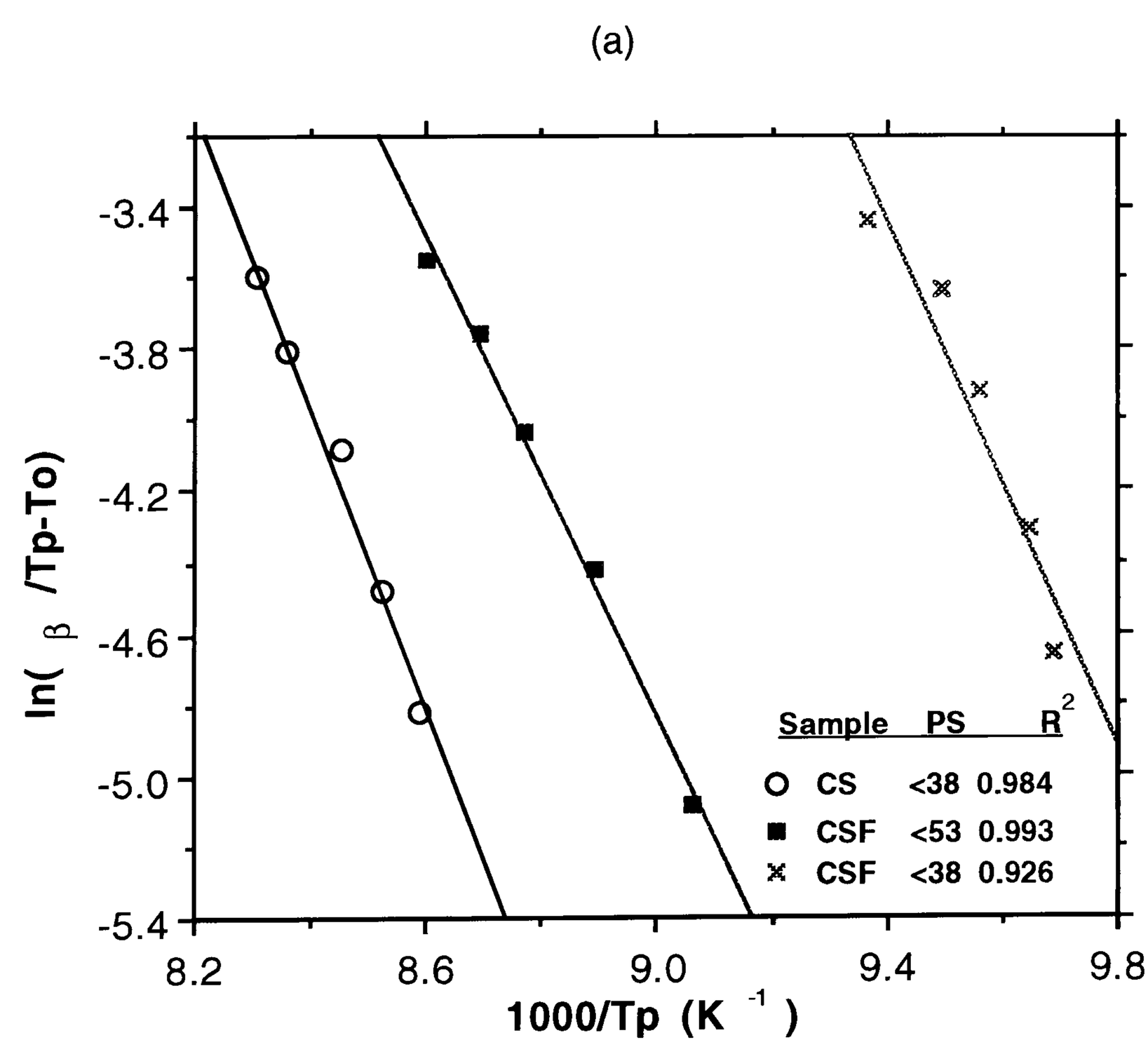
temperatures, respectively and in CSF by 100 and 80°C, respectively, which implies that the free surface facilitates crystallisation because it provide heterogeneous nucleation sites. Nucleation probability increases with the total surface area; therefore, the finer size glass powder was more likely to produce a large amount of nucleation sites.

Finally, several temperatures in CS were shifted in favour of sintering to be completed before crystallisation started. From Table 4-1, the isothermal T_g of CS powder glass, 677°C, was 74°C higher than that of CSF, and the isothermal temperature where crystallisation started, T_x, of CS glass, 832°C, was 141°C higher than that of CSF glass. It can be deduced that the T_x-T_g in CS glass is approximately 67°C greater than that of CSF glass. The higher the difference between T_x and T_g, the longer the time the sintering can proceed before crystallisation starts. Because viscosity of the sample can increase due to crystallisation because of the higher SiO2 content of residual glass and the viscosity of a glass decreases exponentially with increasing temperatures, small variation in T_x-T_g with composition will cause large variations in viscosity at T_p [Pampuch & Lis 1989]. Hence sintering should progress at a faster rate in CS glass and the CS compact should achieve higher densification than CSF.

Figure 4-4 illustrates Arrhenius plots calculated via Kissinger's and Augis-Bennett's methods for CS and CSF powder glass. The activation energies (E_a) for crystallisation of CS and CSF glass powders are given in Table 4-2. It can be seen that E_a was decreased with fluoride addition and with an increase in particle size of the CSF glass powder. The activation energy for crystallisation of CS powder was within about 6% of the value obtained from bulk glass, indicating that the transformation occurred in both states involves equivalent amount of rearrangement by a similar mechanism in the glass structure. In contrast, the activation energy for CSF glass powder (308 kJ/mol) is approximately two times higher than the value in bulk glass (132 kJ/mol), implying that the kinetics for the crystallisation was changed from diffusion controlled in the bulk glass to viscous flow in the powder glass. Possible explanations were discussed in section 3.3.1.1.



(a)



(b)

Figure 4-4 Arrhenius plots via (a) Kissinger's and (b) Augis-Bennett's methods for calculation of E_a.

Table 4-1 Thermal characteristics constants of bulk cast CS and CSF samples.

Heating rate	CS			CSF		
	T_g	T_x	T_p	T_g	T_x	T_p
7	685	841	891	610	679	759
10	686	853	900	607	732	764
15	688	853	910	609	734	773
20	699	864	924	613	730	780
25	700	873	931	619	730	795
Isotherm	677	832	877	603	691	744
R^2	0.890	0.932	0.990	0.744	0.373	0.984

Table 4-2 The apparent activation energy for crystallisation and Avrami exponent in CS and CSF glass powders.

Sample		E_C (kJ/mol)		Avrami exponent
Composition	Particle size (μm)	Kissinger	Augis-Bennett	
<u>1st peak</u>				
CS	<38	347	354	4.94
CSF	<38	302	308	1.04
CSF	<53	273	278	1.50
<u>2nd peak</u>				
CSF	<53	247	254	-

The E_a of the second peak in CSF glass corresponds to the crystallisation of wollastonite and, as previously discussed for bulk samples, is much lower than the E_a for crystallisation of wollastonite in the corresponding CS glass. This suggests that the crystallisation of cuspidine in CSF (1st peak) assists formation of wollastonite. However, it should be noted that the value is subject to inaccuracy since the T_p is not clearly identifiable at high heating rates. E_a for crystallisation in CSF bulk is lower than that for powder CSF. Von Schweitzer [1994] also found E_a for crystallisation of diopside in silceram glass-ceramics was higher in powder sample than in bulk ones.

The high surface area of the powdered glass plays an important role in altering the mode of crystallisation and the Avrami constant. The Avrami exponent of CS powder indicates that crystallisation occurred in three-dimensional growth mode whereas surface crystallisation, one-dimensional growth, was predominated in CSF glass powder. On the contrary, the Avrami exponents from bulk glasses imply that crystals in CS glass grow one dimensionally and in CSF glass grow three dimensionally as discussed in section 3.3.1.1. Because of the high surface area of the powder, CSF glass crystallised instantaneously when the glass was undergoing heat treatment, and crystallisation occurred mainly on the surface of the particles. As a consequence, sintering was halted and the glass particles remained separate entities. But CS glass powder sinters and forms bulk glass before crystallisation occurs. It has been suggested [Rabinovich 1979] that the coalescence of glass particles before crystallisation causes a reduction of a significant portion of the surface, but even after particle coalescence, the traces ("memory") of the original surface could remain as sites for the initial stages of crystallisation. Therefore, the apparent crystallisation seems to be homogeneous throughout the bulk glass. This indicates that particle size effects are important for controlled sintering and crystallisation.

4.3.3 Densification Study

4.3.2.1 Constant heating rate treatment

Dilatometric curves obtained for CS and CSF glass samples at 15°C/min are shown in Figure 4-5. The dilatometric shrinkage of CSF glass occurred in the temperature range

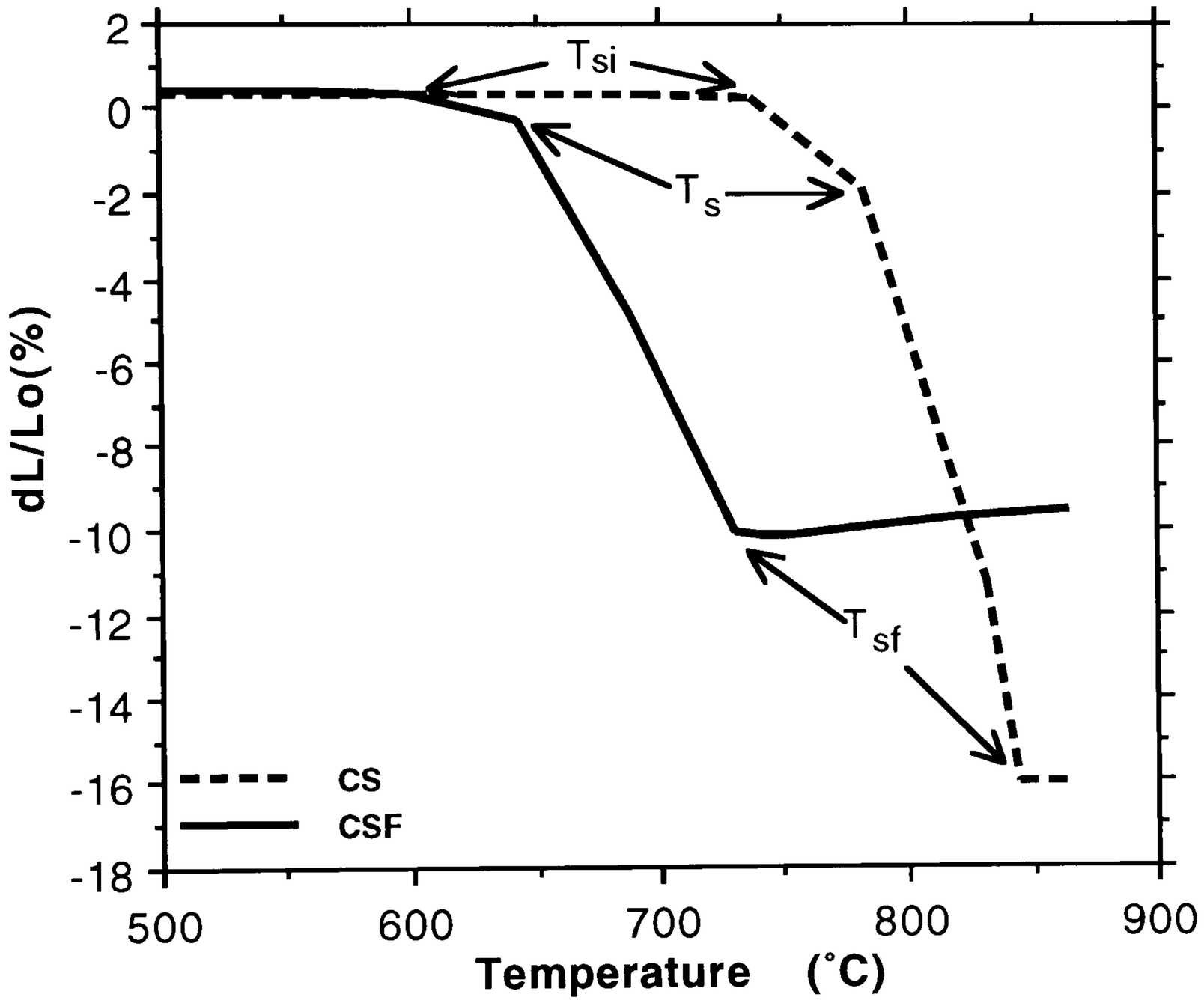


Figure 4-5 Dilatometric plots showing effects of temperature on densification of CS and CSF glass powders.

from 643 to 731°C and achieved smaller densification (7%) compared with that of CS glass (16%). CSF starts and finishes shrinking before CS and the shrinkage rate was 0.11 and 0.21 %/°C for CSF and CS glass respectively, thus the CSF shows less shrinkage in total. The sintering starting, T_{si}, and completion, T_{sf}, temperatures are indicated in the figure and are tabulated in Table 4-3, together with the glass transition, T_g, and crystallization starting, T_x, temperatures and peak temperatures, T_p, obtained from DTA using the same glass powder and the same heating rate. It can be seen that, the values of T_x-T_{sf} for CS and CSF are 16°C and -65°C, respectively; i.e. sintering is completed before crystallization commences in CS but is incomplete at the commencement of crystallization in CSF and continues until eventually halted by the degree of crystallization.

4.3.2.2 Isothermal treatment

(i) CS

Isothermal shrinkage data for different temperatures are compared with CHR shrinkage data obtained from CS glass powder in Figure 4-6. Figure 4-7 illustrates the isothermal shrinkage as a function of time. Samples shrink by viscous flow and spring pressure

Table 4-3 Significant thermal points reference glass transition temperature from DTA (T_g), sintering temperature from dilatometer (T_s) and temperature starting and finishing crystallization from DTA (T_x and T_f respectively) for CS and CSF (<38 mm) powders at 15°C/min, within accuracy of ±5°C

Thermal characteristics	CS T/°C	CSF T/°C
DTA		
T_g	688	609
T_x	861	666
T_p	910	773
Dilatometry		
T_{si}	736	600
T_s	781	643
T_{sf}	845	731

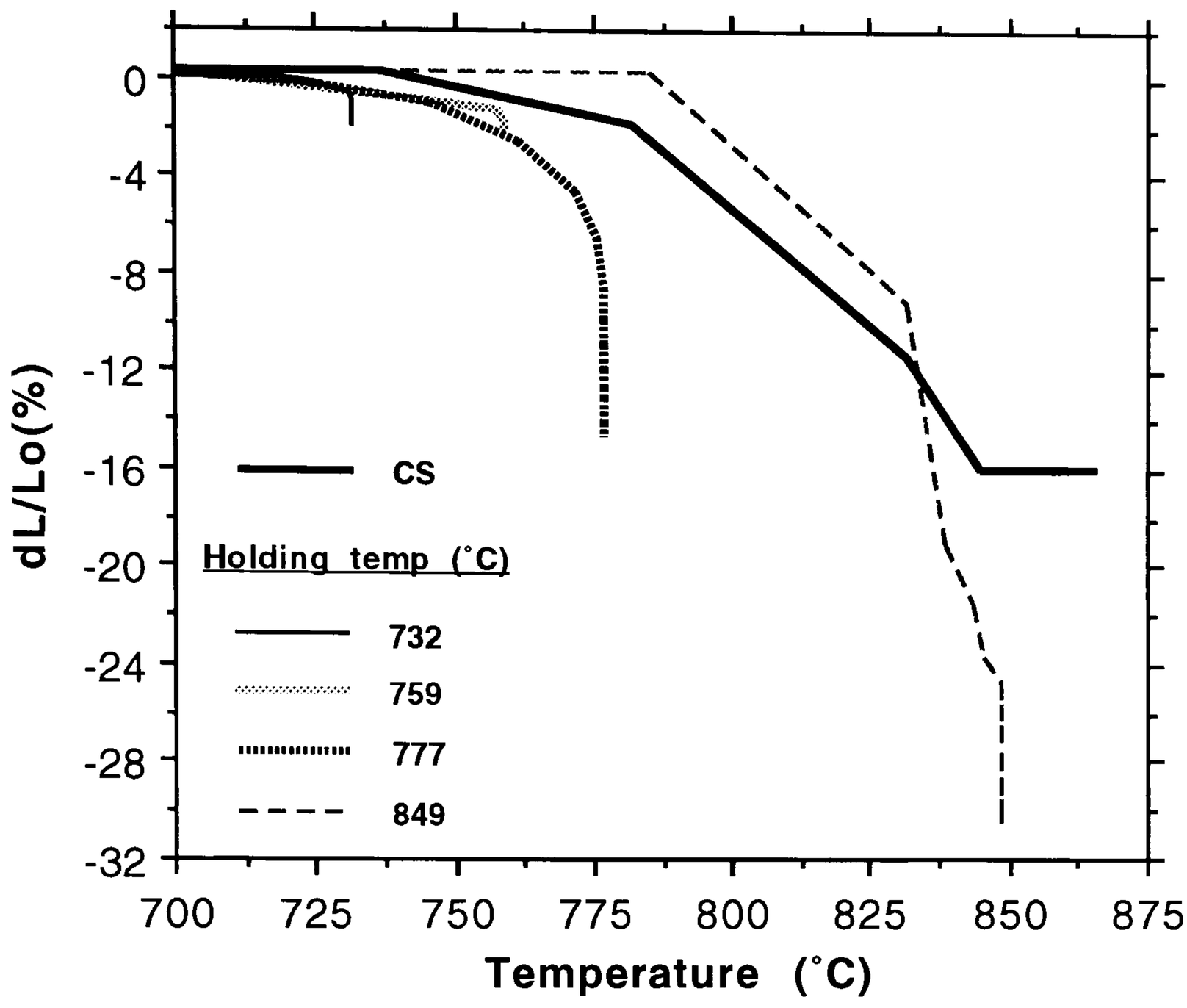


Figure 4-6 Linear shrinkage of CS glass heat treated at 15˚C/min compared with those heat treated isothermally at 732, 759, 777, and 849˚C. The shrinkage at the holding temperature is represented by the vertical drop on the plots.

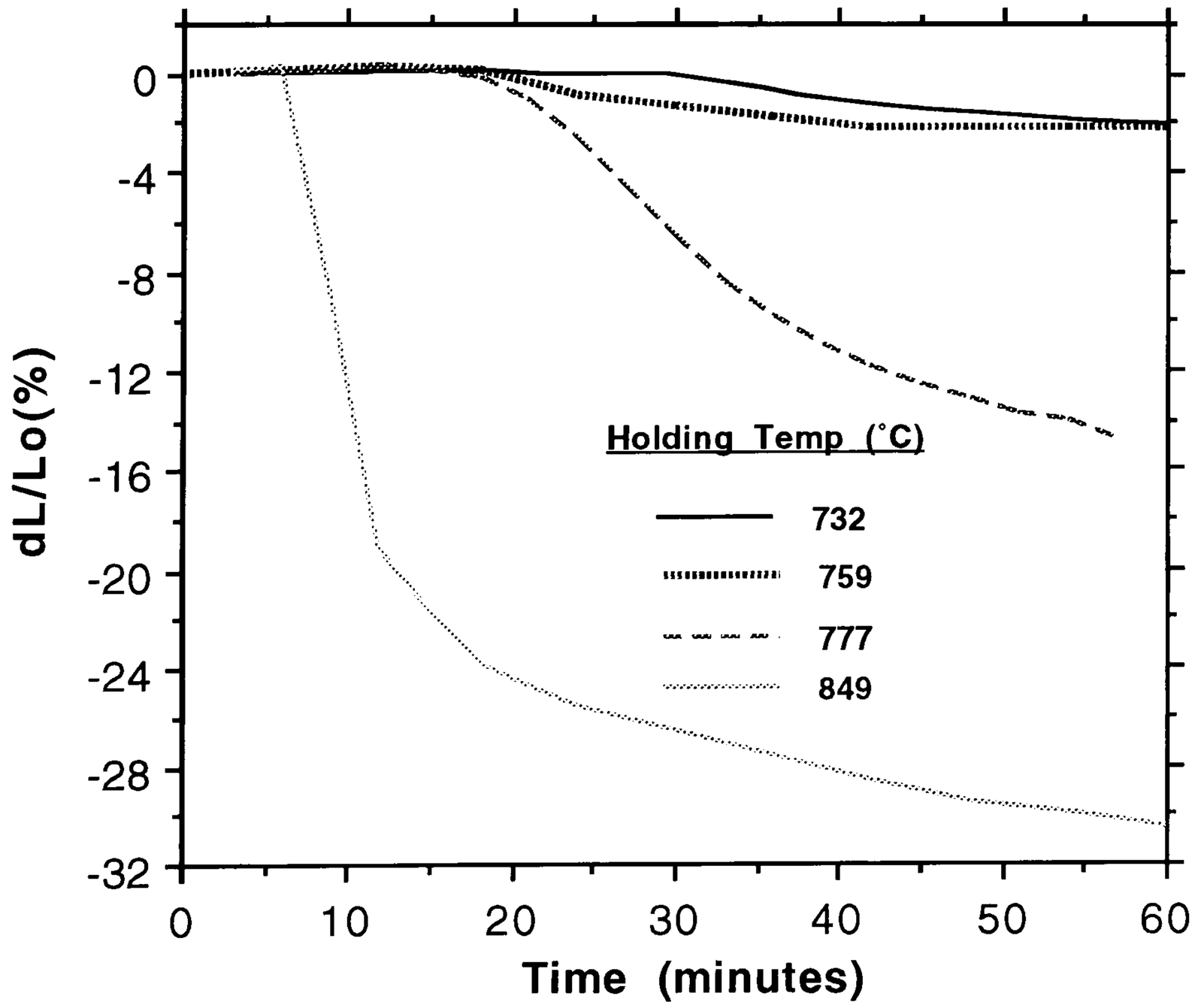


Figure 4-7 Isothermal treatment of CS glass under dilatometry at 750, 780, 800, and 850˚C.

from the dilatometer rod. At earliest stages of sintering, at temperature range between T_g and T_{si}, mass transport by surface diffusion should bring about an insignificant overall shrinkage and, at the same time, should decrease the capillary driving force for densification first by increasing the radius of curvature of the neck surface between the particle and, next, by coalescence of the particles. Hence, there should be a competition between the effects of mass transport by surface diffusion and the effects of volume and grain-boundary diffusion producing an approach of grain centres and shrinkage [Pampuch & Lis 1989]. At T_{sf}, the rather abrupt halt in shrinkage demonstrates the sudden onset of crystallisation [Panda *et al* 1989].

Holding temperature in the range between T_s and T_x makes the CS sample shrink more than the sample heat treated at constant heating rate up to T_p. The decrease in sample size corresponds to the intermediate stage where the viscosity is greatly decreased and the densification is controlled by viscous flow at the boundary between glass particles. The shrinkage rates derived from the linear shrinkage part are plotted against the holding temperature in Figure 4-8. The shrinkage rate remains constant at holding temperature lower than T_s and greatly increases at higher temperatures. The sample heat treated at 849°C sintered at a very high shrinkage rate within 10 minutes and was observed to deform a great deal in both longitudinal and radial directions and showed glossy texture when cooled down.

The isothermal dilatometric plots also provide the direct information of percentage of shrinkage at certain time and temperature. If the shrinkage is assumed to occur only in longitudinal direction and the effect of the dilatometric push-rod was negligible, the data for the progressive change in size of sintered compacts may be inserted into Eq. 4-5), the sintering kinetics of polydisperse glass powders is then given by

$$K = \frac{1}{t} ln \frac{dL}{L_0} \qquad [4\text{-}7]$$

where K is the rate constant of sintering,

dL/Lo is the shrinkage of the sintered compact after time t.

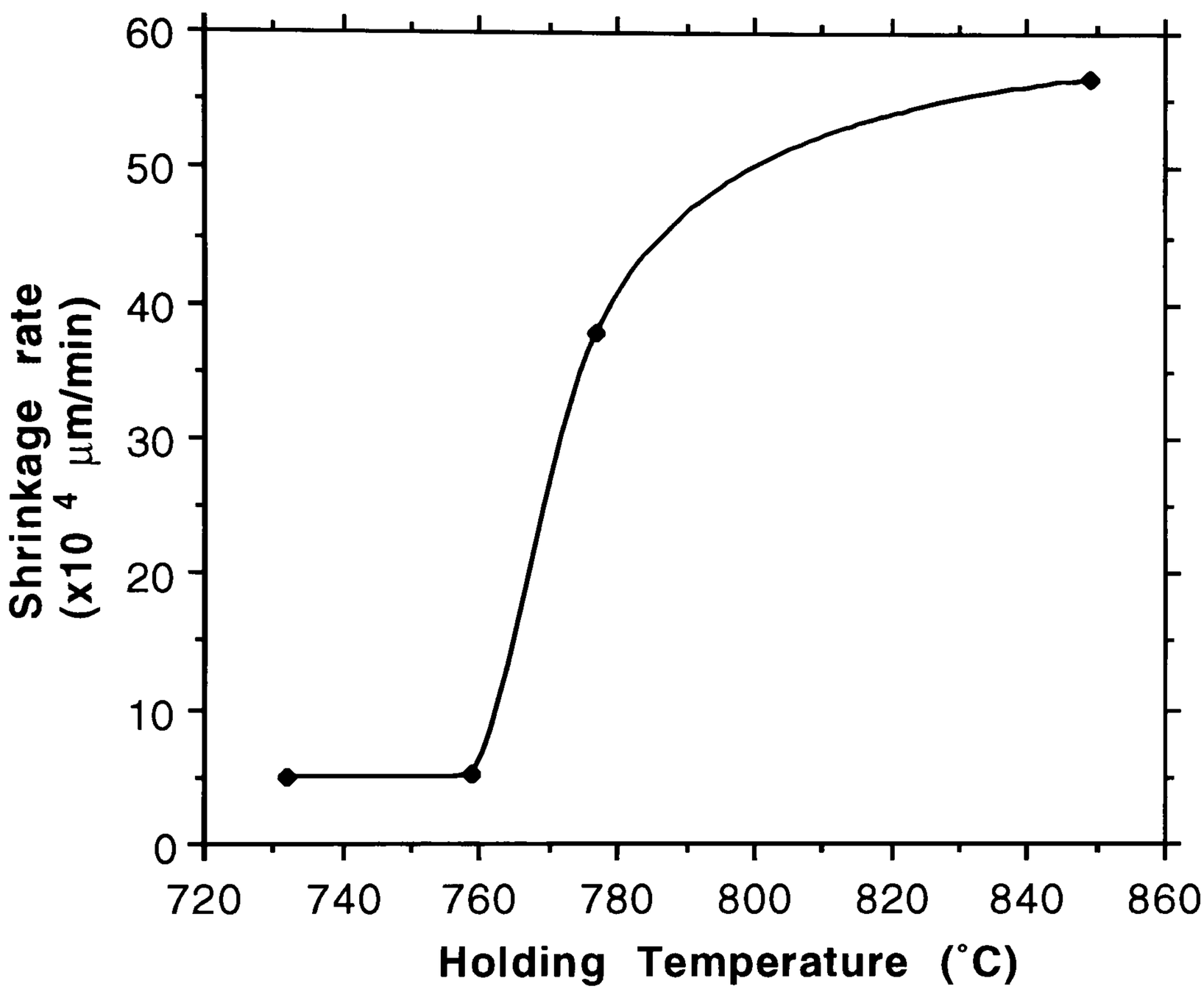


Figure 4-8 Shrinkage rate of CS powder derived from Figure 4-7.

The resultant plot between the sintering constant (K) values at time (t) is shown in Figure 4-9. The rate of change in K was separated into initial and intermediate stages. Arrhenius plots of the rate constant of sintering vs reciprocal of isothermal temperature are illustrated in Figure 4-10. The activation energy for sintering, E_s, can not be directly compared with the values obtained from DTA technique, because of different settings; e.g. the mode of heat treatment, temperature range and the limitations described below. However, E_s in the initial stage (90 kJ/mol) was 25% higher than the value obtained from the 2nd stage (70 kJ/mol), which implies that the sintering kinetics in the initial stage involves more of viscous flow than diffusion compared to the E_s in the intermediate stage.

Some limitations for this technique are (a) the shrinkage occur in both longitudinal and radial directions, especially when heat treated at temperature higher than T_s [Cutler 1969, Panda *et al* 1989, Panda & Raj 1989], (b) the temperature in the dilatometer is assumed to be constant, but practically the dilatometer required approximately 20 minutes to heat the sample up to the designated temperature and an inevitable degree of shrinkage was certainly occurred at this period, and (c) the pressure of the silica rod touching the powder compact (~ 0.1 MPa) also takes part in the sintering process. However, qualitatively, it provides guideline for the significant kinetics controlling the sintering process. Furthermore, the value is readily obtained form dilatometry which is an important tool for the densification study.

SEM micrographs of sintered CS, shown in Figure 4-11, agree well with dilatometric results that densification does not occur explicitly upto T_s (780°C). The samples isothermally heat treated at temperature lower than T_s (732°C as shown in Figure 4-11a and 4-11b) form necks at contact points between particles and insignificant shrinkage was detected; i.e. these micrographs represent the first stage of sintering.

The second stage occurs at temperature between T_s and T_{sf}, the samples shrink and the pores are connected (Figure 4-11c and 4-11d). Figure 4-11c shows non-homogeneous densification. Several factors may cause the heterogeneous densification; e.g. a wide

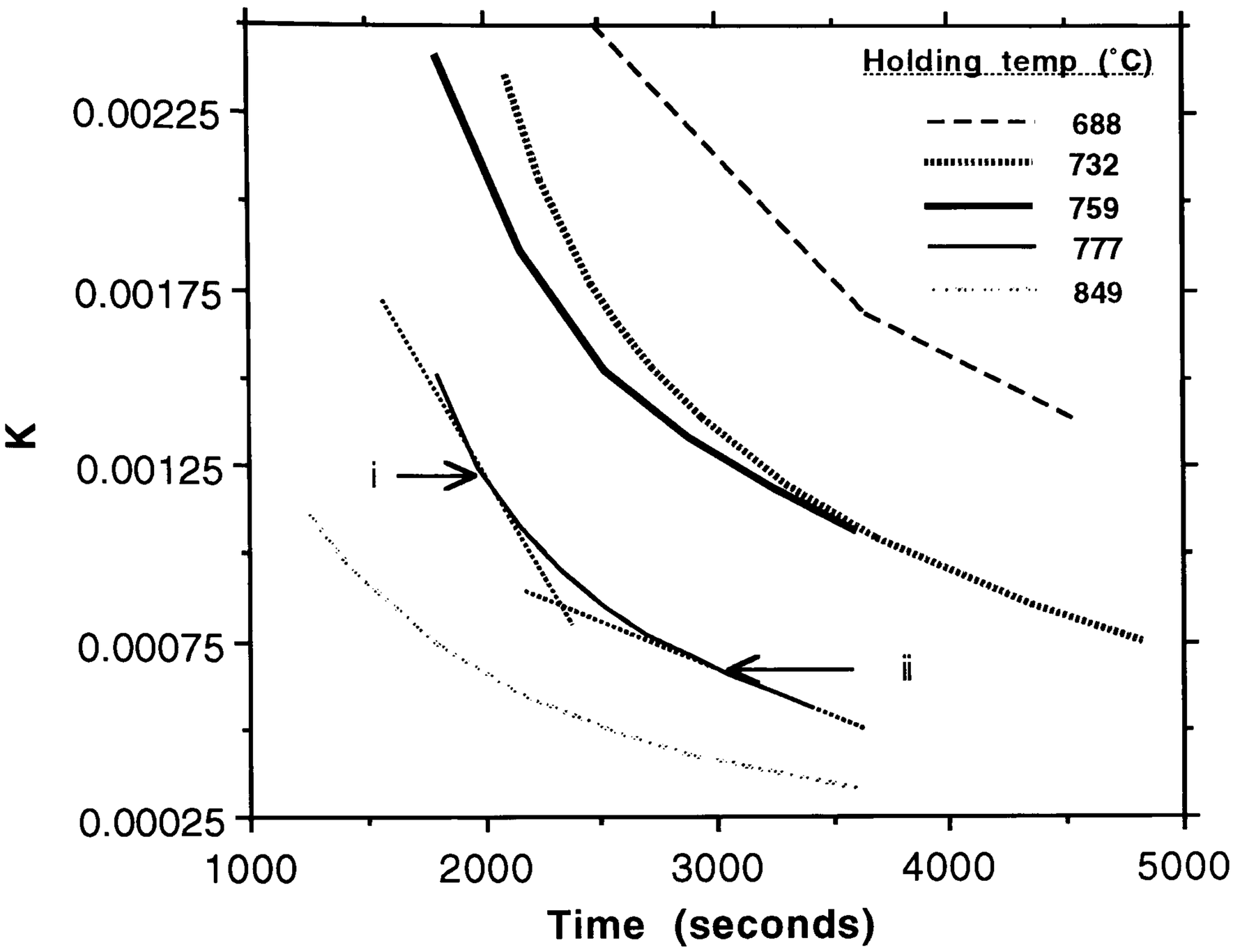


Figure 4-9 K values derived from Petru's equation (eq.4-6) as a function of sintering temperature (the samples undergone isothermal treatment in a dilatometer).

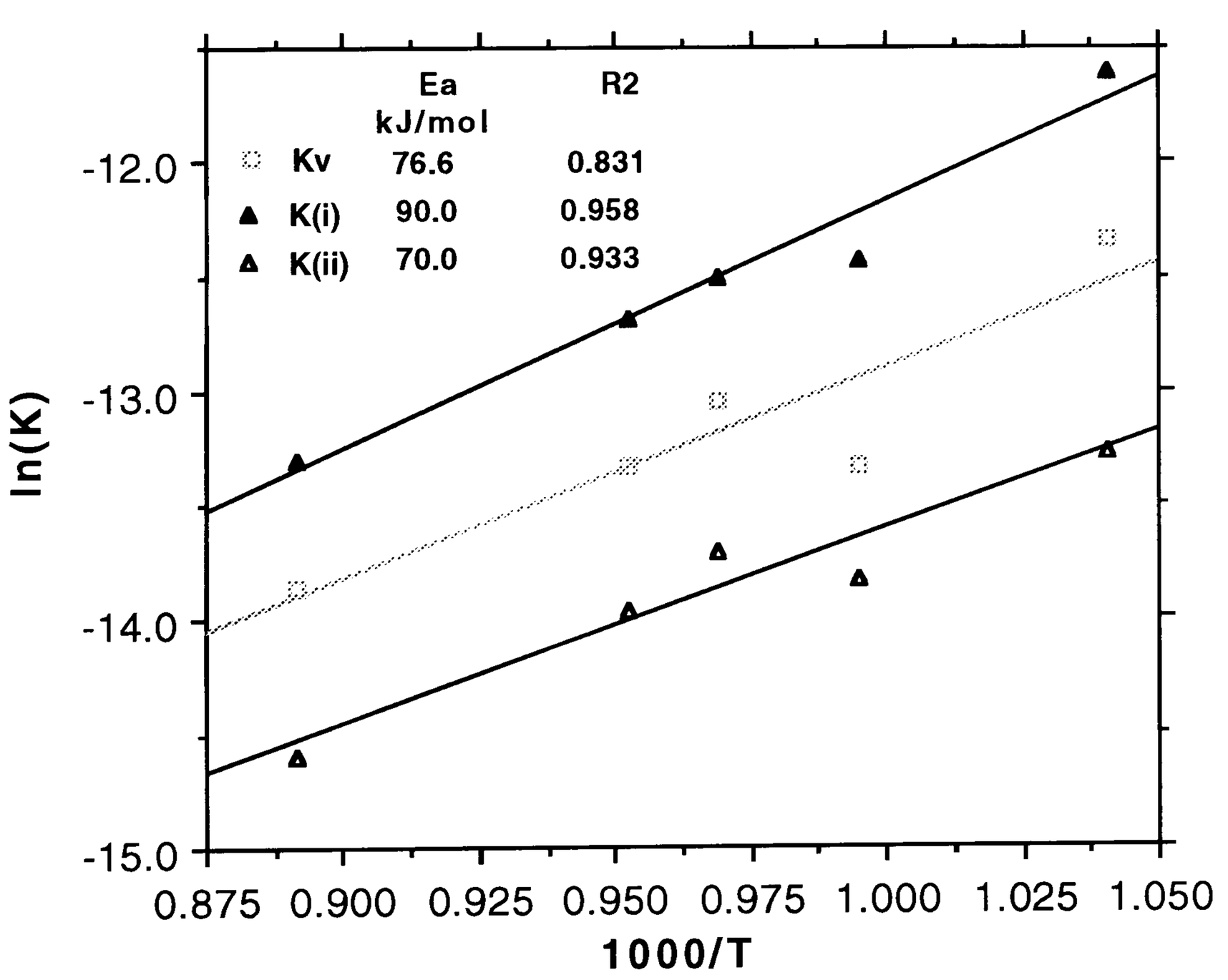
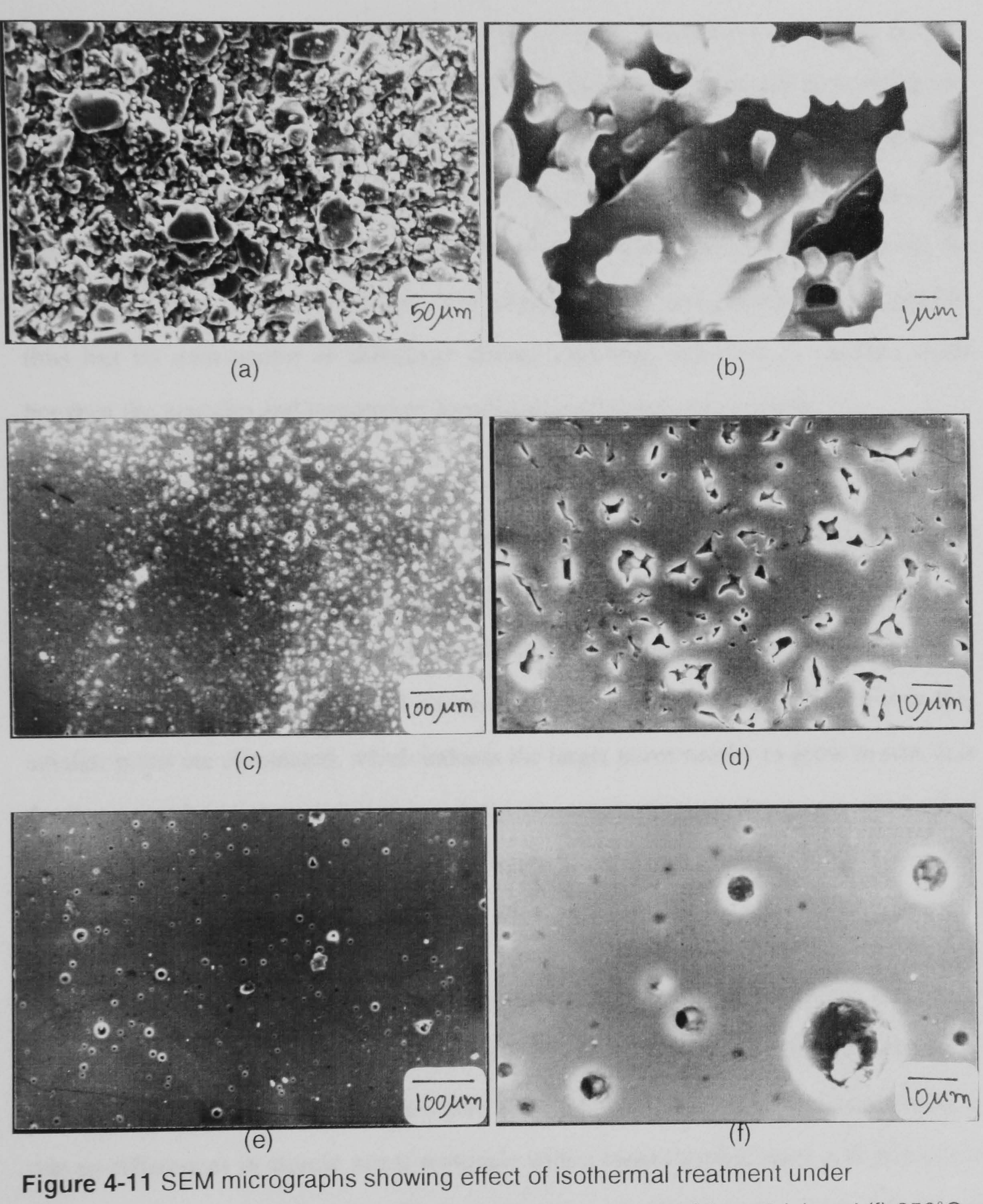


Figure 4-10 Arrhenius plots of the rate constant of sintering (K) vs reciprocal of isothermal temperature for the calculation of activation energy for sintering.



(a) (b) (c) (d) (e) (f)

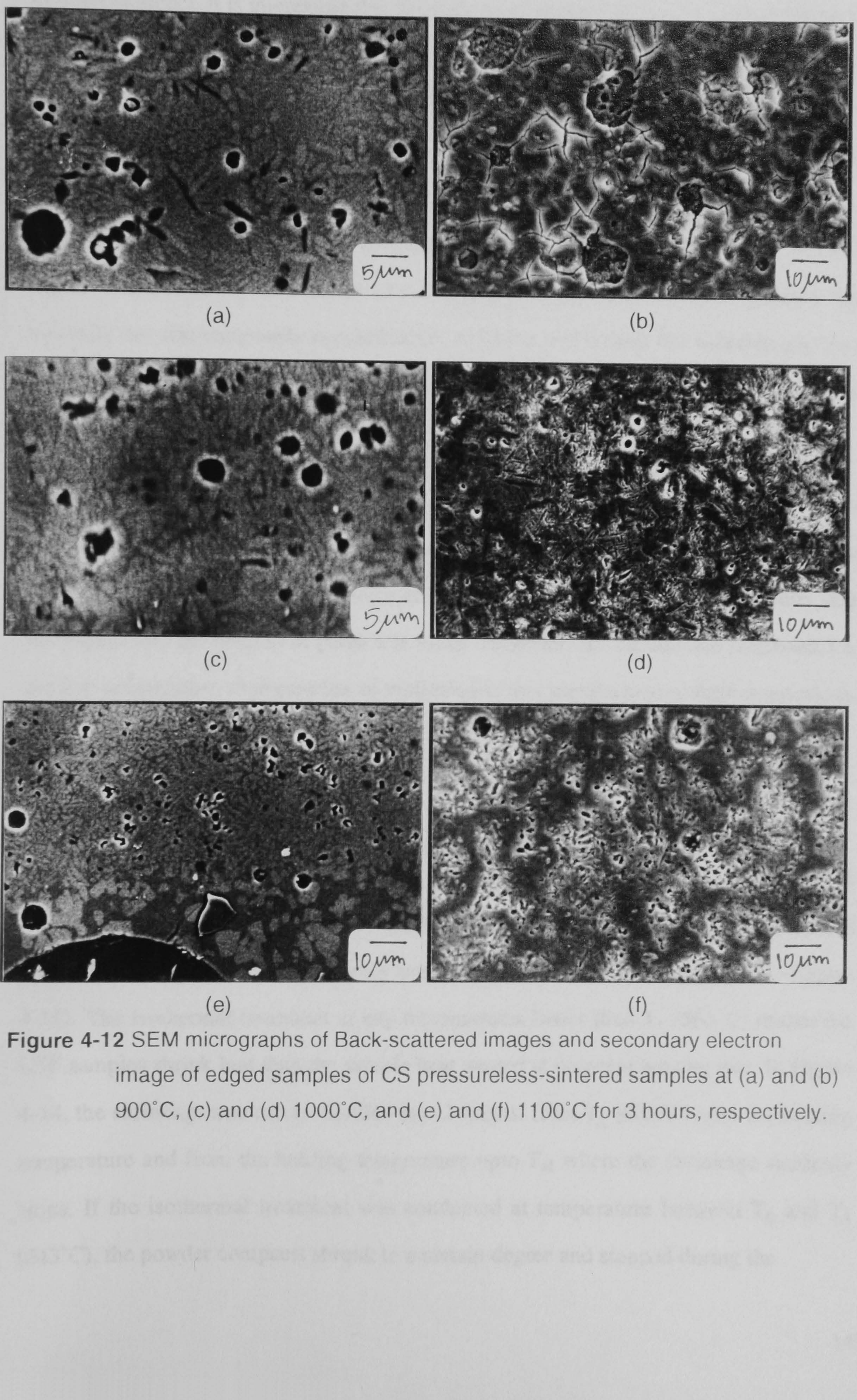
Figure 4-11 SEM micrographs showing effect of isothermal treatment under dilatometry at (a) and (b) 750°C, (c) and (d) 800°C, and (e) and (f) 850°C on sinterability of CS glass powder.

additional hydrostatic stress components in systems composed of small particles [Evans 1987].

The discontinuity in powder compact can lead to many centres for shrinkage. In such multimodel sintering, discontinuities widen as shrinkage occurs in opposite directions, there as explaneed earlier by lowering the overall density. Precompaction and granulation of the powder will enhance the packing efficiency in final compaction. However, excessive precompaction pressure results in hard granules which survive the final compaction process and retain their identity in the green compact. Each granule thus has its own centre of shrinkage during sintering, resulting in residual voids between the granules and incomplete densification of compact as a whole.

The final stage (Figure 4-11e and 4-11f), where the fine porosity is preferentially eliminated, occurs at temperature between T_{sf} and T_x. The preferential annihilation of the fine porosity during sintering is typical and expected. The pores are rounded, and very little shrinkage occurs compared with intermediate stage. The zones composed of agglomerates densify in early and intermediate stages of sintering in such a way that smaller pores are eliminated, which induces the larger pores nearby to grow in size. It is further considered that coalescence and grain coarsening occurs in morphological changes in the intermediate stage should be due to the elimination of smaller pores and the increase in size of large pores.

The back-scattered image of pressureless-sintered CS glass samples heat treated for 3 hours at temperature higher than T_p (877˚C), 900˚C, 1000˚C and 1100˚C, are shown in Figure 4-12. The contrast of light and dark areas using backscattered electron imaging is due to differences in atomic mass; materials with a higher atomic mass will produce a brighter contrast on the micrographs. It is therefore expected that the black regions are due to residual glass as the relatively low atomic weight (Na) is predominantly located within the glass regions. Also presented in Figure 4-12 are the microstructure of etched CS samples. Etching the glass-ceramic removes the glassy phase and the results displayed can provide a rough estimate of the degree of crystallinity present in the glass.



(a) (b) (c) (d) (e) (f)

Figure 4-12 SEM micrographs of Back-scattered images and secondary electron image of edged samples of CS pressureless-sintered samples at (a) and (b) 900˚C, (c) and (d) 1000˚C, and (e) and (f) 1100˚C for 3 hours, respectively.

At 900°C, wollastonite crystals developed in the sintered samples are very similar to those developed in bulk cast samples but they are distributed homogeneously in the sintered compact. It is interesting that the outlines of crystals of 10 to 15 μm in length is in agreement with the mean particle diameter estimated from the size distribution analysis of ground glass powder (see Figure 4-1). The densification achieved was similar to that of the samples sintered in the dilatometer (i.e. sintered with small pressure), but the pores were not spherical, compared to the results from dilatometry, indicating that sintering stopped in the late intermediate stage or beginning of final stage. This seems to be a result of using higher temperatures which reduces the viscosity but simultaneously crystallization develops and retards the sintering process. The sintered at 900°C body composed of a high degree of glass phase and pores of a few microns in diameter.

A microcrystalline mass of interlocking crystals has developed at 1000°C. The microstructure obtained was very similar to those of 900°C but the pores are a few microns bigger with higher percentage of crystallinity. At 1100°C, the crystallinity was the highest and the number of pores was lower. However, the surface was overfired; i.e. the low temperature configuration of wollastonite was transformed to high temperature configuration and large pores, bigger than 50 μm, are formed in the surface.

(ii) CSF

The isothermal heat treatment was performed slightly different from those done for CS glass; i.e. the samples were heat treated upto designated isothermal temperature and held at the temperature for 60 minutes and then heated at 15°C/min upto 850°C (Figure 4-13). The isothermal treatment at any temperatures lower than T_x (666°C) makes the CSF samples shrink less than the sample heat treated at constant heating rate. In Figure 4-14, the shrinkage rate can be divided into 2 stages: from T_g (603°C) upto the holding temperature and from the holding temperature upto T_{sf} where the shrinkage suddenly stops. If the isothermal treatment was conducted at temperature between T_g and T_s (643°C), the powder compacts shrunk to a certain degree and stopped during the

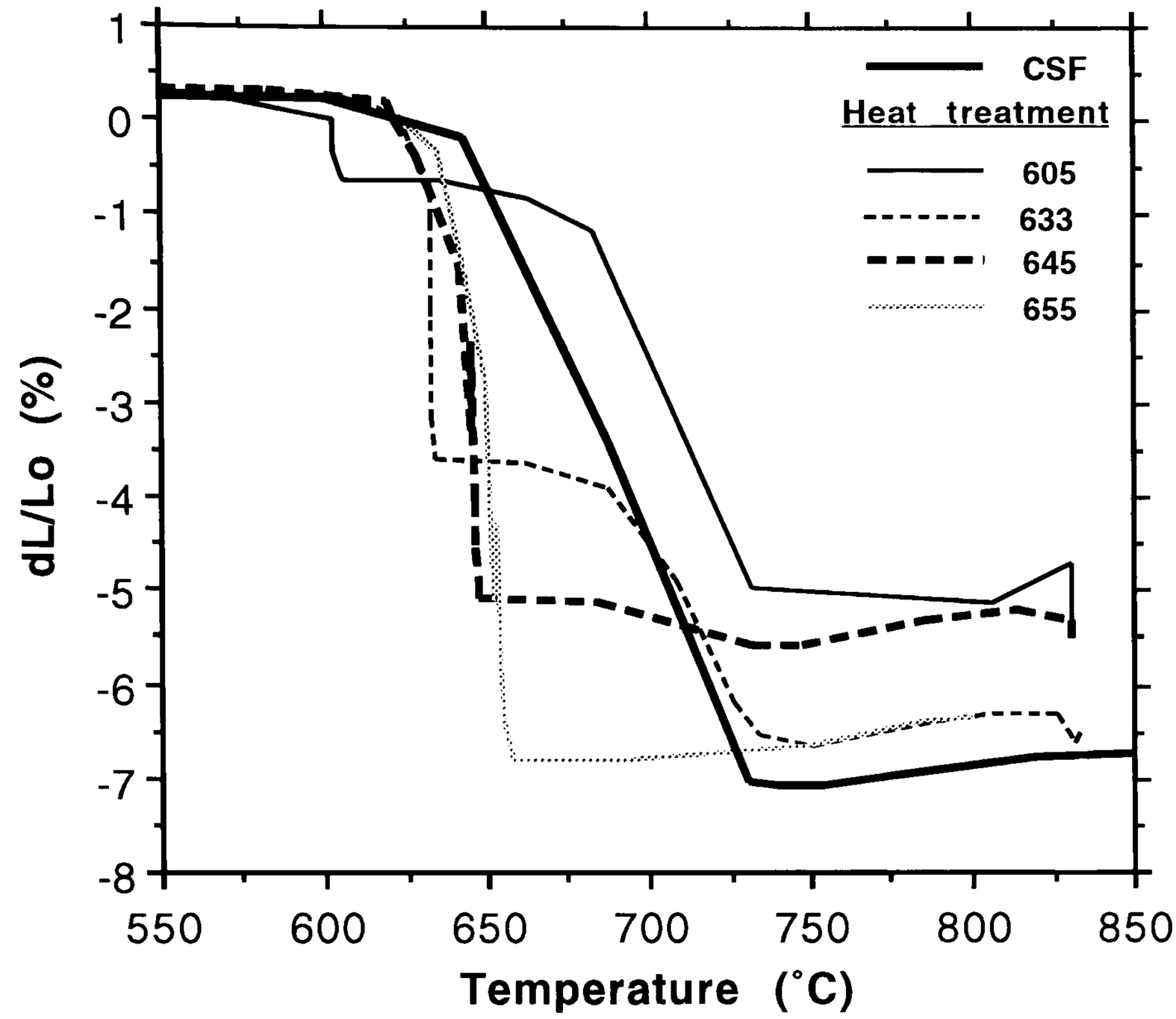


Figure 4-13 Dilatometry plots for CSF glass specimens tested at constant heating rate or with isothermal treatment at 609, 633, 645, and 665˚C. The shrinkage at the holding temperature is represented by the vertical drop on the plots.

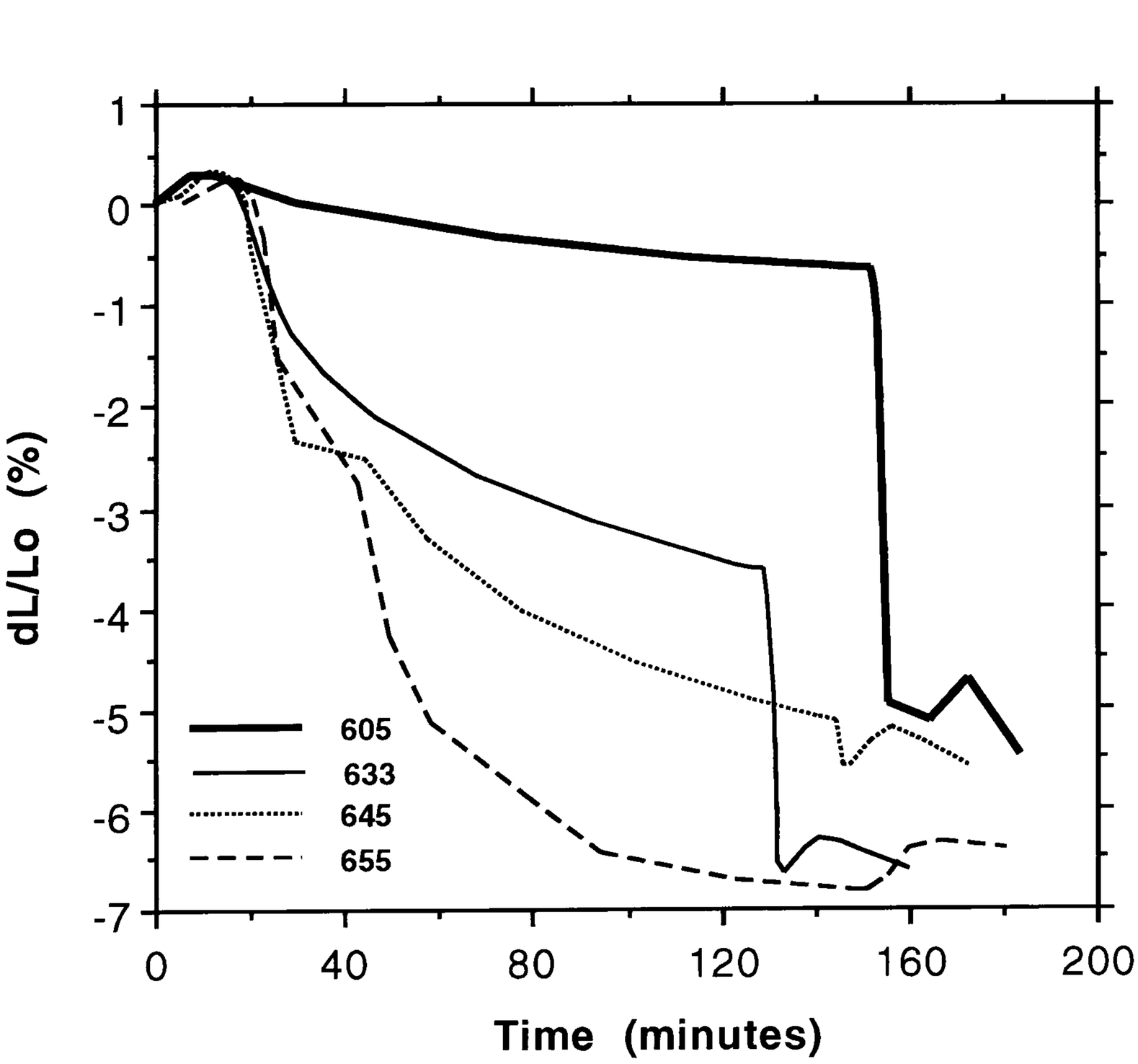


Figure 4-14 Isothermal treatment of CSF glass vs time under dilatometry at 605, 633, 645, and 655˚C.

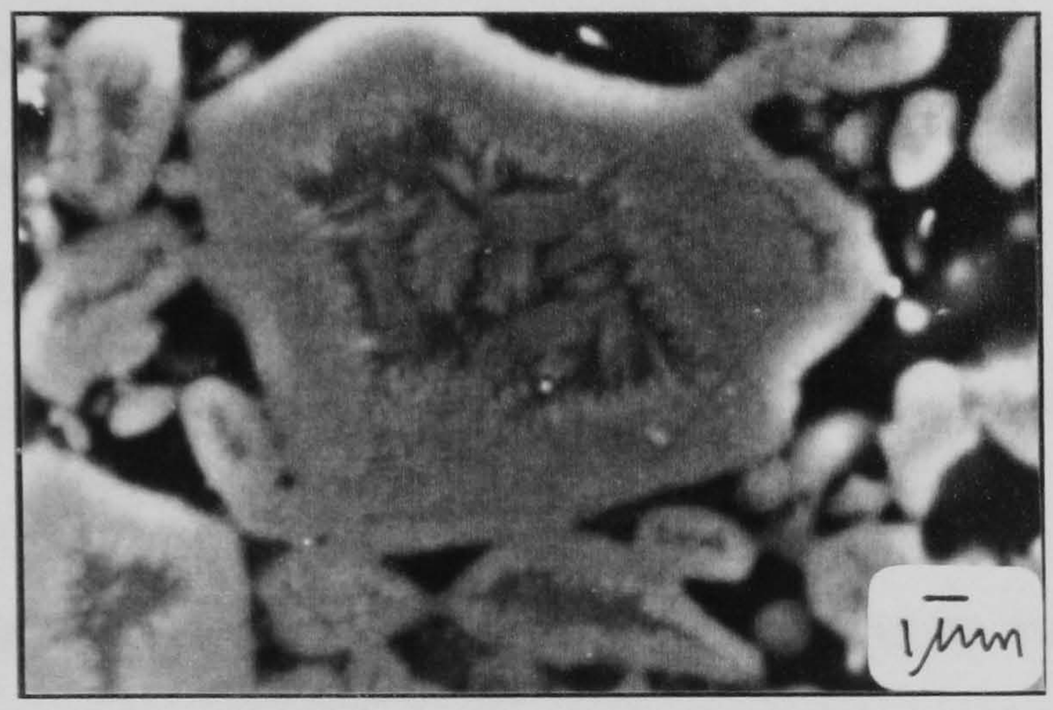
holding temperature, then continued shrinking in the CHR stage before suddenly stopping again at approximately 730°C. If the isothermal treatment was conducted at temperature higher than T_s, a high shrinkage rate resulted but the shrinkage stopped at a lower temperature. As a consequence, the densification achieved was very close to that of CHR treatment.

The shrinkage rate at the isothermal and CHR treatments and total shrinkage in CSF glass are shown in Table 4-4. It appears that the shrinkage rate in the isothermal stage increased with temperature, whereas the shrinkage rate in the CHR stage decreases with increasing isotherm. Moreover, in the CHR stage, if the isotherm was conducted at temperature lower than T_s, shrinkage results, while isothermal treatment at temperature higher than T_s leads to expansion (negative shrinkage rate). The abrupt expansion after crystallization is not unique to this composition, similar results have been obtained in different silicate systems by Kim [1989] and Taylor [1995]. The expansion at T_{sf} was proposed to be the 'springback' (elastic effect due to alteration of Elasticity) effect of crystallization occurring in viscous glass.

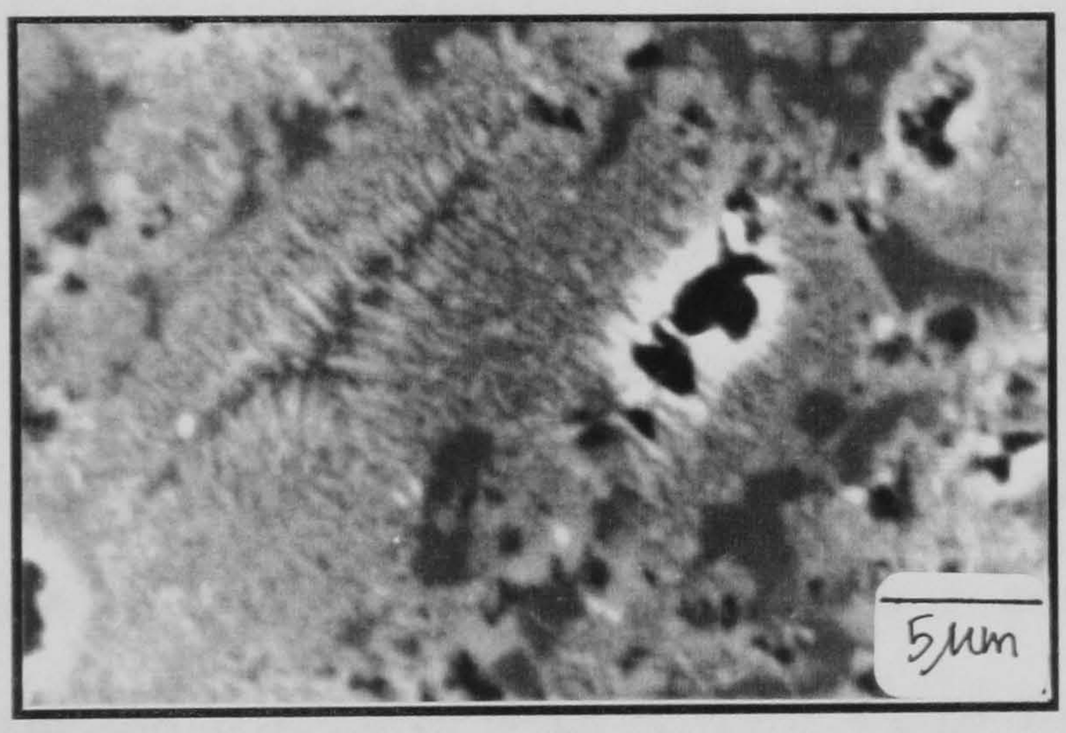
Microstructure observation by SEM in CSF sintered compacts revealed that surface crystallization predominates from early stage of sintering. Figure 4-15a shows that the crystallization developed from the surface in each glass particle and severely retarded sintering. The microstructure of CSF glass compacts heat treated between T_{si} and T_s, to allow viscous flow, before heat treatment at higher temperature produced a body with

Table 4-4 Shrinkage rate of CSF powder derived from the former Figure (Isothermal stage: temperature between T_g to the isotherm and CHR stage: temperature between the isotherm to T_{sf}).

Temperature (°C)	Shrinkage rate (%/min)		Total shrinkage (%)
	Isothermal stage	CHR stage	
605	0.000533	1.104	5.49
633	0.0252	0.7508	6.64
645	0.0261	0.1464	5.61
655	0.0327	-0.0434	6.42



(a)



(b)

Figure 4-15 SEM micrographs and Back-scattered images of CSF samples pressureless-sintered at (a) 750˚C and (b) 900˚C for 3 hours, respectively.

lower porosity than that in the sample heat treated at temperature higher than T_s (Figure 4-15b). It can be tentatively concluded at this stage that CS powder glass can achieve higher densification and has more potential in utilising as a matrix for composites than in CSF.

4.3.2.3 Effect of rigid inclusions

Typical particle size distribution and morphology of reinforcement particles employed; i.e. Al_2O_3, SiC, and ZrO_2, in the present study were presented in Figure 4-1 and 4-2. Densification results from the sintering experiments conducted at 15°C/min in the dilatometer on the CS glass matrix composites with 10 volume percent of Al_2O_3, ZrO_2, or SiC particulates of different sizes are presented in Figure 4-16. The addition of the rigid particles hinders sintering to different degrees. Alumina inclusions delay sintering by shifting the temperatures for starting and finishing sintering by approximately 10°C which is attributed to the incorporation of Al^{3+} into the glass and glass-ceramic networks [Volf 1984]. Aluminium forms tetrahedra in the multi-component glass. $[AlO_4]$ and $[SiO_4]$ tetrahedra are of similar sizes, so that in the silicate network, the former are capable of isomorphous partial substitution of the latter with almost no stress induction. This results in a stronger and stable structure of glass-ceramics. Similar results were obtained in BaO.2SiO2 glass [Sridharan & Tomozawa 1992]. Although the viscosity was expected to be lowed when the T_x is shifted to higher temperature and assisted sintering, the effect of the Al_2O_3 inclusion was predominant. As a result, the composite sintered at lower shrinkage rate than the matrix and achieve lower densification (13.5%) in total.

Another possible explanation is that the glass powder upon heating decreases in viscosity and wets the alumina surface, acting as a mortar to the alumina particles [Auborn & Haber 1991]. Assuming an ideal case of perfect mixing and monosized spherical alumina and glass particles, the glass will shrink evenly in all directions, fill the void spaces, and draw the alumina particulates together. The driving force for this is capillary pressure, but since particle size varies in a real case scenario, the diameter of

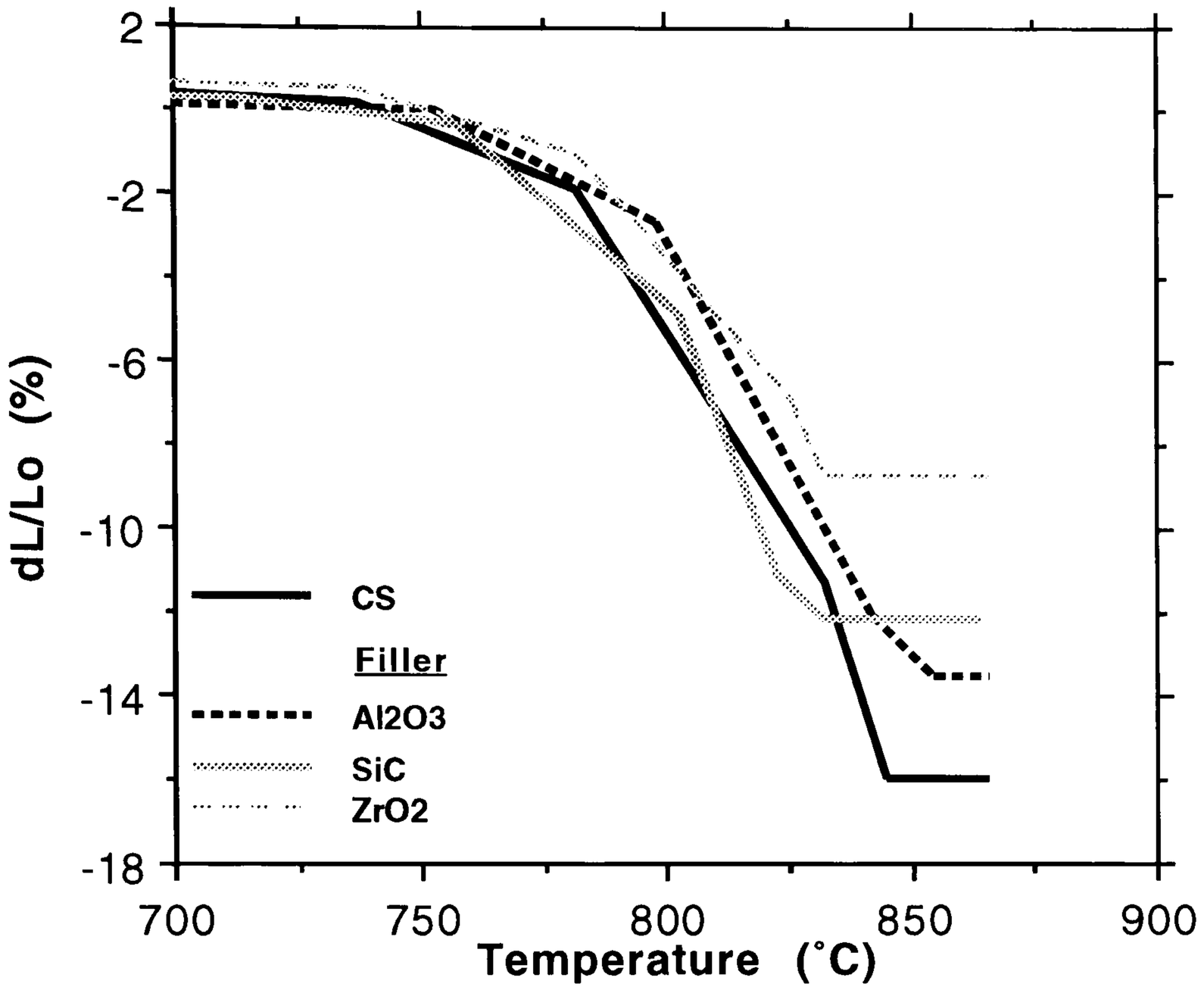


Figure 4-16 Effect of addition of reinforcements on densification of CS glass.

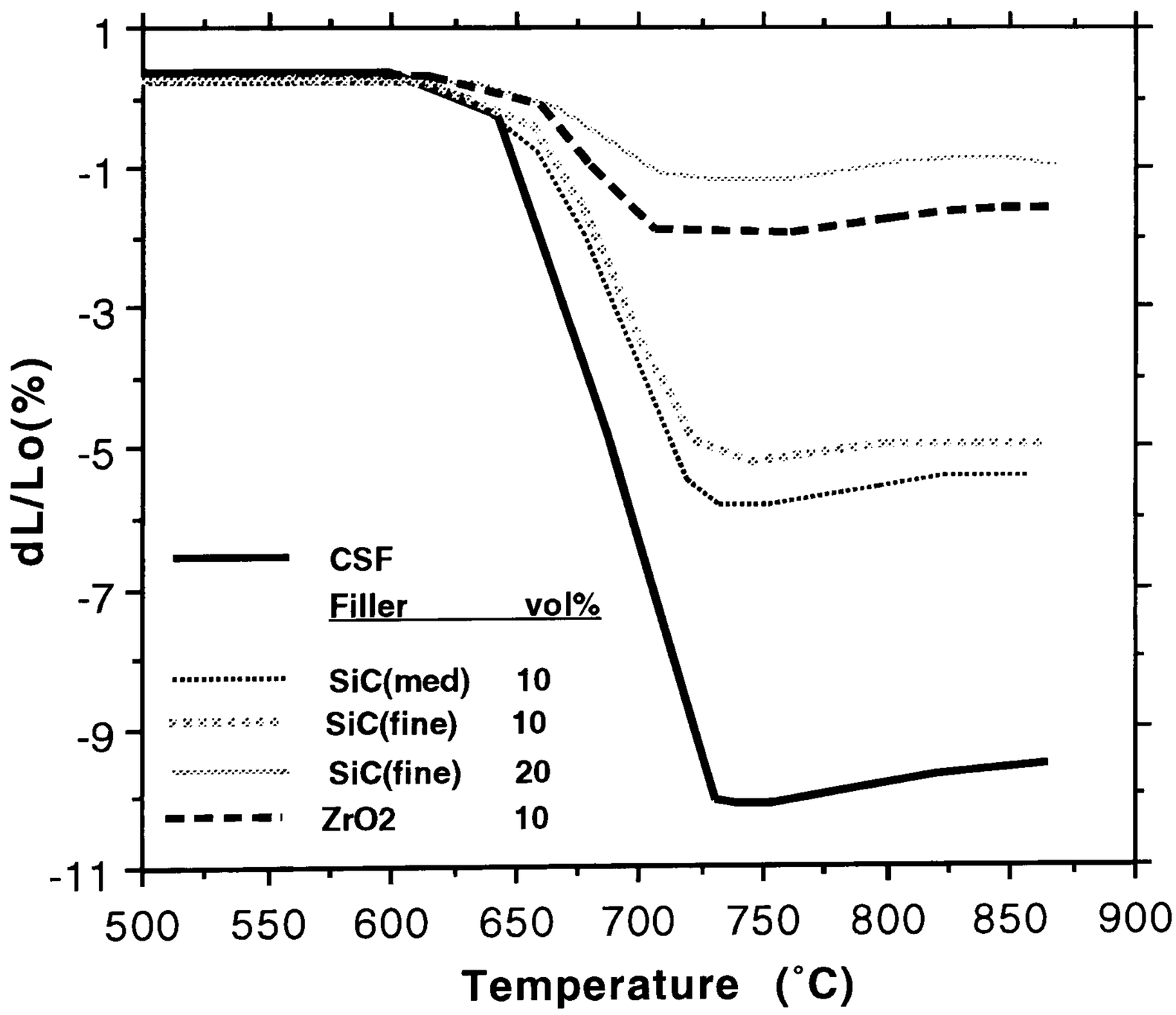


Figure 4-17 Effect of reinforcement type and volume fractions on densification of CSF glass

the capillaries also vary. Pores will develop from uneven capillary pressure, and added force is required to densify these materials.

SiC particles also delay the starting temperature of sintering (T_{si}) and the sintering stops before the monolithic matrix and yields total shrinkage of 12%. The ZrO_2 hinders sintering by lower the shrinkage rate and halts the sintering at lower temperature than those of the monolithic matrix. The addition of 10 vol% of ZrO_2 particles lower the shrinkage to approximately 9% total shrinkage. Although it is generally agreed that the sintered density achieved has an inverse relationship with the viscosity at the crystallization temperature, namely, the lower the viscosity at crystallization temperature, the higher is the sintered density achieved. The effective sintering rates of glass-ceramic with rigid particles is not only governed by viscosity and crystallization but also by percolation events; i.e. the formation of extended clusters of contacting hard inclusions [Stauffer 1985], thus the shrinkage rate was largely diminished.

The effects of rigid particles on sintering of CSF glass was similar to those obtained in CS glass, in that they hinder sintering, densification was severely restricted and hence much lower shrinkage occurred than for the monolithic CSF (Figure 4-17). Al_2O_3 particles also delayed sintering in CSF but the sintering occurred at a much slower rate than in CS, and stopped at only 3.8% total shrinkage at 746°C. Although the effect of SiC was alleviated in CSF by sintering occurring at a lower temperature and finish at a temperature higher than those of CS glass, the shrinkage rate was very low. ZrO2 acts in such a similar way in CSF as in CS glass that very limited sintering was achieved. Table 4-5 shows the effect of these rigid fillers in terms of time for sintering, temperature where sintering started, maximum sintering rate, and finished with total shrinkage obtained.

Microscopic examination showed a homogeneous distribution of reinforcement particles for Al_2O_3 and SiC particles in the matrices but ZrO_2 was agglomerated (Figure 4-18). Good physical bonding is expected when the thermal expansion coefficients (CTE) of the matrices were found to be higher than the CTEs of Al_2O_3, SiC, and ZrO_2. The matrices were, therefore, expected to contract around the particles on cooling after

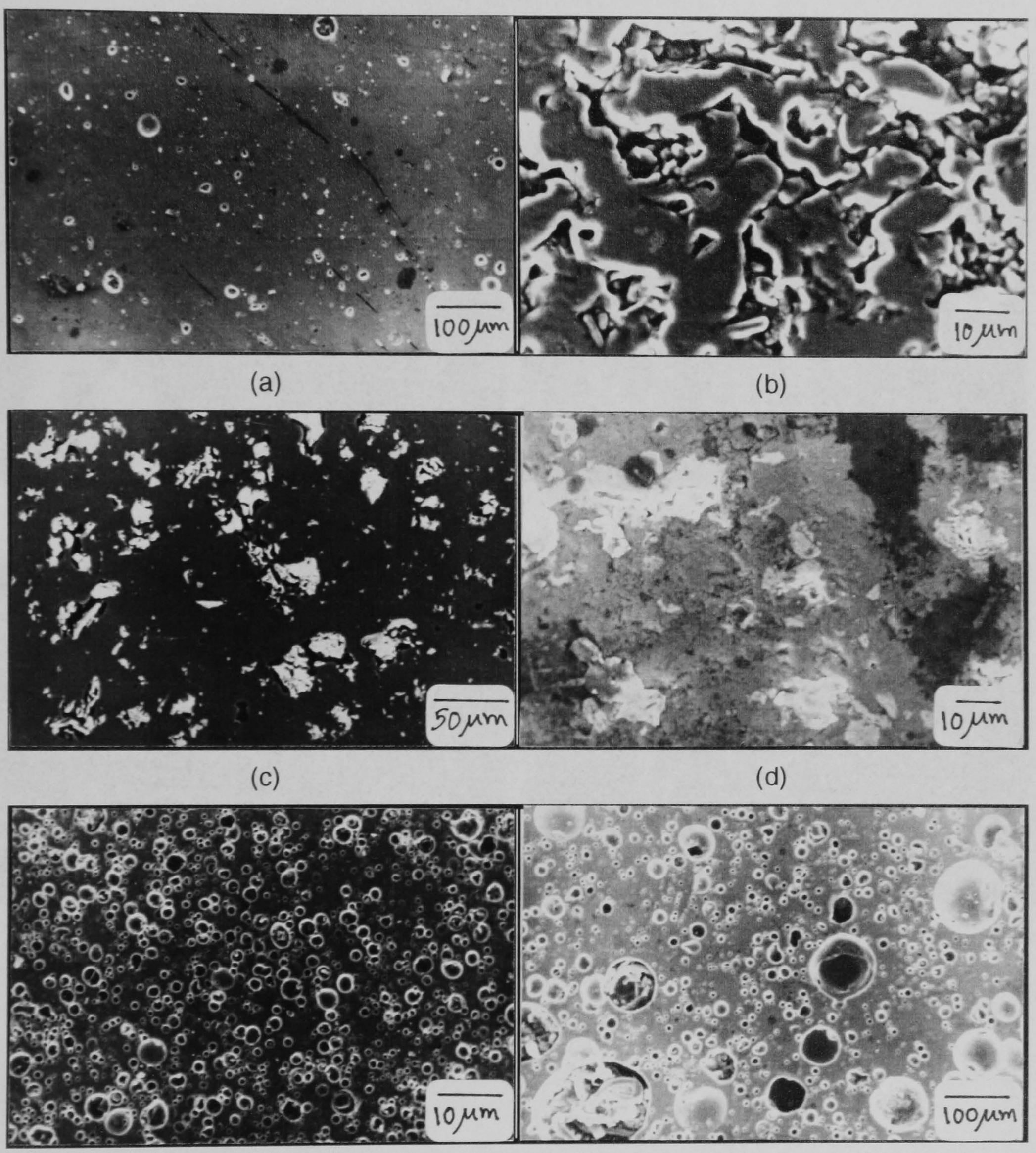
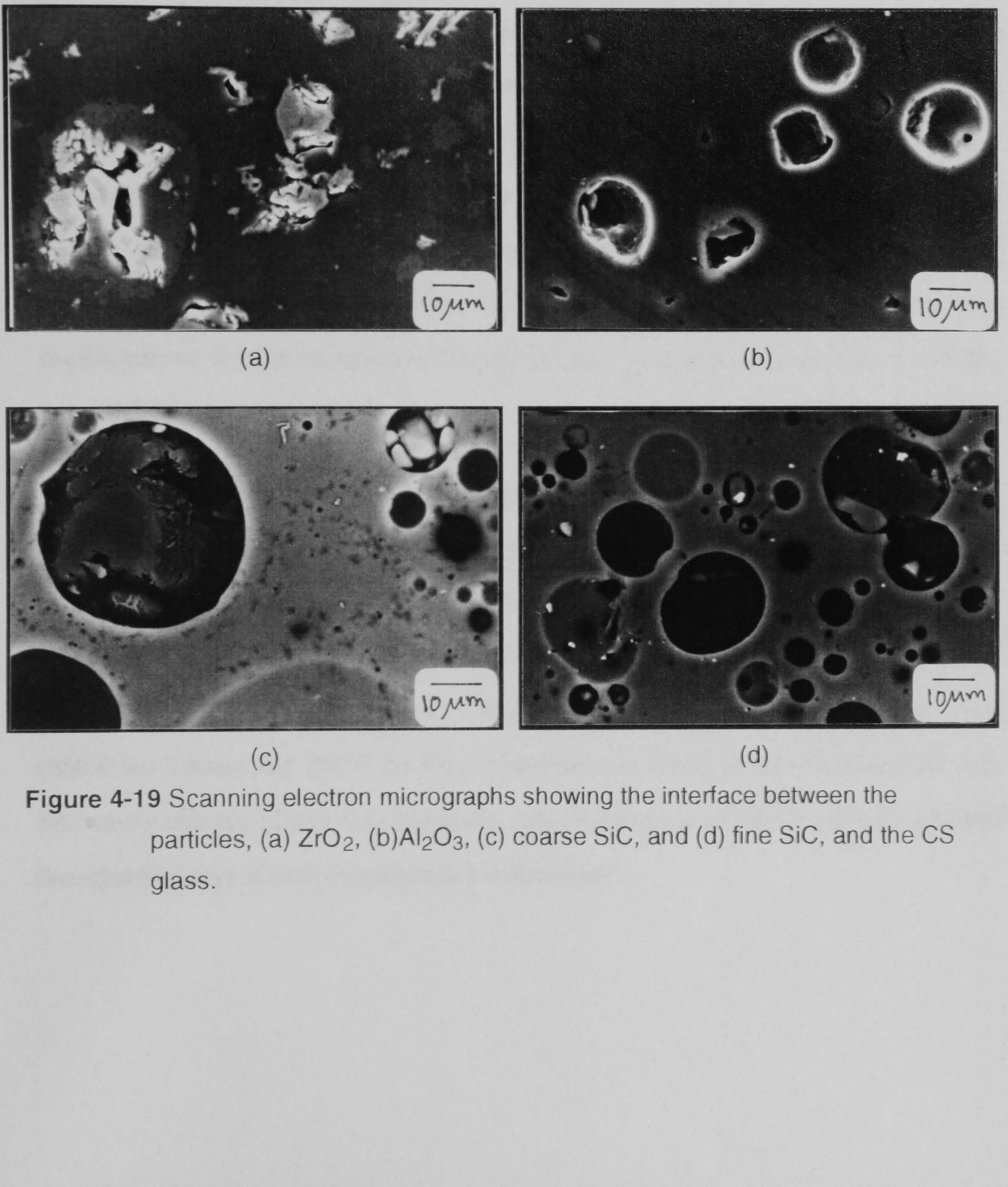


Figure 4-18 Scanning electron micrographs showing the effect of (a) and (b) Al_2O_3, (c) and (d) ZrO_2 on sinterability in CS and CSF glasses and , (e) SiC(fine), and (f) SiC (coarse) particles on sinterability in CS, all heat treated at 900°C for 3 hours.



(a) (b)

(c) (d)

Figure 4-19 Scanning electron micrographs showing the interface between the particles, (a) ZrO_2, (b)Al_2O_3, (c) coarse SiC, and (d) fine SiC, and the CS glass.

fabrication. However, this can only be applied to the Al_2O_3 case. The problem with SiC particulates was due to oxidation at the interface. Large gaps were observed at the interface and severely affected the mechanical properties of the composites (see section 5.3.2.3). Al_2O_3 particle forms good interface with the matrix, whilst ZrO_2 exhibited a reaction layer typically 2-4 μm, as far as sinterability is concerned, thick at the ZrO_2-matrix interface (Figure 4-19). The layer also forms good bonding with the matrix but the problem is the ZrO_2 agglomeration. The SiC particles do not form reaction layer but they are debonded from the matrix and may therefore act as pseudo pores which are detrimental to structural properties of the sintered body. The debonding may be caused by the oxidation of carbon in SiC during the processing at high temperature. In addition, powder surface crystallization can be expected to hinder the wetting of a rigid particle by the surrounding glass and limit the development of a good bond between them. The coefficients of thermal expansion of the glasses and glass-ceramics are shown in Table 2-6 and Table 3-8 respectively.

X-ray diffraction analysis of all CS glass and CS composites reveals that no crystallization occurred, or the crystallinity was lower than the sensitivity of the machine, when heat treated at 850°C for 1 hour. On the other hand, cuspidine was developed in CSF glass and CSF with either SiC or ZrO_2 composites when heat treated at 660°C for 3 hours followed by 775°C for 1 hour, and when heat treated at longer time (660°C for 3 hours and 775°C for 3 hour) wollastonite also precipitated from CSF with SiC reinforcements (Table 4-6). However, the incorporation of Al_2O_3 particles deferred the crystallization of both cuspidine and wollastonite.

Table 4-5 Summary of sinterability of CS powder with rigid inclusions

Sample	Vol. fraction (%)	t_s (mins)	T_{si} (˚C)	T_s (˚C)	T_{sf} (˚C)	Total shrinkage (%)
CS		8.4	736	781	845	16.01
Al_2O_3	10	9.9	753	797	855	13.52
SiC	10	8.1	757	803	832	12.19
ZrO_2	10	7.5	736	782	833	8.80
CSF		10.5	600	644	731	7.10
Al_2O_3	10	11.4	586	657	746	3.82
Al_2O_3	20	9.3	611	659	748	3.05
SiC	10	9.6	598	666	737	5.21
SiC	15	9.0	653	678	715	2.12
SiC	20	8.7	631	666	709	1.18
ZrO_2	10	8.4	617	659	709	1.95

Table 4-6 XRD results of sintered CSF composites (x : 3h660˚C + 1h775˚C and y : 3h660˚C +3h775˚C)

Sample	Vol.(%)	Heat treatment	Cuspidine	Wollastonite	Glass	Particle
CSF	-	x	√	-	§	-
CSF	-	y	√	√	§	-
<u>Filler</u>						
Al_2O_3	10	x	-	-	√	√
Al_2O_3	10	y	-	-	√	√
ZrO_2	10	x	√	-	§	√
ZrO_2	10	y	√	-	§	√
SiC(fine)	10	x	√	-	§	√
SiC(fine)	10	y	√	√	§	√
SiC(fine)	20	x	√	-	§	√
SiC(fine)	20	y	√	√	§	√

§: small amount

4.4 Summary

The production of glass-ceramics via a powder route is very much affected by the crystallization characteristics of the glass. The driving force for sintering being reduction in surface energy, an increase in the surface area of the powder may be expected to result in an increase in the sinterability of the powder compact. However, the availability of high surface energy in the powder also favours the crystallization of the glass. In the optimum process the glass should sinter to full density before the onset of crystallization. To achieve this, the relative rates of crystallization and densification can be controlled by changing heating rate, reflecting the fact that crystallization depends upon two kinetics steps whilst densification depends only upon viscous flow.

The differential thermal analysis (DTA) and dilatometry are essential techniques in the selection of glass powder with or without rigid particle system which exhibits appropriate crystallization and sintering characteristics for the production of glass-ceramic and glass-ceramic-matrix-composite (GCMC). In the present study, CS glass can achieve 94% of true density at temperature as low as 850°C, while in CSF glass, early crystallization is so high as to hinder sintering and prevent completion of densification. Of the two temperatures characteristic of crystallization, namely T_x and T_p, T_x is more relevant in determining sinterability; i.e. the viscosity at T_x has better correlation with the viscous sinterability of crystallisable glass systems.

The criteria which determine the sinterability of a glass powder are the size distribution and the mean diameter of the glass powder, mode (surface or bulk) and temperature of crystallization. CS glass, in which sintering was completed before crystallization started, can achieve higher densification than CSF glass. It appears that the size of the original glass powder plays an important role by limiting the crystallite size.

Although the addition of 'reinforcements' did not change the temperature at which the maximum rate occurs, the temperature range of sintering has been reduced significantly, by approximately 50°C; i.e. the addition of the reinforcements hinders the sinterability of the glass-ceramic matrix. There are two possible explanations for this:-1. This may

be due to the physical barrier for sintering glass powders created by the reinforcement phase, impeding viscous flow of the glass. Particles will induce differential sintering rates which in turn will produce transient stresses during sintering. These stresses can locally retard the densification rate of the composite and generate flaws. 2. As mentioned earlier, wollastonite has a tendency to surface nucleate. The phenomenon of fine crystallisation around the particulate reinforcements was seen with composites produced at 900°C. Thus the nucleation upon the particles may have accelerated the crystallisation processes which in turn increases the viscosity of the glass inhibiting full densification.

CHAPTER 5

MECHANICAL PROPERTIES

5.1 Introduction

Glasses and ceramics are inherently brittle at ambient temperature. The brittleness is a consequence of the strong covalent bonding, or the lack of a sufficient number of independent slip systems for dislocation motion to provide general plasticity [Quinn 1991]. This chapter is concerned with a study of the mechanical properties of CS and CSF glasses and glass-ceramics. The mechanical testings will be focused on flexural strength, fracture toughness, and Vicker's indentation. The effect of heat treatment and fabrication techniques will be examined. In the following section, a concise survey of mechanical testing techniques, brittle fracture and toughness, and toughening mechanisms is presented.

5.1.1 Strength

The "strength" of material is usually defined as the maximum stress the material can be subjected to without it "failing". Three strength testing techniques commonly used by material scientists are tensile, compression, and bending tests (Figure 5-1). Theoretically, the simplest testing technique is tensile test (Figure 5-1a). Experimentally, however, it is difficult to ensure true axial loading. Moreover, gripping the specimen is likely to be a problem because of the sensitivity to stress concentrations, and the machining of ceramic specimens is comparatively time consuming and expensive. The compression test is shown in Fig.5-1b. For metals the strength measured in compression is the same as that measured in tension. But for brittle solids, the compressive strength is roughly 15 times larger. Fracture is not caused by the rapid unstable propagation of one crack, but the slow extension of many cracks to form a

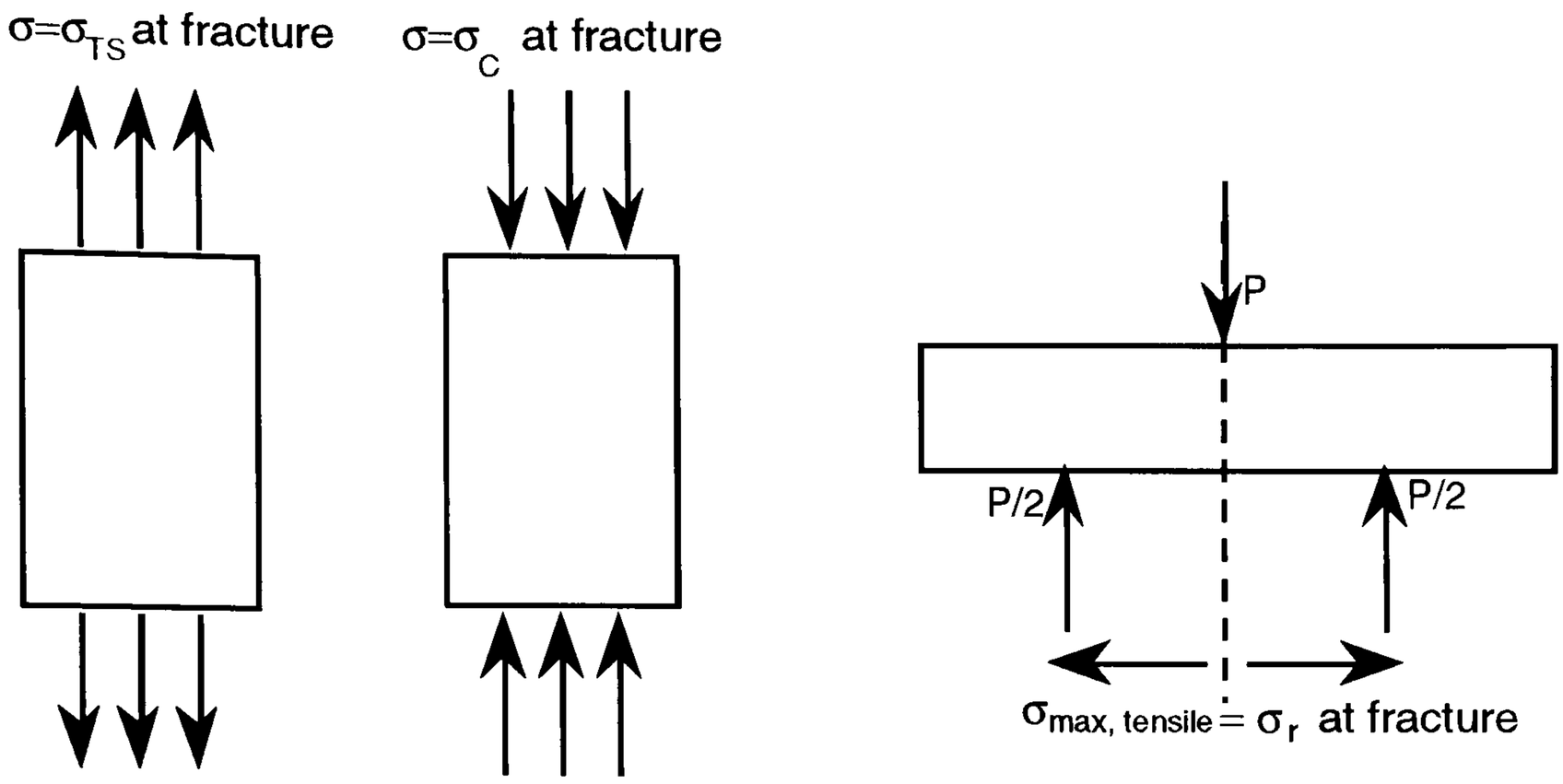


Figure 5-1 Common strength tests (a) tensile, (b) compression, and (c) three-point bending tests.

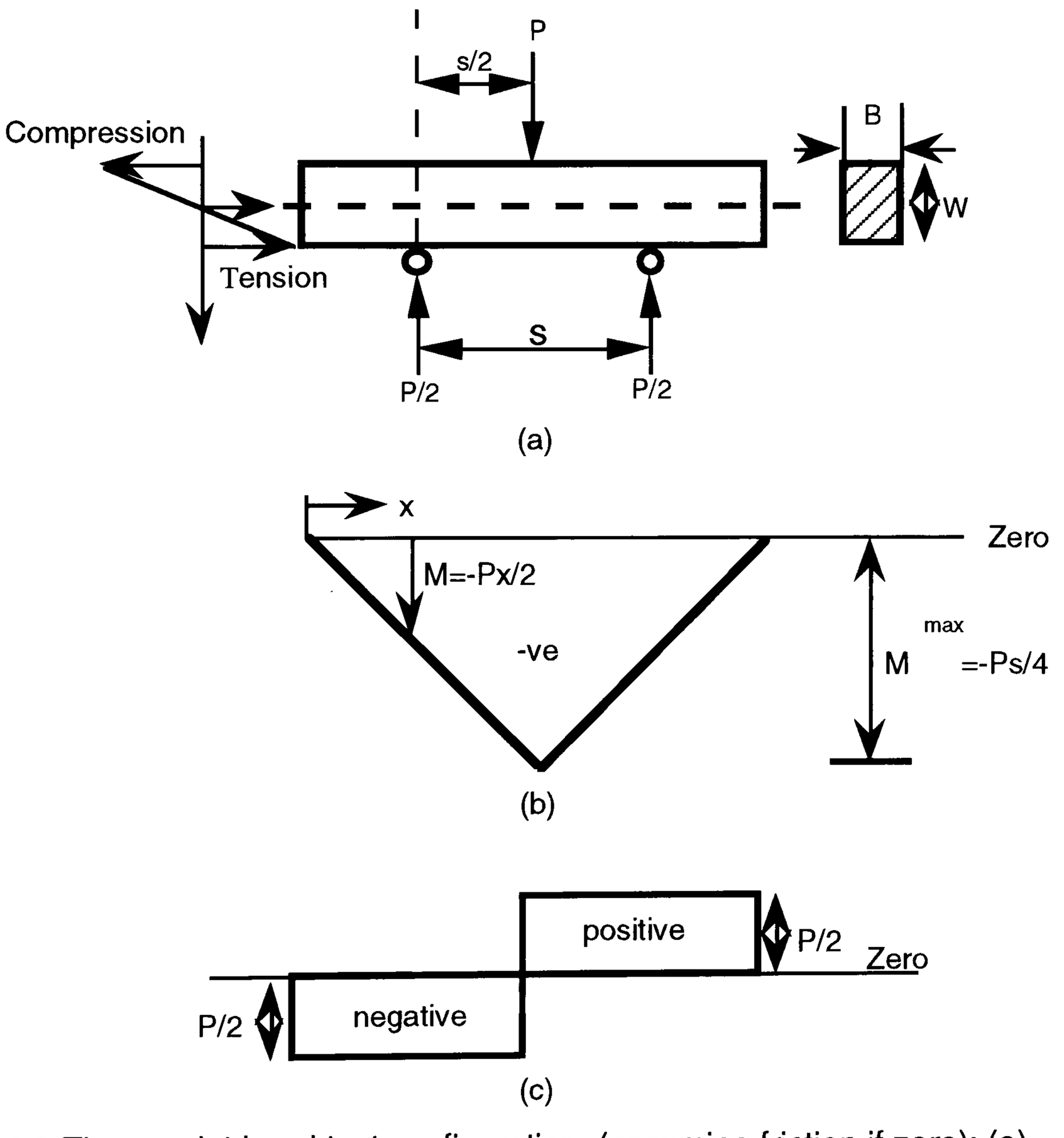


Figure 5-2 Three point bend test configuration, (assuming friction if zero): (a) schematic diagram of a beam subject to 3-point loading, (b) Bending moment diagram (M = f(X)), and (c) Shear force diagram (σ = f(X) = dM/dX.

crushed zone. Therefore, the most commonly used test is the bend-stress test which gives a non-uniform stress field in the specimen.

The bend test (Figure 5-1c) involves loading a beam specimen using three- or four-point simple loading; the theoretical bending moment and shearing force diagram for three-point bend test is shown in Figure 5-2. The bending moment for three-point loading varies linearly from zero at the supports to a maximum at the mid-span position, i.e. at the loading line; hence the tensile bending stress is a maximum at mid-span. The non-uniform bending moment induces a shear stress in the beam perpendicular to the neutral axis and hence a complementary shear stress parallel to the neutral surface which varies parabolically from zero at the top of the beam to zero at the bottom of the beam with a maximum at the neutral surface. Cross-sections normal to the neutral axis cannot remain plane after bending because the resulting shear strain must also vary parabolically in the same way, with zero shear strain at the top and bottom surfaces and maximum shear strain at the neutral surface. Note that since the shear force magnitude is constant along the beam either side of the mid-span the deformation of all cross-sections in identical; thus the bending moment and the distribution of bending stress either side of the mid-span are unaffected by shear strains.

The nominal test specimen cross-section dimensions were such that W=2B, while the nominal span-to-depth ratio (s/W) was 4 (see Figure 5-2). The stress, σ, at a point x is

$$\sigma = \frac{My}{I} \qquad [5\text{-}1]$$

where y is the vertical distance at X from the neutral axis plane NA =W/2, and

M is the maximum bending moment at X = s/2 due to the applied forces =Ps/4.

For a sample with a rectangular section

$$I = \frac{BW^3}{12} \qquad [5\text{-}2]$$

where W is depth of the beam, and

B is width.

Thus maximum bending stress on the tensile surface is

$$\sigma_{max} = \frac{3Ps}{2BW^2} \qquad [5\text{-}3]$$

This value is used for comparison with literature results as these tend to be presented without a correction.

5.1.1.1 Strength of glass

Strength of glass depends primarily on the condition of any surface that is under tensile stress. When a glass article breaks, the fracture nearly always originates from a single point situated somewhere on the surface of the article. The stress on the material close to the tip of a crack is very much higher than the average stress over the whole cross section of the specimen so that bonds may be broken at the tip and then fracture will take place progressively across the specimen. The main characteristics of a fracture formed when the stress is high is that the cracks move at high speed, i.e. the article appear to fragment instantaneously. Another important general feature of tensile strength of all brittle materials is that values measured on apparently identical specimens nearly always show a considerable variation. A coefficient of variation of 10-15% is not unusual [Bansal 1986]. Other important factors are thermal history, rate of load application, environmental conditions, and specimen size [Taylor 1991].

The theoretical strength, σ_{th}, required to break atomic bonds and pull a structure apart, suggested by Orawan [1949], is calculated from equation

$$\sigma_m = \sqrt{\frac{E\gamma}{a_0}} \qquad [5\text{-}4]$$

where E is the Elasticity of the material

γ is fracture surface energy of new surfaces created by the fracture, and

a_o is the interatomic distance.

For many commercial glasses, E is approximately 10^{10} N m^{-2} and a_0 is approximately $2\text{x}10^{-10}$ m using a value of 3 J m^{-2} for γ, one finds that σ_m is $4\text{x}10^4$ MPa, a value very much higher than is normally found in practice. Typical fracture stresses for commercial glassware are in the range 50-150 MPa. It is worth noting that, for the range of commercial glass compositions, none of the terms in the Orawan equation is much

affected by changes in glass composition. Thus the theoretical strength of glass is about the same for all glasses of practical interest.

Brittle failure in monolithic, linearly elastic materials can be well modelled by Griffith's criterion for fracture [Griffith 1924], where it can be shown that a critical balance of strain-energy release rate is offset by the energy to create new fractured surfaces. For fracture from inherent flaws in the material, the fracture stress, σ_f, can be represented by the following general relationship

$$\sigma_f = \sqrt{\frac{2E\gamma_i}{YC}} \qquad [5\text{-}5]$$

where γ_i is the effective surface energy for fracture initiation,

Y is a constant dependent on loading geometry, and

C is the crack length of a surface crack.

This approach does not consider the details at the tip, such as the crack tip radius. Nevertheless, the Griffith equation has been considered sufficient for understanding the strength of brittle materials.

5.1.1.2 Strength of glass-ceramics

Mechanical strength of a glass-ceramic is dependent upon the distribution of a glass and a crystalline phase. There are some uncertainties as to where the strength-damaging flaws reside [McMillan 1979]. One suggestion is that the critical flaws are present in the crystalline phase like normal polycrystalline ceramics, hence strength is proportional to mean grain diameter in the manner of

$$\sigma = Kd^{-1/2} \qquad [5\text{-}6]$$

Comparing this to the Griffth equation would imply that crack length c is proportional or equal to the grain diameter.

The second alternative is that the fracture-initiating flaws exist in the residual glass phase, making it the controlling feature of the strength of glass-ceramics. If this is the case, the mechanical strength must be related to the volume and distribution of the

glass, in particular the mean free path of the glass λ. An expression for the mean free path is given below.

$$\lambda = \frac{d(1-v)}{v} \qquad [5\text{-}7]$$

where v is the volume fraction of the crystalline phase and d is the mean crystal diameter. At high volume fractions and small particle size, the mean free path becomes very small, probably smaller than the original flaw size in the glass phase. When this occurs, the flaw size in the glass-ceramic will be controlled by the inter-crystal spacing and strength will be proportional to $\lambda^{-1/2}$.

The morphology of the crystal phase also influences the strength of the crystallized glass. For instance, Table 5-1 shows the significance of the transformation of $BaO{\cdot}SiO_2$ glass to glass-ceramics of different microstructure on the flexural strength [Freiman *et al* 1971]. The glass-ceramics exhibited higher strength than the glass and glass-ceramics with lath-like structure showed higher strength than that of spherulite structures.

5.1.2 Fracture toughness

The fracture toughness of a material is defined as its resistance to the catastrophic, rapid propagation under stress of a pre-existing flaw in the material. The early work of Griffith has been greatly extended in recent years. This modern study of the process of fracture is known as "Fracture Mechanics", wherein the stress intensity factor K_I at the tip of sharp cracks in a linearly elastic material is expressed as:

Table 5-1 Effect of heat treatment on morphological transformation and flexural strength of $3BaO{\cdot}5SiO_2$ glass-ceramics [Freiman *et al* 1971].

Heat treatment	Microstructure	Flexural strength (MPa)
600˚C 2hrs	Glass	5.2
700˚C 48 hrs + 825˚C 1hr	100% spherulites 1-2 μm diameter	9.5
700˚C 48 hrs + 825˚C 48hr	Secondary crystallization of 1-2 μm spherulites	12.7
700˚C 48 hrs + 825˚C 1hr + 1000˚C 24 hrs	Lath-like crystals	16.4

$$K_I = Y\sigma\sqrt{c} \qquad [5\text{-}8]$$

where σ is the applied far-field stress,

c is crack length, and

Y is dimensionless shape factor that describes the severity of a defect and geometrical considerations.

Fracture occurs when the level of K_I reaches a critical level, K_{1C} which is a material property known as fracture toughness. The design strength of a ceramic, then, is determined by its fracture toughness and by the size of the microcracks it contains. Therefore, two ways of improving the strength of ceramics are decreasing *c* by careful quality control, and increasing K_{1C} by making the ceramic into a composite. Monolithic ceramics have a fracture toughness between 0.2 and 2 MPa $m^{1/2}$ whereas values as high as 20 MPa $m^{1/2}$ have been recorded for continuous fibre composites [Brennan & Prewo 1982, Prewo *et al* 1986].

In the present work the plane strain fracture toughness (K_{1C}) was calculated from the experimental data in units of MPa $m^{1/2}$ using the following equation:

$$K_{IC} = Y * \frac{3Ps}{2Bw^2}\sqrt{a} \qquad [5\text{-}9]$$

where P: the load at fracture,

s: the span length,

B: the specimen breadth,

W: specimen width,

a: the notch depth, and

Y: the compliance factor is given by

$$Y = \frac{1.99 - \left(\frac{a}{w}\right)\left[1 - \left(\frac{a}{w}\right)\right]\left[2.15 - 3.93\left(\frac{a}{w}\right) + 2.7\left(\frac{a}{w}\right)^2\right]}{\left[1 + 2\left(\frac{a}{w}\right)\right]\left[1 - \left(\frac{a}{w}\right)\right]^{3/2}} \qquad [5\text{-}10]$$

5.1.2.1 Critical Flaw Size (a_c)

Once the values of K_{1C} and MOR had been found it was possible to estimate the critical flaw size (size of defect from which fracture initiated) of the material studied. This was evaluated using equation [Bansal 1976]

$$a_c = \left(\frac{ZK_{1C}}{Y\sigma_f} \right)^2 \qquad [5\text{-}11]$$

where Z is the flaw shape parameter and a_c is the critical flaw size. For a straight through-thickness crack (Griffith flaw), Z is given by

$$\left(\frac{Z}{Y} \right)^2 = \frac{1}{1.21\pi} \qquad [5\text{-}12]$$

For a penny-shaped crack, Z is given by

$$\left(\frac{Z}{Y} \right)^2 = \frac{2}{\pi} \qquad [5\text{-}13]$$

5.1.2.2 Fracture surface energy (γ_f)

The term "fracture surface energy (γ_f)" is very similar to "fracture initiation energy (γ_i)". The fracture surface energy indicates the amount of energy absorbed by a unit area of fractured surface at the moment of crack propagation. For an ideal brittle material the crack tip zone of non-plastic flow is extremely small, therefore one can assume $\gamma_f = \gamma_i$ and measures in the region of 1 J m^{-2}. In a very ductile material γ_f is extremely high (>1000 Jm^{-2}) and differs increasingly from γ_i as the fracture surface energy increases. Fracture energy (γi) can be estimated using [Wahi & Ilshner 1980].

$$\gamma_i = \frac{K_{Ic}^2}{2E}(1-\upsilon^2) \qquad [5\text{-}14]$$

where υ is the material Poisson ratio.

This equation requires that the test is carried out under conditions of plane strain and that strain cannot be relieved by general plastic deformation. For ceramic materials and their composites this condition is nearly always satisfied.

5.1.3 Hardness and Indentation Toughness

Hardness is defined in the conventional sense as a means of specifying the resistance of a material to deformation, scratching, and erosion. Interest in the indentation fracture technique stems from its simplicity, the small volume of material required enabling the study of the effect of small superficial defects on the fracture of brittle, homogeneous material [Tanaka 1987]. Hardness tests are based on indenting the sample with a hard indenter, which may be spherical, conical, or pyramidal. It should be noted that each test method only defines a self-consistent resistance of a material, and a comparison of hardness values from one test method with those from another for a given material is to be avoided.

Figure 5-3 depicts the effect of the loading and unloading process that occur as a result of indentation. Loading produces a stress field. The stress field is seen as building up from (i) the applied load and (ii) the stress between the bulk of the sample around the indented area, which is only moving in accord with the elastic modulus and material which has flowed plastically from the indent volume. Since this will be present when applied load is removed, it is called the residual stress.

The applied load as in (i) above causes a tension in the bulk material which has a maximum at the interface between the elastic body and the plastically deformed zone, in turn causing microcracking dependent upon the surface flaw population and the nucleation mechanisms of slip. Microcracks nucleated develop into a penny-shaped crack below the indenter and shallow Palmqvist cracks in the surface region. These are the median and radial cracks.

The pressure surface under the indenter causes compression, not tension; this acts in opposition to the residual stress. As the indenter is withdrawn, the surface compression decreases to zero. The residual stress now acts toward the surface and on it to produce cracks with surface traces that can be seen in the microscope on suitably polished surfaces; these are radial cracks. Radial and medians have combined to give semi-elliptical cracks, called half-penny cracks, whose surface diameter is about twice the

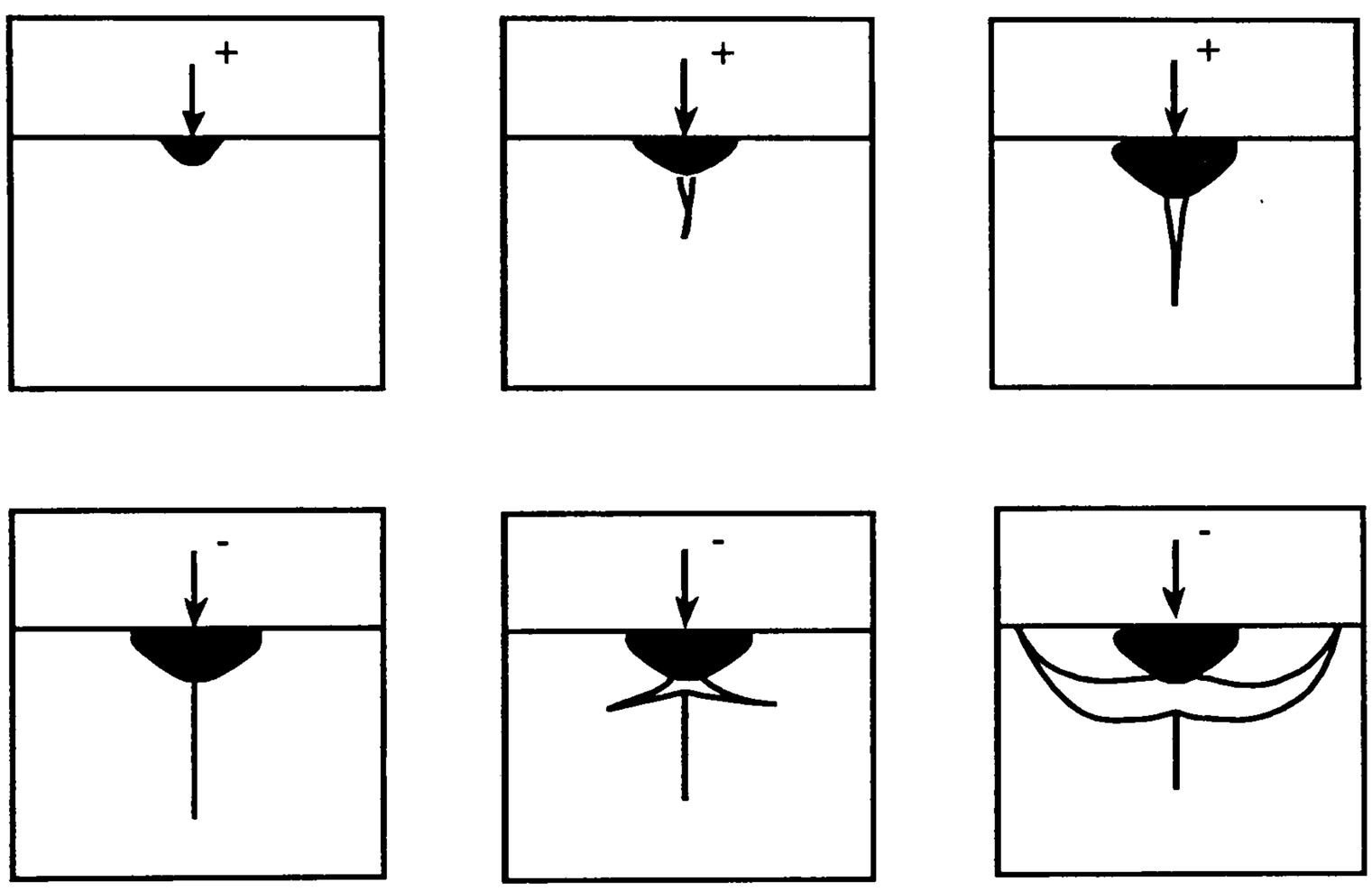


Figure 5-3 Cracking sequences obtained by Vickers indentation test during loading (+) and unloading (-) [Hamidouche *et al* 1994].

maximum depth. Fully developed radials are in mechanical equilibrium and have crack dimensions that are determined by K_{1C}; hence this parameter can be measured.

However, confusion has been engendered by the multitude of models and equations in the literature relating the degree of cracking to the fracture toughness. Ponton and Rawlings [1989] reviewed nineteen of these equations and formulated them into standardised forms. Generic equations which can be employed for Vickers' hardness (H_v) and indentation fracture toughness (K_c) are shown respectively.

$$H_v = 1.85436\frac{P}{d^2} \qquad [5\text{-}15]$$

where H_v is the Vicker's hardness (kg/mm^2)

P is the applied load (kg)

d is the average indent diagonal (mm).

$$K_c = 0.0824\frac{P}{C^{3/2}} \qquad [5\text{-}16]$$

where P is indenter load (N) and

C is mean square radial crack length (mm)

5.1.4 Fractography

The fracture surface displays certain zones or features which can provide information on how the propagation occurred and, in some cases, information on the cause of the failure. The "post-mortem" study of the pieces of fractured material is known as *fractography* [Zarzycki 1991]. Fractography appears to reflect real crack-growth conditions and was found to be the only means by which to identify the effects of microstructure on crack path.

Markings on fracture surfaces can give information about the origin and direction of fracture propagation, as well as about material inhomogeneities and local stress effects [Bansal 1986]. The appearance of the fracture surface may also gives qualitative information on toughening mechanism. Stable cracks, produced by indentation, can be used to obtain a reasonable measure of the crack front profile. The radial cracks along

the surface provide a reliable deflection profile, if the distribution of angles along the surface trajectory is equivalent to that along the subsurface crack front.

5.1.5 Toughening mechanisms in glass-ceramics

Fracture of glass-ceramic materials is controlled by the direct effect of microstructure on the crack tip. When the material fractures, resistance to crack growth comes from the atomic forces that hold the solid together. Crack growth occurs only when atoms bonds at the crack tip have been stretched to the breaking point. Consequently, fracture toughness is achieved by modifying the microstructure of the solid to reduce the stress near the crack tip. The following authors provide an updated summary of the toughening mechanisms [Wiederhorn 1984; Rice 1985; Clarke & Faber 1987; and Freiman 1988].

Analytical tools, such as scanning electron microscope (SEM), have led to major advances in understanding the strength of ceramics and in the characterization of defects. The application of fracture mechanics analysis to ceramics has increased the fundamental understanding of the factors that control fracture phenomena. Fracture in glasses and glass-ceramics is now understood to be a consequence of the stress intensification that occurs in the vicinity of defects. The advent of fine scale, isotropic ceramic composites with either second phases or particulate reinforcement has brought about the exciting prospect of tough and very strong ceramics. These composites employ a variety of means to impede or resist crack propagation, including crack deflection or branching, microcracking (to blunt the crack or dissipate the stress concentration), crack-particle interactions, or wake toughening (bridging of the crack faces by reinforcement -- very effective in fibre reinforcement). Figure 5-4 illustrates simple and sharp cracks in glass and glass-ceramics compared with those in toughened and composite structures.

Crack deflection is a commonly observed fracture characteristic in brittle materials, associated either with crack attraction or repulsion by second phase particles (due to residual stresses) or with the presence of low resistance interfaces [Faber & Evans

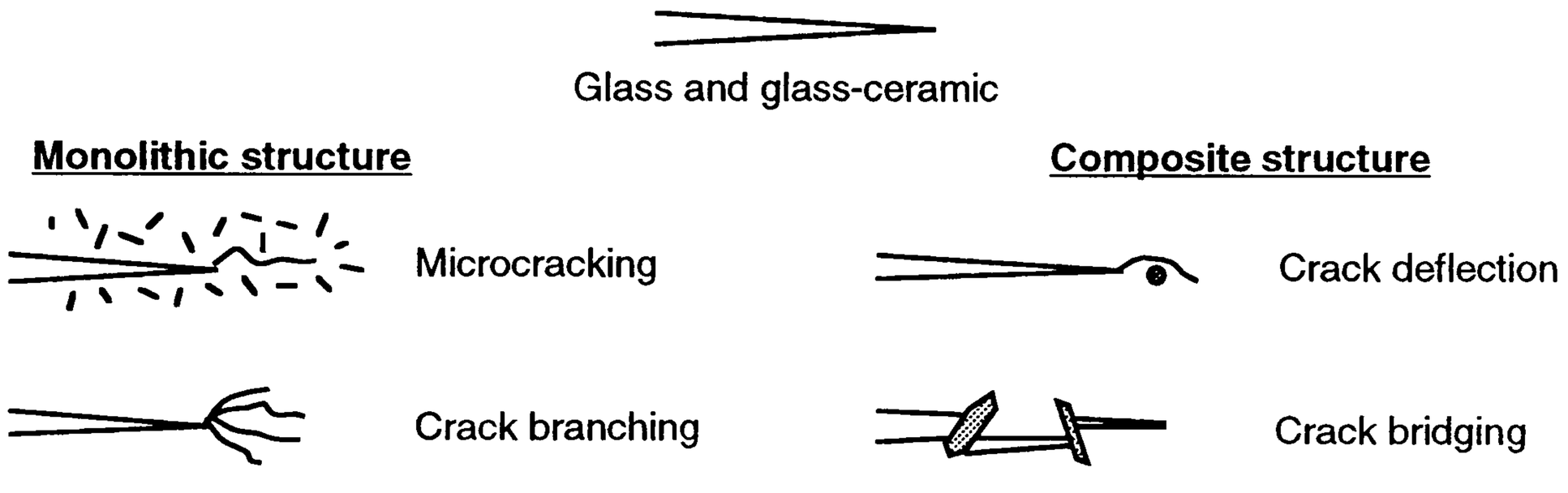


Figure 5-4 Schematic drawings illustrates typical sharp crack in glass and glass-ceramic materials and toughening mechanisms in monolithic and composite structures.

1983]. There is evidence that some porosity can also lead to substantial increases in fracture energy due to crack deflection [Rice 1985]. The coefficient of thermal expansion (CTE) of the composite constituents can also affect toughening, a crack will be attracted towards particles of lower CTE and repelled in the opposite situation. It has been suggested that these systems offer increased total fracture areas thus increasing the composite toughness [Faber & Evans 1983, Watchman *et al* 1989].

Microcracking can arise form the result of 1) difference in elastic moduli, 2) thermal expansion anisotropy in single-phase materials or thermal expansion mismatch in two-phase or multiphase systems, and 3) the volume expansion associated with a transformation. The tendency for microcracking exhibited by a single phase material depends on the scale of the dominant microstructural entity, namely grain size [Rice & Freiman 1981]. The microcracking can be distinguished from crack branching by noting the origin of the secondary crack. Branched cracks always originate from the main crack; microcracks can nucleate away from the main crack, followed by coalescence [Faber & Evans 1983]. However, it should be noted that microcrack toughening always leads to a drop in strength because, as suggested by Orowan [1949] and Griffith [1924], the fracture stress is inversely proportional to the crack length.

The ability of the second phase to reduce crack propagation in the composite, depends on factors such as its strength, particle size, volume fraction, and microstructural homogeneity. While the particulate strength is a material property and cannot be altered, the volume fraction, particle size, and homogeneity can be controlled. The homogeneity in particular increases the probability of crack front-particle interactions. To ensure this microstructural uniformity, processing factors such as the initial particle size and mixing procedures are the most important.

5.2 Experimental procedure

5.2.1 Flexural strength

The fracture strength of the glass and glass-ceramic samples produced via casting and controlled crystallization (Chapter 3) and via a powder route (Chapter 4) were measured by means of the three-point bend test technique performed on beam specimens. The beam specimens were of nominal dimensions of 25mm x 5mm x 2.5mm. The longitudinal edges of the specimens were carefully given a rounded profile on 1200-grit SiC abrasive paper to remove edge flaws produced during the fabrication process which may act as sites of stress concentration and thus cause premature failure of the specimen. The intended tensile face of the specimens was polished down to a 1 μm finish on the diamond lapping wheel. The tests were carried out at room temperature on an Instron testing machine. The span was 20 mm., giving a span-to-depth ratio of 4 and the cross-head speed employed was 0.5 mm/minute.

5.2.2 Plane strain fracture toughness

The plane strain fracture toughness (K_{1C}) of cast and sintered specimens was determined using single-edge notched beam (SENB) bend specimens. The beam specimens were prepared as described for the strength specimens except that the intended tensile faces were not polished with 1 μm finishing nor were the longitudinal edges of the intended tensile faces rounded. Instead, a notch with a nominal width of 0.15 mm and depth of 17% of the width of the specimen was machined in the tensile face of each specimen at the mid-length position, using a 0.165 mm thick diamond slitting disc on a Jones and Shipman 540P surface grinding machine. The notches were cleared of debris using strips of thin, stiff tracing paper prior to the measurement of their depths by an optical microscope with a graduated and calibrated eyepiece. Measurement were taken from both sides of the specimens and the bigger value recorded. The dimension of the SENB specimens were measured at the ends and at the centre, to within 0.01 mm accuracy with a screw micrometer, and the average of the three readings was taken.

5.2.3 Vicker's microhardness and Indentation toughness

The Vickers indentation test method was used to evaluate fracture toughness and surface hardness of the materials. The samples were polished down to a 1 μm surface finish using various grades of the diamond polishing wheels, so as to eliminate residual stresses and surfaces flaws. The microhardness was measured using a Leitz Wetzlar 8423 microhardness tester with x10 and x50 objective lenses. The samples were loaded to 490 N for 15 seconds. At least 8 indentation were taken for each sample, and the average value of surface hardness and indentation fracture toughness were calculated using equations 5-15 and 5-16 respectively.

5.2.4 Elasticity

The elasticity was determined using a non-destructive testing based on the impulse excitation technique. The major interests in using a dynamic method for the elasticity determination came from the accuracy and good reproducibility of the results. As a non-destructive test, it allowed the use of the samples for other measurements.

The instrument used was a Grindosonic MK4i supplied with EMOD version 9.12 software. The frequency of the natural vibration is dependent upon the specimen dimensions, its weight, and elastic properties. The sample was quickly struck with a ball bearing to cause an instantaneous impact. A transducer picked up the analogue signal and it was initially fed to a two stage amplifier. A zero crossing detector marked off the signal periods. When the incoming signal began to decay the peak detector validates the data and successive period measurements begin. All available periods are recorded and are stored in its memory. Finally when the incoming signal has died away the processor selects the measurement corresponding to the purest wave form and outputs the data.

5.3 Results and discussion

The microstructural differences observed for the various heat treatments cause large changes in the mechanical properties. The major effects of heat treatment, as discussed previously, are crystallization in bulk cast glass-ceramics, Chapter 3, and of sintering and crystallization in glass-ceramics produced via the powder route, Chapter 4.

The mechanical testings were performed on CS and CSF glasses, CSF glass-ceramics with a range of crystallinity, sintered CS and CSF glasses, glass-ceramics, and glass-ceramic matrix reinforced with either alumina, silicon carbide, or zirconia particles. The CSF bulk cast samples utilised in mechanical testing were produced under controlled heat treatment to obtain different degrees of crystallinity and spherulite sizes (see section 3.3.3). Sintered samples were produced by taking into consideration the crystallization and sintering characteristics to obtain different amounts of porosity and crystallization. The preparation and characterization of the cast and sintered samples were described in section 3.3.3 and 4.3.2.2, respectively.

The mechanical properties measured were the Elasticity (E), Vicker's hardness (H_v), fracture toughness (K_c), flexural strength (σ), and plane strain fracture toughness (K_{1c}). However, it should be borne in mind that each testing technique had its technical or mechanical limitations. In addition, the purpose of these tests was not to acquire a full range of mechanical properties, but rather to search for a system which is suitable for structural application and has a possibility to be improved by controlling the fabrication process or making a composite.

5.3.1 Elasticity

The Elasticity of CS and CSF glasses and glass-ceramics were measured only in bulk cast samples because the heterogeneity and porosity in sintered samples severely affect the transient natural vibration of elastic wave and thus give rise to inconsistent measured values. The Elasticities of CS and CSF glasses and glass-ceramics produced by different heat treatment are shown in Table 5-2. The structure of CSF glass is less

Table 5-2 Elasticity of CS and CSF cast glasses and glass-ceramics

Sample	Nucleation		Growth		Crystallinity	Phase present		E	
	T (°C)	t*	T (°C)	t*	(%)	C§	W§	Av (GPa)	SD
CS	-	-	-	-	0	-	-	75	18
CSF	-	-	-	-	0	-	-	70	8
FR1	-	-	800	10m	32.8	√	-	71	8
FR2	-	-	820	60m	50.6	√	-	68	8
FR3	660	30m	820	60m	73.4	√	-	78	7
FR4	600	72h	750	48h	73.8	√	-	76	6
FS1	-	-	900	10m	23.9	√	-	67	6
FS2	660	15h	900	5m	42.2	√	-	64	6
FS3	-	-	800	24h	91.0	√	-	92	3
FS4	660	48h	800	24h	89.4	√	√	75	14
FS5	-	-	850	60m	99.0	√	√	84	7

t*: in m (minutes) or h (hours)
§: C = cuspidine, W = wollastonite

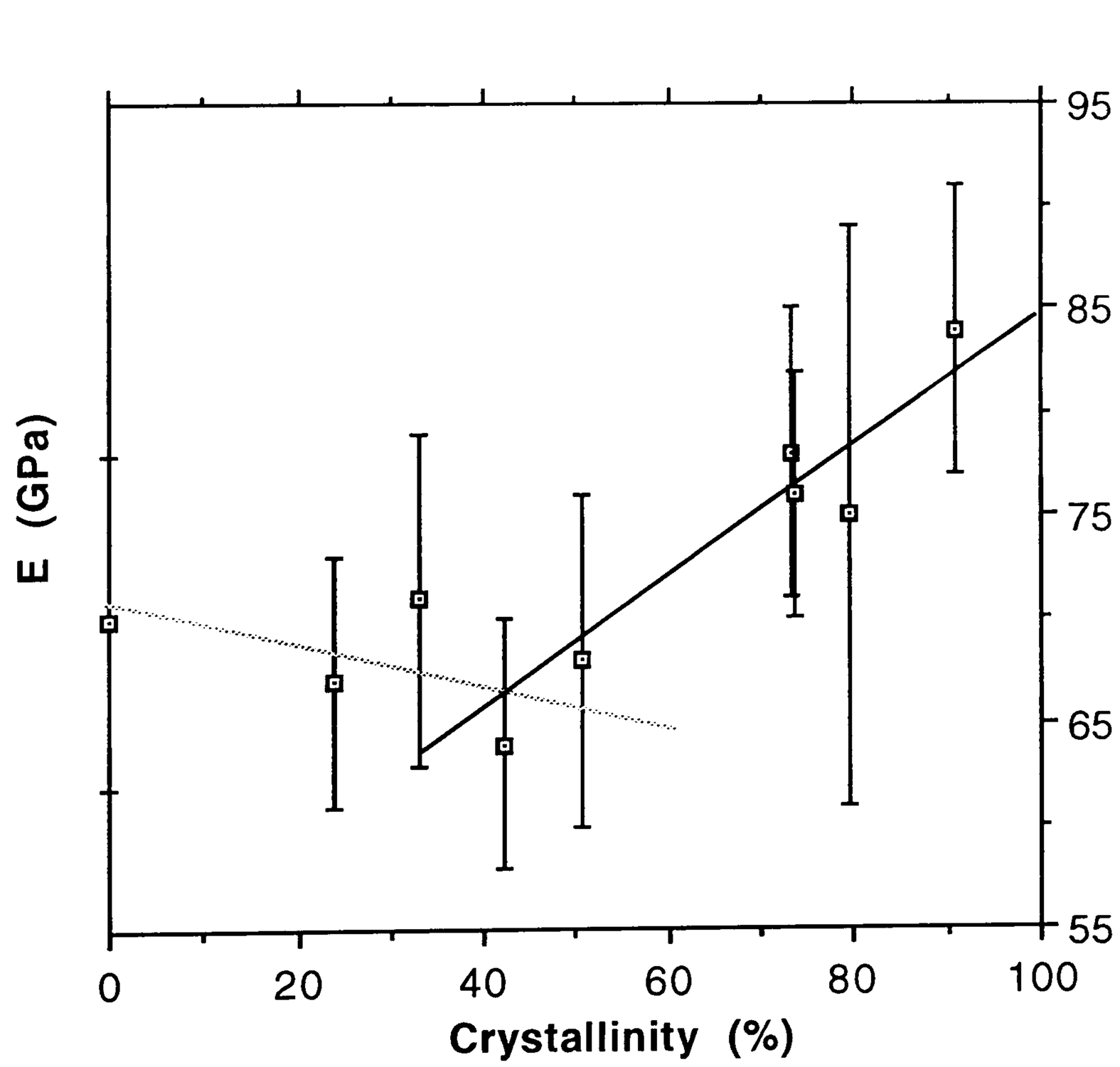


Figure 5-5 The relationship between crystallinity and Elasticity of cast CSF glasses.

rigid than that of CS because fluorine affects the glass structure in such a way that it breaks the Si-O bonds; i.e. acts as network breaker. Thus, CS glass exhibits higher Elasticity value than that of CSF glass.

Figure 5-5 shows the effect of crystallinity in CSF glass-ceramics on the elasticity. The Elasticity appeared to be little changed until the degree of crystallinity exceeds 50% despite the fact that it is expected to have high value because of low fluorine content in the residual glass and crystal structure could be expected to have a higher elasticity value than that of the glass structure. A possible explanation was that the composition of residual glass changes gradually with time/temperature and the Elasticity of the glass-ceramics of low crystallinity are expected to be dominated by the glassy phase. As shown in Table 3-9, the residual glass was rich in sodium. As the crystallization proceeds, the glassy phase will exhibit the Elasticity value lower than that of the original glass. In contrast, at higher crystallinity, the Elasticity was controlled by the crystal phase(s), and thus showed a marked increase.

5.3.2 Flexural strength

5.3.2.1 Bulk cast glass and glass-ceramics

Visual examination of broken flexural strength samples showed that fracture initiates on the tensile side perpendicular to the surface and exits on the compressive side not perpendicular to the surface. The crack does not pass straight through the thickness, but instead follows contours consistent with microstructure and the stress fields it encounters.

Table 5-3 displays the effect of spherulite size and crystallinity of crystallized CSF glasses. The flexural strength can be divided, according to spherulite morphology, into two categories: round and sheaf (Figure 5-6). The flexural strength of the former category decreased with spherulite radius and crystallinity. Similar results were obtained by Utsimi and co-workers [1970]. But the flexural strength of the samples in the latter category the was reduced by the presence of spherulite at low crystallinity, while it was increased at crystallinity higher than 70%, or more obvious with spherulite

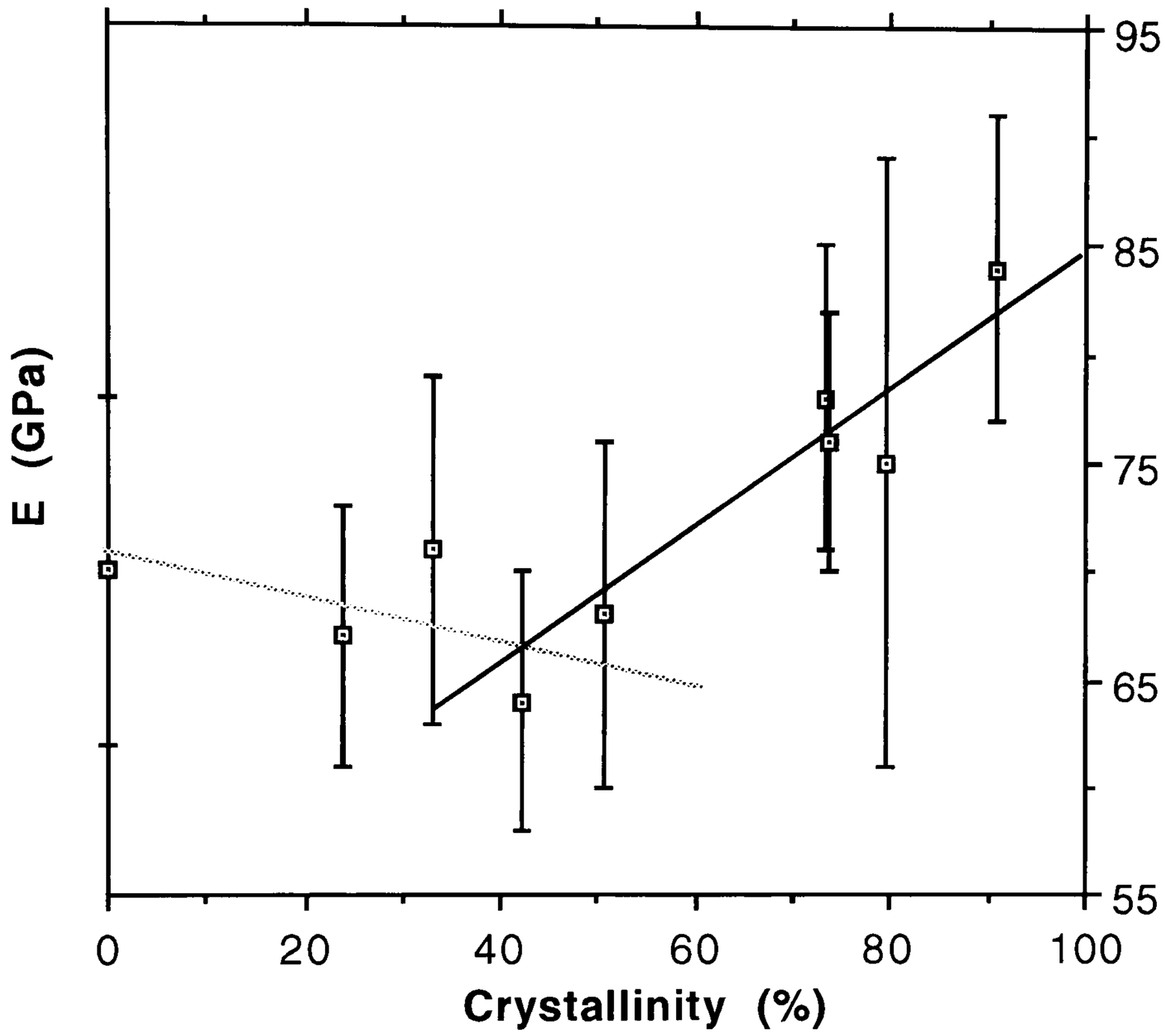


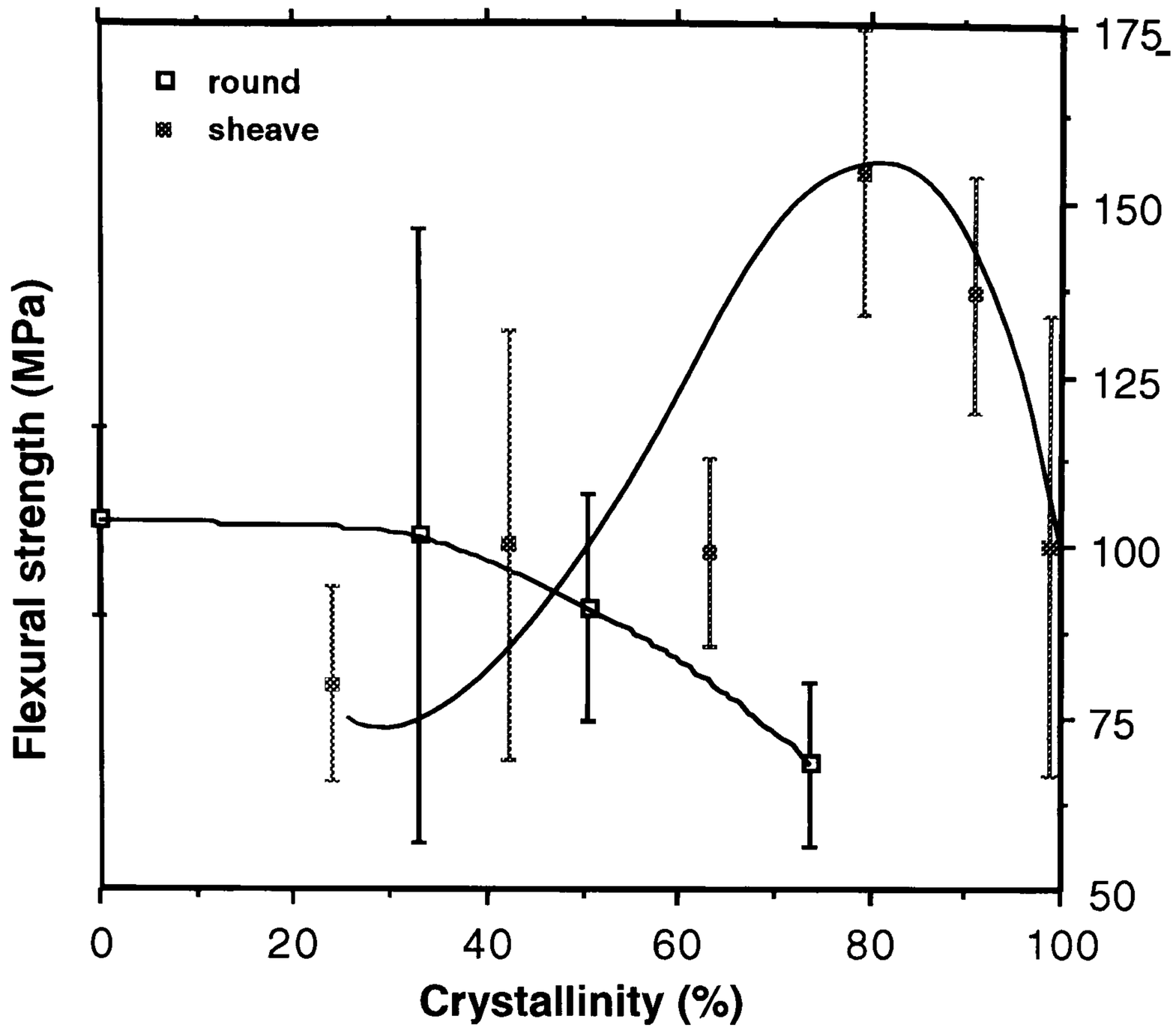
Figure 5-5 The relationship between crystallinity and Young's modulus of cast CSF glasses.

Table 5-3 Modulus of rupture (MOR) of CS and CSF cast glasses compared with those of crystallized CSF classified by morphology, size and crystallinity.

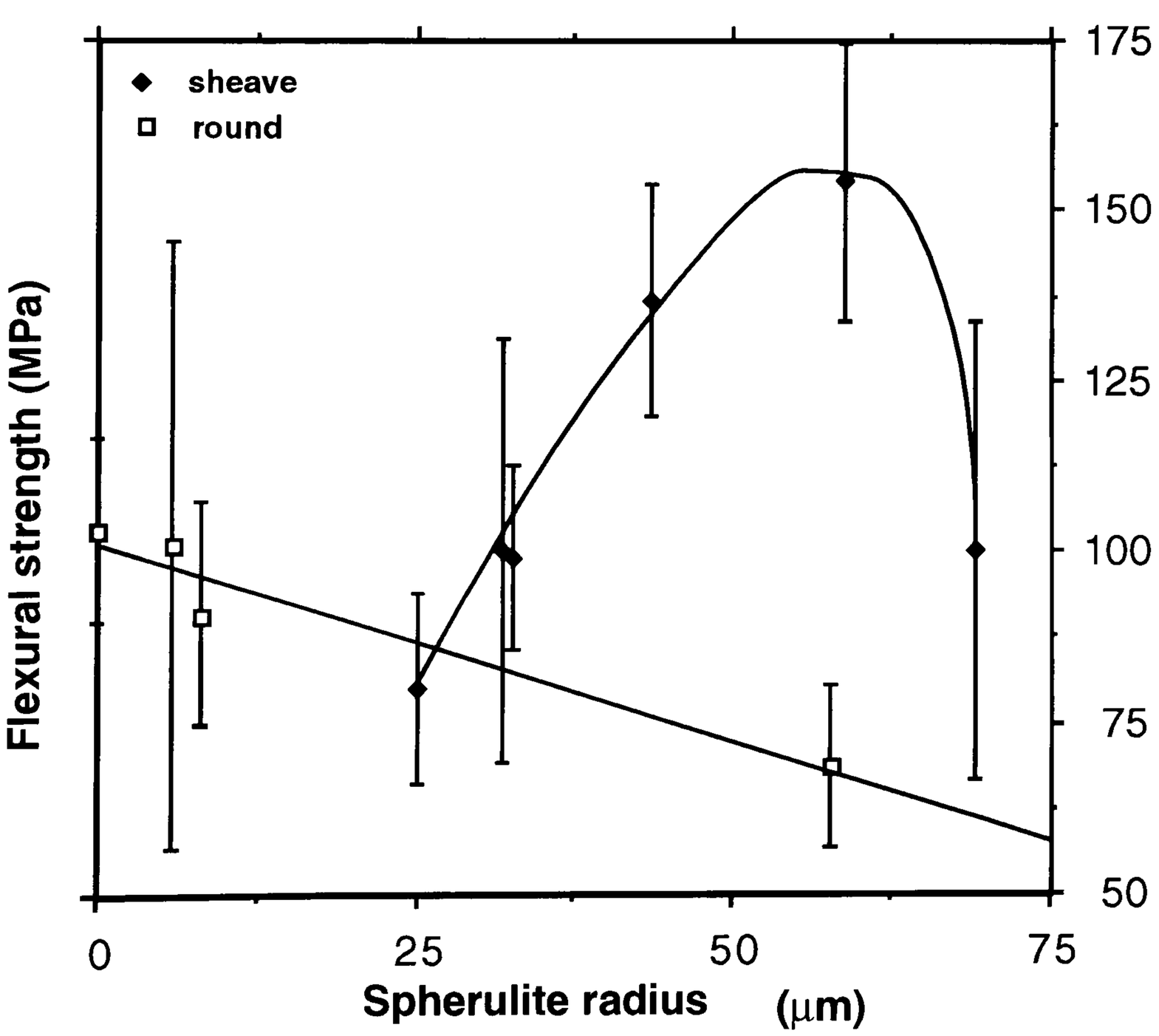
Sample	Morphology	Spherulite radius (μm)	Crystallinity (%)	Flexural st.	
				σ	SD
CS	-	-	0	127	20
CSF	-	-	0	105	13
FR1	round	5.9	32.8	101	44
FR2	"	8.2	50.6	91	16
FR3	"	32.5	73.4	99	13
FR4	"	57.8	73.8	68	12
FS1	sheaf	25	23.9	80	14
FS2	"	31.9	42.2	100	31
FS3	"	43.5	91	137	17
FS4	"	58.9	89.4	154	20
FS5	"	69.3	99	100	34

radius; i.e. strength increased with the radius up to ~ 60 μm, and then dropped at larger radius. The reason for the strength drop was because of the presence of microcracks.

Figure 5-7 displays micrographs of the fracture surfaces of these samples. In order to explane the differences in the surface topography, the local stress concentration based on the difference in modulus of elasticity between the two phases, in this case the glass matrix and the spherulites, would have to be taken into account [Utsumi & Sakka 1970]. It has long been recognised [Goodier 1933] that the stress concentration occurs at the time of application of an external force if a particle of different modulus of elasticity is present in the matrix. When the elasticity of the spherical particle is lower than that of the matrix, maximum tensile stress occurs at the ends of the diameter perpendicular to the direction of the external force [Edwards 1951]. This microstress may help the formation of cracks inside the particle or in the matrix, depending upon whether the particle is weaker or stronger. Furthermore, the thermal mismatch between the spherulites and residual glass components can generate internal stresses in the glass-ceramic which may unfavourably lead to lower strengths. The reduction in strength may also be due to inducement of microcracking by the thermal mismatch between the



(a)



(b)

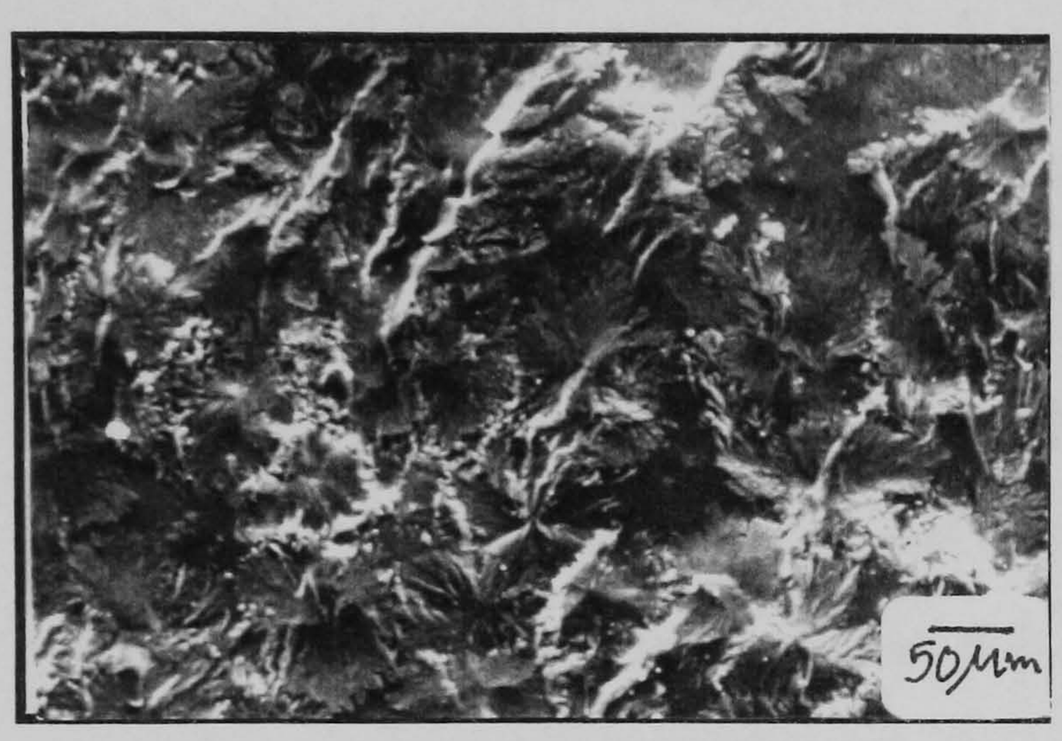
Figure 5-6 A plot showing the effect of morphological parameters, (a) crystallinity and (b) spherulite radius, on flexural strength of CSF glass.



FR2



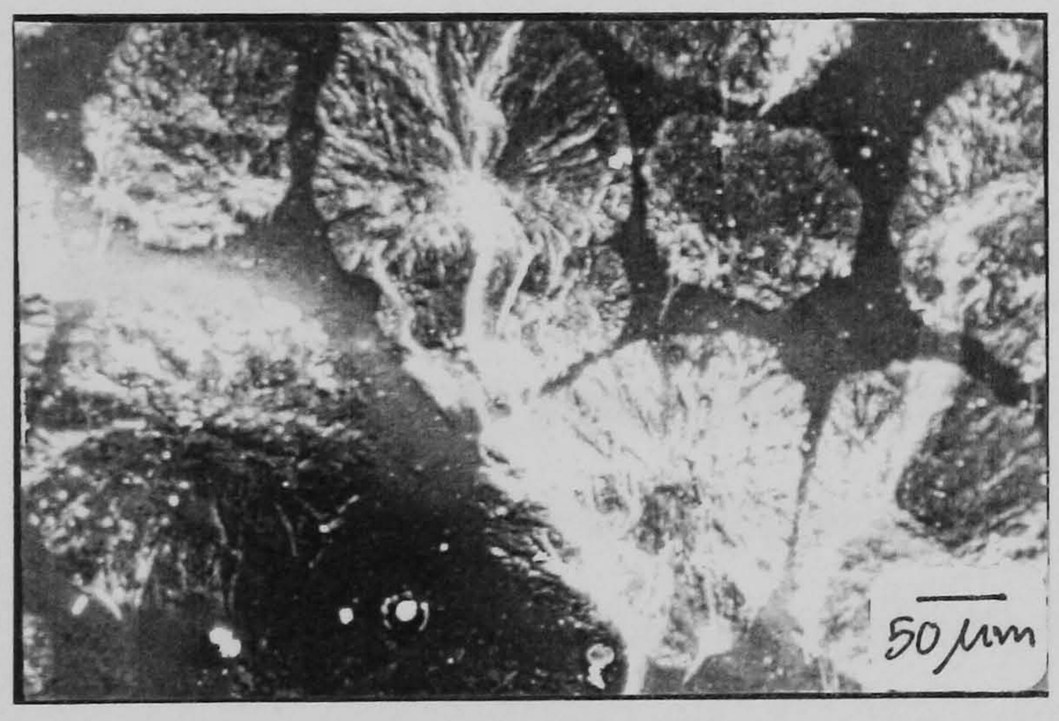
FS1



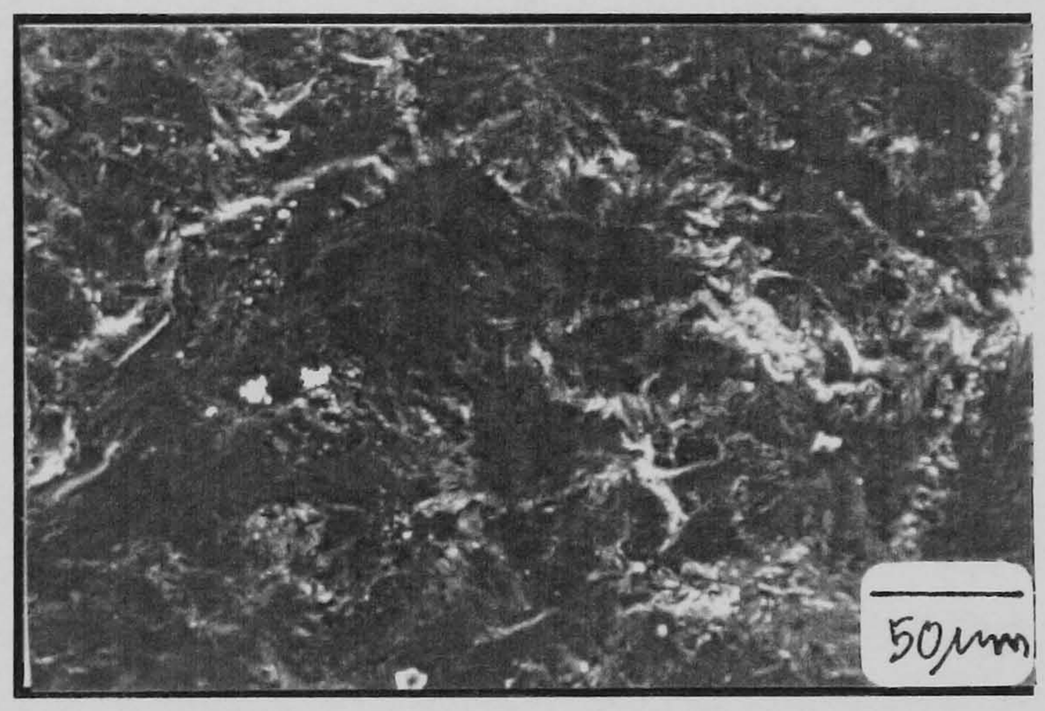
FR3



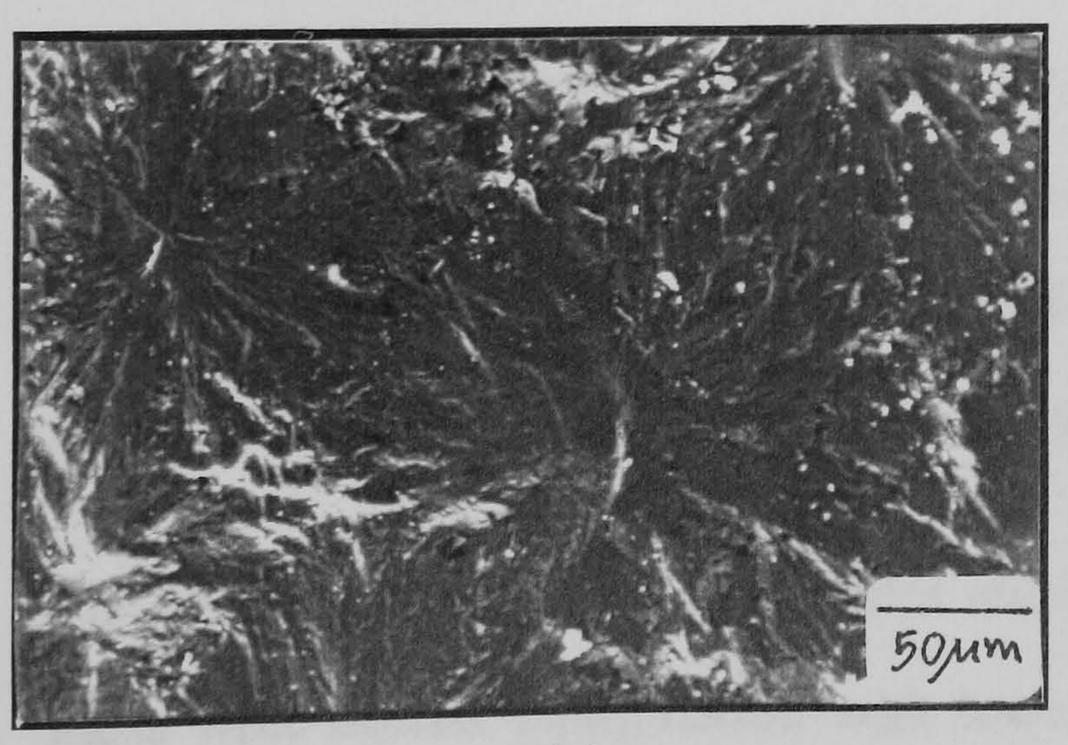
FS2



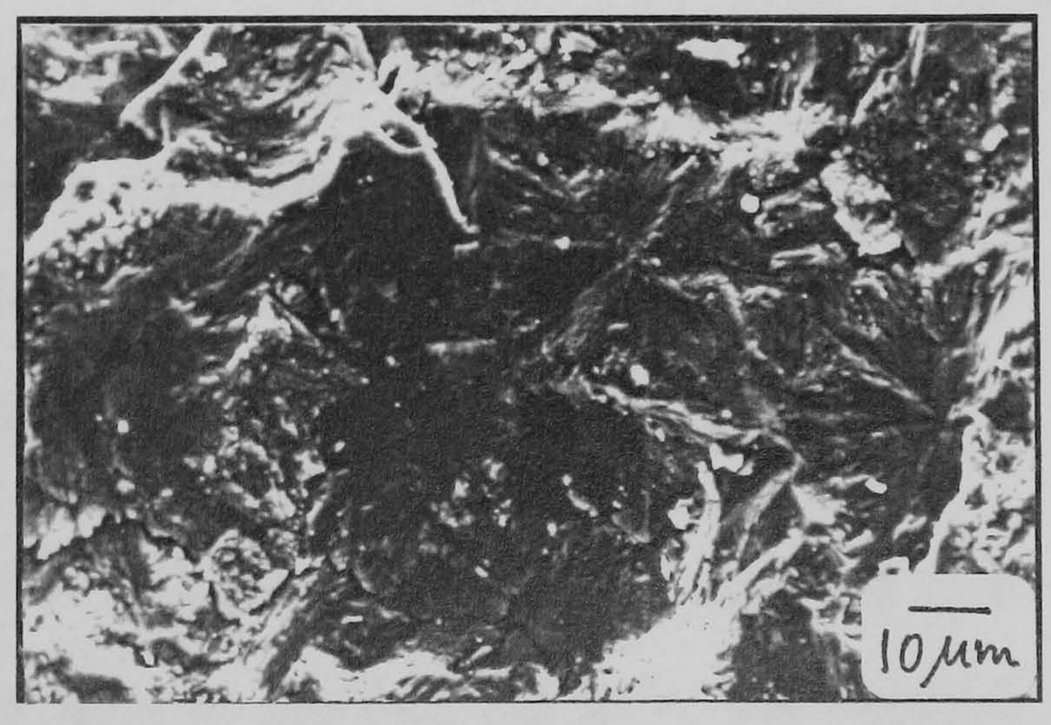
FR4



FS3



FS4



FS5

Figure 5-7 Scanning electron micrographs showing broken surface of CSF cast glass-ceramics (compared to Figure 3-26).

crystalline and residual glass components, which can generate internal stresses in the glass-ceramics. Sample FR4, which showed evidence of microcracking (Figure 5-7), gave flexural strength of 68±12 MPa, which is lower than those for samples of the same degree of crystallinity.

The samples in the former category were subject to heat treatments which gave rise to round spherulites. The micrograph of broken surfaces of these samples (Figure 5-7) reveals relatively smooth surface, resembling those of the first category. It may be deduced that the spherulites attract the crack and act as stress concentrators.For the second category, the fracture observed produced rough fracture surfaces which is characteristic of intergranular fracture. The surface topography became more tortuous with increasing crystallinity. The crack fronts interact with elastic waves produced by collision of the crack front with the spherulites. This interaction has the effect of modifying the plane of propagation of the cracks and produces a mark. The greater irregularity is associated with increased energy required for fracture.

5.3.2.2 Sintered glass and glass-ceramics

Sintered CS samples showed a severe deterioration in strength when compared with those of bulk cast glass (Table 5-4). Electron micrographs of these samples were displayed in Figure 4-12. Because of time limitation, degree of crystallinity of sintered samples were not measured. The porosity was slightly increased in size with increasing sintering temperature but the degree of sintering achieved was very similar. Although the strength was expected to increase with sintering temperature due to the increase in crystallinity, the major microstructural feature determining strength appeared to have been porosity. Consequently, the strength fell (Figure 5-8) as pores decrease the cross-sectional area on which the load is applied and also act as stress concentrators.

The flexural strength in CSF samples was not different from the value obtained from glass with similar composition with lower fluorine content, 2.8 wt%. The strength increased with increasing sintering temperature up to 900°C, then it fell when sintered at 950°C. The values obtained by sintering at 900°C and 950°C exceeded that of cast

Table 5-4 Effect of heat treatment, and crystallinity, on flexural strength of sintered glass-ceramics.

Sample	Holding temperature (°C)	MOR (MPa)	
		σ	SD
CS sintered	900	96	24
"	1000	85	11
"	1100	64	14
CSFsintered	750	62	10
"	800	57	16
"	850	104	19
"	900	132	37
"	950	126	20

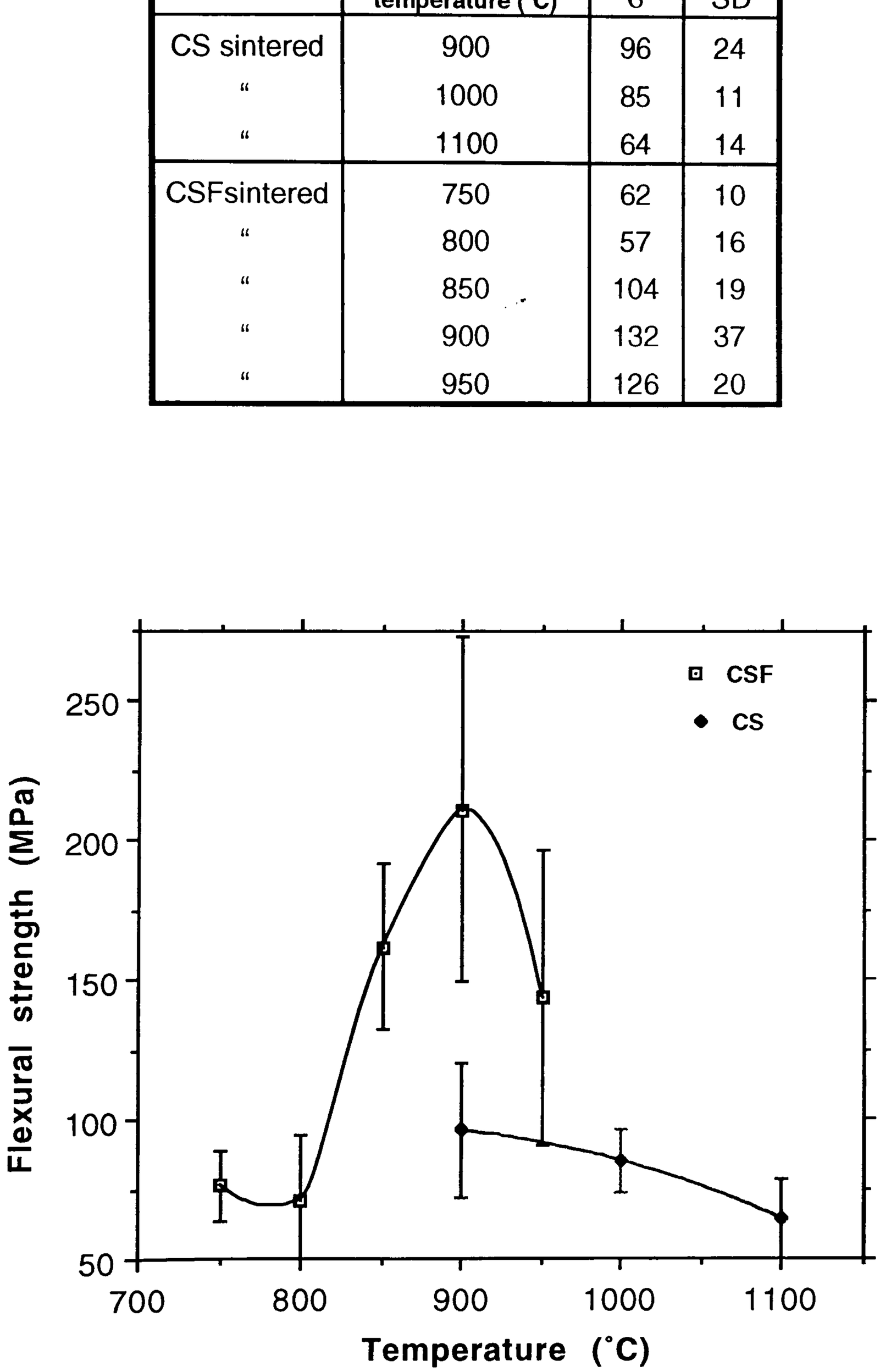


Figure 5-8 Plot showing the effect of sintering temperature on flexural strength.

CSF parent glass but were inferior to those of the best cast glass-ceramics. The improvement in strength with sintering temperature is attributed to the crystals developed in CSF being much finer than those in CS samples. The optimal strength value was achieved because the competition two driving forces for densification; i.e. sintering and crystallization, were balanced and thus given a small porosity content and high degree of crystallinity with a small crystal size.

In CSF the rate of reduction in viscosity with sintering temperature must have been so high in the temperature range 850°C to 900°C that the glass particles achieved a high degree of sintering before crystallization was initiated. This behaviour was not initially predicted from the densification study in Chapter 4. The key factor for this discrepancy from the densification study is the heating rate. The procedure for the preparation of samples for mechanical testing was such that the samples were dried at approximately 120°C and then transferred directly to a furnace set at the required sintering temperature. The temperature of the samples was expected to reach the furnace temperature within 5 minutes. So the heating rate was so high (> 150°C/min) that the crystallization was delayed. However, at higher temperature, 1000°C, the microstructure shown in Figure 4-12 reveals lower number of larger pores than those developed at 900°C. The drop in strength must have been related to the size of the pore.

5.3.2.3 Glass- and glass-ceramic matrix composites

The flexural strength of CS and CSF glass and glass-ceramic matrix composites are displayed in Table 5-5. The strength of all samples deteriorated significantly by the addition of particulate 'reinforcements' although the performance of the Al2O3 reinforced composites was superior to the rest. The microstructures of the samples are shown in Figure 4-18 and Figure 4-19. It can be seen that only Al_2O_3 reinforcements form a good bond with the matrix. The good bonding between phases allows load transfer, and thus greater improvements in strength than would otherwise be observed. In the case of weakly bonded interface or indeed no bond present (as observed in ZrO_2 and SiC reinforced composites) not only will the opposite case apply, but the

Table 5-5 Effect of particulate 'reinforcements' on the flexural strength of sintered CS and CSF (all heat treated for 3 hours at 900˚C)

Matrix	Filler		Strength (MPa)	
	reinforcement	VF*	Av	SD
CS	Al_2O_3	20	93	15
	Zr	10	37	7
	SiC(fine)	15	19	6
		20	14	6
CSF	Al_2O_3	20	47	8
	ZrO_2	10	18	6
	SiC(coarse)	10	17	5

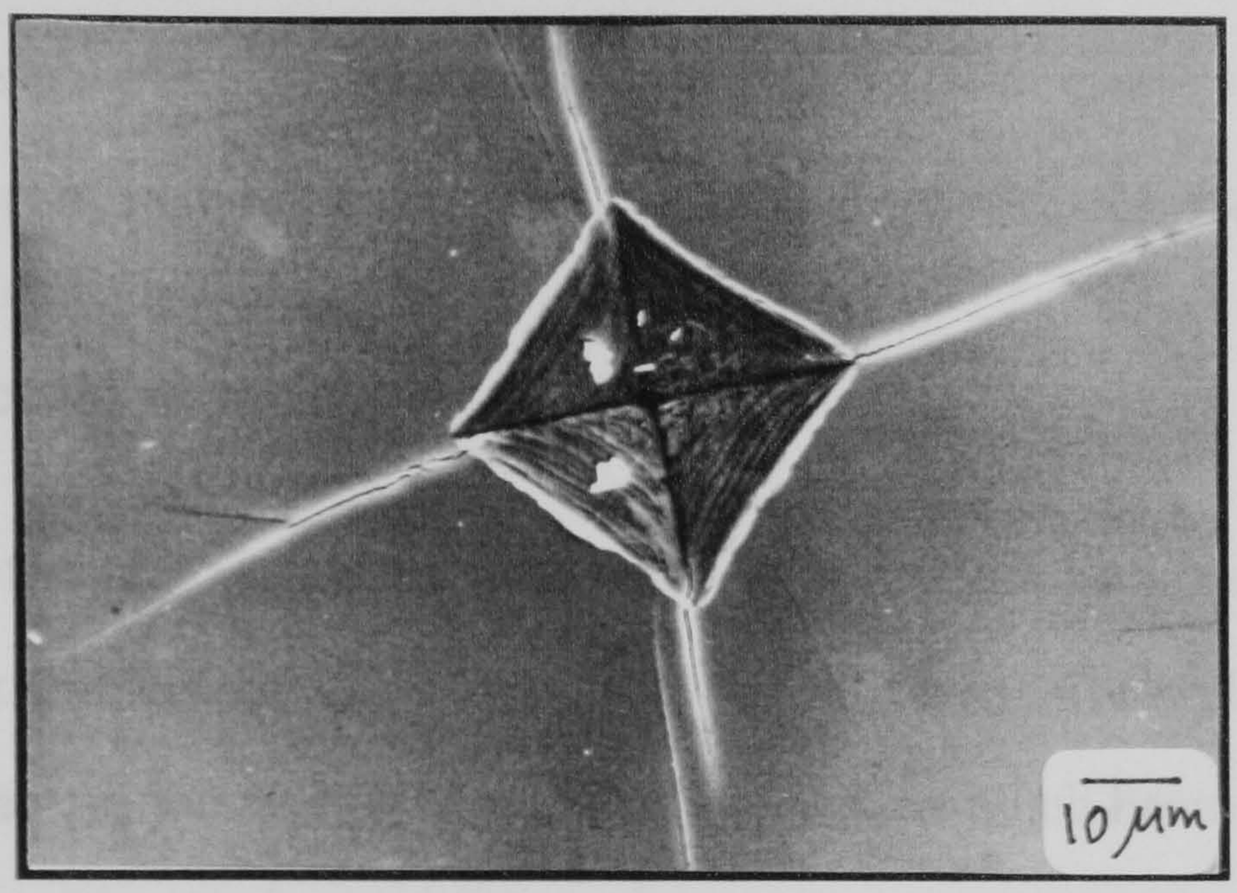
*: VF= volume fraction

psuedopores developed at the interface also act as stress concentrators and severely decrease the strength.

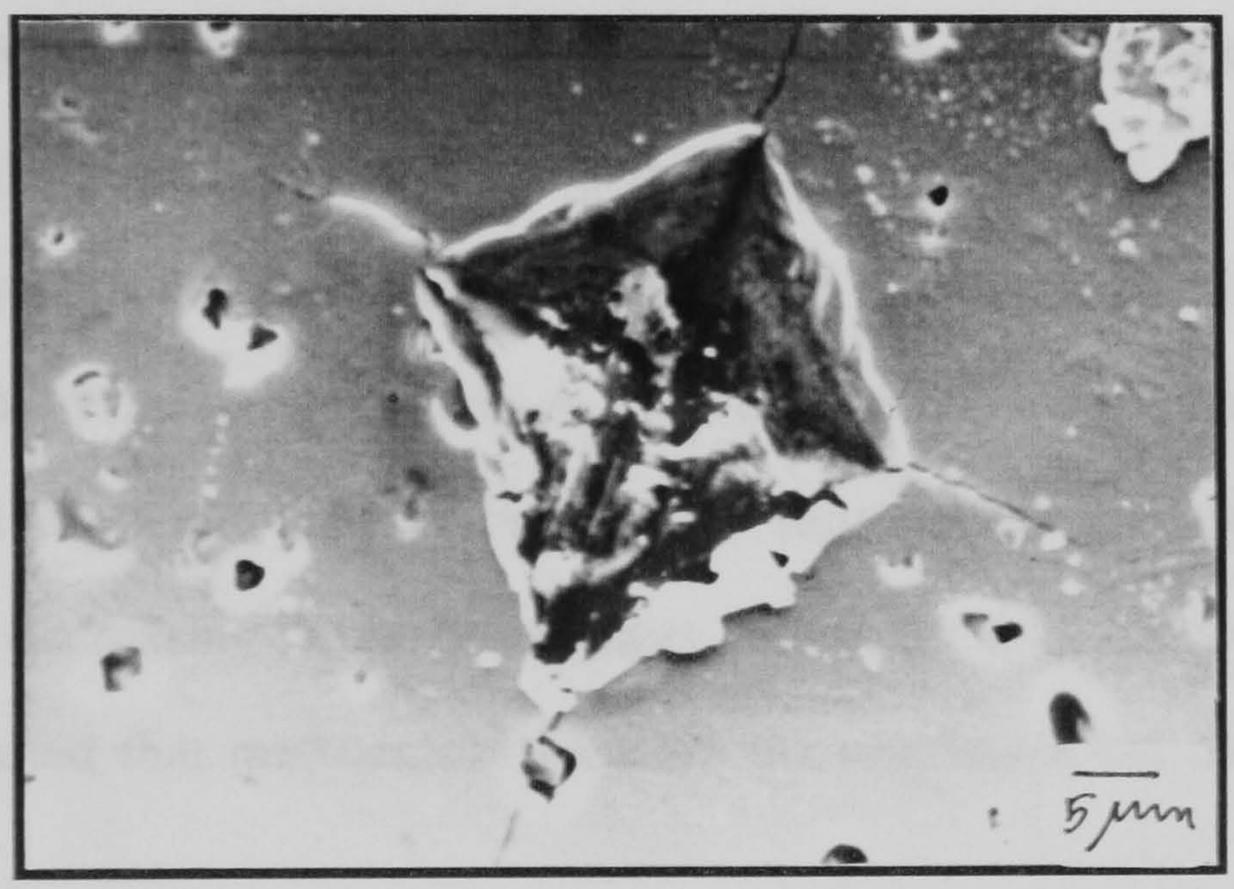
5.3.3. Vicker's microhardness

Cracks which are introduced onto the polished surfaces of samples using a Vickers diamond indenter give some indication as to the inherent fracture characteristics of the material. Typical indents in cast and sintered samples are shown in Figure 5-9. In cast glass the indentation and the cracks, which emanated from the diagonal corners, are clearly defined. In some sintered sample, material broke away from one side of the indentation, but only indents with clear diagonal and cracks were measured. The calculated H_v (using eq. 5-15) of CS and CSF glasses are 5.7±0.2 GPa and 5.4±0.2 GPa, respectively. Table 5-6 shows the Vicker's hardness values of CSF glasses with different degree of crystallinity. Figure 5-10 depicts the effect of heat treatment on H_v of the CSF cast samples. H_v values were approximately invariant with crystallinity. However it should be noted that none of the heat treatment produced a Hv value higher than that of CSF cast glass.

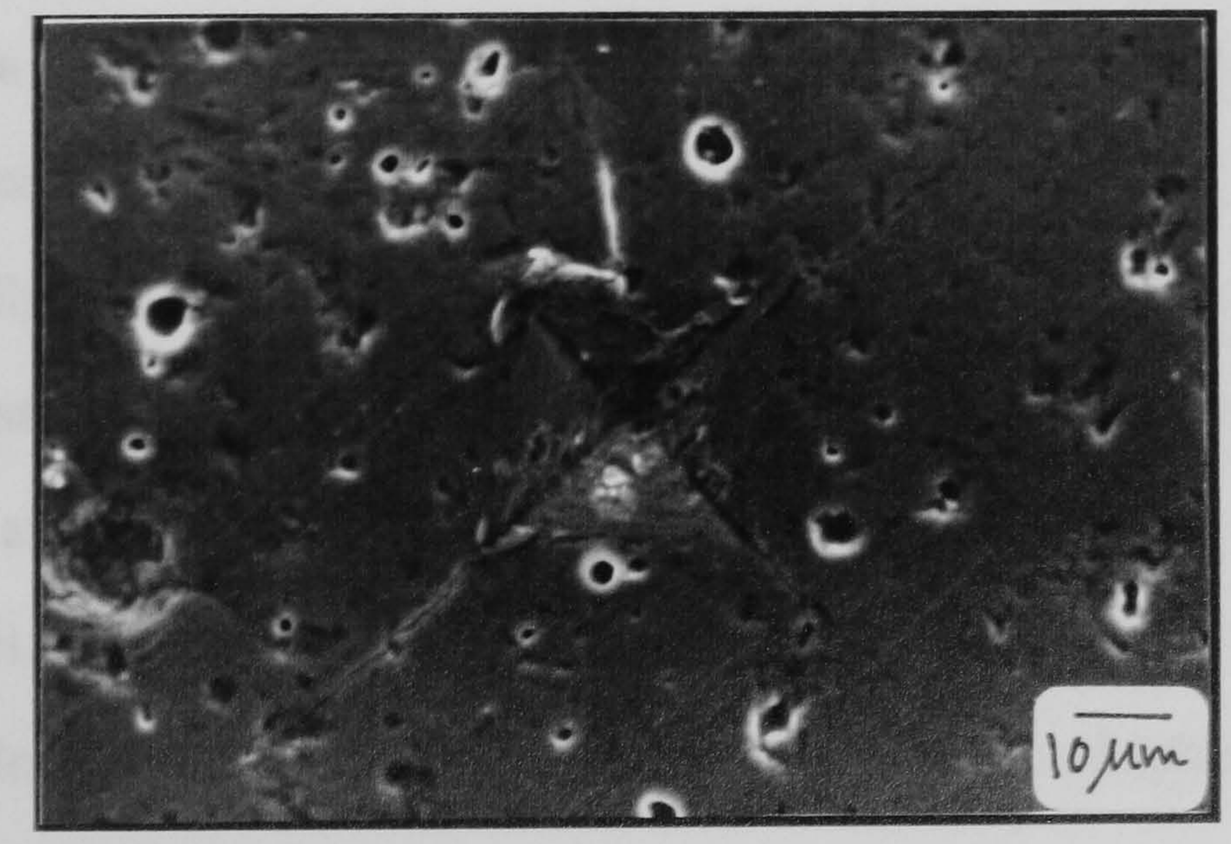
The effect of heat treatment on H_v of sintered CS and CSF are shown in Table 5-7. The hardness, H_v, of CS sintered is approximately invariable with heat treatment but H_v of CSF sintered is highest at temperature between 850-900˚C (Figure 5-11) which is the



(a)



(b)



(c)

Figure 5-9 SEM micrographs of typical indents obtained in (a) cast CS and CSF glasses, (b) sintered CS glass-ceramics, and (c) sintered CSF glass-ceramics.

optimum the temperature range sintering and also produced the highest strength values (see 4.3.2.2). Therefore, the Vicker's hardness reflects well the degree of sintering occurred in the samples. The highest Hv values achieved in sintered samples are, within experimental error, in the same range as those obtained from cast samples.

5.3.4 Fracture toughness

Two types of fracture toughness were measured: fracture toughness, K_c, determined from the cracks which emanated from diagonal of Vicker's microhardness indent and plane strain fracture toughness, K_{1c}, from single edged notch beam (SENB) technique. The fracture toughness values of CS cast glass are 1.68±0.23 MPam1/2 and 1.10±0.09 MPam1/2 for K_c and K_{1c}, respectively. The fracture toughness in CSF glass is higher than those in CS glass. Table 5-8 gives the fracture toughness of CSF cast glass and glass-ceramics with various spherulite diameter, D_s. The critical flaw size (size of defect from which fracture initiated), A_c, was calculated from equation 5-11, assuming that the cracks are penny-shaped. Figure 5-12 suggests that the critical flaw size, A_c, increased with decreasing fracture toughness, except for samples with low crystallinity. It should be noted that microcracks increase the toughness but decrease the flexural strength.

The increase in toughness can be explaneed in terms of crack propagation behaviour. The observed cracks running at the boundaries between spherulites (Figure 5-10) must have profoundly affected the crack path. The mismatch in the coefficient of thermal expansion must have played a role, as the CTE of CSF glass and fully-crystallized glass-ceramic are 10.64 x 10^{-6} K^{-1} and 6.00 x 10^{-6} K^{-1}, respectively. Therefore three microstructural characteristics which favour high fracture toughness in cast glass-ceramics are elongated crystals, high crystallinity (>80%), and spherulite with diameter larger than the critical flaw size.

The fracture toughnesses of sintered samples were measured by indentation method. Although the calculated values were exaggerated by porosity halting the cracks, the

Table 5-8 Effect of heat treatment, and crystallinity, spherulite radius (Rs), mean free path (λ), and critical flaw size on fracture toughness of cast CSF glass.

Sample	Crystallinity	Rs	λ	Critical flaw		K_c (MPam$^{1/2}$)		K_{1c} (MPam$^{1/2}$)	
	(%)	(μm)	(μm)	Gr.	Pe.	Av	SD	Av	SD
CSF	-	-	-	26.2	154	1.81	0.16	2.01	0.25
FR1	32.8	5.91	38	8.3	49	1.59	0.09	1.11	0.09
FR3	73.4	32.5	37	9.0	53	1.84	0.18	1.13	0.17
FR4	73.8	57.8	65	45.3	266	1.54	0.29	1.75	0.40
FS1	23.9	25	250	26.2	154	§	§	§	§
FS4	91	43.5	14	10.3	61	3.74	0.80	1.63	0.14
FS5	79.4	58.9	48	19.5	114	3.69	0.93	2.59	1.14
FS6	99.0	69.3	2.2	95.0	557	4.08	1.78	3.71	1.17

§ not measured.

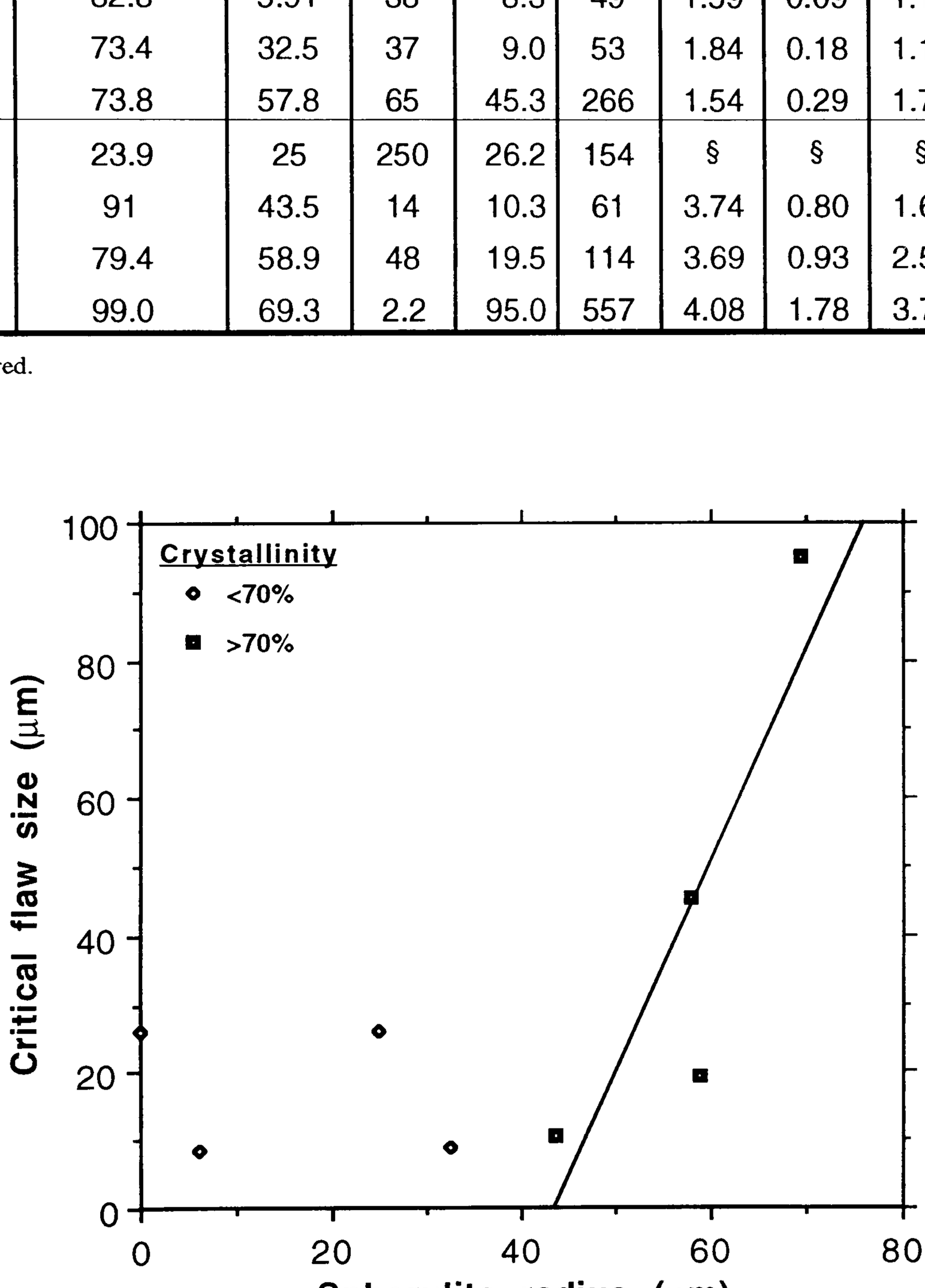


Figure 5-12 The effect of spherulite radius on critical flaw size.

Table 5-9 Effect of heat treatment at different temperatures for 3 hours on indentation toughness of sintered CS glass.

Sample	Temperature (°C)	K_c (MPa ·$m^{1/2}$)	
		Av	SD
CS cast	-	1.68	0.23
CSF cast	-	1.81	0.16
CS sintered	900	3.05	0.64
	1000	9.79	3.30
	1100	6.24	2.61
CSFsintered	800	0.88	0.21
	850	4.45	2.22
	900	12.73	2.54
	950	6.54	2.85

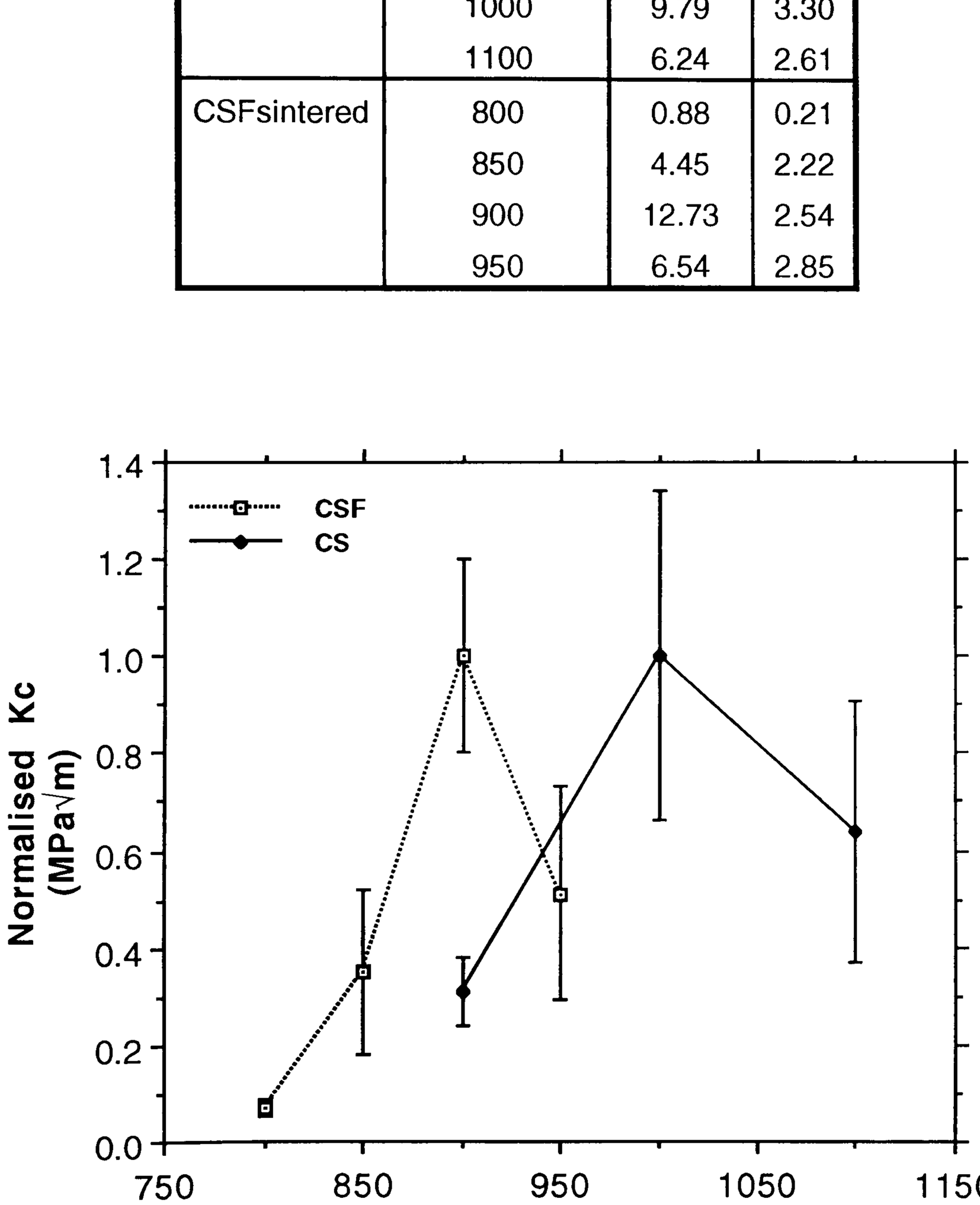


Figure 5-13 Plot shows the effect of sintering temperature on normalised fracture toughness (K_c).

indentation tests made it possible to rank the ability of the material to resist crack propagation and the crack path (Figure 5-12). The fracture toughness values (shown in Table 5-9) were normalised and plotted in Figure 5-13. The highest K_c for CS and CSF were obtained from samples heat treated at 900°C and 1000°C, respectively. The microstructure of the CSF samples with high and low K_c are shown in Figure 4-15. Both composed of fine crystals but the sintering in samples with low K_c was very limited and the glass particles remain separated, on the other hand, the sintering in samples with high K_c was well-advanced and the fine crystals were initiated from the particle surface and interlocked when the crystal fronts met.

5.4 Summary

The addition of 4.8 wt% fluoride in CS glass affects the mechanical properties in such a way that the elasticity, flexural strength, and Vicker's microhardness are decreased but the fracture toughness is increased. The mechanical properties of cast CS cannot be improved by ceramisation of the glass because of the surface crystallization as discussed in Chapter 3. However, the mechanical properties of CSF glass can be enhanced by controlled crystallization.

Maximum flexural strength of 154±20 MPa was obtained from the glass-ceramic (FS5) with high crystallinity (>80%) of elongated wollastonite crystals. This material also had a reasonable toughness of 2.59 MPa $m^{1/2}$. Improved toughness, 3.71±1.17 MPa $m^{1/2}$, was obtained in glass-ceramics with microcracks running at the boundary of spherulites with diameter larger than the critical flaw size. Inevitably, the presence of microcracks led to lower flexural strength of 137±17 MPa.

The strength of sintered CS glass-ceramics is inferior to those of cast glass but the toughness, as assessed by indentation, appears to be better. Although the crystallinity was increased with sintering temperature, the mechanical strength seemed to be more affected by the porosity. On the other hand, the mechanical properties of sintered CSF glass-ceramics show more promise. The flexural strength of 123±8 MPa was obtained

when heat treated at 900°C for 3 hours. This heat treatment also resulted in the higher indentation toughness. It is suggested key factor for the success is the heating rate.

None of the particulate 'reinforcement' (ZrO_2, SiC, and Al_2O_3) improved mechanical performance. ZrO_2 and SiC had a disastrous effect on strength which was attributed to a very poor reinforcement-matrix bond. The bonding was better in the case of Al_2O_3 and consequently the deterioration in strength was not as marked as for the other reinforcements.

CHAPTER 6

SUMMARY

6.1 Kinetics considerations

Fluoride addition and fabrication routes profoundly affect the crystallization behaviour in glass in the systems under investigation. Table 6-1 summarises the characteristic temperatures and activation energies for viscous flow and for crystallisation in CS and CSF glasses produced by bulk and powder routes. Generally, the characteristic temperatures; i.e. glass transition temperature (T_g), dilatometric temperature (T_d), crystallization started temperature (T_x), and crystallization peak temperature (T_p), in CS glass are higher than those in CSF. In other word, fluorine weakens the glass network. These conditions favour the formation of CSF glass and glass-ceramics because of the ease of melting and, as suggested by the large reduction in activation energy for crystallization, the ease which crystallization can be induced by reheating of the glass to a temperature within or just above the annealing range. Additionally, the Avrami

Table 6-1 Characteristic temperatures in ˚C; glass transition temperature (T_g), dilatometric temperature (T_d), crystallisation start temperature (T_x), and crystallisation peak temperature (T_p), and activation energies; for viscous flow (E_η), for crystallisation (E_c), and Avrami exponent.

Kinetic	**CS**		**CSF**	
parameter	bulk	powder	bulk	powder
T_g	686	677	613	603
Td	770*	781†	664*	644†
T_x	958	832	802	691
T_p	1108	877	822	744
E_η	985	875	616	652
$E_c(T_x)$	994	409	572	984
$E_c(T_p)$	374	354	146	308
n	0.78	4.94	3.01	1.04

* heating rate 10˚C/minute

† heating rate 15˚C/minute

exponent indicates that CS crystallized one-dimensionally, whereas CSF crystallized predominantly in three-dimension which assists the formation of homogeneous glass-ceramic.

The kinetics of crystallization in the CS and CSF glasses are much more complicated in the production of glass-ceramics by the powder route. Apparently, the presence of high surface area facilitates the reduction in the characteristic temperatures in both CS and CSF glasses. In CS glass powder the activation energies for viscous flow and for crystallization at T_p were approximately 10% lower than those in CS bulk glass; but the activation energy at T_x dropped to lower than 50% of that in bulk glass. This implies that the initiation of crystallization was markedly accelerated in CS glass powder. The Avrami exponent also indicates that the crystallization mode switched from surface-nucleated to bulk-nucleated. This is possible if the glass powder sintered and formed homogeneous glass bulk before crystallization was initiated. However, the surface of glass particles are normally alkali-depleted, and this uneven composition distribution give rise to 'traces' of the particle surface which act as nucleation sites.

In contrast, all the activation energies for crystasllisation in CSF glass formed from powder are increased, especially those for T_x and T_p which are almost twice the corresponding valuesof bulk glass. This implies that the controlling factor for thermal reactions was altered from diffusion of alkali ions to viscous flow, or crystallization was largely halted by the presence of high surface area. The Avrami exponent also implies that the crystallization was essentially one-dimensional growth from the surface of each particle.

6.2 Thermodynamic considerations

The nominal composition of the system under investigation is approximately $CaO{\cdot}2SiO_2$. In CS glass the equilibrium phase should be wollastonite ($CaO.SiO_2$) and silica (SiO_2). Whereas in CSF, a metastable phase, cuspidine ($CaF_2.3CaO.2SiO_2$), crystallized first. At temperature higher than 800°C, the cuspidine reacts with the

residual glass to form the more stable phase, wollastonite. It is proposed that the fluorine, from cuspidine, reacts with the sodium ions in the residual glass.

6.3 Controlled crystallization

The changes of composition of the residual glass which accompany the first development of the crystal phase causes an increase in viscosity. The distribution and number of nuclei in the glass determines the characteristic structure after completion of the crystallization process. In CS bulk glass, the crystals grow inwards from the glass surface in the form of needles and quite often they are oriented at 90° to the glass surface so that the two "fronts" of the crystal growth meet in the centre of the glass. The crystals are generally large and the orientation effect is such that the material will be mechanically weak.

A more acceptable microstructure; i.e. large number of small crystals distributed evenly throughout the bulk, can be obtained in CSF bulk glass. It was found that the microstructure was profoundly controlled by the heat treatment. Requirements for glass-ceramics with good mechanical properties are high volume fraction (>70%) of stable crystals having an interlocking fibrous morphology.

High crystallinity can be produced by either undergoing heat treatment at lower temperature for a long time or at higher temperature for a shorter period. Heat treatment at temperatures lower than T_x was found to produce crystals of fine fibrous structure but it may take an impractically long period for the crystallinity to be high enough for the crystals to be interlocked. However, rapid growth at temperature higher than T_p implies that conditions for coarsening of the microstructure exist in which small crystals redissolve and large crystals are enlarged. Thus, the mechanical properties are degraded. Consequently, it is suggested that the CSF bulk glass undergoing heat treatment in the nucleation range, T_d (664°C) < T < T_x (802°C), to induce the formation of fine crystals before undergoing heat treatment in the growth range, T_x (802°C) < T < T_p (822°C), to achieve high crystallinity.

6.4 Controlled sintering and crystallization

The densification study of CS glass powder, which had undergone an isothermal and constant heating rate (15°C/min) treatment, produced more promising results than from a similar study on CSF glass powder. Crystallization in sintered-CS glass was not observed even when heat treated at temperatures higher than T_p (877°C) for one hour. This suggests that although the viscosity was low enough to fill pores, and thus a high degree of densification was obtained, it was too high for crystallization to occur readily. On the contrary, the crystallization rate in CSF glass powder was so high that heat treatment at temperatures lower than T_d (643°C) leads to sintering being halted after only 5% shrinkage.

Crystallization in CS was observed when the sample was sintered pressurelessly at 900°C for 3 hours. The crystal morphology was similar to that obtained in bulk CS where rapid growth of the crystals occurs. Therefore, in order to obtain CS glass-ceramic with fine fibrous structure it is necessary that the glass compact is sintered at temperatures lower than T_p; however, a long period of heat treatment will be required.

Much finer crystals were developed in CSF glass even when heat-treated at 900°C. Moreover, it is interesting to note that a high degree of densification was obtained when the glass compact was sintered at temperature between 850°C and 900°C. This means the heating rate was so high that the crystallization was shifted and the glass of low viscosity has time to fill pores before crystallization started. At lower temperature, the viscosity was not low enough and at higher temperature the crystallization rate was too high. In both cases, sintering was halted before a high degree of densification was achieved.

Therefore, the major factors controlling the sintering and crystallization in glass powder are viscosity, heating rate, and crystallization temperature. In CS glass with high viscosity, low heating rate and sintering at a temperature lower than T_p is preferred. Conversely, CSF glass with low viscosity requires high heating rate and sintering at

temperature higher than T_p ; however, the sintering range in this glass is short and precautions have to be taken not to sinter at too low or too high a temperature.

It is only possible to reinforce CS glass with particles because in CSF the crystallizability is so high that it severely hinders sintering. On the choice of a suitable reinforcement, it was found that the interfacial bond plays a major role. It was shown that either the addition of SiC or ZrO_2 particles into the CS and CSF matrices are detrimental to the composites. SiC gave a poor interfacial bond due to poor wetting and ZrO_2 was agglomerated and acts as nucleating agent, as observed from interaction layer and crystal formation at the interface. Only Al_2O_3 gave a reasonable bond but however no strength improvement was achieved because Al_2O_3 increased the viscosity of the composite and this led to relatively high amount of porosity.

6.5 Mechanical properties

The elasticity of glass-ceramics depends on crystallinity. At low crystallinity the modulus depends mainly on the properties of the glassy phase, but on the stiffness of the crystal phase at high crystallinity. So, the elasticity of the glass-ceramics was constant, or slightly decreased, at low crystallinity and considerably increased with extent of crystallinity at high crystallinity.

Bulk CS glass had a low strength and could not be successfully heat-treated to produce a glass-ceramic with a desirable microstructure. In contrast, improved strength can be obtained in bulk CSF by controlled heat treatments to give glass-ceramics, the highest value achieved being 154±20 MPa. Strength depends on morphology and size of spherulites and the degree of crystallinity. Round spherulites led to poor strength and the strength was lowered, the larger the spherulites. Improved strength was attained from sheaf spherulites. In this case, the strength was generally better the larger the spherulite size and also a marked increase in strength was obtained in glass-ceramics with crystallinity higher than 75%. However, care should be taken not to produce spherulites which are too large because microcracks may develop and lead to a drop in

strength. But if high toughness is required, a controlled amount of microcracks is beneficial. The microcracking originated from CTE mismatch and the high rate of crystallization. The growth of crystalline phases, which may differ markedly in thermal expansion coefficient from the parent glass, can lead to the generation of high stresses in the glass due to the differential contraction which occurs on cooling.

Strength in sintered samples is controlled by porosity and crystal morphology. In CS, the strength degrading effect of the porosity outweighed the small improvement in strength associated with the development of coarse crystal structure. Thus the strength obtained was lower than that of cast glass. In CSF, the development of fine crystals gave rise to higher mechanical strength than that of the cast glass but lower than the best value obtained from a cast glass-ceramic.

The strength of the glass-ceramics was severely degraded with added 'reinforcement'. Factors controlling the choice of 'reinforcements' are the interaction between the 'reinforcements' and the matrix; i.e., interfacial bonding, reactions between matrix and 'reinforcement' phase, and role of the interface on the viscosity of the composites.

6.6 Conclusion

The $Na_2O{\cdot}CaO{\cdot}Al_2O_3{\cdot}SiO_2$ glass system gives relatively high strength (127 MPa) but very low fracture toughness (1.1 $MPam^{1/2}$). The toughness was improved by adding fluorine but other mechanical properties; i.e. strength, hardness, and the elasticity, are worsened. In kinetic terms, F increases crystallizability and lowers viscosity.

Mode of crystallization is very important for the production of glass-ceramics from bulk cast glass. The surface crystallization in bulk CS glass lead to anisotropic crystal growth which is accompanied by microcracking and planes of weakness. Thus crystallized CS glass is not acceptable for mechanical application. On the contrary, bulk crystallization was obtained in CSF and can be controlled to achieve good mechanical properties.

Factors controlling the mechanical performance were natures of crystalline phase, crystallinity, and extent of spherulite morphology and size.

The production of glass-ceramics via the powder route gave opportunity to utilise CS glass and to produce composites. Although the knowledge of crystallization kinetics in bulk glass is useful, the powder route is much complicated by the high surface area of the particles. The main factors controlling the sintering and crystallization processes were viscosity and crystallizability. These kinetics and thermodynamic factors can be manipulated by controlling the heating rate. For CS, which is of high viscosity and low crystallizability, slow heating rate is beneficial to facilitate densification. In contrast, the CSF is of low viscosity but readily crystallized from a powder. A high heating rate is recommended because the crystallization temperature is shifted to higher temperatures and the glass can quickly densify during the time lag period. Improved properties are obtained from the fine microcrystals in CSF. Similar fine microstructures and properties may be obtainable with CS glass if long heat treatments are used.

The CS glass may be used as matrix for glass-ceramic matrix composites if the reinforcements are carefully selected to have good bonding and to delay crystallization. From the preliminary study, alumina has the potential to be used in these matrices. The CSF glass may be used as a matrix phase if the crystallizability is diminished, possibly by reducing the amount of fluoride.

CHAPTER 7

SUGGESTIONS FOR FURTHER WORK

7.1 On matrix characterization

1. Quantitative XRD analysis for glassy phase, cuspidine and wollastonite in order to estimate the composition of the residual glass which significantly affects the crystallization characteristics.

2. Measure the fracture toughness of the sintered CS and CSF materials by single edged notch beam method.

3. Determine the crystallinity in pressureless sintered samples so that a direct effect of crystallization can be compared with those obtained from cast samples.

4. Control the heating rate to produce sintered CS with fine crystal structure and measure the mechanical properties.

7.2 On improvement of the materials

1. Study lower fluorine contents in order to obtain more information about the nucleation process in cast material and in sintered glass-ceramic to observe if the sinterability and crystallizability of the glass powder is significantly affected.

2. Hot press monolithic CS and CSF glasses by using low heating rate for CS glass and high heating rate for CSF glass up to temperature where crystallization is initiated and then heat isothermally to achieve high densification.

3. If the hot-press study is successful, explore the range of reinforcement interaction with the matrix. Al_2O_3 is recommended for preliminary study.

7.3 On application

1. Since a glass-ceramic composition similar to CSF has been used before as a glass-ceramic seal for sealing molybdenum to alumina or platinum to alumina [Rogers et al 1969]. The effect of crystallinity on coefficient of thermal expansion can be controlled to match other materials. A range of vacuum sealing techniques based on CSF may be explored.

2. Since good strength and toughness values have been obtained in CSF glass-ceramics. Fatigue-testing may be investigated to estimate the life span of the material if utilised under mechanical loading.

References

Anderson,M.P.; Srolovitz,D.J.; Grest,G.S.; and Sahni,P.S. **[1984]** "Computer simulation of grain growth: I. Kinetics" Acta.Metall. 32[5]783-91

Anon [1957] Am.Cer.Soc.Bull. 36[7]279-80

Auborn,J.N. and **Haber**,R.A. **[1991]** "The effects of particulate grain size and volume fraction on the mechanical properties of alumina-glass composites" Cer.Trans: Vol.19 Advanced composite materials 789-95

Augis,J.A. and **Bennett**,J.E. **[1978]** "Calculation of the Avrami parameters for heterogeneous solid state reactions using a modification of the Kissinger method" J.Ther.Anal. 13[2]283-92

Avrami,M. [1939] "Kinetics of phase change: I." J.Chem.Phys. 7,1103; "II." J.Chem.Phys. [1940] 8,212; "III." J.Chem.Phys. [1941] 8,177

Bansal,G.K. **[1976]** "Effect of flaw shape on strength of ceramics" J.Am.Cer.Soc. 59[1-2]87-8

Bansal,G.K. and **Doremus**,R.H. **[1986]** Handbook of glass properties Academic press

Bansal,N.P. and **Doremus**,R.H. **[1984]** "Determinations of reaction kinetic parameters from variable temperature DSC and DTA" J.Therm.Anal. 29[1]115-19

Bansal,N.P.; Doremus,R.H.; Bruce,A.J.; and Moynihan,C.T. **[1983]** "Kinetics of crystallization of ZrF4-BaF2-LaF3 glass by differential scanning calorimetry" J.Am.Cer.Soc. 66[4]233-38

Barringer,E.; Jubb,B.; Fegley,B.; Pober,R.L.; and Bowen,H.K.**[1984]** "Processing monosized powders" in Hench,L.L. and Ulrich,D.R. [eds] Ultrastructure processing of ceramics, John Wiley, 315-33

Bartels,J.; Schweitzer,F.; and Schmelzer,J. **[1990]** "Non-stationary nucleation and cluster growth in quasi-binary non-ideal solutions" J.Non-Cryst.Solids 125,129-38

Bauer,R.R.; Copeland,J.R.; and Santini,K. **[1994]** "Wollastonite" in D.D.Carr [ed] Industrial Minterals and Rocks Soc.of Mining, Metallurgy, and Exploration,Inc. USA. p.1119-228 ISBN 0-87335-103-7

Bergeron,C.G. and **De Luca**,J.P. **[1967]** "Crystal growth at bubble surfaces in glass" J.Am.Cer.Soc. 50[2]116-7

Borchardt,H.J. **[1956]** "Differential thermal analysis" J.Chem.Education 33[3]103-7

Bordia,R.K. and **Raj**,R. **[1986]** "Analysis of sintering of a composite with a glass or ceramic matrix" J.Am.Cer.Soc. 69, C55-7

Bordia,R.K. and **Scherer**,G.W. **[1988]** "On constrained sintering: Part 1, 2, and 3" Acta.Mettal. 36[9]2393-2416

Brennan,J.J. and **Prewo**,K.M. [1982] "Silicon carbide fibre reinforced glass-ceramic matrix composites exhibiting high strength and toughness" J.Mater.Sci. 17, 2371-83

Budworth,D. **[1968]** "Theory of pore closure during sintering" A432t-D434t, 29-31

Buri,A.; Marotta,A.; and Giordano,O.P. **[1971]** Proc. 9th Inter.Congr.Glass: Vol.1, section A 1.3 International Commission on Glass, Charleroi, p.343

Burnett,D.G. and **Douglas**,R.W. **[1971]** "Nucleation and crystallization in the soda-baria-silica system" Phys.Chem.Glasses 12[5]117-24

Cahn,J.W. **[1969]** "The metastable liquidus and its effect on the crystallization of glass" J.Am.Cer.Soc. 52[3]118-21

Cahn,J.W. and **Heady**,R.B. **[1970]** "Analysis of capillary forces in liquid-phase sintering of jagged particles" J.Am.Cer.Soc. 53,406-9

Carpenter,P.R.; Campbell,M.; Rawlings,R.D.; and Rogers,P.S. **[1986]** "Spherulitic growth of apatite in a glass-ceramic system" J.Mater.Sci. 5,1309-12

Charles,R.J. **[1969]** "The origin of immiscibility in silicate solutions" Phys.Chem.Glasses 10[5],169-78

Clark,T.J. and **Reed**,J.S. **[1986]** "Kinetic processes involved in the sintering and crystallization of glass powders" J.Am.Cer.Soc. 69[11]837-46

Clinton,D.; Mercer,R.A.; and Miller, R.P. **[1970]** J.Mater.Sci. 5,171

Coble,R.L **[1958]** "Initial sintering of alumina and hematite" J.Am.Cer.Soc. 41,55

Cutler,I.B. **[1969]** "Sintering of glass powders during constant rates of heating" J.Am.Cer.Soc. 52[1]14-17

Cutler,I.B. and **Henrichsen**,R.E. **[1968]** "Effect of particle shape on the kinetics of sintering of glass" J.Am.Cer.Soc. 51[10]604-5

De Bruijn,T.J.W.; DeJong,W.A.; and Van Den Berg,P.G. **[1981]** "Kinetic parameters in Avrami type reactions from isothermal and non-isothermal experiments" Thermochim.Acta 45[3]315-25

Dietzel,A. **[1942]** Z.Electrochem 9, 48

Doremus,R.H. **[1973]** Glass Science John Wiley & Sons USA ISBN 0-471-21900-2

Drummond III,C.H. **[1990]** "Glass formation and crystallization in high-temperature glass-ceramics and Si3N4" J.Non-Cryst.Solids 123,114-28

Dumas,P.; Corset,J.; Carvalho,W.; Levy,Y.; and Neuman,Y. **[1982]** "Fluorine doped vitreous silica analysis of fibre optic preforms by vibration spectroscopy" J.Non-Cryst. Solids 47[2]239-42

Evans,A.G. **[1982]** "Considerations of inhomogeneity effects in sintering" J.Am.Cer.Soc. 65[10]497-501

Exner,H.E. **[1980]** "Solid-state sintering: Critical assessment of theoretical concepts and experimental methods" Powder Metallurgy 4,203-9

Faber,K.T. and **Evans**,A.G. **[1983a]** "Crack deflection processes- I. Theory" Acta Metall. 31[4]565-75

Faber,K.T. and **Evans**,A.G. **[1983b]** "Crack deflection processes- II. Experiment" Acta Metall. 31[4]577-84

Freiman,S.W. and **Hench**,L.L. **[1972]** "Effect of crystallization on the mechanical properties of Li2O-SiO2 glass-ceramics" J.Am.Cer.Soc. 55[2]86-90

Freiman,S.W.; Onoda,G.Y.,Jr.; and Pincus,A.G. **[1971]** "Spherulitic crystallization in glasses" in Advances in Nucleation and Crystallization in Glasses L.L.Hench and S.W.Freiman [eds] Am.Cer.Soc., Columbus, OH, p.141-50

Freiman,S.W.; Onoda,G.Y.,Jr.; and Pincus,A.G. **[1972]** "Controlled spherulitic crystallization in 3BaO-5SiO2 glass" J.Am.Cer.Soc. 55[7]354-59

Frenkel,J. **[1945]** "Viscous flow of crystalline bodies under the action of surface tension" J.Phys. (USSR) 9[5], 385-91

Frishchat,G.H. **[1970]** "Sodium diffusion in natural quartz crystals" J.Am.Cer.Soc. 53, 357

Geiger,G. **[1993]** "Thermal analysis for improved quality" Am.Cer.Soc.Bull. 72[11] 54-62,129

Geiss,E.A.; Fletcher,J.P.; and Herron,L.W. **[1984]** "Isothermal sintering of cordierite-type glass powders" J.Am.Cer.Soc. 67[8]549-522

German,R.W. **[1991]** "Fundamentals of sintering" Engineered materials handbook vol.4: Ceramics and glassed, ASM international, 260-8

Goldschmidt,V.M. Skrifter Norke Videnskaps Akad [Oslo],I. Math-Naturwiss. K1. 8, p.7

Greer,A.L. and **Kelton**,K.F. **[1991]** "Nucleation in lithium disilicate glass: A test of classical theory by quantitative modeling" J.Am.Cer.Soc. 74[5]1015-22

Griffith,A.A. **[1924]** Phil.Trans.R.Soc. A221, 163-98

Guillemet,C. and **Denocin**,J. **[1982]** "Kinetics of the precipitation of wollastonite in industrial soda-lime silicate glasses" in Nucleation and crystallisation in Glasses J.H.Simmons, D.R.Uhlmann, and G.H.Beall (eds) Am.Cer.Soc., Columbus, 193-203

Gutzow,I.; Avramov,I.; and Kastner,K. **[1990]** "Glass formation and crystallization" J.Non-Cryst.Solids 123,97-113

Haller,W. and **Macedo**,P.B. **[1968]** "The origin of phase connectivity in microheterogeneous" Phys.Chem.Glasses 9[5]153-5

Hammel,J.J. **[1966]** "Direct measurements of homogeneous nucleation rates in a glass-forming system" J.Chem.Phys. 46[6]2234-44

Hamidouche,M.; Louahdi,R.; Bouaouadja,N.; and Osmani,H. **[1994]** "The fracture of soda-liime glass" Glass Technology 35[4]183-5

Hasselman,D.P.H. and **Fulrath**,R.M. **[1966]** "Proposed fracture theory of a dispersion-strengthened glass matrix" J.Am.Cer.Soc. 49,68-72

Hayward,P.J.; Vance,E.R.; and Doern,D.C. **[1987]** "DTA/SEM study of crystallization in sphene glass-ceramics" Am.Cer.Soc.Bull 66[11]1620-6

Hilliard,J.E. and **Cahn**,J.W. **[1961]** "An evaluation of procedures in quantitative metallography for volume-fraction analysis" Trans.Met.Soc.AIME 221,344-52

Hirayama,C. & **Camp**,F.E. **[1969]** "The effect of fluorine and chlorine substitution on the viscosity and fining of soda-lime and a potassium-barium silicate glass" Glass Technol. 10[5]123-7

Holloway,D.G. **[1973]** The Physical Properties of Glass Wykeham Publications, London, ISBN 0 85109 320 5

James,P.F. **[1982]** "Nucleation in glass-forming systems - a review" in J.H.Simmons; D.R.Uhlmann; and G.H.Beall [eds] Advanced in Ceramics vol.4: Nucleation and crystallization in glasses, American Ceramic Society,

James,P.F. **[1985]** "Kinetics of crystal nucleation in silicate glasses" J.Non-Cryst.Solids 73,517-40

Johannsen,A. **[1931]** A Descriptive Petrography of Igneous Rocks Univ. of Chicaco Press, Chicago, IL

Johnson,W.A. and **Mehl**,R.F. **[1939]** "Reaction kinetics in processes of nucleation and growth" Trans.AIME 135[8]416-42

Kalinina,A.M.; Jurizin,N.S.; Foking,W.M.; and Filipovich, W.N. **[1986]** Proc.of the National Conf. on Glassy State Leningrad

Keith,H.D. and **Padden**,F.J. **[1963]** "A Phenomenological theory of spherulitic crystallization" J.Appl.Phys. 34[8]2409-21

Kelton,K.F.; Greer,A.L.; and Thompson,C.V. **[1983]** J.Chem.Phys. 79,6261

Kim,H.S. **[1989]** "Development of a fibre-reinforced glass-ceramic composite" PhD Thesis, Imperial College, London

Kingery,W.D. & **Berg**,M. **[1955]** "Study of the initial stage of sintering solids by viscous flow, evaporation-condensation, and self-diffusion" J.Appl.Phys. 26,1205

Kingery,W.D. **[1960]** "Implication of sintering theories with regard to process controls" Transactions of the VIIth International Ceramic Congress Institute of Ceramics, London, 461-71

Kingery,W.D.; Bowen,H.K.; and Uhlman,D.R. **[1976]** Introduction to ceramics John Wiley and Sons

Kissinger, H.E. **[1957]** "Reaction kinetics in differential thermal analysis" Anal.Chem. 29[11]1702-6

Kissinger, H.E. **[1956]** "Variation of peak temperature with heating rate in DTA" J.Res.Natl. Bur. Stand. [US] 57[4]217-21

Klingsberg,C. **[1964]** "Bubble-induced nucleation and crystal growth in glass" J.Am.Cer.Soc. 47[2]97-100

Koide,M.; Matusita,K.; and Komatsu,T. **[1990]** "Viscosity of fluoride glasses at glass transition temperature" J.Non-Cryst.Solids 125,93-7

Kuczynski,G.C. **[1949]** "Self-diffusion in sintering of metallic particles" Trans.AIME 185, 169

Kuczynski, G.C. and **Zaplatynskyj**,I. **[1956]** "Sintering of glass" J.Am.Cer.Soc. 30[10]349-50

Lange,F.F. and **Metcalf**,M. **[1983]** "Processing-related fracture origins: II. Agglomerate motion and cracklike internal surfaces caused by differential sintering" J.Am.Ceram.Soc. 66[6]398-406

Lange,F.F. and **Radford**,K.C. **[1971]** J.Mater.Sci. 6,197

Lewis, M.H.; Metcalf-Johansen,J.; and Bell,P.S. **[1979]** "Crystallization mechanisms in glass-ceramics" J.Am.Cer.Soc. 62[5-6]278-88

Liniger,E.G. and **Raj**.R. **[1988]** "Spatial variations in the sintering rate of ordered and disordered particle structures" J.Am.Cer.Soc. 71[9]C408-10

Mackenzie,J.K. and **Shuttleworth**,R. **[1949]** "A phenominological theory of sintering" Proc. Phys.Soc., London, Sect.B, 62, 833-52

Marotta,A. and **Buri**,A. **[1978]** "Kinetics of devitrification and differential thermal analysis" Thermochim.Acta 25,155-60

Marotta,A.; Buri,A.; Branda,F.; and Saiello,S. **[1982]** "Nucleation and crystallization of Li2O.2SiO2 glass - A DTA study" in J.H.Simmons, D.R.Uhlmann, and G.H.Beall [eds] Advances in Ceramics: Vol.4 Nucleation and crystallization in glasses American Ceramic Society, Columbus, OH, p.146-52

Mattox,D.M. **[1967]** "Contamination-nucleated crystal growth at bubble surfaces in glalss" J.Am.Cer.Soc. 50[12]683

Matusita,K. and **Sakka**,S. **[1979a]** "Study on crystallization kinetics in glass by differential thermal analysis" Thermochim.Acta 33,351-4

Matusita,K. and **Sakka**,S. **[1979b]** "Kinetic study of the crystallization of glass by differential scanning calorimetry" Phys.Chem.Glasses 20,81-4

Matusita,K.; Sakka,S.; and Matsui,Y. **[1975]** "Determination of the activation energy for crystal growth by differential thermal analysis" J.Mat.Sci. 10,961-6

McCoy,M.A. and **Heuer**,A.H. **[1988]** "Microstructure characterization and fracture toughness of cordierite-ZrO_2 glass-ceramics" J.Am.Cer.Soc. 71[8]673-7

McMillan,P.W. **[1979]** Glass-Ceramics [2nd ed.] Academic Press, London. ISBN 0-12-485660-8

Morey,A. **[1930]** J.Am.Cer.Soc. 13, 683

Moynihan,C.T. **[1993]** "Correlation between the width of the glass transition region and the temperature dependence of the viscosity of high-Tg glasses" J.Am.Cer.Soc. 76[5]1081-7

Mukherjee,S.P. and **Rogers**,P.S. **[1967]** "Nucleation and crystal growth in silicate glasses containing fluorides" Phys.Chem.Glasses 8[3]81-7

Ohlberg,S.M.; Golob,H.R.; and Strickler,D.W. **[1962]** in M.K.Reser; G.Smith; and H.Insley [eds] Symposium on Nucleation and Crystallization of Glasses and Melts, Am.Cer.Soc. Columbus,OH, p.55-62

Ohsato,H. and **Sugimura**,T. **[1986]** "Morphology of synthetic β-wollastonite and para-wollastonite" J.Cryst.Growth 74,656-8

Orowan,E. **[1949]** Rep.Prog.Phys. 12,185-232

Pampuch,R. and **Lis**,J. **[1989]** "Specific aspects of sintering of micropowders" Solid State Phenomena 8&9, 83-94

Panda,P.C. and **Raj**.R. **[1989]** "Sintering and crystallization of glass at constant heating rates" J.Am.Cer.Soc. 72[8]1564-66

Panda,P.C.; Mobley,W.M.; and Raj,R. **[1989]** "Effect of the heating rate on the relative rates of sintering and crysallisation in glass" J.Am.Cer.Soc. 72[2]2361-64

Partridge,G. **[1994]** "An overview of glass ceramics Part 1 Development and principal bulk applications" Glass Technology 35[3]116-27

Paul,A. **[1990]** Chemistry of glasses 2nd ed. Chapman & Hall. ISBN 0-412-27820-0

Petru,Z. **[1981]** "The sintering kinetics of crystallising glasses" Silikaty, 25,[check in Clark & Reed 1986]

Phillips,D.C. **[1991]** "Ceramic composites- their current status and some requirements for future development" Comp.Sci.Tech. 40[1]1-17

Ponton,C.B. and **Rawling**,R.D. **[1989]** "Dependence of the Vickers indentation fracture toughness on the surface crack length" J.British Cer.Trans. 88, 83-90

Prewo,K.M. and **Brennan**,J.J. **[1982]** "Silicon carbide fibre reinforced glass-ceramic matrix composites exhibiting high strength and toughness" J.Mat.Sci. 17,2371-83

Prewo,K.M.; Brennan,J.J.; and Layden,G.K. **[1986]** "Fibre reinforced glasses and glass ceramics for high performance applications" Am.Ceram.Soc.Bull. 65,305-13 and 322

Quinn,G.D. **[1991]** "Strength and proof testing" Engineering materials handbook vol.4: Ceramics and Glasses, ASM international, 585-98

Rabinovich,E.M. **[1979]** "Crystallization and thermal expansion of solder-glass in the PbO-B2O3-ZnO system with admixture" Am.Cer.Soc.Bull. 58[6]595-605

Rabinovich,E.M. **[1982]** "Cordierite glass-ceramics produced by sintering" in J.H.Simmons, D.R.Uhlmann and Beall,G.H. [eds] Advances in ceramics vol.4: Nucleation and crystallization in glass Am.cer.Soc. Ohio 327-33.

Rabinovich,E.M. **[1983]** "On the structural role of fluoride in silicate glasses" Phys.Chem.Glass 24[3]54-6

Rabinovich,E.M. **[1985]** "Review: Preparation of glass by sintering" J.Mater.Sci. 20,4259-97

Rabinovich,E.M.; Krol,D.M.; Kopylov,N.A.; and Gallagher,P.K. **[1989]** "Retention of fluorine in silica gels and glass" J.Am.Cer.Soc. 72[7]1229-32

Rahaman,M.N. and De **Jonghe**,L.C. **[1987]** "Effect of rigid inclusions on the sintering of glass powder compacts" J.Am.Cer.Soc. 70[12]C348-C351

Raj,R. **[1981]** "Morphology and stability of the glass phase in glass-ceramic systems" J.Am.Cer.Soc. 64[5]245-8

Ray,C.S. and **Day**,D.E. **[1990]** "Determining the nucleation rate curve for lithium disilicate glass by differential thermal analysis" J.Am.Cer.Soc. 73[2]439-42

Richter,A. **[1989]** "Transient nucleation in glass formation" in O.V.Mazuring [ed] Glass'89 XV International congress on glass: Vol.1b, Leningrad, p.245–8

Rice,R.W. **[1991]** "Porosity dependence of mechanical and other properties of materials" Mater.Res.Soc.Symp.Proc. 229-33

Rogers,P.S.; Butler,J.; and Steele,B.C.H. **[1969]** "A simple technique for sealing molybdenum to alumina or platinum to alumina by means of a glass-ceramic seal" J.Sci.Instruments [J.Phys.E] 2[2]102

Ross,J.W.; Miller,W.A.; Weatherly,G.C. **[1982]** Acta Metall. 30,203

Sakka,S.; Matusita,K.; and Kamiya,K. **[1977]** "Thermal analysis studies on the crystallization of glass" in H.Chihara [ed] Ther.Anal. [Kagaku Gijutsu-sha, Tokyo] 10-13

Salama,S.N. **[1990]** "Catalytic effect of fluoride on crystallization and phase transformation of some silicate systems" Silicate Industriels 5-6,171-6

Saraswati,V. **[1990]** "Additive induced crystallization of mica phase in K2O.SiO2.MgO.F glass-ceramic" J.Non-Cryst.Solids 124,254-7

Schaeffer,H.A. **[1975]** "Silicon and oxygen diffusion in oxide glasses" in Cooper and Heuer [eds] 311-25

Scherer,G.W. **[1987]** "Sintering with rigid inclusions" J.Am.Cer.Soc. 70[10] 719-25

Scherer,G.W. **[1990]** "Theories of relaxation" J.Non-Crystalline Solids 123, 75-89

Schweitzer,C.B.V. **[1994]** "Precessing and properties of silceram glass-ceramics particulates reinforced composites" Ph.D. thesis, Imperial College, London

Seward,T.P.; Uhlmann,D.R.; and Turnbull,D. **[1968]** "Development of two-phase structure in glasses, with special reference to the system BaO-SiO2" J.Am.Cer.Soc. 51[11]634-42

Shen,D.; Xu,G.; Huang,R.; and Chen,X. **[1989]** "Phase separation and crystallization of a CaO-Al2O3-SiO2 system glass" Glass'89 vol.4, 17-22

Shields,J.E. **[1991]** "Porosity, density, and surface area measurement" Engineering materials handbook vol.4: Ceramics and Glasses, ASM international, 580-4,

Shyu,J.J. and **Wu**,J.M. **[1991a]** "Effects of composition changes on the crystallization behaviour of MgO-CaO-SiO2-P2O5 glass-ceramics" J.Am.Cer.Soc. 74[9]2123-30

Shyu,J.J. and **Wu**,J.M. **[1991b]** "Spherulitic growth of apatite in a MgO-CaO-SiO2-P2O5 glass" J.Am.Cer.Soc. 74[7]1532-40

Singer,G.M. & **Tomozawa**,M. **[1989]** "Cordierite-based oxyfluoride glasses and glass ceramics Part 1: Glasses" Phys.Chem.Glasses 30[3]86-95

Sridharan,S. and **Tomozawa**,M. **[1992]** "Effect of various oxide additives on sintering of BaO-SiO2 system glass-ceramics" J.Mat.Sci. 27,6747-54

Stauffer,D. **[1985]** "Introduction to percolation theory" Taylor and Francis, London and Philadelphia

Stephenson,I.M. and **White**,J. **[1967]** "Factors controlling microstructure and grain growth in 2-phase [1 solid+1 liquid] and in 3-phase [2 solid+1 liquid] systems" Transaction of the British Ceramic Society vol.66,443-83

Stookey,S.D. **[1960]** USP 2 920 971

Strnad,Z. **[1986]** Glass-Ceramic Materials Elsevier, Amsterdam ISBN 0-444-99524-2

Sudre,O. and **Lange**,F.F. **[1992]** "Effect of inclusions on densification: I. Microstructural development in an Al2O3 matrix containing a high volume fraction of ZrO2 inclusions" J.Am.Cer.Soc. 75,519-524

Sun,K.H. **[1947]** J.Am.Cer.Soc. 30,277

Tamman,G. **[1925]** The states of aggregation, D.van Nostrand & Co.

Tanaka,K. **[1987]** "Elastic/plastic indentation hardness and fracture toughness" J.Mater.Sci. 22,1501-8

Tang,T.B. and **Chaudhuri**,M.M. **[1983]** "Comment on kinetics of crystallization of ZrF4-BaF2-LaF3 glass by differential scanning calorimetry" J.Am.Cer.Soc. 66[11]C-218

Tashiro,M. **[1985]** "Crystallization of glasses: Science and technology" J.Non-Cryst. Solids 73,575-84

Taylor,B.A. **[1995]** "Development of a bioactive glass-ceramic incorporating metal particles" PhD Thesis, Imperial College, London

Taylor,T.D.**[1991]** "Structure and properties of glasses" Engineering materials handbook vol.4: Ceramics and Glasses, ASM International, 564-9

Turnbull,D. [1961] Turnbull,D. [1988] "Phase stability of glasses" J.Non-Cryst.Solids. 102,117-24

Uhlmann,D.R. **[1969]** "Crystal growth and glass formation" 465-78

Uhlmann,D.R. **[1972]** "A kinetic treatment of glass formation" J.Non-Cryst.Solids 7,337

Urbain,G.; Cambier,R.; Deletter,M.; and Ansean,M.R. **[1981]** "Viscosity of silicate melts" J.Br.Ceram. Soc. 80,139-41

Utsumi,Y.; Sakka,S.; and Tashiro,M. **[1970]** "Experimental study on the bending strength of glass in relation to liquid-liquid phase separation" Glass Tech 11[3]80-5

Utsumi,Y. and **Sakka**,S. **[1970]** "Ball indentation strength of phase separated glasses" Glass Tech 11[3] 86-91

Varshal,B.G. **[1989]** "Structure aspects of the crystallization of silicate glasses" Glass and Ceramics 46[5-6]271-4

Volf,M.B. **[1984]** Chemical approach to glass, Elsevier, Amsterdam

Warren,R. **[1992]** Ceramic-Matrix Composites Blackie and Son, Chapman Hall, NY ISNB 0 216 92682 3

Weinberg,M.C. **[1991]** "On the analysis of non-isothermal thermoanalytic crystallization experiments" J.Non-Cryst.Solids 127,151-8

Weinberg,M.C. and **Zanotto**,E.D. **[1989]** "Re-examination of the temperature dependence of the classical nucleation rate: Homogeneous crystal nucleation in glass" J.Non-Cryst.Solids 108,99-108

Wendlandt,W.W. **[1974]** Thermal Methods of Analysis, 2nd edition, Ch. 5, Wiley, New York.

Whittemore,O.J. and **Varela**,J.A. **[1987]** "Pore growth and shrinkage during sintering" 4th International symposium on Science and Technology of Sintering, Tokyo, 4-6 November 1987

Yinnon,H. and **Uhlmann**,D.R. **[1983]** "Application of thermoanalytical techniques to the study of crystallization kinetics in glass-forming liquids part I: Theory" J.Non-Cryst.Solids 54,253-75

Zachariasen [1932] J.Am.Cer.Soc.54,3841

Zanotto,E.D. and **James**,P.F. **[1988]** "Experimental test of the general theory of transformation kinetics: Homogeneous nucleation in a $BaO\text{-}2SiO_2$ glass" J.Non-Cryst.Solids 104,70-2

Zanotto,E.D. and **Weinberg**,M.C. **[1988]** "Saturation effects in homogeneous and heterogeneous crystal nucleation" J.Non-Cryst.Solids 105,53-62

Zarzycki,J. **[1991]** Glasses and the Vitreous State [Cambridge solid state science series] Cambridge, G.B.

Zdaniewski,W.A. **[1978]** "Microstructure and kinetics of crystallization of $MgO.Al_2O_3.SiO_2$ glass-ceramics" J.Am.Cer.Soc. 61[5]199-204

Appendix A
Urbain Viscosity model

The following is a brief summary of the 'Urbain Model' for predicting viscosity from the absolute temperature and composition of the silicate melts. Firstly, the constituent oxides are split into three categories: glass formers, modifiers, and amphoterics. These categories are then used to predict the viscosity of the melts. The method is summarised as follows:

1) Convert oxide weight % into mole fractions.

2) Sum the mole fractions of the modifiers, multiplying each individual mole fraction be the number of oxygen atoms present in that oxide.

3) Calculate the value of α from the equation

$$\alpha = \frac{\Sigma \text{ modifier mole fractions}}{\Sigma \text{ modifier mole fractions} + \text{mole fraction of amphoterics}}$$

4) Using α, calculate B_n from the equations

$B_0 = 13.8+39.9355\alpha - 44.049\alpha^2$

$B_1 = 30.481-117.1501\alpha+129.997\alpha^2$

$B_2 = -40.9429+234.0486\alpha-300.04\alpha^2$

$B_3 = 60.7619-153.9276\alpha+211.1616\alpha^2$

5) Using B_n and N, the mole fraction of glass formers, calculate B (units are in Kelvin, K):

$B=B_0+B_1N+B_2N^2+B_3N^3$

6)Calculate A from B (units are in Poise/K)

$-\ln A=0.2693B+11.6725$

7) Calculate the viscosity, using the absolute temperature (known), T, and the values of A and B calculated above:

$$\eta = AT\exp^{\frac{10^3 B}{T}}$$

In the present study, the constituent oxides were split into three categories as follows:

The glass former: SiO_2

The modifiers: CaO, Na_2O, CaF_2

The amphoteric: Al_2O_3

Appendix C

Critical size for nucleus formation

The kinetics of formation of nuclei involves both the free energy of formation of the small region, including its surface energy, and the rate of atom transport at the interface boundary. If we assume for simplicity that the new nucleus is spherical and has a radius of r, the free-energy of reaction, ΔG is given by

$$\Delta G = 4\pi r^2 \Delta G_s + \frac{4}{3}\pi r^3 \Delta G_v \qquad [C\text{-}1]$$

where ΔG_s is the free energy of the surface and ΔG_v is the free energy change per unit volume for the phase transition, neglecting interfacial energy.

As the particle first increases in size, its free energy also increase until the radius r* is reached. Particles of radius less than r* will tend to redissolve, thus lowering the free energy. However, particles of radius larger than r* will lower free energy for growing. From Figure C-1, it is clear that ΔG^* and r* may be calculated by maximizing equation C-1. By setting the first derivative equal to zero, one obtain

$$r^* = -\frac{2\Delta G_s}{\Delta G_v} \qquad [C\text{-}2a]$$

$$\Delta G^* = \frac{16\pi \Delta G_s^3}{3\Delta G_v^2} \qquad [C\text{-}2b]$$

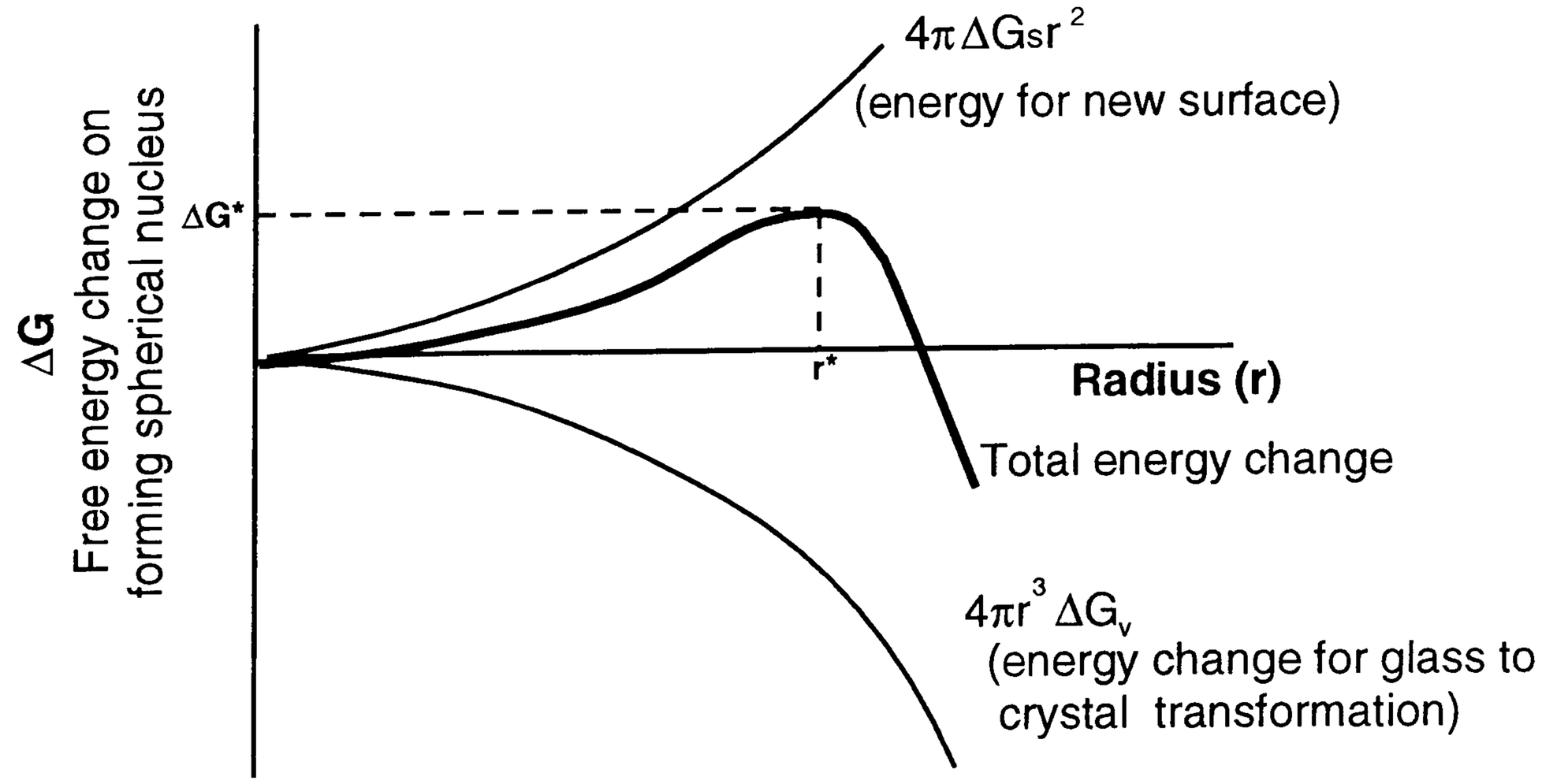


Figure C-1 Free energy of nucleus as a function of size. Some critical size must be exceeded before the nucleus becomes stable.

If the total number of particles of the new solid phase is n0, the number of nuclei n* may be calculated by

$$n^* = n_0 e^{-\Delta G^*/kT} \qquad [C\text{-}3]$$

The nuclei grow by addition of atoms, the final step in nucleation. The rate of addition is proportional to the frequency of motion (ν) into the nucleus for a single atom, multipied by the number of atoms (m*) which is the immediate neighbours to the nucleus. Consequently,

$$I = n^* \nu m^* \qquad [C\text{-}4]$$

where I is the rate of nucleation measured in units of nuclei per second. The motion of atoms into the nucleus is diffusive and therefore

$$\nu \alpha e^{-\Delta G_D/kT} \qquad [C\text{-}5]$$

where ΔG_D is the activation energy for diffusion. m* is geometrical and depends on the shape and size of the nucleus. The previous three equations may be combined to give

$$I \alpha m^* e^{-\left(\frac{\Delta G^* + \Delta G_D}{kT}\right)} \qquad [C\text{-}6]$$

for the temperature variation. As the tempreature drops, ΔG^* falls violently and the nucleation rate increases. Soon, however, ΔG^* becomes negligible compared to ΔG_D and ΔG_D thus dominates equation C-6, and I then decreases with temperature. Consequently, there is a maximum in the homogeneous nucleation rate which may be considerably below the melting point.